TECHNICAL REPORT

CISPR 16-3

First edition
2000-05

INTERNATIONAL SPECIAL COMMITTEE ON RADIO INTERFERENCE

Specification for radio disturbance and immunity measuring apparatus and methods –

Part 3:
Reports and recommendations of CISPR

Spécifications des méthodes et des appareils de mesure des perturbations radioélectriques et de l'immunité aux perturbations radioélectriques –

Partie 3:
Rapports et recommandations du CISPR

Numéro de référence
Reference number
CISPR 16-3/TR:2000(E)

Revision of this publication

The technical content of IEC and CISPR publications is kept under constant review by the IEC and CISPR, thus ensuring that the content reflects current technology.

Information on the subjects under consideration and work in progress undertaken by the technical com-mittee which has prepared this publication, as well as the list of publications issued, is to be found at the following IEC sources:

- **IEC web site***
- **Catalogue of IEC publications**
  Published yearly with regular updates
  (On-line catalogue)*
- **IEC Bulletin**
  Available both at the IEC web site* and
  as a printed periodical

Terminology used in this publication

Only special terms required for the purpose of this publication are defined herein.

For general terminology, readers are referred to IEC 60050: *International Electrotechnical Vocabulary* (IEV), which is issued in the form of separate chapters each dealing with a specific field, the General Index being published as a separate booklet. Full details of the IEV will be supplied on request.

For terms on radio interference, see Chapter 902.

Graphical and letter symbols

For graphical symbols, and letter symbols and signs approved by the IEC for general use, readers are referred to:

– IEC 60027: *Letter symbols to be used in electrical technology*;

– IEC 60617: *Graphical symbols for diagrams*;

The symbols and signs contained in the present publication have either been taken from IEC 60027 or IEC 60617, or have been specifically approved for the purpose of this publication.

* IEC web site

TECHNICAL REPORT

CISPR 16-3

First edition
2000-05

INTERNATIONAL SPECIAL COMMITTEE ON RADIO INTERFERENCE

Specification for radio disturbance and immunity measuring apparatus and methods –

**Part 3:
Reports and recommendations of CISPR**

Spécifications des méthodes et des appareils de mesure des perturbations radioélectriques et de l'immunité aux perturbations radioélectriques –

*Partie 3:
Rapports et recommandations du CISPR*

International Electrotechnical Commission 3, rue de Varembé Geneva, Switzerland
Telefax: +41 22 919 0300 e-mail: inmail@iec.ch IEC web site http://www.iec.ch

Commission Electrotechnique Internationale
International Electrotechnical Commission
Международная Электротехническая Комиссия

CODE PRIX
PRICE CODE XH

Pour prix, voir catalogue en vigueur
For price, see current catalogue

CONTENTS

INTERNATIONAL ELECTROTECHNICAL COMMISSION

SPECIFICATION FOR RADIO DISTURBANCE AND IMMUNITY MEASURING APPARATUS AND METHODS –

Part 3: Reports and recommendations of CISPR

FOREWORD

1) The IEC (International Electrotechnical Commission) is a worldwide organization for standardization comprising all national electrotechnical committees (IEC National Committees). The object of the IEC is to promote international co-operation on all questions concerning standardization in the electrical and electronic fields. To this end and in addition to other activities, the IEC publishes International Standards. Their preparation is entrusted to technical committees; any IEC National Committee interested in the subject dealt with may participate in this preparatory work. International, governmental and non-governmental organizations liaising with the IEC also participate in this preparation. The IEC collaborates closely with the International Organization for Standardization (ISO) in accordance with conditions determined by agreement between the two organizations.
2) The formal decisions or agreements of the IEC on technical matters express, as nearly as possible, an international consensus of opinion on the relevant subjects since each technical committee has representation from all interested National Committees.
3) The documents produced have the form of recommendations for international use and are published in the form of standards, technical specifications, technical reports or guides and they are accepted by the National Committees in that sense.
4) In order to promote international unification, IEC National Committees undertake to apply IEC International Standards transparently to the maximum extent possible in their national and regional standards. Any divergence between the IEC Standard and the corresponding national or regional standard shall be clearly indicated in the latter.
5) The IEC provides no marking procedure to indicate its approval and cannot be rendered responsible for any equipment declared to be in conformity with one of its standards.
6) Attention is drawn to the possibility that some of the elements of this International Standard may be the subject of patent rights. The IEC shall not be held responsible for identifying any or all such patent rights.

The main task of IEC technical committees is to prepare International Standards. However, a technical committee may propose the publication of a technical report when it has collected data of a different kind from that which is normally published as an International Standard, for example "state of the art".

Technical reports do not necessarily have to be reviewed until the data they provide are considered to be no longer valid or useful.

CISPR 16-3, which is a technical report, has been prepared by CISPR subcommittee A: Radio interference measurements and statistical methods.

The text of this technical report is based on the following documents:

Enquiry draft	Report on voting
CISPR/A/CO/67 CISPR/A/CO/77	CISPR/A(CO)82 CISPR/A(CO)84

Full information on the voting for the approval of this technical report can be found in the report on voting indicated in the above table.

This publication has been drafted in accordance with the ISO/IEC Directives, Part 3.

This document which is purely informative is not to be regarded as an International Standard.

The text of this report is based on the following documents:

Recommendation 2/2 – p/o CISPR. 7B, 1975; Recommendation 46/1 – p/o CISPR. 11, 1990; Report 33 – p/o CISPR 8, 1969; Report 38 – p/o CISPR 8, 1969; Report 48 – p/o CISPR 8B, 1975; Report 49 – p/o CISPR 8C, 1980; Report 61 = CISPR 23, 1987; Report 59: CIS/A(Sec)58 + CIS/A(Sec)58A, 1983; Report: CIS/A(Sec)67 + CIS/A(Sweden)29; RM 2828/CISPR/A, 1985; CIS/A(CO)32, 1985; CIS/A(Sec)58, 1983; CIS/A(Sec)58A, 1983; CIS/A(Sec)67, 1985; CIS/A(CO)67, 1992; CIS/A(CO)67A, 1993; CIS/A(CO)77A, 1993; CIS/A(CO)81, 1987; CIS/A(CO)82, 1994; CIS/A(CO)84, 1994; CIS/A(Sec)84, 1987; CIS/A(Sec)88, 1988; CIS/A(Sec)88A, 1988; CIS/A(Sec)94, 1989; CIS/A(Sec)115, 1991; CIS/A(Sec)115A, 1991; CIS/A(Sec)116, 1991; CIS/A(Sec)124, 1991; CIS/A(Sec)128, 1992; CIS/A(Sec)132, 1993; CIS/A/166/CD, 1995.

A bilingual version of this publication may be issued at a later date.

SPECIFICATION FOR RADIO DISTURBANCE AND IMMUNITY MEASURING APPARATUS AND METHODS –

Part 3: Reports and recommendations of CISPR

1 General

1.1 Scope

This part of CISPR 16 contains recommendations on statistics of disturbance complaints, on the significance of CISPR limits, on determination of CISPR limits and other specific reports.

Over the years, the CISPR prepared a number of recommendations and reports that have significant technical merit but were not generally available. Reports and recommendations were for some time published in CISPR 7 and 8.

At its meeting in Campinas, Brazil, in 1988, subcommittee A agreed on the table of contents of part 3 and to publish the reports for posterity by giving the reports a permanent place in part 3.

1.2 Reference documents

IEC 60083:1997, *Plugs and socket-outlets for domestic and similar general use standardized in member countries of IEC*

IEC 60364-4, *Electrical installations of buildings – Part 4: Protection for safety*

CISPR 11:1997, *Industrial, scientific and medical (ISM) radio-frequency equipment – Electromagnetic disturbance characteristics – Limits and methods of measurement*

CISPR 13:1996, *Limits and methods of measurement of radio interference characteristics of sound and television broadcast receivers and associated equipment*

CISPR 14-1, *Electromagnetic compatibility – Requirements for household appliances, electric tools and similar apparatus – Part 1: Emission*

CISPR 16-1:1999, *Specification for radio disturbance and immunity measuring apparatus and methods – Part 1: Radio disturbance and immunity measuring apparatus*

CISPR 16-2:1996, *Specification for radio disturbance and immunity measuring apparatus and methods – Part 2: Methods of measurement of disturbances and immunity*

ITU-R BS 468-4, *Measurement of audio-frequency noise voltage level in sound broadcasting*

1.3 Definitions

For the purpose of this part of CISPR 16, the definitions of CISPR 16-1 and IEV 60050(161) as well as the following definitions apply.

1.3.1
bandwidth (B_n)
width of the overall selectivity curve of the receiver between two points at a stated attenuation, below the midband response. The bandwidth is represented by the symbol B_n, where n is the stated attenuation in decibels

1.3.2
impulse bandwidth (B_{imp})

$$B_{imp} = A(t)_{max} / (2G_o \times IS)$$

where

$A(t)_{max}$ is the peak of the envelope at the IF output of the receiver with an impulse area IS applied at the receiver input;

G_o is the gain of the circuit at the centre frequency.

Specifically, for two critically coupled tuned transformers,

$$B_{imp} = 1{,}05 \times B_6 = 1{,}31 \times B_3$$

where B_6 and B_3 are respectively the bandwidths at the –6 dB and –3 dB points (see 1.3-A.2 in annex 1.3-A for further information)

1.3.3
impulse area (sometimes called impulse strength) (IS)
the voltage-time area of a pulse defined by the integral:

$$IS = \int_{-\infty}^{+\infty} V(t)\,dt \text{ (expressed in µVs or dB(µVs))}$$

NOTE Spectral density (D) is related to impulse area and expressed in µV/MHz or dB(µV)/MHz. For rectangular impulses of pulse duration T at frequencies $f << 1/T$, the relationship D (µV/MHz) = $2 \times 10^6/IS$ (µVs) applies since D is calibrated in r.m.s. values of a corresponding sine wave.

1.3.4
electrical charge time constant (T_C)
time needed after the instantaneous application of a constant sine-wave voltage to the stage immediately preceding the input of the detector for the output voltage of the detector to reach 63 % of its final value

NOTE This time constant is determined as follows. A sine-wave signal of constant amplitude and having a frequency equal to the mid-band frequency of the i.f. amplifier is applied to the input of the stage immediately preceding the detector. The indication, D, of an instrument having no inertia (for example, a cathode-ray oscilloscope) connected to a terminal in the d.c. amplifier circuit so as not to affect the behaviour of the detector, is noted. The level of the signal is chosen such that the response of the stages concerned remains within the linear operating range. A sine-wave signal of this level, applied for a limited time only and having a wave train of rectangular envelope is gated such that the deflection registered is 0,63D. The duration of this signal is equal to the charge time of the detector.

1.3.5
electrical discharge time constant (T_D)
time needed after the instantaneous removal of a constant sine-wave voltage applied to the stage immediately preceding the input of the detector for the output of the detector to fall to 37 % of its initial value

NOTE The method of measurement is analogous to that for the charge time constant, but instead of a signal being applied for a limited time, the signal is interrupted for a definite time. The time taken for the deflection to fall to 0,37D is the discharge time constant of the detector.

1.3.6
mechanical time constant (T_M) of a critically damped indicating instrument

$$T_M = T_L / 2\pi$$

where T_L is the period of free oscillation of the instrument with all damping removed.

NOTE 1 For a critically damped instrument, the equation of motion of the system may be written as

$$T_M^2(d^2\alpha / dt^2) + 2T_M(d\alpha / dt) + \alpha = ki$$

where

α is the deflection;

i is the current through the instrument;

k is a constant.

It can be deduced from this relation that this time constant is also equal to the duration of a rectangular pulse (of constant amplitude) that produces a deflection equal to 35 % of the steady deflection produced by a continuous current having the same amplitude as that of the rectangular pulse.

NOTE 2 The methods of measurement and adjustment are deduced from one of the following:

a) The period of free oscillation having been adjusted to $2\pi T_M$, damping is added so that $\alpha_{TM} = 0{,}35\ \alpha_{max}$.

b) When the period of oscillation cannot be measured, the damping is adjusted to be just below critical such that the overswing is not greater than 5 % and the moment of inertia of the movement is such that $\alpha_{TM} = 0{,}35\ \alpha_{max}$.

1.3.7
overload factor
ratio of the level that corresponds to the range of practical linear function of a circuit (or a group of circuits) to the level that corresponds to full-scale deflection of the indicating instrument.

The maximum level at which the steady-state response of a circuit (or group of circuits) does not depart by more than 1 dB from ideal linearity defines the range of practical linear function of the circuit (or group of circuits)

1.3.8
symmetric voltage
in a two-wire circuit, such as a single-phase mains supply, the symmetric voltage is the radio-frequency disturbance voltage appearing between the two wires. This is sometimes called the differential mode voltage. If *Va* is the vector voltage between one of the mains terminals and earth and *Vb* is the vector voltage between the other mains terminal and earth, the symmetric voltage is the vector difference (*Va* – *Vb*)

1.3.9
asymmetric voltage
radio-frequency disturbance voltage appearing between the electrical mid-point of the mains terminals and earth. It is sometimes called the common-mode voltage and is half the vector sum of *Va* and *Vb*, i.e. (*Va* + *Vb*)/2.

1.3.10
unsymmetric voltage
amplitude of the vector voltage, *Va* or *Vb* defined in 1.3.8 and 1.3.9. This is the voltage measured by the use of an artificial mains V-network

1.3.11
CISPR indicating range
range specified by the manufacturer which gives the maximum and the minimum meter indications within which the receiver meets the requirements of this part of CISPR 16

2 Statistics

2.1 Recommendation 2/3: Statistics of complaints and sources of interference (this recommendation replaces Recommendation 2/2 in CISPR 7B)

The CISPR,

CONSIDERING

a) that many administrations regularly publish statistics on interference complaints;

b) that it would be useful to be able to compare the figures for certain categories;

c) that, at present, varied and ambiguous presentation often renders this comparison difficult,

RECOMMENDS

1 that the statistics supplied by National Committees should be in such a form that the following information may be readily extracted:

1.1 number of complaints as a percentage of the total number of receiving licences for television, sound broadcasting and other services;

1.2 the relative aggressivity of the various sources of interference in the different frequency bands;

1.3 the comparison of the interference caused by the same source in different frequency bands;

1.4 the effectiveness of limits (CISPR or national) and other counter-measures on subclauses 1.1, 1.2 and 1.3;

2 that the terms used in publication of statistics as recommended in clause 3 should have the following meaning:

2.1 *complaint:* a request for assistance made to the interference service by a listener or a viewer who complains that his reception is degraded by interference. For the purpose of these statistics, one complaint will be recorded for each frequency band for which a confirmed complaint has been received;

2.2 *source:* a source of interference is the apparatus or installation which causes interference. Interference may be caused by a group of devices, for example, a number of fluorescent lamps on one circuit. In such cases, the number to be entered in the statistics is determined by the interference service;

NOTE To facilitate comparison of statistics, the method used to determine the number of sources should be stated.

one source may cause many complaints and one complaint may be caused by more than one source. Therefore, it is clear that the number of sources and the number of complaints against any classification code may not be related;

for the purpose of these statistics, both active generators of electrical energy and apparatus and installations which cause interference by secondary effects (secondary modulation) are included. See also Appendix II for a complete list;

2.3 *cause of complaint other than a source:* a reason for unsatisfactory reception in a case in which no source is concerned. See also Appendix II for a complete list;

3 that statistics should cover a complete calendar year; they should whenever possible be presented in the following form, without necessarily employing the finer categories listed in Appendix II. It s not intended to exclude further subdivisions; these are desirable, but they should fit into the scheme of the standard form;

the code numbers refer to the items listed in Appendices I and II;

Statistics of interference complaints

Source of interference or other cause of complaint			Number of complaints per service from each source					
Classification code	Description	Total number in each classification	Broadcasting [a]					Other services [b]
			Sound [c]		Television [c]			
			LF/ MF/ HF	II	I	III	IV/V	
A 1 1								
2 1								
etc. as in the appendices								
		Totals						

[a] LF = low frequency (long waves);

MF = medium frequency (medium waves);

HF = high frequency (short waves).

These three bands may either be grouped together, as shown, or dealt with separately.

II = Band II (VHF/FM)

I = Band I (VHF/television)

III = Band III (VHF/television);

IV/V = Band IV/V (UHF/television).

[b] The service and band affected should be stated.

[c] At the time of receipt of complaints of interference, i.e. before they have been investigated fully, it may not be possible to apportion the complaints accurately to the various broadcasting services. If this is so, then the number of complaints should be stated separately for sound broadcasting and television.

Appendix I to Recommendation 2/3: Classification of sources of interference and other causes of complaint

Main categories

Classification code	Description of the source
A	Industrial scientific and medical RF apparatus
A.1	Industrial and scientific RF apparatus
A.1.1	Apparatus tuned to free radiation frequency
A.1.2	Apparatus not tuned to free radiation frequencies
A.2	Medical radio-frequency apparatus
A.2.1	Apparatus tuned to free radiation frequencies
A.2.2	Apparatus not tuned to free radiation frequencies
A.3	Sparking apparatus (except ignition)
B	Electric power supply, distribution and traction
B.1	AC voltages exceeding 100 kV
B.1.1	Power lines overhead
B.1.2	Generating and switching stations
B.2	DC voltages exceeding 100 kV
B.2.1	Power lines overhead
B.2.2	Converting stations

Classification code	Description of the source
B.3	Voltages 100 kV to 1 kV (subdivision as for B.1)*
B.4	Voltages 1 kV to 450 kV (subdivision as for B.1)*
B.5	Low tension power supply and distribution (<450 V)
B.5.1	Power lines overhead
B.5.2	Generating and switching stations
B.6	Electric traction
B.6.1	Railways
B.6.2	Tramways
B.6.3	Trolley buses
C	Electricity consumers' equipment (industrial and similar)
C.1	Generators
C.2	Motors (P > 700 W)
C.2.1	Rated power P: 700 W < $P \leq$ 1 000 W
C.2.2	Rated power P: 1 000 W < $P \leq$ 2 000 W
C.2.3	Rated power P: 2 000 W < P
C.3	Contacts
C.4	Ignition
C.5	Rectifiers
C.6	Convertors
C.7	Diode thyristor and thyratron control equipment
C.8	Cattle fences
D	Low-power appliances as normally used in households, offices and small workshops
D.1	Motors (up to and including 700 W)
D.2	Contact devices
D.3	Diode, thyristor and thyratron control equipment (less than 1 000 W)
E	Gaseous discharge and other lamps
E.1	Fluorescent lamps
E.2	Neon signs
E.3	Filament lamps
F	Receiving installations
F.1	Sound broadcast receivers
F.2	Television receivers
F.3	Amplifiers and common aerial reception systems for broadcasting
F.4	Non-broadcasting receivers
G	Ignition systems of internal combustion engines
H	Identified sources other than those specified

* For convenience of analysis, the same subdivision is used for all voltage ranges. In those cases where a classification does not apply, for example, corona for low voltages, the category should remain blank

Classification code	Description of the source
I	Other causes of complaint
I.1	Telecommunication
I.1.1	Radio communication transmitters
I.1.1.1	Fundamental radiation
I.1.1.2	Harmonic radiation
I.1.1.3	Spurious radiation
I.1.2	Telecommunication by wire
I.2	Faults of the receiving installations
I.3	Receiver characteristics
I.4	Weak or faulty signals
I.5	Atmospheric disturbances
I.6	Unidentified sources of interference
I.7	Interference not observed
J	Information technology equipment
J.1	Data processing equipment (DPE)
J.1.1	Large DPE in computer rooms
J.1.2	Smaller plugable DPE not in dedicated rooms
J.1.3	Home computers and home video games
J.2	Local area network
J.3	Commercial video games
J.4	Telephone exchanges and other digital telecommunication equipment

Appendix II to Recommendation 2/3: Classification of sources of interference and other causes of complaint

Detailed categories

Classification code	Description of the source
A	Industrial scientific and medical RF apparatus
A.1	Industrial and scientific RF apparatus
A.1.1	Apparatus tuned to free radiation frequency
A.1.1.1	Drying non-metals
A.1.1.2	Plastic pre-heaters
A.1.1.3	Plastic seam welders
A.1.1.4	Wood glue drying
A.1.1.5	Microwave heating
A.1.1.6	Microwave cooking
A.1.1.7	Ultrasonic soldering and cleaning
A.1.1.8	Food treatment heaters (for example, fish thawing)
	...
A.1.1.20	Other
A.1.2	Not tuned to free radiation frequencies
A.1.2.1 to A.1.2.20	As for A.1.1.1 to A.1.1.20
A.2	Medical radiofrequency apparatus
A.2.1	Apparatus tuned to free radiation frequencies
A.2.1.1	Diathermy
A.2.1.2	Ultrasonic medical
A.2.1.3	Cauterization
	...
A.2.1.20	Other
A.2.2	Apparatus not tuned to free radiation frequencies
A.2.2.1 to A.2.2.20	As for A.2.1.1 to A.2.1.20
A.3	Sparking apparatus (except ignition)
A.3.1	RF excited arc welder
A.3.2	Surface erosion of plastics
A.3.3	Surface erosion of metals
A.3.4	Spectrograph
A.3.5	Spark diathermy
	...
A.3.20	Other
B	Electric power supply, distribution and traction
B.1	AC voltages exceeding 100 kV
B.1.1	Power lines overhead
B.1.1.1	Corona effect
B.1.1.2	Insulators
B.1.1.3	Presence of foreign objects on line
	...
B.1.1.20	Other

Classification code	Description of the source
B.1.2	Generating and switching stations
B.1.2.1	Generating stations
B.1.2.2	Switching stations
B.1.2.3	Transformer stations
B.1.2.4	Saturated transformers
	…
B.1.2.20	Other
B.2	DC voltages exceeding 100 kV
B.2.1	As for B.1.1
B.2.2	Converting stations
B.3	Voltages 100 kV to 1 kV (subdivision as for B.1)*
B.4	Voltages 1 kV to 450 V (subdivision as for B.1)*
B.5	Low tension power supply and distribution (<450 V)
B.5.1	Power lines overhead
B.5.1.1	Presence of foreign objects on line
B.5.1.2	Equipment faults
	…
B.5.1.20	Other
B.5.2	Generating and switching stations
B.5.2.1 to B.5.2.20	
B.6	Electric traction
B.6.1	Railways
B.6.1.1	Overhead distribution, high voltage
B.6.1.2	Overhead distribution, medium voltage
B.6.1.3	Rail distribution
B.6.1.4	Locomotive
	…
B.6.1.20	Other
B.6.2	Tramways
B.6.3	Trolley buses
C	Electricity consumers' equipment (industrial and similar)
C.1	Generators
C.2	Motors (P > 700 W)
C.2.1	Rated power P: 700 W < $P \leq$ 1 000 W
C.2.1.1	Lifts
C.2.1.2	Central heating
	…
C.2.1.20	Other
C.2.2	Rated power P: 1 000 W < $P \leq$ 2 000 W
C.2.2.1	Lifts
C.2.2.2	Central heating
	…
C.2.2.20	Other
* Appendix A of CISPR Recommendation 22/3 gives a list of such appliances	

Classification code	Description of the source
C.2.3	Rated power P: 2 000 W < P
C.2.3.1	Lifts
C.2.3.2	Central heating
	…
C.2.3.20	Other
C.3	Contacts
C.3.1	Lifts
C.3.2	Central heating
	…
C.3.20	Other
C.4	Ignition
C.4.1	Central heating
	…
C.4.20	Other
C.5	Rectifiers
C.6	Convertors
C.7	Diode thyristor and thyratron control equipment
C.8	Cattle fences
	…
C.20	Other installations
D	Low power appliances as normally used in households, shops, offices and small workshops
D.1	Motors (up to and including 700 W)*
D.1.1	Tools
D.1.1.1	Portable
D.1.1.2	Fixed
D.1.2	Household appliances
D.1.3	Shop and office appliances
	…
D.1.20	Other
D.2	Contact devices**
D.2.1	Thermostats
D.2.2	Other contact devices
D.3	Diode, thyristor and thyratron control equipment (less than 1 000 W)
E	Gaseous discharge and other lamps
E.1	Fluorescent lamps
E.2	Neon signs
E.3	Filament lamps
E.3.1	Vacuum
E.3.2	Gas filled
	…
E.20	Other

* Appendix A of CISPR Recommendation 22/3 gives a list of such appliances.

** See Appendix III of CISPR Recommendation 50.

Classification code	Description of the source
F	Receiving installations
F.1	Sound broadcast receivers
F.1.1	AM receiver
F.1.2	FM receiver
F.2	Television receivers
F.2.1	Local oscillator
F.2.1.1	Fundamental
F.2.1.2	Harmonic
F.2.2	Intermediate frequency radiation
F.2.3	Time base oscillator
F.2.4	Time base parasitic oscillation is, for example, Barkhausen oscillations
	...
F.2.20	Other
F.3	Amplifiers and common aerial reception systems for broadcasting
F.4	Non-broadcasting receivers
G	Ignition systems of internal combustion engines
G.1	Motor vehicles
G.2	Boats
G.3	Powered appliances (for example, lawn mowers)
	...
G.20	Other engines
H	Identified sources other than those specified
I	Other causes of complaint
I.1	Telecommunication
I.1.1	Radio communication transmitters
I.1.1.1	Fundamental radiation
I.1.1.1.1	Broadcasting stations
I.1.1.1.2	Amateur stations
I.1.1.1.3	Land mobile stations
	...
I.1.1.1.20	Other
I.1.1.2	Harmonic radiation
I.1.1.2.1	Broadcasting stations
I.1.1.2.2	Amateur stations
I.1.1.2.3	Land mobile stations
I.1.1.3	Spurious radiation
I.1.1.3.1 to I.1.1.3.20	As for I.1.1.1
I.1.2	Telecommunication by wire
I.2	Faults of the receiving installation
I.2.1	Inefficient aerial installation
I.2.2	Faulty receivers
I.2.3	Maladjustment of receiver
I.2.4	Low mains voltage

Classification code	Description of the source
I.3	Receiver characteristics
I.3.1	Second (image) channel response
I.3.2	Other spurious responses
I.3.3	Intermodulation
I.3.4	Inadequate receiver immunity
I.4	Weak or faulty signals
I.4.1	Outside service area
I.4.2	Shadow area
I.4.3	Multipath reception
I.4.3.1	Power lines
I.4.3.2	Other
I.5	Atmospheric disturbances
I.6	Unidentified sources of interference
I.7	Interference not observed
J	Information technology equipment
J.1	Data processing equipment
J.1.1	Large DPE in computer rooms
J.1.2	Smaller plugable DPE not in dedicated rooms
J.1.3	Home computers and home video games
J.2	Local area network
J.3	Commercial video games
J.4	Telephone exchanges and other digital telecommunication equipment

2.2 Report 48: Statistical considerations in the determination of limits of radio interference
(identical with the text taken from CISPR 8B)

2.2.1 Introduction

Compliance of mass-produced appliances with radio interference limits should be based on the application of statistical techniques that have to ensure the consumer with an 80 % degree of confidence that 80 % of the appliances of a type being investigated are below the specified radio interference limit. This so-called 80 %/80 % rule protects the consumer from appliances with too high a radio interference level, but it says hardly anything about the probability that a batch of appliances from which the sample has been taken will be accepted. This acceptance probability is very important to the manufacturer. The manufacturer knows only that if 20 % of the items of the batch are above the relevant limit, the acceptance probability is 20 % and knowledge is necessary about the dependence of the acceptance probability on the sample size and the fraction items of the batch that are above the relevant limit. The curves representing the acceptance probability versus fraction items above the limit and the sample size as a parameter, are called the operating characteristic curves. These curves can be calculated using either the non-central *t*-distribution (sampling by variables) or the binomial distribution (sampling by attributes).

The Poisson distribution cannot be used since the fraction appliances above the limit should be very small (<1 %) and the sample size large (more than 20 items). Besides sampling of batches, it is also possible to ensure conformity of the production by means of control chart techniques. These methods provide a continuous recording of the wanted information – for example, the radio interference level of the appliances being produced.

2.2.2 Tests based on the non-central *t*-distribution (sampling by variables)

The following condition must be fulfilled:

$$\overline{X} + k\,S_n \leq L$$

and has to ensure, with an 80 % degree of confidence, that 80 % of the appliances produced on a large scale are below a specified radio interference limit L.

Meaning of the symbols used in this expression:

$\overline{X}$ = mean value of the interference level of the sample with size n of the appliances to be tested; $\overline{X}$ is known;

S_n = standard deviation of the interference level of the sample with size n of the appliances to be tested; S_n is known;

$$\overline{X} = \frac{1}{n}\sum_{i=1}^{n} X_i \qquad\qquad S_n = \sqrt{\frac{\sum\left(X_i - \overline{X}\right)^2}{n-1}}$$

k = constant to be determined in such a way that the above-stated rule is satisfied;

L = the permissible radio interference limit; L is an upper limit.

2.2.2.1 Determination of the constant k

It is assumed that the production being investigated has a normal distribution with the following parameters:

μ = mean value of the radio interference level of all appliances; μ is unknown;

σ = standard deviation of the radio interference level of all appliances; σ is unknown.

Assume: p fraction that is above the limit L (fraction defective) and $(1 - p)$ fraction of the lot below the specified limit L.

Define a constant K_p:

$$p = \int_{K_p}^{\infty} \frac{1}{\sqrt{2\pi}} e^{-\frac{y^2}{2}} dy$$

in which $f(y) = \frac{1}{\sqrt{2\pi}} e^{-\frac{y^2}{2}}$ is the standardized normal density function.

K_p can be determined from appropriate tables of the normal distribution function.

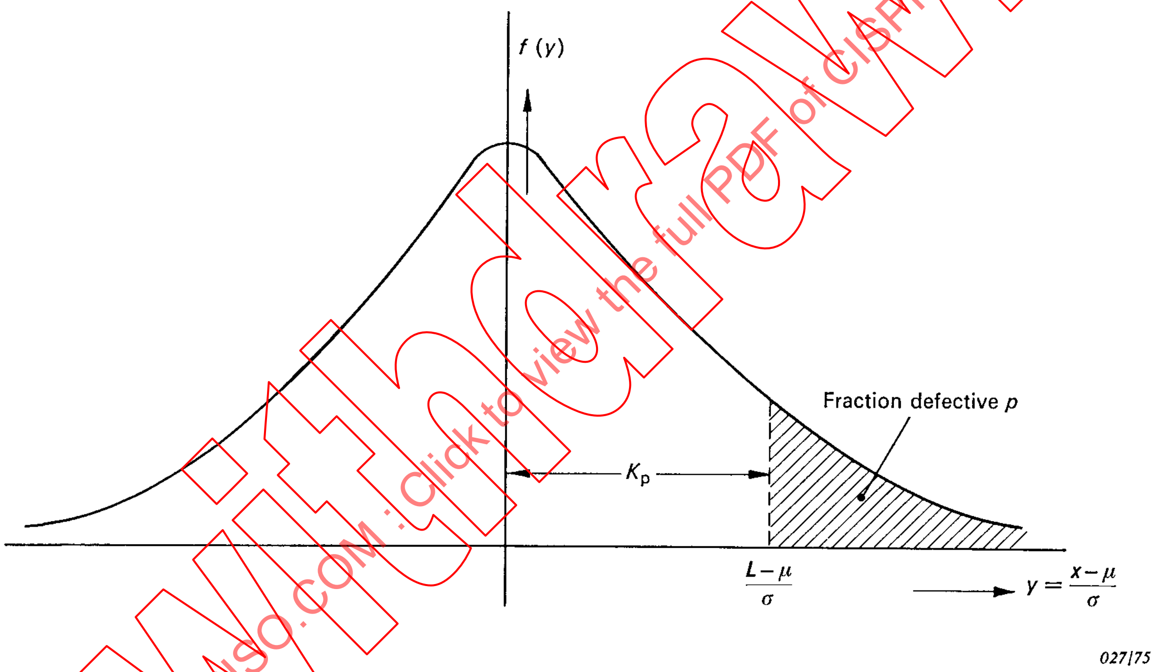

From the definition of K_p as well as the figure drawn above it follows that:

$$L = \mu + K_p\sigma \qquad K_p > 0$$

since L is an upper limit.

According to the CISPR, p = 0,2, then K_p = 0,84. The test instruction can now be read as follows:

$$p\left(\overline{X} + \mathrm{k}S_n \geq L \,/\, L = \mu + K_p\sigma\right) = 1 - \alpha$$

The probability α of a batch with a fraction defective p being accepted gives the *consumer's risk.*

For CISPR, α = 0,2 ($1 - \alpha$ = 0,8 → 80 %) and K_p = 0,84.

To determine the constant k, the expression should be rewritten as follows:

$$p\left(\overline{X} + \mathrm{k}S_{\mathrm{n}} \geq L \,/\, L = \mu + K_{\mathrm{p}}\sigma\right) = 1 - \alpha$$

$$= p\left(\frac{\overline{X} - \mu}{\sigma/\sqrt{n}} - \frac{L - \mu}{\sigma/\sqrt{n}} \geq -\frac{\mathrm{k}S_{\mathrm{n}}}{\sigma/\sqrt{n}} \Big/ L = \mu + K_{\mathrm{p}}\sigma\right)$$

$$= p\left(\frac{-\dfrac{\overline{X} - \mu}{\sigma/\sqrt{n}} + \dfrac{L - \mu}{\sigma/\sqrt{n}}}{S_{\mathrm{n}}/\sigma} \leq \mathrm{k}\sqrt{n} \Big/ L = \mu + K_{\mathrm{p}}\sigma\right)$$

By definition:

$$t_{\mathrm{n.c.}} = \frac{-\dfrac{\overline{X} - \mu}{\sigma/\sqrt{n}} + \dfrac{L - \mu}{\sigma/\sqrt{n}}}{S_{\mathrm{n}}/\sigma}$$

$t_{\mathrm{n.c.}}$ is a non-central *t*-distribution with non-centrality parameter

$$(L - \mu)/\left(\sigma/\sqrt{n}\right) = K_{\mathrm{p}}\sqrt{n}$$

and (n – 1) degrees of freedom.

The non-centrality parameter follows from the condition that not more than a fraction p of the lot being investigated is above the permissible limit.

$$p\left(t_{\mathrm{n.c.}} \leq \mathrm{k}\sqrt{n}\right) = 1 - \alpha$$

$$p\left(\frac{t_{\mathrm{n.c.}}}{\sqrt{n-1}} \leq \mathrm{k}\sqrt{\frac{n}{n-1}}\right) = 1 - \alpha$$

This probability function has been tabulated in [1] and [2]. Some figures are given below.

With α = 0,2, p = 0,1 (1 – α = 80 %, 1 – p = 80 %), the following values for k will be obtained for different sample sizes:

n	4	5	6	7	8	9	10	11	12
k	1,68	1,51	1,42	1,35	1,30	1,27	1,24	1,21	1,20

2.2.2.2 Determination of the sample size *n*

The producer wants to know the probability of the appliances being accepted and has to know:

$$p\left(\overline{X} + \mathrm{k}S_{\mathrm{n}} \leq L \,/\, L = \mu + K_{\mathrm{p}}\sigma\right)$$

By definition, this expression is equal to $\beta(p)$, the acceptance probability. The probability $1 - \beta(p)$ of a batch with a fraction defective p being rejected gives the *producer's risk*.

This can be rewritten as follows:

$$p\left(\frac{t_{\text{n.c.}}}{\sqrt{n-1}} \geq \text{k}\sqrt{\frac{n}{n-1}}\right) = \beta(p)$$

For a lot with the same fraction defective p as in clause 1, $\beta(p)$ equals α. With $p = 0{,}2$, $\alpha = 0{,}2$ (CISPR values) $\beta(0{,}2)$ is 0,2. From the producer's point of view, $\beta(p)$ should be maximized by improving the production (a smaller percentage of defective) since $\beta(p)$ depends on the defective fraction.

Generally the manufacturer needs an acceptance probability as high as 95 %. The function representing the dependence of the acceptable probability $\beta(p)$ on the fraction defective p is called the operating characteristic if the test and $1 - \beta(p)$ the power curve of the test. The mathematical representation for the O.C. curve:

$$\beta(p) = p\left(\frac{t_{\text{n.c.}}}{\sqrt{n-1}} \geq \text{k}\sqrt{\frac{n}{n-1}}\right)$$

for fixed n.

In Graph 1, a few curves are given for $\alpha = 0{,}2$. From these curves it can be seen that in order to ensure the same acceptance probability $\beta(p)$, the percentage of defectives will increase with the sample size. The so-called discriminatory power of the operating characteristic curve increases as the sample size increases and is ideal if n equals the total number of appliances to be approved.

2.2.2.3 Example (see Graph 1)

A batch of appliances has to be checked according to the 80 %/80 % rule with a sample size $n = 6$, we have k = 1,42. The consumer has an 80 % degree of confidence that 80 % of the batch lies below the limit.

The acceptance probability $\beta(p)$ is 20 % at $p = 0{,}2$ (80 % below the limit). To obtain a greater acceptance probability, the percentage defective p should be decreased. At $p = 0{,}035$ (96,5 % below the limit), the acceptance probability is 80 %. From each 10 samples consisting of six units taken from lots with $p = 0{,}035$, eight samples will on average yield a positive result. At $p = 0{,}009$ (99,1 % below the limit), the acceptance probability is 95 %. In the latter case, the manufacturer has to apply a μ and σ which fulfil the expression $\mu + 2{,}4\,\sigma \leq L$.

2.2.3 Tests based on the binomial distribution (sampling by attributes)

The number of defective units c that occur in a sample of size n has to ensure with an 80 % degree of confidence that 80 % of the appliances produced on a large scale are below a specified radio interference limit L. An item has to be considered defective as soon as its radio interference level is above the specified value L.

2.2.3.1 Determination of constant *c*

The occurrence of defective units by sampling a batch of appliances should satisfy the requirement that the occurrences are statistically independent and not more than one occurrence takes place at the same moment.

The binomial distribution is characterized by the fraction defective *p* of the batch of appliances being tested and the sample size *n*.

The probability that a sample of size *n* has exactly *c* defective items is given by:

$$p(x = c) = \binom{n}{c} p^{c}(1 - p)^{n-c} \quad n,\ c \text{ integers}$$

and that this sample contains *c* defective items or less by:

$$p(x \le c) = \sum_{x=0}^{c} \binom{n}{x} p^{x}(1 - p)^{n-x} \quad n,\ x,\ c \text{ integers}$$

$p\ (x \le c)$ represents the distribution function.

The probability that a sample with size *n* contains more than *c* defective items should be $(1 - \alpha)$ if the batch of appliances being tested has the maximum allowed fraction defective, hence:

$$p(x \le c\ /\ p) = 1 - \alpha$$

$$p(x \le c\ /\ p) = \sum_{x=0}^{c} \binom{n}{x} p^{x}(1 - p)^{n-x} = \alpha$$

According to the CISPR requirements: $\alpha = 0{,}2$ and $p = 0{,}2$. The corresponding *c* and *n* values are given in the left-hand table. The right-hand table represents the values for *c* and *n* if $\alpha = 0{,}05$ and $p = 0{,}2$. *c* represents the allowed number of defective items and *n* the sample size.

c	n
0	7
1	14
2	20
3	26
4	32
5	38
for a consumer's risk of 20 %	

c	n
0	13
1	22
2	29
3	36
4	43
5	50
for a consumer's risk of 5 %	

To have an 80 % degree of confidence that 80 % of the appliances are below the limit *c* and *n* should correspond with the values listed in the left-hand table.

2.2.3.2 Determination of sample size *n*

Analogue to 2.2, the acceptance probability follows from:

$$p(x \le c\ /\ p) = \beta(p)$$

If $p = 0{,}2$ then $\beta(0{,}2) = \alpha = 0{,}2$. The probability $1 - \beta(0{,}2)$ of the batch of appliances being rejected is 0,8.

The operating characteristic curve is given by

$$\beta(p) = \sum_{x=0}^{c} \binom{n}{x} p^{x} (1-p)^{n-x}$$

Curves have been drawn in graph 2.

2.2.3.3 Control charts

The use of control charts (3) provides information about the influence of the production process on the values to be statistically controlled and indicates the deviations from the original values. In this way, an insight can be gained into the performance of the production process.

Generally the sample average $\overline{X}$ and the sample standard deviation S_n give a good estimation of the quality characteristics to be studied. For mass-produced appliances, a sufficient number of samples can be taken to ensure conformity of $\overline{X}$ and S_n with the required mean value μ and standard deviation σ. The confidence intervals for various fractions of the production may be predicted from these values.

Control chart techniques can easily be applied in such a way that the consumer has the required 80 % confidence that 80 % of the production is below the permissible limit, whereas at the same time the use of small samples is avoided.

2.2.4 Bibliography

[1] *Tables of the non-central t-distribution*, Resnikoff, G.J., and Lieberman, G.J., Stanford University, California, 1957.

[2] CISPR/WG 8 (Groenveld/Neth.)1, March 1972.

[3] *Statistics and Experimental Design I*, pp 298-348, Johnson, N.L., and Leone, F.C., Wiley and Sons, New York, 1964.

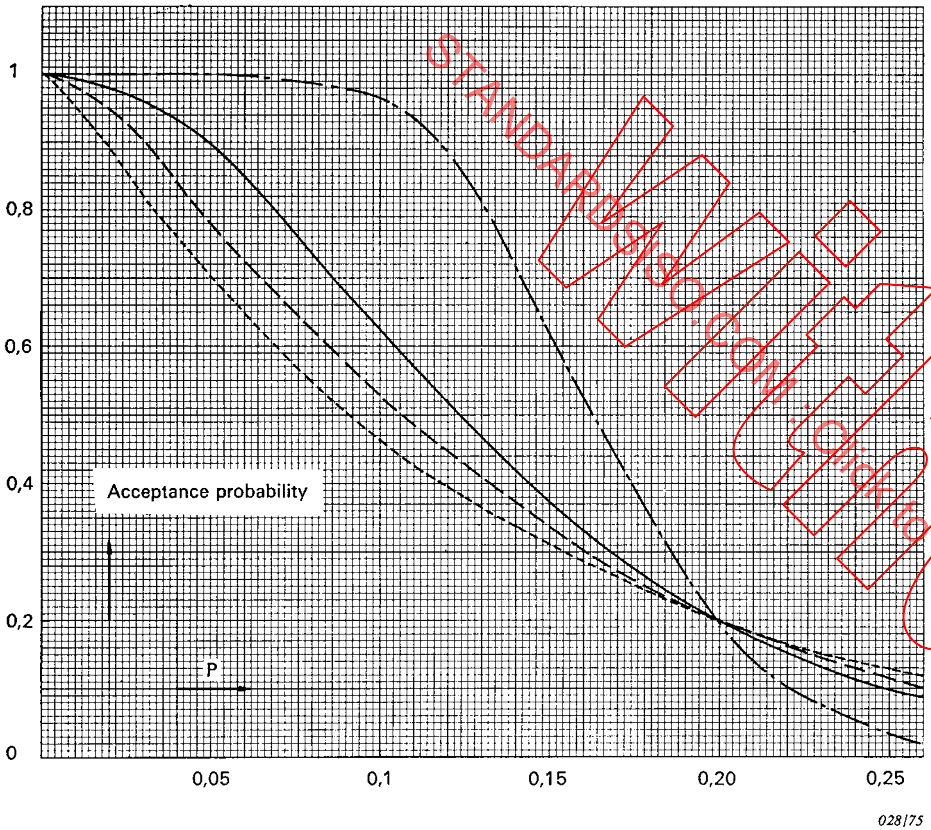

Graph 1

Operating characteristic curves for non-central *t*-distribution

-------------------	$n = 6$; $k = 1{,}42$
— — — — — —	$n = 8$; $k = 1{,}30$
————————	$n = 12$; $k = 1{,}20$
—·—·—·—	$n = 51$; $k = 0{,}99$

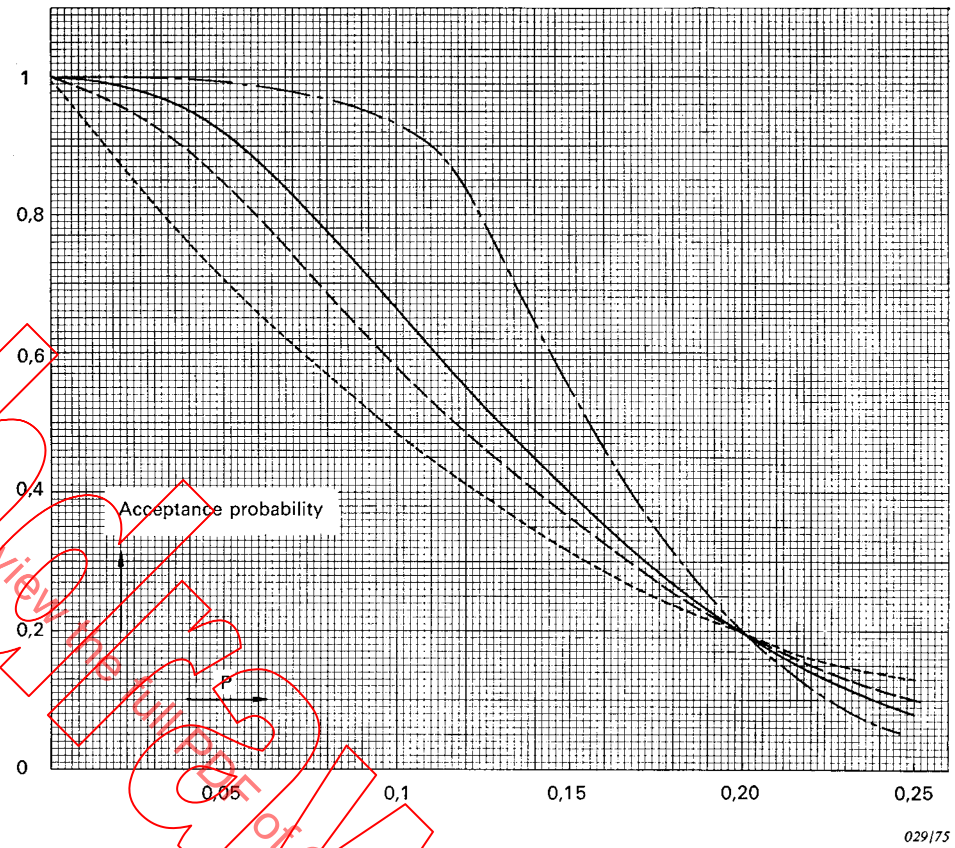

Graph 2

Operating characteristic curves for binomial distribution

-------------------	$n = 7$; $k = 0$
— — — — — —	$n = 14$; $k = 1$
————————	$n = 20$; $k = 2$
—·—·—·—	$n = 49$; $k = 7$

2.3 Recommendation 46/2: Significance of a CISPR limit (this recommendation replaces Recommendation 46/1, contained in CISPR 7B)

The CISPR,

CONSIDERING

a) that the abatement of interference aims that the majority of the appliances to be approved shall not cause interference;

b) that the CISPR limits should be suitable for the purpose of type approval of mass-produced appliances as well as approval of single-produced appliances;

c) that to ensure compliance of mass-produced appliances with the CISPR limits, statistical techniques have to be applied;

d) that it is important for international trade that the limits shall be interpreted in the same way in every country;

e) that the National Committees of the IEC which collaborate in the work of the CISPR should seek to secure the agreement of the competent authorities in their countries,

RECOMMENDS

that the following interpretation of CISPR limits and of methods of statistical sampling for compliance of mass-produced appliances with these limits should be adopted:

1 a CISPR limit is a limit which is recommended to National Authorities for incorporation in national standards, relevant legal regulations and official specifications. It is also recommended that international organizations use these limits;

2 the significance of the limits for type-approved appliances shall be that, on a statistical basis, at least 80 % of the mass-produced appliances comply with the limits with at least 80 % confidence;

3 type tests can be made;

3.1 on a sample of appliances of the type with statistical evaluation in accordance with clause 5 below;

3.2 for simplicity, on one item only (see clause 4);

4 subsequent tests from time to time on items are taken at random from the production are necessary especially in 3.2 above;

in the case of controversy involving the possible withdrawal of a type approval, withdrawal shall be considered only after tests on an adequate sample in accordance with 3.1 above;

5 that statistically assessed compliance with limits shall be made according to one of the two tests described below or to some other test which ensures compliance with the requirements of clause 2;

5.1 test based on the non-central *t*-distribution. This test should be performed on sample of not less than five items of the type, but if in exceptional circumstances five items are not available, then a sample of three shall be used. Compliance is judged from the following relationship:

$$\bar{x}_n + kS_n \leq L$$

where

$\bar{x}_n$ = arithmetic mean value of the levels of *n* items in the sample;

$$S_n^2 = \sum \left(x - \bar{x}_n \right)^2 \Big/ (n-1);$$

x = level of individual item;

k = the factor derived from tables of the non-central t-distribution with 80 % confidence that 80 % of the type is below the limit; the value of k depends on the sample size n and is stated below:

L = the permissible limit

the quantities x, $\bar{x}_n$, S_n and L are expressed logarithmically (dB(μV), dB(μV/m) or dB(pW));

n	3	4	5	6	7	8	9	10	11	12
k	2,04	1,69	1,52	1,42	1,35	1,30	1,27	1,24	1,21	1,20

5.2 test based on the binomial distribution. This test should be performed on a sample of not less than seven items. Compliance is judged from the condition that the number of appliances with an interference level above the permissible limit may not exceed c in a sample of size n;

n	7	14	20	26	32
c	0	1	2	3	4

5.3 should the test on the sample result in non-compliance with the requirements in 5.1 or 5.2, then a second sample may be tested and the results combined with those from the first sample and compliance checked for the larger sample.

6 Immunity tests

6.1 Application of the CISPR 80 %/80 % rule to immunity tests

In the assessment of the immunity of appliances and equipment in large-scale production, consideration should be given to the specification of the statistical method to be used in the CISPR sampling scheme. Two methods have been standardized: one using the binomial distribution and the other using the non-central t-distribution.

The binomial distribution method is essentially sampling by attributes. Hence, this method should be used in an immunity test in which the immunity level cannot be determined, with the result that it is only possible to verify whether an appliance or equipment complies with the immunity limit or not, i.e. only a pass or fail test at a specified immunity level is possible.

The non-central t-distribution method is essentially sampling by variables. Hence, this method is suitable for an immunity test in which the immunity level or the level of a signal that is a measure of the degradation of operation, can be determined. The latter level shall be expressed in logarithmic units before applying the non-central t-distribution method.

6.2 Application guidelines

Subclause 6.1 only gives conditions related to the choice of statistical test method to be used in the assessment of the immunity of appliances and equipment in large-scale production after it has been decided by the relevant Product Committee that a statistical evaluation is needed. A Product Committee may also decide that a type-test alone is adequate.

In the formulation of 6.1, use has been made of the IEC definitions of immunity level, immunity limit and degradation, which read

– the *immunity level* is the maximum level of a given electromagnetic disturbance, incident in a specified way on a particular device, equipment or system, at which no degradation of operation occurs;

– the *immunity limit* is the minimum required immunity level;

– *degradation* is an undesired departure in the operational performance of any device, equipment or system from its intended performance.

6.2.1 Sampling by attributes

When testing the immunity of an equipment under test (EUT), the combination of type of disturbance signal and type of susceptible part in the EUT might result in damage to the EUT if the immunity level is exceeded. In such a case, only an immunity test on Pass/Fail or (Go/No Go) basis will be possible, i.e. a test which verifies only whether the EUT complies or does not comply with the immunity limit. Consequently, only two test results are possible: the EUT passes or the EUT fails. The properties "pass" and "fail" are attributes of the EUT, so the method based on the binomial distribution has to be used.

An immunity test on a Pass/Fail basis is not necessarily associated with damage to the EUT. If the test is to be carried out with a fixed-level electromagnetic disturbance, it may also be possible to use only the Pass/Fail criterion. Also in this case the sampling method based on the binomial distribution has to be used.

An example of an immunity test on Pass/Fail basis in view of the possibility of damaging the EUT is the testing of telecommunication equipment for immunity to transients caused by lightning. An example of such a test in view of the fixed-level disturbance is the electroacoustic discharge test on (digital) information technology equipment.

6.2.2 Sampling by variables

If the EUT and the chosen immunity test allow the determination of the immunity level or the level of a signal that is a measure of the degradation of operation, these levels will be variables and, hence, a Product Committee may decide to opt for sampling by variables. In that case, the sampling method based on the non-central *t*-distribution has to be used.

Note the above formulation "may decide", as a Product Committee can always decide to opt for a test on a Pass/Fail basis. In addition, note that if the EUT is sufficiently immune, it might not be possible to determine the levels mentioned. This does not exclude, however, the possibility of sampling by variables. Such a situation is completely comparable with the situation in an emission test when the emission level is lower than the noise level of the CISPR receiver.

The determination of the immunity level in an immunity test is, generally speaking, not very practical. It always causes over-exposure of the EUT to the applied disturbance signal, and may easily lead to unforeseen effects during immunity testing. Nevertheless, there is no need to exclude this determination beforehand.

A signal which is a measure of the degradation of operation of the EUT may be available for sampling by variables; for example, the demodulated signal when testing several samples of EUT, say an audio equipment, for their immunity to amplitude-modulated RF signals of constant level and frequency. The level of the demodulated signal is then a measure of the degradation of the EUT. Another example is the bit-error rate when performing immunity tests on digital communication equipment.

2.4 Report 59: An analytical assessment of statistical parameters of radio disturbance in the case of an incompletely defined sample

CISPR Recommendation 46/2 specifies the requirements for the statistical assessment of series-produced equipment. The assessment is based on the non-central *t*-distribution and it requires that the actual levels of the radio *disturbance* generated by each equipment in a sample is measured. The assessment of acceptability is then made during the mean and the standard deviation of the radio *disturbance* levels measured.

In a number of cases, it may not be possible to measure the levels of radio *disturbance* generated by all the *units of* the equipment in the sample because of insufficient sensitivity of the testing apparatus used. In such cases the available distribution of the values of radio *disturbance* levels (expressed in decibels) is truncated from below, giving a one-sided and incomplete determination of the distribution.

Figure 1 shows the probability density function $\varphi(\gamma,\gamma_0)$ of a normal distribution of radio *disturbance* values truncated from below.

Figure 2 shows the function $\Phi(\gamma,\gamma_0)$, which is an alternative illustration of the same truncated distribution.

This report presents the analytical method of assessment of mathematical expectation and standard deviation of radio *disturbance* values distributed according to a normal law, on the basis of the known parameters of truncated distribution and the degree of truncation.

Assume that for the determination of the statistical parameters of the distribution of radio *disturbance* values one takes a sample of *n units* from the parent population which is a normal distribution $N(\mu x;\sigma)$. In this sample $n_0 < n$ *units* have a radio disturbance level $X < X_L$, where X_L is the limit of sensitivity of the measuring apparatus, this limit being the point of truncation. Hence, in a sample of the size *n* there are only $n - n_0$ *units* with radio *disturbance* values which are greater than X_L, and for these units only can the radio *disturbance* levels be measured. It is possible to consider $n - n_0$ of radio *disturbance* values as the measurements from truncated distribution with the truncation degree $\Phi(\gamma_0)$. The ratio n_0/n is the assessment of the degree or truncation $\Phi(\gamma_0)$.

The average $\overline{X}$ and the standard deviation *S* of the measured radio d*isturbance* values are an estimation of the parameters μ_x and σ in the parent population of the equipment. $\overline{X}$ and *S* are determined from the expressions:

$$\overline{X} = \overline{X}_y - \frac{S_y}{\left(\frac{1-\Phi(\gamma_0)}{\varphi(\gamma_0)}\left(\frac{1-\Phi(\gamma_0)}{\varphi(\gamma_0)} + \gamma_0\right) - 1\right)^{1/2}} \qquad (1)$$

$$S = \frac{S_y}{\left(\frac{\varphi(\gamma_0)}{1-\Phi(\gamma_0)}\left(\gamma_0 - \frac{\varphi(\gamma_0)}{1-\Phi(\gamma_0)}\right) + 1\right)^{1/2}} \qquad (2)$$

where

$\gamma_0 = (X_L - \mu)/\sigma$ is a specified truncation point;

$\Phi(\gamma_0)$ is a value of the normal distribution function

$$\Phi(\gamma) = \frac{1}{\sqrt{2\pi}} \int_{-\infty}^{\gamma} e^{-\frac{x^2}{2}}\, dx$$

$\varphi(\gamma_0)$ is a value of a probability density function of a normal distribution

$$\varphi(\gamma) = \frac{1}{\sqrt{2\pi}} e^{-\frac{\gamma^2}{2}}$$

The values of the sampling parameters $\overline{X}_y$ and S_y of the truncated distribution included in the formulas (1) and (2) are determined from the following expressions:

$$\overline{X}_y = \frac{1}{n - n_0} \sum_{i=1}^{n-n_0} X_i \qquad (3)$$

$$S_y = \left(\frac{1}{n - n_0 - 1} \sum_{i=1}^{n-n_0} \left(X - \overline{X}_y \right)^2 \right)^{1/2} \qquad (4)$$

The mathematical expectation and standard deviation of a radio disturbance value in the parent population of equipment, which has normal distribution, are determined from the parameters of an incompletely determined sample in the following succession:

a) the radio disturbance values produced by all the units of the sample of the size n are measured;

b) the degree of truncation $\Phi(\gamma_0) = \frac{n_0}{n}$ is determined;

c) the values of the specified point of truncation γ_0 are determined from the tables of a function of the normal distribution on the basis of the known values of $\Phi(\gamma_0)$;

d) from the tables of a probability density function of normal distribution the values of $\varphi(\gamma_0)$ are found;

e) the values of the statistical parameters of the truncated distribution of measured disturbance produced by the articles of a sample of the size $n - n_0$ are determined from formulae (3) and (4);

f) the values of the statistical parameters of the complete distribution of disturbance levels from the sample of equipment of size n are determined from formulae (1) and (2).

NOTE An example calculation is given in the appendix.

The confidence interval of the parameter $\overline{X}$ with the confidence $1 - \alpha$ is determined by the expression:

$$\overline{X} - U_p S \sqrt{\frac{\mu_x \gamma_0}{n}} < \mu_x < \overline{X} + U_p S \sqrt{\frac{\mu_x \gamma_0}{n}}$$

where

$U_p = U_{1-\frac{\alpha}{2}}$ is a quartile of distribution N(0.1);

$\mu_x(\gamma_0)$ is a function of truncation degree determined from table 1.

Table 1 (relative to Recommendation 46/2)

γ_0	–3,0	–2,5	–2,1	–2,0	–1,9	–1,8	–1,7	–1,6	–1,5	–1,4
$\mu_x(\gamma_0)$	1,000	1,001	1,002	1,003	1,004	1,005	1,006	1,009	1,011	1,015
γ_0	–1,3	–1,2	–1,1	–1,0	–0,9	–0,8	–0,7	–0,6	–0,5	–0,4
$\mu_x(\gamma_0)$	1,019	1,025	1,032	1,042	1,054	1,069	1,089	1,114	1,147	1,189
γ_0	–0,3	–0,2	–0,1	0	0,1	0,2	0,3	0,4	0,5	0,6
$\mu_x(\gamma_0)$	1,243	1,312	1,401	1,517	1,667	1,863	2,118	2,453	2,893	3,473
γ_0	0,7	0,8	0,9	1,0	1,1	1,2	1,3	1,4	1,5	1,6
$\mu_x(\gamma_0)$	4,241	5,261	6,623	8,448	10,90	14,22	18,73	24,89	33,34	44,99
γ_0	1,7	1,8	1,9	2,0						
$\mu_x(\gamma_0)$	61,13	83,64	115,2	159,7						

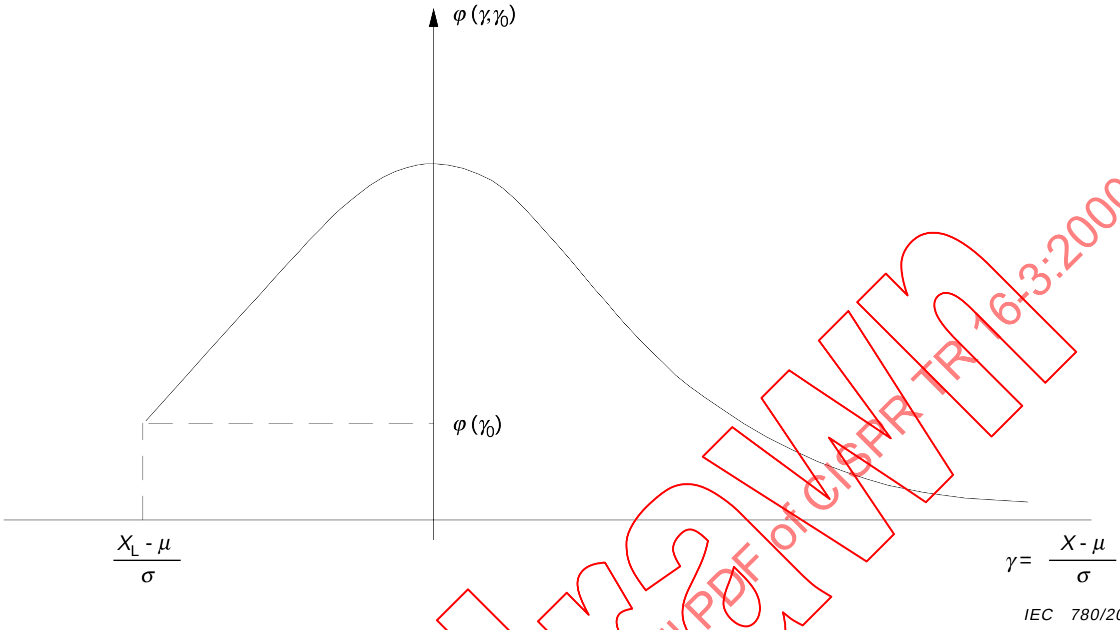

Figure 1 – The probability density function $\varphi(\gamma;\gamma_0)$

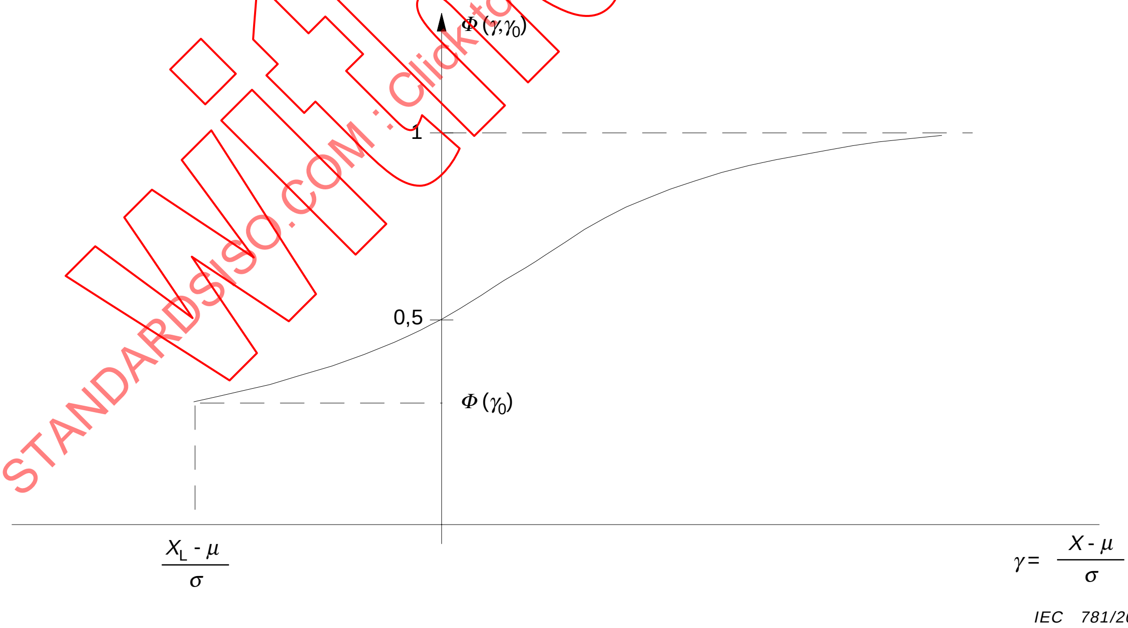

Figure 2 – The truncated distribution function $\Phi(\gamma;\gamma_0)$

Appendix to Report 59

A numerical example is given of the calculation of the average value $\overline{X}$ and the standard deviation S of the radio *disturbance* values in the case of an incompletely determined sample. In this example calculation, the sample size is six *units of equipment* (n = 6) The value of radio *disturbance* from two units (n_0 = 2) is below the limit of sensitivity of the measuring apparatus ($X < X_L$).

As outlined in the main text the calculation is performed as follows:

a) the radio *disturbance* values produced by the six units of equipment of the sample are measured. These are presented in the table below.

Unit of equipment number	1	2	3	4	5	6
The value of radio disturbance dB	19	23	20	21	$X < X_L$	$X < X_L$

b) The degree of truncation is:

$$\Phi(\gamma_0) = \frac{n_0}{n} = \frac{2}{6} = 0{,}333$$

c) Using the known value of $\Phi(\gamma_0) = 0{,}333$, the value of the normalized point of truncation is determined from the tables of the normal-distribution functions The value is: $\gamma_0 = -0{,}43$

d) From the tables of the probability density function of a normal distribution

$$\varphi(\gamma) = \frac{1}{\sqrt{2\pi}} e^{-\frac{\gamma^2}{2}}$$

$\varphi(\gamma_0) = 0{,}364$ is found.

e) From the formulae (3) and (4) assessments of the values of the statistical parameters of the truncated distribution of *disturbance* are made

$$\overline{X}_y = \frac{1}{n - n_0} \sum_{i=1}^{n-n_0} X_i = 20{,}8 \text{ dB}$$

$$S_y = \left(\frac{1}{n - n_0 - 1} \sum_{i=1}^{n-n_0} \left(X_i - \overline{X}_y \right)^2 \right)^{1/2} = 1{,}7 \text{ dB}$$

f) From the formulae (1) and (2) assessments of the values of the statistical parameters of the complete distribution of the interference values are made.

$$\overline{X} = \overline{X}_y - \frac{S_y}{\left(\frac{1 - \Phi(\gamma_0)}{\varphi(\gamma_0)} \left(\frac{1 - \Phi(\gamma_0)}{\varphi(\gamma_0)} + \gamma_0 \right) - 1 \right)^{1/2}}$$

$$\overline{X} = 20{,}8 - \frac{1{,}7}{\left(\frac{1 - 0{,}333}{0{,}364} \left(\frac{1 - 0{,}333}{0{,}364} - 0{,}43 \right) - 1 \right)^{1/2}}$$

$$\overline{X} = 19{,}4 \text{ dB}$$

$$S = \frac{S_y}{\left(1 + \frac{\varphi(\gamma_0)}{1 - \Phi(\gamma_0)}\left(\gamma_0 - \frac{\varphi(\gamma_0)}{1 - \Phi(\gamma_0)}\right) + 1\right)^{1/2}}$$

$$S = \frac{1{,}7}{\left(1 + \frac{0{,}364}{1 - 0{,}333}\left(-0{,}43 - \frac{0{,}364}{1 - 0{,}333}\right) + 1\right)^{1/2}}$$

S = 2,5 dB

The sample of equipment is then assessed for compliance with the limits as required in the application of non-central *t*-distribution using the formula

$$\overline{X} + kS < L$$

In this particular example, the requirement is 19,4 + 1,42 · 2,5 < *L*.

3 A model for the calculation of limits

3.1 Introduction

A harmonized method of calculation is an important pre-condition for the efficient discussion of CISPR limits by National Committees and the adoption of CISPR Recommendations.

3.1.1 Generation of EM disturbances

CISPR Recommendations are developed for protection of radio communications and often several types of radio networks are to be protected by a single emission limit.

Most electrotechnical equipment have the potential to interfere with radio communications. Coupling from the source of electromagnetic disturbance to the radio communications installation may be by radiation, induction, conduction, or a combination of these mechanisms. Control of the pollution of the radio spectrum is accomplished by limiting at the source the levels of appropriate components of the electromagnetic disturbances (voltage, current, field strength, etc.). The choice of the appropriate component is determined by the mechanism of coupling, the effect of the disturbance on radio communications installations and the means of measurement available.

3.1.2 Immunity from EM disturbances

Most electronic equipment has the potential to malfunction as the result of being subjected to EM disturbances.

Protection of equipment is accomplished by hardening the appropriate disturbance entry route. The choice is determined by the mechanism of coupling, the effect of the disturbance on the electronic equipment and the means of measurement available.

3.1.3 Planning a radio service

Before planning radio communication service, it is necessary to decide upon the reliability of obtaining a predetermined quality of reception. This condition can be expressed in terms of the probability of the actual signal-to-interference ratio at the input of a receiver being greater than the minimum permissible signal-to-interference ratio. That is:

$$P\left[R(\mu_R;\sigma_R) \geq R_P\right] = a$$

where

$P[\ ]$ is the probability function;

$R(\mu_R;\sigma_R)$ is the actual signal-to-interference ratio as a function of its mean value (μ_R) and standard deviation (σ_R);

R_p is the minimum permissible signal-to-interference ratio;

a is a specified value representing the reliability of communications.

This probability condition is the basis for the method of determining limits.

3.2 Probability of interference

In order to make recommendations to protect adequately the radio communications systems of interest to the ITU considerable attention is paid within CISPR to the probability of interference occurring. The following is an extract from ITU-R Report 829.

3.2.1 Derivation of probability of interference

The Radio Regulations, No. 160, defines interference as "the effect of unwanted energy due to one or a combination of emissions, radiations, or inductions upon reception in a radio communication system, manifested by any performance degradation, misinterpretation, or loss of information which could be extracted in the absence of such unwanted energy".

3.2.1.1 Probability of instantaneous interference

Let

A denote "The desired transmitter is transmitting";

B denote "The wanted signal is satisfactorily received in the absence of unwanted energy";

C denote "Another equipment is producing unwanted energy";

D denote "The wanted signal is satisfactorily received in the presence of the unwanted energy".

All of these statements refer to the same small-time period. Then, according to the definitions, interference means "A and B and C and D*", where D* is the negation or opposite of D: Let $P(x)$ denote the "probability of X" and $P(x|y)$ denote the "probability of x, given y". Then, the probability of interference during the small-time period is

$$P(\mathrm{I}) = P(\mathrm{A \text{ and } B \text{ and } C \text{ and } D^*}) \tag{3.1}$$

It can be shown that this can be expressed in terms of known or computable quantities:

$$P(\mathrm{I}) = [P(\mathrm{B}|\mathrm{A}) - P(\mathrm{D}|\mathrm{A \text{ and } C})]\, P(\mathrm{A \text{ and } C}) \tag{3.2}$$

It may be preferable to consider the probability of interference only during the time that the wanted transmitter is transmitting. This probability is:

$$P'(\mathrm{I}) = P(\mathrm{B \text{ and } C \text{ and } D^*}|\mathrm{A}) \tag{3.3}$$

which can be reduced to:

$$P'(\mathrm{I}) = [P(\mathrm{B}|\mathrm{A}) - P(\mathrm{D}|\mathrm{A \text{ and } C})]\, P(\mathrm{C}|\mathrm{A}) \tag{3.4}$$

3.2.1.2 Discussion of equations (3.2) and (3.4)

First, consider the difference between equation (3.2) and (3.4). The probability of interference can be interpreted as the fraction of time that interference exists. In equation (3.2), this fraction is the number of seconds of interference during a time period divided by the number of seconds of interference divided by the number of seconds the wanted transmitter is transmitting during the time period. This second fraction is larger than the first unless the wanted transmitter is on all the time. $P(\mathrm{B}|\mathrm{A})$ is just the probability that a wanted signal will be correctly received when there is no interference, often expressed as the probability that $S/N \geq R$ where S is the signal power, N is the noise power, and R is the signal-to-noise ratio required for satisfactory service. In some services, this probability is called the reliability, and is often computer when the system is designed. It can be computed if system parameters (for example, transmitter and receiver location, power, required S/N) are known using statistical data on transmission loss (for example, Recommendation 370) and statistical data on radio noise (for example, Reports 322 and 670).

Many systems, such as satellite or microwave relay point-to-point systems, are designed so that $P(\mathrm{B}|\mathrm{A}) \approx 1$. In other services, such as long-distance ionospheric point-to-point services, or mobile services near the edge of the coverage area, $P(\mathrm{B}|\mathrm{A})$ may be quite small. In this latter case, the probability of interference will not be small regardless of the other probabilities.

$P(\mathrm{D}|\mathrm{A}$ and $\mathrm{C})$ is the probability that the wanted signal will be correctly received even when the unwanted energy is present. It can be computed if there is sufficient information about the location, frequency, power, etc. of the source of unwanted energy. For examples, see the references in Report 656.

Notice that it has been assumed that $P(\mathrm{D}|\mathrm{A}$ and $\mathrm{C}) \leq P(\mathrm{B}|\mathrm{A})$; that is, if the signal can be received satisfactorily in the presence of unwanted energy, then it can surely be received satisfactorily in the absence of the unwanted energy. Thus $P(\mathrm{I})$ cannot be negative.

$P(\mathrm{A}$ and $\mathrm{C})$ is the probability that the wanted transmitter and the source of unwanted energy are on simultaneously. In some situations, the wanted transmitter and source of unwanted energy may be operated independently. For example, they may be on adjacent channels, or beyond a coordination distance. In this case, $P(\mathrm{A}$ and $\mathrm{C}) = P(\mathrm{A})P(\mathrm{C})$, where $P(\mathrm{A})$ is the fraction of time that the wanted transmitter is emitting, and $P(\mathrm{C})$ is the fraction of time that the unwanted source is on.

In other situations, the operation may be highly dependent. For example, the transmitters may be co-channel stations in a disciplined mobile service. In this case $P(\mathrm{A}$ and $\mathrm{C})$ is very small, but perhaps not zero, because a station can be located so that it causes interference even when it cannot hear the other transmitter.

The two transmitters might both operate continuously. For example, one might be part of a microwave point-to-point service, and the other a satellite sharing the same frequency band. In this case, $P(\mathrm{A}$ and $\mathrm{C}) = 1$, and the probability of interference depends entirely on the factor in square brackets in equation (3.2).

Similarly, $P(\mathrm{C}|\mathrm{A}) = P(\mathrm{C})$ if the transmitters operate independently. $P(\mathrm{C}|\mathrm{A})$ is very small if the two transmitters are co-channel stations in a disciplined land mobile service; and $P(\mathrm{C}|\mathrm{A}) = 1$ if the unwanted transmitter is on all the time.

In general, all the terms in equations (3.2) and (3.4) affect the probability of interference, although their relative importance is different in different services.

3.3 Circumstances of interferences

In this part, general criteria are laid down for establishing RFI limits. In this case, a distinction is made for areas where close coupling exists between noise sources and victim equipment and for areas with remote coupling.

3.3.1 Close coupling and remote coupling

Although an ill-defined borderline exists between areas of close and remote coupling these concepts are generally used in the following terms.

Close coupling refers to a short distance between noise source and receiving antenna (for example, 3-30 m) which is the case for residential sources interfering with broadcasting and land mobile receivers in residential areas. In general, frequencies up to 300 MHz are considered.

Remote coupling refers to longer distances, usually 30-300 m, which are normal between professional or semi-professional sources and receivers as in the case of individual areas. The relevant frequency spectrum is much broader: 10 kHz to 18 GHz.

For the statements given above, it follows that some similarity exists between closed coupling and near-field radiation conditions on the one hand and between remote coupling and far-field radiating conditions on the other hand. However, these concepts do not fully correspond since at frequencies below 1 MHz remote coupling may occur under near-field conditions whereas for frequencies above about 30 MHz close coupling may occur under far-field conditions. In the majority of the practical situations, however, the good correspondence between close/remote coupling and near/far-field conditions is useful in the evaluation of coupling aspects.

It should be noted that field strength measurements, which are normally used for evaluating remote coupling characteristics, are actually carried out under near-field conditions in the lower end of the frequency range.

Whereas close and remote coupling are generally used to describe a direct coupling path between noise source and receiving antenna by means of electric, magnetic or radiation fields, an additional coupling mode is conduction coupling. In this case, the noise signal is conducted by the mains network from the mains output of the source to the mains input of the receiver. Inside the receiver the noise signal is coupled from the mains terminals to sensitive circuits of the receiver.

Some well-known differences exist between near-field and far-field radiation characteristics, and therefore also for most close and remote coupling cases.

– Under far-field conditions with free-space propagation the relation between electric and magnetic components of the field is fixed and well defined, the relation under near-field conditions is completely undefined.
– Under far-field conditions the attenuation formula is

$$y = kd^{x} \tag{3.5}$$

where

y = attenuation factor;

d = distance;

x = propagation coefficient, which is 1 in free-space propagation and somewhat higher (1 to 1,5) for non-free-space propagation.

Under near-field conditions the propagation coefficient x is more complex and dependent on the magnetic or electric component with values between 2 and 3.

For this reason, it is much easier to develop a model for remote coupling conditions than for close coupling situations and for conduction coupling paths. Such a model is necessary to derive emission limits for a general interference environment.

3.3.2 Measuring methods

The measuring method is of major importance for the specification of an RFI limit. Several measuring methods are applied and a short survey is given in the following paragraphs. In all measurements, the measuring instrument is a selective RFI meter (CISPR receiver) as specified for the relevant frequency range.

3.3.2.1 Interference voltage at the mains terminals

In the lower frequency range up to about 30 MHz, the mains network may conduct any injected RF energy to nearby users connected to the mains and/or couple part of the RF energy to nearby antennas in the electric, magnetic or radiation mode. Electric or magnetic field coupling to nearby antennas in this frequency range, however, is in most cases of minor importance compared with conduction coupling through the mains network. Because of the RF output voltage conduction mainly coupling through the mains network, the RF output voltage at the mains terminals is used as a measure for the interfering potential of a source in this frequency range.

This RFI voltage at the mains terminals is measured by means of an artificial mains network which isolates the source from the mains at RF frequency and which furnishes a standardized RF load to the source. The artificial mains network generally recommended by CISPR is a 50 Ω/50 µHV-network which introduces a parallel impedance of 50 Ω/50 µH V-network between each mains terminal and reference ground.

Although not recommended by CISPR yet, the asymmetric current in the mains lead, measured by means of a current probe, might be used as a measure for the radiation capability of the source.

3.3.2.2 Interference voltage at the signal terminals

Imperfections of the symmetry in circuits carrying wanted symmetrical signals will produce unwanted asymmetric signals at the terminals. In asymmetric (coaxial) terminals unwanted external currents can be conducted in the screen because of imperfect screening. These asymmetric signals and external screen currents may couple energy by inductive or radiation fields to nearby or remote antennas.

The asymmetric voltages can be measured by means of an artificial loading network. In this case the use of a delta network instead of a V-network is preferred.

3.3.2.3 RFI power measurements with the absorbing clamp

The asymmetric RF current in a lead or on the outer surface of the screen of a screened cable will radiate energy to nearby or remote antennas depending on frequency, length and configuration of the connected cable. This is particularly important at VHF and UHF in which frequency ranges the external lead of the appliance has a length which is in the order of a half wavelength or longer.

The absorbing clamp is a device which gives measuring results in a good correspondence with the interference power that can be radiated from the external lead of the appliance.

The main part of an absorbing clamp is a ferrite cylinder clamped around the disturbance carrying lead which attenuates conducted asymmetric currents by absorption. At the input end of the cylinder a current probe is fixed.

The ferrite cylinder operates as an isolator for RFI signals between mains and noise source and offers a specified, resistive impedance to the lead at the position of the current probe. So the output voltage of the current probe is a measure for the RFI power entering the absorbing clamp.

The device is clamped around the lead under test and moved along the lead to a position of maximum output reading. This operation actually adjusts the determination between source impedance and clamp input impedance (maximizing the RFI output power) through the variable lead section between source and clamp.

Under this condition the RFI power conducted through the mains lead and measured by the absorbing clamp is a good measure for the disturbance potential. If the dimensions of the source are not small compared with wavelength, a larger part of the RFI energy will be radiated directly and the absorbing clamp measurement is less reliable.

Because broadband disturbance is, in general, of less importance at frequencies above 300 MHz the absorbing clamp was originally recommended for the measurement of small appliances in the frequency range 30 MHz to 300 MHz. There is, however, a tendency to use the absorbing clamp in the frequency range up to 1 000 MHz.

The use of the clamp is restricted at the lower part of the frequency region because of the poor absorbing characteristics of the ferrite material. It is therefore recommended for frequencies above 30 MHz.

3.3.2.4 Field-strength measurement

The unwanted field strength produced by RFI signals is likely to be the most straightforward criterion for the interference potential of an RFI source, because it is more directly comparable with the wanted field strength at the antenna of a radio receiver particularly for remote coupling analysis.

A source radiates RFI energy from its case or cabinet if a coupling path exists between internal noise source and external case or cabinet and if the dimensions of the case or cabinet are of the order of one wavelength. For practical reasons the electric component of the field is measured in the frequency range above 30 MHz (by means of dipole antennas) and the magnetic component of the field below 30 MHz (loop antennas).

Field-strength measurements have a number of practical drawbacks. The influence of surrounding reflections should be eliminated which is usually met by using an open test site. Such a test site introduces inaccuracies by the variable reflections from the operator and from the ground (influence of moisture and season) and by the interference of ambient transmitter fields. It also reduces the work time due to poor weather and other climatic conditions. These drawbacks can be partly eliminated by the use of anechoic rooms in the frequency range above 30 MHz.

Another drawback of field-strength measurements is the complex radiation diagram and its dependence on the test set-up which requires measurements in various directions and an accurately specified test set-up.

3.3.2.5 Radiation substitution measurements

In order to reduce the effect of surrounding reflections in field-strength measurements, the source under test is replaced by a radiator of specified characteristics and an adjustable output level (usually a dipole connected to a calibrated RF generator) to produce the same field strength under equal environmental conditions. The RFI of the appliance is expressed as the equivalent power radiated from the substitution radiator. This method is often used at frequencies above 1 GHz.

3.3.2.6 RFI power measurements with a reverberating chamber

The reverberating chamber method is essentially a radiation substitution method inside a screened cage and is used in the microwave frequency range. By using rotating reflection plates, the standing wave patterns inside the cage are continuously varied in such a way that the time averaged field strength is nearly independent of the position inside the cage. Therefore, the source under test and the substitution source need not be at exactly the same position and the calibration procedure for the radiated power is much simpler than in the normal substitution method.

3.3.2.7 Frequency considerations with respect to measuring methods

As indicated earlier, the radiation of a device and the conduction and radiation of connected cables, particularly the main cables, depend on the size of the device and of the cables compared with wavelength (frequency). The following table gives a general survey of the usefulness of various measuring methods with respect to the frequency bands (subdivided according to CISPR Recommendations). It should be noted that the frequency ranges are only for indication and the quoted valuation given for guidance.

Table 1 – Guidance survey of RFI measuring methods

Frequency MHz	Terminal voltage	Asymm. current	Absorbing clamp	Field strength	Subst. radiation	Reverb. chamber
0,01 – 0,15	+	+	–	0	–	–
0,15 – 30	+	+	–	0	–	–
30 – 300	–	0	+	+	0	–
300 – 1 000	–	0	0	+	+	–
Above 1 000	–	–	–	+	+	+

where

+ = to be recommended;

0 = usable;

– = not normally usable.

3.3.3 RFI signal waveforms and associated spectra

An important aspect is the RFI spectrum which is associated with the signal waveform. As most radio services use relatively narrow frequency channels the spectrum (frequency domain) is considered of major importance compared with the waveform (time domain). Therefore the following distinction is made.

Narrowband RFI effects occur when the disturbance signal occupies a bandwidth smaller than the radio channel of interest or the measuring receiver. The disturbance spectrum may consist of a single frequency produced by a sinewave oscillator of medium or high RF power (ISM equipment) or of low power (electronic circuits, receiver oscillators). The oscillator could be modulated by the mains frequency. Oscillator frequencies can be generated over the entire usable frequency spectrum. The effect of narrowband disturbance is considered by CISPR over the frequency range 10 kHz to 18 GHz.

– Narrowband RFI from a broadband spectrum – Pulse waveforms derived from a digital clock oscillator contain discrete harmonic frequencies in a wide frequency range (broadband spectrum) For fundamental (clock) frequencies appreciably higher than the bandwidth of the radio channel, not more than one separate spectral line can coincide with the radio channel and such a spectral line is considered as narrowband RFI.

– Continuous broadband RFI – Gaussian noise generated by gas discharge devices (lighting) produces continuously a flat spectrum during the operation of the device. Repetitive pulses produce a wide spectrum containing various discrete spectral lines. At repetition rates much lower than the radio channel bandwidth many spectral lines occur within the channel (broadband RFI), for example, pulse derived from the mains frequency (commutator motors, thyristor voltage regulators).

  The frequency curve of repetitive pulses decreases above the transition frequency (the reciprocal of the pulse width) at 20 dB or 40 dB per decade, dependent on the pulse shape. Continuous broadband interference is considered by CISPR over the frequency range 150 kHz to 300 MHz.

– Discontinuous broadband RFI – Switching operations by means of a hard contact (spark) generates short bursts of noise. Short-duration bursts of RFI cause less severe interference effects than long-duration bursts depending, however, on the average repetition rate of the bursts.

  For this reason CISPR allows a relaxation with respect to the limit of continuous interference for short bursts with a duration of less than 200 ms and with a repetition rate N of less than 30 clicks per minute. This relaxation factor equals 20 log 30/N. The frequency spectrum of such clicks is not essentially different from that of continuous broadband interference.

3.3.4 Characteristics of interfered radio services

The characteristics of the interfered radio services with respect to RFI are very important as well. The main radio services in residential areas which suffer from RFI are broadcasting and (land) mobile communication. AM sound broadcasting operates at frequencies below 30 MHz and FM (stereo) sound broadcasting between 64 MHz and 108 MHz. TV broadcasting uses various channels in the range between 50 MHz and 900 MHz, the picture signal being modulated in AM-VSB and the sound signal in either AM or FM depending on the TV standard in use. Broadcasting also takes place in the bands between 11 GHz and 13 GHz.

In residential areas with private receiving antennas the RFI radiation from noise sources and from mains cables is of major importance. Broadcast signals distributed through a cable system are less vulnerable because of the more suitable location which can be selected for the common receiving antenna, but if RFI is coupled to such an antenna the interference is distributed to all subscribers.

Satellite broadcast signals in the 12 GHz range are generally not disturbed by broadband sources because of the limited frequency spectrum of broadband sources. The risk mainly depends upon the frequencies chosen for the first intermediate frequency band at the receiver.

The annoyance to the broadcast signal depends on the RFI waveform. Narrowband and broadband sources produce different types of annoyance. Subjective tests have shown that for equivalent subjective assessment, narrowband RFI should be of significantly lower amplitude than broadband RFI (quasi-peak measured) in the 0,15 MHz to 30 MHz range.

The influence of the repetition rate of rapid pulses in a broadcast channel is accounted for in the quasi-peak detector characteristic, the effect of low rate pulses (clicks) by the 20 log 30/N relaxation to the limit. In mobile communication (mainly narrowband FM), traffic noise sources (ignition interference) are the major source of RFI. In this respect the base station antenna is in a more favourable position with respect to RFI signals than the mobile antenna because of its higher location. Mobile antennas on the other hand change their position continuously and are therefore less vulnerable to stationary noise sources.

Broadcasting and mobile services may be interfered by narrowband sources as well (ISM equipment, data processing equipment, receiver oscillators, etc.). The radiated RF power from ISM equipment may be several orders higher than the level from broadband sources although the distances between those sources (industrial areas) and the victim receivers are normally longer. The disturbing energy, however, is mainly concentrated in a very narrow frequency band. For this reason a number of frequency bands is reserved for typical ISM applications.

Other professional radio services (navigation, fixed services, satellite and microwave communication) are, in general, less vulnerable to radio interference because of the use of higher frequencies (greater than 1 000 MHz in which broadband interference is negligible) more favourable antenna locations, sophisticated systems (modulation, coding, antenna directivity) and technology (screening, filtering).

3.3.5 Operational aspects

Noise sources in residential areas mainly consist of mass-produced devices for domestic and sometimes for professional use. Such appliances are tested according to statistical procedures which implies that a restricted percentage of *p* per cent fulfils the limit with a limited confidence *q* per cent. Small batches reduce the figures *p* and *q* and CISPR recommends a value for both *p* and *q* of 80 per cent (80 %-80 % rule). The rule is in general adequate to protect non-vital radio services like broadcast and most land mobile communication.

For critical or safety services, however, a much higher degree of confidence is necessary. The actual annoyance in an interfered radio service not only depends on the RFI field strength, but on the wanted signal level as well. The radio of wanted-to-unwanted input level which procures a specified quality of performance is called RF protection ratio. The wanted signal level depends on the natural noise level which may be much higher than the receiver noise level, particularly in the lower part of the frequency range.

In establishing limits for various types of noise sources it is important to strive for limits which have an equal effect on the radio services to be protected. The users of such a service are not interested in the type of source which causes RFI. Therefore all types of sources should be suppressed as much as possible to an equal level of noise output.

In some cases, however, this may be in contradiction with other requirements for suppression measures such as feasibility from physical conditions or from electric safety reasons and not in the least from an economic point of view.

3.3.6 Criteria for the determination of limits

3.3.6.1 Remote coupling

For remote coupling situations the field strength at a specified distance from the noise source is used as a characteristic for the interference potential of the source. The following model (see figure 15) was developed to derive radiation limits for the case of in-band interference (in the tuned channel). For the relevant radio services in the allocated frequency bands the protection ratio is determined. This protection ratio in ITU documents is given for disturbing radio service with the same modulation. The protection ratio for any disturbance radiation may be different.

From this protection ratio and from the minimum or nominal wanted field strength (field strength to be protected), the acceptable disturbance field strength at the receiving antenna input is calculated; that means that different types of modulation of the disturbance field strength has to consider a distinct from the protection ratios given in ITU documents. A minimum operational distance between noise source and receiving antenna is specified and with the use of an estimated or empirical propagation factor, the acceptable disturbance field strength at a specified measuring distance is calculated. Next some additional factors should be introduced for the screening factor of buildings and for the probability of actual interference under operational conditions. Such a probability factor should take into account statistics of antenna directivity (in the direction of the wanted transmitter and of the interference source), distance variations, propagation variations, time coincidence, etc.

The final result of this procedure is a calculated limit which is a good basis for an operational limit guaranteeing that the requirements of the protection ratio is met on a statistical basis (*x* % of the actual cases). It should be noted that reliable statistical values for most of the parameters mentioned above are not (yet) available and that in those cases rough estimations are used.

Moreover the interfering effect of out-of-band signals is more complex because of the selectivity and non-linearity characteristics of the receiver which can differ from case to case.

3.3.6.2 Close coupling

A simple model for close coupling situations is given in figure 16. The noise source is considered as an RF generator with an e.m.f. U_s and an internal impedance Z_s for each mains connector/earth combination (for simplicity only one mains connector is shown). The mains network is connected between the noise source and the interfered receiver. The mains network offers an RF-impedance Z_m to the source and transfers the energy from the noise source to the mains input of the receiver.

In addition, part of the conducted RF energy is propagated as a magnetic and electric field. For the close coupling situations generally, near-field conditions exist (ratio electric/magnetic component undefined).

Two coupling paths exist between noise source and receiving antenna:

a) the path of disturbance conducted along the mains network, the mains supply circuit of the receiver and the coupling between supply circuit and antenna/RF circuits inside the receiver;

b) the path of disturbance conducted along and radiated by the mains network and coupled directly to the receiving antenna outside or inside the receiver.

In the case of external antennas, the RF power coupled through the external path b exceeds the power via path appreciably. Moreover the internal coupling is determined by the mains immunity characteristics of the receiver, and it has been shown that it is not difficult to control the mains immunity factor of a receiver to an adequate level. Therefore the attention is mainly focused on path b. For internal (ferrite) antennas no clear distinction can be made between paths a and b.

The approach of the modelling starts in the same way as in the case of remote coupling. The acceptable disturbance field strength at the receiving antenna is calculated from protection ratio and field strength to be protected in the relevant frequency bands. The following step is the coupling factor measured from mains input (RF-voltage) to field strength at the antenna. It is, however, more usual to define a transfer factor as the ratio of the RF-voltage injected into the mains and the antenna output voltage (for a specified antenna). This factor is known as the mains decoupling factor. Because of the wide spread in actual situations, extensive statistical material is needed to found a basis for limits derived from mains decoupling factors.

Another statistical aspect in the calculation of limits in this concept is the variation of the RF-impedance at the mains input. Although individual decoupling factors are determined by the measured voltage, independent of the actual mains impedance, the interference limit is defined for a fixed simulated impedance (artificial mains network impedance), in order to get reproducible measuring results during tests. If a noise source is coupled to an actual mains network the load impedance of that network varies from location to location and from time to time. This aspect should be considered in deriving a limit from mains decoupling measuring data.

3.3.6.3 General

The derivation of limits from a hypothetical model requires the introduction of various experimental data in such a model. As these data, as pointed out earlier, are based on statistical measurements under different actual circumstances, the usefulness of such data for general application is often debatable.

On the other hand, the implementation of suppression measures should be considered on physical, operational, manufacturing and not in the least on economic aspects. Therefore the model should be used as a worthwhile starting point but the final limit value is often the result of an agreement between parties involved after extensive considerations and negotiations.

3.4 Basic model

This section contains the basic mathematical model used. The start-up point is the supposition that there is an identifiable probability inequality to be satisfied, and the assumption that the parameters obey a lognormal distribution.

3.4.1 Generation of EM disturbances

From the mathematical point of view any limit must be calculated with the provision that the inequality

$$z = x/y \geq 1 \tag{3.6}$$

is satisfied with some probability α.

If in (3.6) x and y are random values with log-normal distribution X (dB) and Y (dB) and with parameters μ_x (dB), μ_y (dB), σ_x (dB) and σ_y (dB) will have a normal distribution with the parameters

$$\mu = \mu_x - \mu_y$$

$$\sigma = \left[\sigma_x^2 + \sigma_y^2\right]^{1/2}$$

In this case

$$\alpha = F(\mu/\sigma)_{z=0} \tag{3.7}$$

Solving (3.7) relative to μ_x or μ_y

$$\mu_x = \mu_y + t_\alpha \sigma \tag{3.8}$$

$$\mu_y = \mu_x - t_\alpha \sigma \tag{3.9}$$

where t_α is a quantile of normal distribution, corresponding to the probability level α.

The CISPR limit L is determined for some quantile t_β in distribution of probabilities of the value x or y for which limits are established, in such a way that the following equality is true:

$$L_x = \mu_x + t_\beta \sigma_x \tag{3.10}$$

$$L_y = \mu_y - t_\beta \sigma_y \tag{3.11}$$

where t_β is a quantile for the probability level β.

Substituting (3.8) into (3.10) and (3.9) into (3.11)

$$L_x = \mu_y + t_\alpha \sigma + t_\beta \sigma_x \tag{3.12}$$

$$L_y = \mu_x - t_\alpha \sigma + t_\beta \sigma_y \tag{3.13}$$

one is enabled by the expressions obtained for the calculation of limits for different parameters, which ascertain the radio reception quality.

3.4.2 Immunity from EM disturbances

The inequality (3.6) has the form:

$x/y \geq 1$

where

x is a parameter of receptor immunity;

y is a parameter of electromagnetic environment in respect to which the immunity limit is established.

If the values X (dB) and Y (dB) are satisfactorily approximated by normal distributions with parameters μ_x, σ_x, μ_y, σ_y then

$$\sigma = \left[\sigma_x^2 + \sigma_y^2\right]^{1/2} \tag{3.14}$$

In this case, according to (3.12), the equation for the calculation of receptor immunity limits has the following form:

$$L_x = \mu_y + t_\alpha \left[\sigma_x^2 + \sigma_y^2\right]^{1/2} - t_\beta \sigma_x \tag{3.15}$$

3.5 Application of the basic model

3.5.1 Radiation coupling

This section adapts the basic model for the case where it is wished to protect a radio service when there is radiation coupling from the source of EM disturbance to the radio antenna. The actual signal-to-interference ratio R can be expressed in terms of the wanted signal, the disturbing signal, the propagation losses and the antenna gain, as follows:

$$R = E_w(\mu_w{:}\sigma_w) + G_w(\mu_{Gw}{:}\sigma_{Gw}) - [E_i(\mu_i{:}\sigma_i) + G_i(\mu_{Gi}{:}\sigma_{Gi}) + L_o(\mu_{Lo}{:}\sigma_{Lo}) + L_b(\mu_{Lb}{:}\sigma_{Lb}) \quad \text{dB} \tag{3.16}$$

where

E_w is the actual value of the wanted signal as a function of its mean value (μ_w) and the standard deviation (σ_w);

E_i is the value of the disturbance signal at a preset distance on a test site as a function of its mean value (μ_i) and standard deviation (σ_i);

G_w is the actual value of the antenna gain for the wanted signal as a function of its mean value (μ_{Gw}) and standard deviation (σ_{Gw});

G_i is the actual value of the antenna gain for the disturbance signal as a function of its mean value (μ_{Gi}) and standard deviation (σ_{Gi});

L_o is the actual value of the factor which takes account of the attenuation of the disturbance field strength when it is propagated through free space without obstacles as a function of its mean value (μ_{Lo}) and standard deviation (σ_{Lo});

L_b is the actual value of the factor which takes account of the attenuation of the disturbance field strength caused by obstacles in its propagation path as a function of its mean value (μ_{Lb}) and standard deviation (σ_{Lb}).

It is assumed that all the variables on the right-hand side of equation (3.16) obey a normal distribution law, then the distribution factors are related as follows:

$$\mu_R = \mu_w + \mu_{Gw} - \mu_i - \mu_{Gi} + \mu_{Lo} + \mu_{Lb} \quad \text{dB} \tag{3.17}$$

$$\sigma_R^2 = \sigma_w^2 + \sigma_{Gw}^2 + \sigma_i^2 + \sigma_{Gi}^2 + \sigma_{Lo}^2 + \omega_{Lb}^2 \quad (3.18)$$

With a normal distribution law the reliability of obtaining the preset quality of service can be expressed by the following function of the normal probability-distribution:

$$\Phi\,[-(R_p - \mu_R)\,/\,\sigma_R] = a \quad (3.19)$$

therefore:

$$\mu_R = R_p + t_a\sigma_R \quad (3.20)$$

where $t_a = \Phi^{-1}\,(a)$

By combining equations (3.17), (3.18) and (3.20) an expression is obtained for the permissible mean value of the disturbance field strength at a preset distance from the source of disturbance:

$$\mu_i = \mu_w + \mu_{Gw} - \mu_{Gi} + \mu_{Lo} + \mu_{Lb} - R_p - t_a\,[\sigma_w^2 + \sigma_{Gw}^2 + \sigma_i^2 + \sigma_{Gi}^2 + \sigma_{Lo}^2 + \omega_{Lb}^2]^{1/2} \quad (3.21)$$

The mean value of the disturbance shall be below the limit, and may be specified as follows:

$$E = \mu_i + t_n\sigma_i \quad (3.22)$$

where

E is the limit for disturbance measured on a test site at a specified distance; and

t_n is a normalized argument of the distribution function which corresponds to a probability level of compliance with the limits.

The free space attenuation factor (μ_{Lo}) can be evaluated from

$$\mu_{Lo} = 20\log_{10}\,[r^x/d] \quad (3.23)$$

where

r is an average distance between the disturbance source and the receiving antenna

d is the specified test distance on the measurement site;

x is the exponent which determines the actual free space attenuation rate.

Combining equations (3.21), (3.22) and (3.23) the limit is given by:

$$E = \mu_w + \mu_{Gw} - \mu_{Gi} + 20\log_{10}\,[r^x/d] + \mu_{Lb} - R_p - t_n\sigma_i$$

$$- t_a\,[\sigma_w^2 + \sigma_{Gw}^2 + \sigma_i^2 + \sigma_i^2 + \sigma_{Gi}^2 + \sigma_{Lo}^2 + \omega_{Lb}^2]^{1/2} \quad (3.24)$$

CISPR Recommendation 46/1 (see 2.2) specifies that 80 % of series-produced equipment should meet the disturbance limit, and that the testing should be such that there is 80 % confidence that this is so. For these conditions t_n = 0,84.

3.5.2 Mains coupling

The required quality of radio communications is considered to be fulfilled when the probability that the actual signal-to-disturbance level is greater than the minimum acceptable value exceeds a specified value. That is

$$P(R > R_p) \geq \alpha \tag{3.25}$$

where

R is the signal-to-disturbance ratio;

R_p is the minimum acceptable signal-to-disturbance ratio;

α is a specified value representing the reliability of communications.

The relationship between the signal-to-disturbance ratio and generated electromagnetic disturbance is:

$$R = V_w - V_i + K \quad \text{dB} \tag{3.26}$$

where

V_w is an effective value of wanted signal at the receiver input;

V_i is a value of a specified component of the electromagnetic disturbance (i.e., of voltage, field strength, power, etc.) measured in a specified way using specified equipment (i.e. a quasi-peak detector);

K is a decoupling factor defined as a ratio of V_i to an effective value of electromagnetic disturbance signal at the receiver input.

For the situations where the disturbance is coupled predominantly by conduction (frequencies below 30 MHz):

$$K = K_m + I \quad \text{dB} \tag{3.27}$$

where

K_m is a mains decoupling factor relating V_i measured at the source (by an artificial mains network) to a value of disturbance at the mains input to the receiving installation;

I is a mains immunity factor relating a value of disturbances at the mains input to an equivalent disturbance which, if applied at the antenna input of the receiving installation, would produce the same effect.

It has been established experimentally that probability distributions of V_w (dB), V_i (dB) and K for arbitrarily selected disturbance sources, radio receiving installations and distances between them is well approximated by a normal law.

A limit for electromagnetic disturbances is established for a definite quantile $E_i(p)$ in the probability distribution of E_i. A permissible value L for $E_i(p)$ is selected in such a way that at $E_i(p) = L$ a reliability of guaranteeing a radio reception which has a quality $R \geq R_p$ would be equal to the specified value τ:

$$L_{pr}(V_i) = U_{Ew} + U_k + R_p + t_p\sigma_{Ei} - t_r\left[\sigma_{Ew}^2 + \sigma_{Ei}^2 + \sigma_k^2\right]^{1/2} \tag{3.28}$$

U, σ^2 are expectations/variances of corresponding components; $t_r = \Phi^{-1}$, $t_p = \Phi^{-1}$ are arguments of a normal distribution function which is equal to t_r and p, respectively.

For series-produced articles CISPR recommends that p = 0,8; then t_p = 0,84. A value of τ is selected between 0,8 and 0,99, depending on a type of a radio network (radio broadcasting, air navigation, *et al*). When τ = 0,95, then t_r = 1,64.

It has been found experimentally that σ_k is the most significant factor. A change in the value of σ_k with an equivalent change in the limit for E_i results in no variation from the specified quality and reliability of radio performance. Therefore, limits are calculated for equipment located in similar conditions relative to radio receiving installations of a given radio network. For instance, in order to protect a broadcast reception in dwelling houses, it is enough to consider two groups only:

– equipment located in dwelling houses or connected to their supply mains;

– equipment located outside dwelling houses.

The second group, on the basis of economic considerations and separation distance, is divided into the following subgroups: power lines; electric transport; motor vehicles; industrial equipment located in an assigned territory; etc.

3.6 An alternative method used for ISM equipment

3.6.1 Introduction

The purpose of this clause is to review studies made for the derivation of CISPR limits for the protection of telecommunications from interference from ISM equipment and to conclude from these a recommended method which will meet the objectives of CISPR and ITU. This clause deals only with radiation which occurs outside the bands designated by ITU for ISM use.

3.6.2 Derivation of limits

The full range of parameters to be taken into account in the derivation of limits is shown in table II together with the major services requiring protection. Appendix A provides a model for the calculation of limits.

3.6.2.1 Protection of communication services

The wanted field strength to be protected, the protection ratio required for the different types of ISM equipment, the distance from the source at which protection is necessary and the attenuation law to be used in the calculation are important. These are matters in which ITU support is essential.

3.6.2.2 Proposed model for use in calculating disturbance limits

The factors that have traditionally been included in models for predicting interference from radio-frequency sources are listed in columns 1 to 10 of table 2 by assigning appropriate values to each parameter, for example, field strength to be protection, protection ratio, etc., worst-case limits for protecting the various communication services from interference from ISM equipment may be determined. However, a model which is based on worst-case parameters is both technically and economically unrealistic since it ignores the fact that there have been very few instances of interference attributed to ISM equipment. It is therefore critical that the experience in this subject should be taken into account. Thus, the benefits of worldwide experience in this subject can be included although it is recognized that the probability can only be an estimate at present because so many complex factors are involved as shown in 3.7.2.3. Determination of numerical values of the probability for the various services is urgently required and studies are being undertaken in several countries.

3.6.2.3 Probability factors

Probability of coincidence of adverse factors:

$P = P_1 \times P_2 \rightarrow P_{10}$

where

P_1 is the probability that the major lobe of the ISM radiation is in the direction of the victim receiver;

P_2 is the probability of directional receiving aerials having maximum pick-up in the direction of the disturbing source;

P_3 is the probability that the victim receiver is stationary;

P_4 is the probability of ISM equipment generating a disturbing signal on a critical frequency;

P_5 is the probability that the relevant harmonic is below the limit value;

P_6 is the probability that the type of disturbing signal being generated will produce a significant effect in the receiving system;

P_7 is the probability of coincident operation of the ISM source and the receiving system;

P_8 is the probability of the disturbing source being within the distance at which interference is likely to occur;

P_9 is the probability of coincidence of limit value of ISM radiation with edge of service area condition is for the protected service;

P_{10} is the probability that buildings provide attenuation.

Table 2 – Tabulation of the method of determining limits for ISM equipment 0,150 MHz to 960 MHz

Frequency band	Service to be protected	Signal to be protected dB(µV/m)	Protection ratio dB	Permissible interference field at receiving antenna dB(µV/m)	Distance from equipment at which signal is to be protected m	Attenuation law	Approximate equi-valent interference field at 20 m from equipment dB(µv/m)	Building attenuation dB	Allowance for probability dB	Corresponding practical limit at 30 m from boundary dB(µV/m)	Corresponding limit at 30 m from boundary dB(µV/m)	Proposal for revision of CISPR limits at 30 m on a test site dB(µv/m)
(1)	(2)	(3)	(4)	(5)	(6)	(7)	(8)	(9)	(10)	(11)	(12)	(13)
0,150 to 0,285	LF BC Aero-beacons											
0,285 to 0,490	Aero-beacons											
0,490 to 1,605	MF BC Aero-beacons											
1,605 to 4,00	Fixed links Aeromobile											
4,00 to 15,00	Fixed links Aeromobile											
15,00 to 20,00	Fixed links Aeromobile											
20,00 to 30,00	Fixed links Aeromobile											
30,00 to 68,00	TV BC Land mobile											
854,00 to 960,00	Land mobile											
100,00 to 156,00	FM BC ILS Aero-mobiles Land mobile											

Table 2 *(continued)*

Frequency band	Service to be protected	Signal to be protected dB(µV/m)	Protection ratio dB	Permissible interference field at receiving antenna dB(µV/m)	Distance from equipment at which signal is to be protected m	Attenuation law	Approximate equivalent interference field at 20 m from equipment dB(µv/m)	Building attenuation dB	Allowance for probability dB	Corresponding practical limit at 30 m from boundary dB(µV/m)	Corresponding limit at 30 m from boundary dB(µV/m)	Proposal for revision of CISPR limits at 30 m on a test site dB(µV/m)
(1)	(2)	(3)	(4)	(5)	(6)	(7)	(8)	(9)	(10)	(11)	(12)	(13)
156,00 to 174,00	Land mobile											
174,00 to 216,00	TV BC Land mobile											
216,00 to 400,00	ILS											
400,00 to 470,00	Fixed links Land mobile											
470,00 to 585,00	TV BC											
585,00 to 614,00	Aeronav TV BC											
614,00 to 854,00	TV BC											
854,00 to 960,00	Land mobile											

NOTE Explanation of column headings:

(3) Median value of the field strength to be protected at the edge of service area: to be derived from ITU regulations and ITU recommendations as appropriate.

(4) Protection ratio. The signal-to-interference ratio required to protect the service from interference with the characteristics of the signal generated by ISM equipment (for example, frequency stability, etc.). This is the value to be used in the derivation of limits and is not necessarily the same protection ratio as recommended by ITU for planning purposes.

(6) The mean minimum distance from ISM equipment at which receiving installations of the relevant service are normally installed. Equipment at a different distance will be allowed for in the probability factor.

(9) The attenuation provided by buildings in which the ISM equipment is installed. Experience has shown that 10 dB is a normal practical value.

3.6.3 Application of limits

The CISPR has traditionally adopted the view that there should be only one limit for each type of appliance. This approach has in the past had considerable merit, but is becoming increasingly difficult to sustain. Thus, it has been found useful to introduce several classes of limits for ISM equipment (see CISPR 11).

Annex 3.6-A

Summary of proposals for determination of limits

3.6-A.1 Experience approach

The exponents of this approach state simply that limits in use in their own country have been proved by practical experience to give adequate protection.

This is a powerful argument which cannot be ignored. The technical evaluation of coupling between sources of interference and communication services is very complex and virtually impossible to define precisely in mathematical or practical terms mainly because control of the various parameters is impossible and the spreads on measured values are very wide. Experience is therefore valuable. Unfortunately, the same factors which make experience valuable tend to militate against the acceptance of this approach unless the experience gained in a sufficiently large number of countries leads to similar conclusions. In this case, however, there is not a sufficiently large number of countries supporting the unqualified application of the actual limits but there is clearly a need to support the approach as one factor in the consideration of limits.

3.6-A.2 User and manufacturer responsibility for avoidance of interference

User regulations are in force in a number of countries.

User limits may take one of the several forms outlines as follows:

i) regulations may require users to meet certain limits if interference is caused;

ii) if interference is caused, regulations may require an ISM user to cease operations until the interference is abated;

iii) regulations based on the licensing of apparatus of this category.

These approaches on their own satisfy neither the ITU/CISPR criteria for avoidance of interference nor the CISPR requirements for avoidance of technical barriers to trade. User limits would probably, in any case, be quite unacceptable in a number of countries as they place the user in an unfavourable position legally, financially and technically.

User regulations in conjunction with manufacturer regulations are a different matter. In these the user may be required to maintain suppression to the standard of new equipment and his financial, legal and technical obligations are therefore clear.

Examples of limits which are in use for user-only regulations are those in force in the United Kingdom for industrial radio-frequency heaters in the frequency range 0,15 MHz to 1 000 MHz. These broadly conform with the present CISPR limits with a provision of a 10 dB more stringent limit where interference is caused to safety of life services.

Other examples are the USA regulations which take the form described in item ii) and the German regulations which take the form of item iii). In the USA the limits are considerably less stringent than those recommended by CISPR.

3.6-A.3 Calculation of limits on a worst-case basis

This method of arriving at limits is intended to provide a high degree of protection for all radiocommunication services. Limits are calculated using minimum values of field strength to be protected, high values of protection ratio, maximum coupling between disturbance sources and radiocommunication receivers, and minimum values of attenuation with distance of the disturbing signal.

At first sight, this approach might seem to be ideal as it would, if implemented, lead to an ideal situation of very low values of man-made ambient radio-frequency noise. The cost to society of the adoption of such limits, however, would be high and it would be impossible, with present technology, to continue to operate many electrical devices which do not contribute to the welfare and heath of the human race.

3.6-A.4 Statistical evaluation approach

This approach states that the control of radio interference has to be treated statistically because the many factors involved are not under the control of the engineer and those parameters which are capable of measurement have very wide spreads of values.

The statistical evaluation approach has to overcome these difficulties. It should satisfy the communicator that communication services will receive adequate protection under normal circumstances of correct use and the manufacturers and users of electrical equipment that economic, operational and safety considerations are being correctly taken into account.

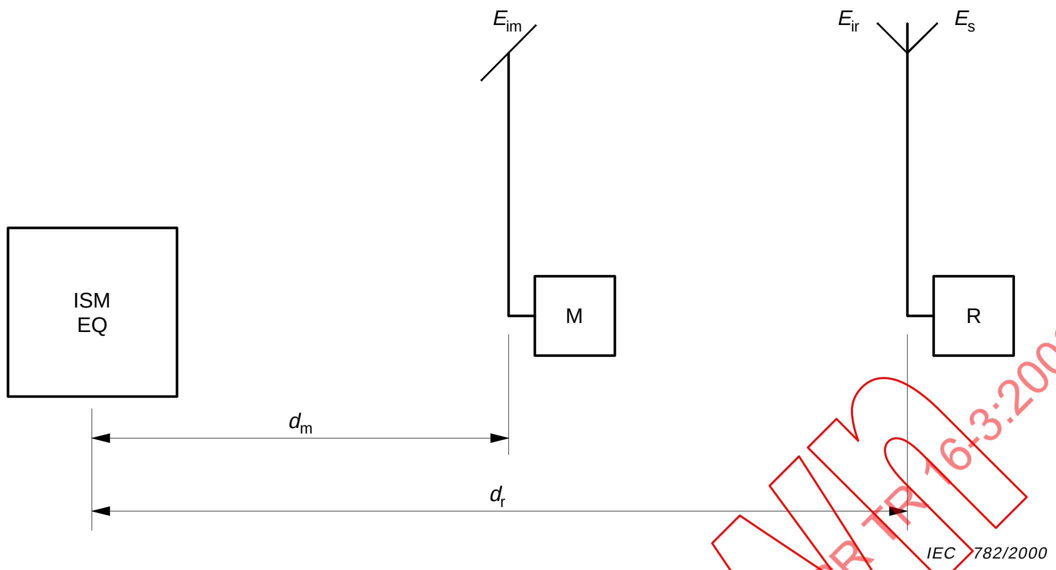

$$E_{ir} = E_w / S$$

E_w = wanted signal field strength to be protected

S = protection ratio

$$E_{im} = E_{ir}\ \alpha\ p\ (d_r / d_m)^x$$

E_{im} = regulated interference field strength at measuring distance d_m

α = screening factor of building

p = statistical probability factor

x = propagation coefficient

Figure 15 – Model for remote coupling situation derived disturbance field strength E_{ir} at receiving distance d_r (see 3.3.6.1)

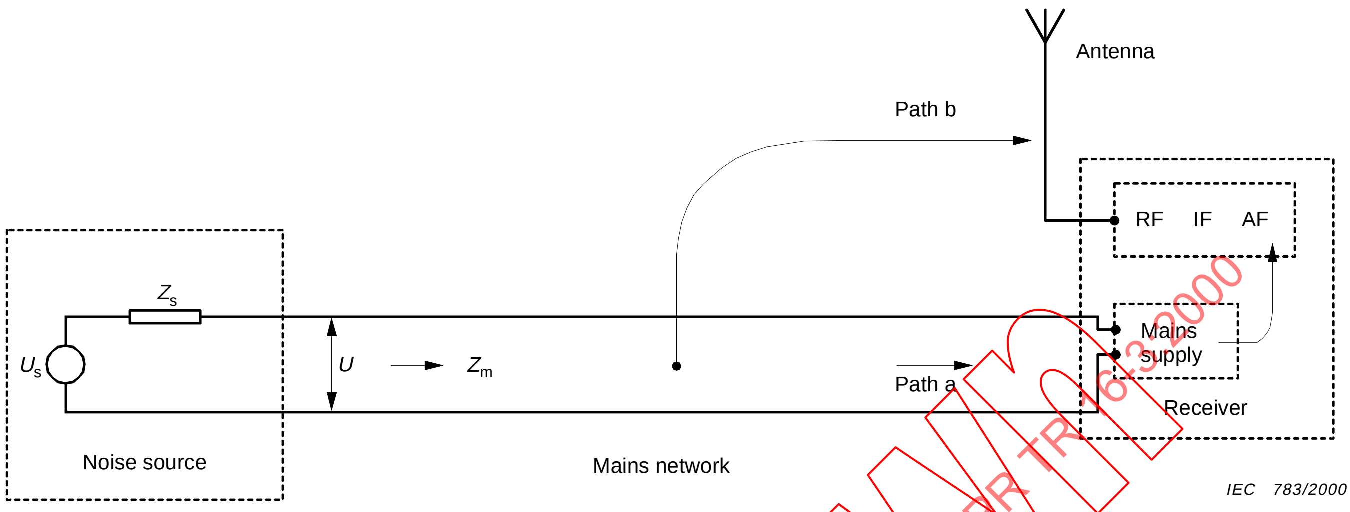

Figure 16 – Model for close coupling situations (see 3.3.6.2)

4 Technical reports

4.1 Correlation between measurements made with apparatus having characteristics differing from the CISPR characteristics and measurements made with CISPR apparatus

4.1.1 Introduction

CISPR standards for instrumentation and methods of measurement have been established to provide a common basis for controlling radio interference from electrical and electronic equipment in international trade.

The basis for establishing limits is that of providing a reasonably good correlation between measured values of the interference and the degradation it produces in a given communications system. The acceptable value of signal-to-noise ratio in any given communication system is a function of its parameters including bandwidth, type of modulation and other design factors. As a consequence, various types of measurements are used in the laboratory in research and development work in order to carry out the required investigations.

The purpose of this subsection is to analyse the dependence of the measured values on the parameters of the measuring equipment and on the waveform of the measured interference.

4.1.2 Critical interference measuring instrument parameters

The most critical factors in determining the response of an instrument for measuring interference are the following: the bandwidth, the detector, and the type of interference being measured. Considered to be of secondary importance, but, nevertheless, quite significant in correlating instruments under particular circumstances, are: overload factor, AGC design (if used), image and other spurious responses, and meter time constant and damping.

For purposes of discussion, reference is made to three fundamental types of radio noise: impulse, random and sine wave. The dependence of the response to each of these on the bandwidth and the type of detector is given in table 4.1-1. In this table, δ is the magnitude of the impulse strength, Δf_{imp} is the impulse bandwidth, Δf_{rn} is the random noise bandwidth, $P(\alpha)$ is the pulse response for the quasi-peak detector, f_{PR} is the pulse repetition frequency, and E' is the spectral amplitude of the random noise. The relative responses of various detectors to impulse interference for one instrument are shown in figure 4.1-1.

Table 4.1-1 shows that the dependence of the noise meter response on bandwidth is different for all three types of interference. If the waveform being measured can be defined as being any of the three types listed in table 4.1-1, and if a standard source provides that type of waveform, then by using the substitution method, a satisfactory calibration can be obtained for any instrument with adequate overload factor independent of its bandwidth. Thus, with a purely random interference or a purely impulsive interference of known repetition rate, calibration can be made using a corresponding source, or a correlation factor calculated on the basis of known circuit parameters.

If a particular interference waveform is of a type intermediate between these three types, then the correction or correlation factors will also be intermediate. In any given case, it will be necessary to classify the noise waveform in such a manner that a significant correlation factor can be established. Hence, in order to develop this subject to any significant extent, it will be necessary to examine typical interference sources and to determine the extent to which they are of impulsive, random, or sine-wave type.

If an interference measuring set with several types of detectors is available, for example, peak, quasi-peak and average, the type of interference can be assessed by measuring the ratios of the readings obtained with these detectors. These ratios will, of course, depend upon the bandwidth and other characteristics of the instrument being used for the measurement.

4.1.3 Impulse interference – Correlation factors

The quasi-peak detector response of any interference measuring set to regularly repeated impulses of uniform amplitude can be determined by the use of the "pulse response curve" which is shown in figure 4.1-2. This figure shows the response of the detector in percentage of peak response for any given bandwidth and value of charge resistance and discharge resistance. Applying this curve, it should be noted that the peak itself is dependent upon the bandwidth, so that as the bandwidth increases, peak value increases, but the percentage of peak, which is read by the detector, decreases; over a narrow range of bandwidth, these effects tend to counteract each other. The bandwidth used in this curve is the 6 dB bandwidth, which, for the passband characteristics typical of most interference measuring equipment, is about 5 % less than the so-called impulse bandwidth. A theoretical comparison of instruments having various bandwidths and detector parameters with the CISPR instrument is shown in figure 4.1-3.

The response of the average detector to impulsive noise is an interesting case. The reading of an average detector for impulsive noise is independent of the bandwidth of the pre-detector stages. It is, of course, directly proportional to the repetition rate. In most cases, the reading obtained with an average detector for impulsive noise is so low as to be of no practical value unless the noise meter bandwidth is exceedingly narrow, such as of the order of a few hundred hertz. For a repetition rate of 100 Hz and a bandwidth of the order of 10 kHz, the average value would be approximately 1 % of the peak value. Such a value is too low to measure with any degree of precision. Furthermore, for many communication systems, the annoyance effect may be well above the reading obtained with the average meter. This, of course, is one of the justifications for the use of the quasi-peak instrument.

4.1.4 Random noise

The response of a noise meter to random noise is proportional to the square root of the bandwidth. This result is independent of the type of detector used. The ratio of the random noise bandwidth to the 3 dB bandwidth is a function of the type of filter circuit. On the other hand, it has been shown that for many circuits typical of those used in interference measuring equipment, a ratio of effective random noise bandwidth to the 3 dB bandwidth of about 1,04 is a reasonable figure.

4.1.5 The r.m.s. detector

One of the advantages of the r.m.s. detector in correlation work is that for broadband noise the output obtained from it will be proportional to the square root of the bandwidth, i.e. the noise power is directly proportional to the bandwidth. This feature makes the r.m.s. detector particularly desirable and is one of the main reasons for adopting the r.m.s. detector to measure atmospheric noise. Another advantage is that the r.m.s. detector makes a correct addition of the noise power produced by different sources, for example, impulsive noise and random noise, thus for instance allowing a high degree of background noise.

The r.m.s. values of noise often give a good assessment of the subjective effect of interference to a.m. sound and television reception. However, the very wide dynamic range needed when using very wide-band instruments for measuring impulsive noise, limits the use of r.m.s. detectors to narrow-band instruments.

4.1.6 Discussion

The preceding paragraphs have indicated the theoretical basis for comparing measurements obtained with different instruments. As mentioned previously, the possibility of establishing significant correlation factors depends upon the extent to which noise can be classified and identified so that the proper correlation factors may be used. In many frequency ranges, impulsive interference appears to be the most serious; however, for power lines where corona interference is the primary concern, random interference would be expected to be more characteristic. Additional quantitative data are needed on typical interference characteristics. Another important parameter is the overload factor.

4.1.7 Application to typical noise sources

Commutator motors

The noise generated by commutator motors is usually a combination of impulse and random noise. The random noise originates in the varying brush contact resistance, while the impulse noise is generated from the switching action at the commutator bars. For optimum adjustment of commutation the impulse noise can be minimized. However, where variable loading is possible, measurements have confirmed that for the peak and quasi-peak detectors, the dominant noise is of impulse type and the random component may be neglected. While the repetition rate may be of the order of 4 kHz, the effective rate is lower because the amplitude of the impulses is usually modulated at twice the line frequency. Hence, experimental results have shown that quasi-peak readings are consistent with bandwidth variations if the repetition rate of the impulse is assumed to be twice the line frequency.

Peak measurements show fluctuating levels on such noise because of the irregular nature of the commutator switching action.

The quasi-peak to average ratio is lower than would be obtained for pure impulse noise for two reasons.

1) The modulation of the commutator switching transients by line frequency produces many pulses below the measured quasi-peak level. These pulses do not contribute to the quasi-peak value but do contribute to the average.
2) The relatively low level, but continuous, random noise can likewise contribute substantially only to the average value. Experimental values of quasi-peak to average ratio ranged from 13 dB to 23 dB with the highest ratios for the widest bandwidths (120 kHz).

Impulsive sources

Tests on an ignition model, commutator motor appliances, and appliances using vibrating regulators showed reasonable agreement on instruments with the same nominal bandwidth, but with time constant ratios of the order of 3 to 1 on restricted portions of the output indicator scale. Deviations at higher scale values are without explanation. Relatively poor correlation was obtained on sources producing very low repetition rate pulses.

Ignition interference

CISPR Recommendation 35 recognizes that correlation between quasi-peak and peak detectors can be established as a practical matter. The conversion factor of 20 dB is explained partly on the basis of theory for uniform repeated impulses, and partly on the basis of the actual irregularity of the amplitude and wave shape of such impulses.

Noise from high-voltage lines

Comparative tests were made with an instrument meeting CISPR specification and one meeting those of the U.S.A. Standards Institute. The latter read 0 dB to 1 dB higher in one test and 1 dB to 3 dB higher in another (see IEEE Special Publication 31C44).

Dependence on bandwidth

Comparisons of measurements made in the U.K. with two instruments having bandwidths of 90 kHz and 9 kHz respectively have been reported to show that for most interference sources, the values obtained are in the ratio 14 dB to 18 dB. This figure is consistent with the concept that the interference is dominated by impulse type noise but that some random components are present.

4.1.8 Conclusions

Analysis of data comparing the responses of various instruments shows that it is possible to explain in almost every case the differences in measured values on the basis of theoretical and practical considerations. In many instances, it is indicated that waveform characteristics are known to predict correlation factors adequately with an accuracy of 2 dB to 4 dB.

Further studies are needed

a) to characterize in some detail the waveforms of various sources of interference, and

b) to correlate these waveform characteristics with measured values and the instrument parameters.

Table 4.1-1 – Comparative response of slideback peak, quasi-peak and average detectors to sine wave, periodic pulse and Gaussian waveform

Input waveform	Detector type			
	Slideback peak (sb)	**Quasi-peak:1/600 (qp)**	**Field intensity (average)**	**RMS**
CW sine wave	*e*†	*e*	*e*	*e*
Periodic pulse (no overlap)	1,41 $\delta\,\Delta f_{imp}$	1,41 $\delta\,\Delta f_{imp}\,P(\alpha)$*	1,41 $\delta\,f_{PR}$+	1,41 $\delta\,\sqrt{f_{PR}\,\Delta f_{imp}}$
Random ++	–	1,85 $\sqrt{\Delta f_{rn}\,E'}$ **	0,88 $\sqrt{\Delta f_{rn}\,E'}$	$\sqrt{\Delta f_{rn}\,E'}$

† *e* is the r.m.s. value of the applied sine wave.

* *P*(*α*) is given in figure 4.1-2.

** *E′* is spectral strength in r.m.s. volts/hertz bandwidth.

\+ *δ* is impulse strength. It is assumed the instrument is calibrated in terms of the r.m.s. value of a sine wave.

++ It is assumed that characteristics of the envelope are measured by the detector on random noise.

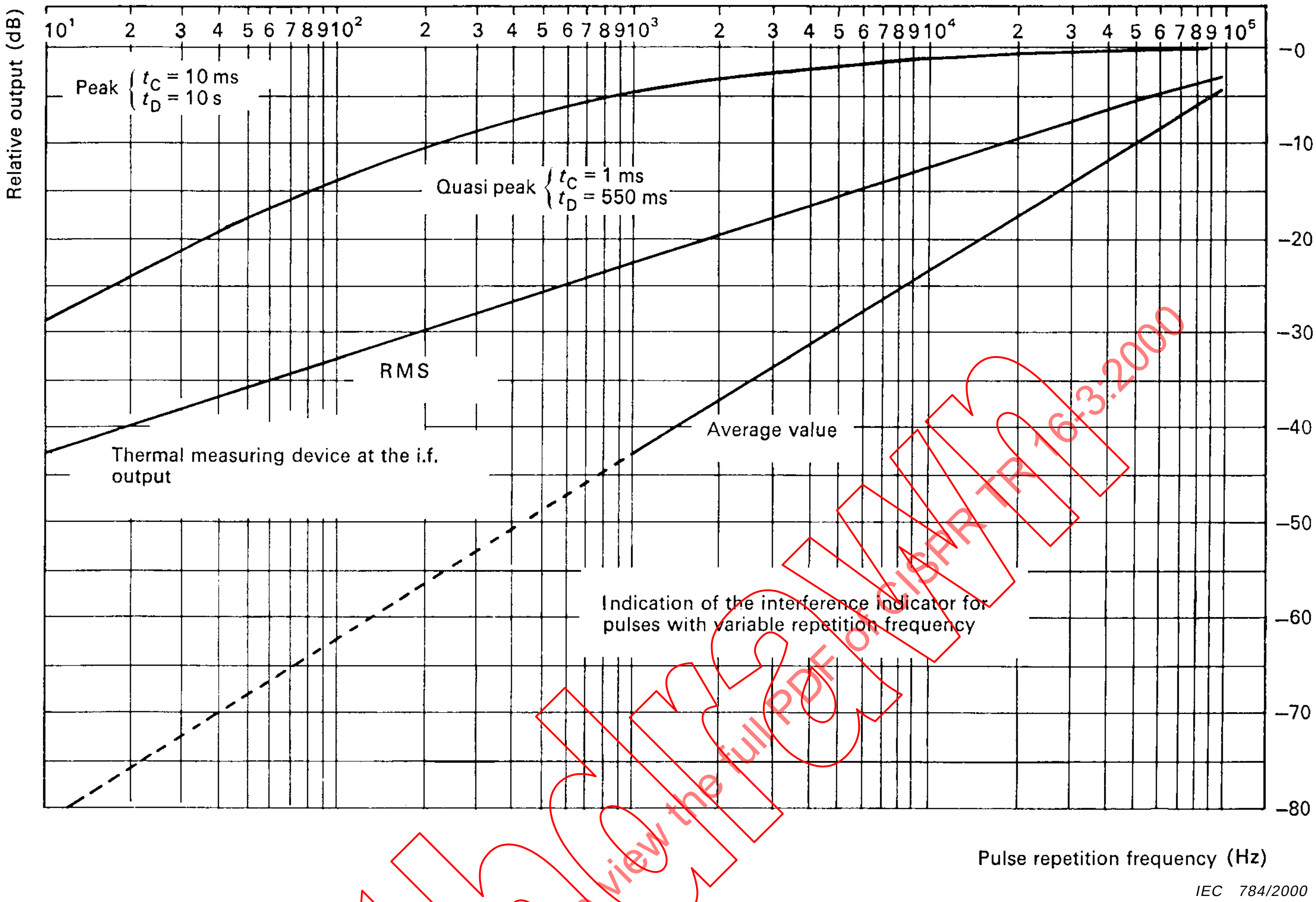

Figure 4.1-1 – Relative response of various detectors to impulse interference

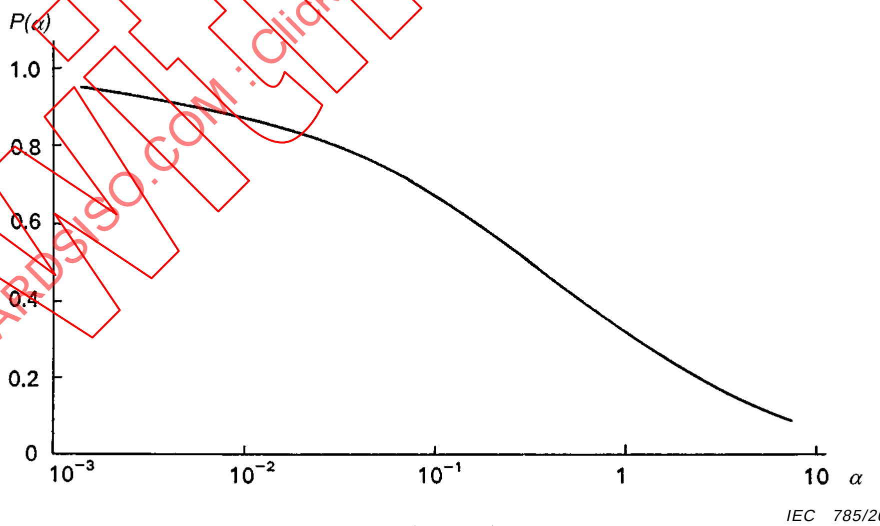

$$\alpha = \frac{(\pi R_c \Delta F)}{(R_d f_{PR})}$$

R_c = charging resistance, in ohms

R_d = discharging resistance, in ohms

ΔF = 6 dB bandwidth, in hertz

f_{PR} = pulse repetition frequency, in hertz

Figure 4.1-2 – Pulse rectification coefficient $P(\alpha)$

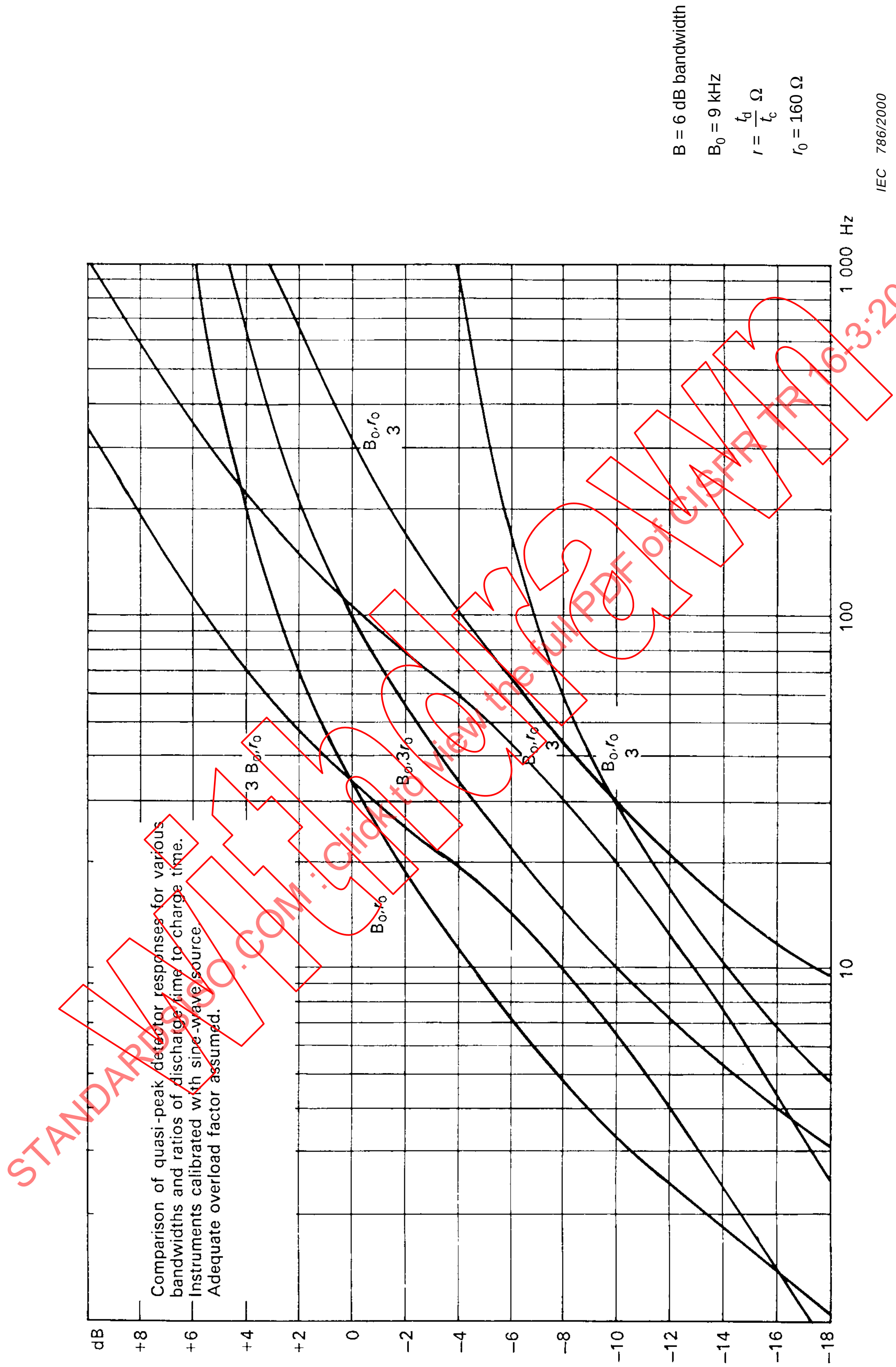

Figure 4.1-3 – Pulse repetition frequency

4.2 Interference simulators

4.2.1 Introduction

Interference simulators can be used for various applications, in particular to study signal processing in systems and equipment in the presence of interference (for example, over-loading of receivers, synchronization of TV receivers, error rate of data signals, etc.) and for assessment of the annoyance caused by disturbances in broadcast and communication services.

A simulator should produce a stable and reproducible output signal, which requirement is normally not fulfilled by an actual interference source, and the simulator output waveform should show a good resemblance to the actual interference signal.

4.2.2 Types of interference signals

The following interference sources can be simulated.

a) Narrowband interference sources generating sine-wave signals, for example receiver oscillators and ISM equipment. These sources can be simulated by an appropriate RF standard signal generator. ISM interference is often modulated by the mains voltage which can be simulated by modulating the RF signal with a full-wave rectified mains signal.

b) Broadband interference sources producing continuous broadband noise, for example, gaseous discharges and corona. For simulating purposes a standard broadband noise source (saturated vacuum tube diode, zener diode or gas tube followed by a suitable broadband amplifier) can be used. In mains-fed sources of this type, mains modulation is present, but because of the non-linear behaviour of gaseous discharges the envelope of the actual noise signal can deviate appreciably from the normal full-wave rectified mains waveform. In this case, gating the noise of the simulator at a repetition frequency of twice the mains frequency can yield a good correspondence with the actual interference signal.

c) Thyristor controlled regulators with phase control generate in a RF-channel narrow pulses of constant amplitude at a repetition frequency equal to twice the mains frequency. They can be simply simulated by standard pulse generators with narrow output pulses (10^{-7} s to 10^{-9} s width) of the same repetition frequency.

d) Ignition systems, mechanical contacts and commutator motors generate short periods (bursts) of quasi-impulsive noise. This type of noise is caused by very short pulses of regular or irregular height at random time intervals; if the average interval between adjacent pulses is less than the reciprocal of the channel bandwidth under test ($\tau_{av} < 1/B$) the pulses overlap and because of the random phase conditions a random fluctuating output signal (noise) results. Therefore, bursts of quasi-impulsive interference of this type can be simulated by a gated broadband noise signal.

The duration and the repetition frequency of the bursts depend on the type of interference source (see table 4.2-1).

Ignition interference is characterized by burst durations between 20 µs and 200 µs and repetition frequencies between 30 bursts/s and 300 bursts/s depending on the number of cylinders and revolutions/minute of the engine.

Mechanical contacts produce bursts (clicks) which can vary between some milliseconds (snap-off switches) and more than 200 ms. In the case of a contact device in a mains-fed circuit, the noise during the burst is modulated with the full-wave rectified mains voltage.

Commutator motors produce much shorter bursts with durations between 20 µs and 200 µs at repetition frequencies between 10^3 bursts/s and 10^4 bursts/s, depending on the number of commutator bars and revolutions/minute of the rotor. Also in this case, mains supply causes a similar envelope modulation of the noise bursts.

4.2.3 Circuits for simulating broadband interference

Simulators of this type should generate gated noise bursts with or without mains modulation according to the characteristics laid down in table 4.2-1. Figure 4.2-1 shows a straightforward design with a noise source followed by an appropriate amplifier of 70 dB to 80 dB gain, a gating circuit to simulate the bursts, a mains envelope modulator and an output attenuator to adjust the required output level.

Table 4.2-1 – Characteristics of gate generator and modulator to simulate various types of broadband interference

Simulator signal	Burst duration	Burst repetition frequency	Mains modulation [a]
Gaseous discharge		Continuous	Yes/no [b]
Ignition	20-200 µs	30-300 bursts/s	No
Switches	5-500 ms	0,2-30 bursts/min or single	Yes/no
Commutator motors	30-300 µs	10^3-10^4 bursts/s	Yes/no

[a] Depending on a.c. or d.c. supply.

[b] In the case of mains modulation, gating at a repetition frequency $2f_{mains}$ and gate width of 1 ms to 2 ms may be more appropriate.

The disadvantage of this layout is that a wide usable frequency range requires a broad bandwidth for the entire circuit between noise source and output terminal. The most critical part in this respect is the high-gain amplifier. For applications in a wide frequency range (for example, 0 MHz to 1 000 MHz) such a range can be split up in several smaller ranges or a tunable amplifier may be used. Such a design complicates the construction of the simulator appreciably.

Another way to produce a gated wideband noise signal is given in the diagram of figure 4.2-2. In this design, nanosecond pulses are generated in the output stage, for example, a step recovery diode or similar device. These pulses of constant height are triggered at random time intervals and at a sufficiently high repetition rate to cause overlap in the RF channel under test in order to result in quasi-impulsive noise in the output of the channel. Average repetition rates of a few megahertz are required for measurements in a TV channel of at least 100 kHz for measurements in an FM channel and of at least 10 kHz in an AM channel. The random occurrence of the trigger pulses is obtained from the zero crossings of a broadband signal. For this purpose the output of a noise source is fed to an appropriate amplifier which is followed by a gating circuit for burst simulation. The gated noise signal is fed to a bistable multivibrator which converts the zero crossings into pulses of random varying width from which narrow trigger pulses at random distances are generated by the monostable multivibrator.

The advantage of this system over the circuit of figure 4.2-1 is that the usable frequency range is determined by the output pulses of the step recovery diode only. An example of such a circuit is given in figure 4.2-3, in which circuit output pulses are generated by the step recovery diode HP0102, the pulse width is determined by the length of a short-circuited coaxial cable *L*. Ringing effects are suppressed by the fast switch diode HP2301 and mains modulation can be effected simply by modulating the supply voltage of the step recovery diode with a full-wave rectified mains voltage. Pulses of 1 ns duration and 5 V amplitude are applicable and offer an output spectrum flat to about 500 MHz. Such a single pulse causes a 50 mV pulse in a TV channel and a 1 mV pulse in an FM channel; overlapping pulses add up, and the peak and quasi-peak value of the resulting signal is considerably higher.

The bandwidth of the preceding stages which generate the trigger signal (noise source, amplifier and gating circuit) should be sufficient for the required pulse repetition rate, so for measurements in a TV channel a bandwidth of 5 MHz to 10 MHz is quite satisfactory. Moreover, the linearity of these stages is not critical because only the position of the zero crossings is important. The multivibrators have to generate steep pulses of short duration (about 0,1 µs) to drive the step recovery diode.

In summary, the circuit according to figure 4.2-1 is very useful for broadband interference simulators to be operated in a limited frequency range, whereas the circuit of figure 4.2-2 is more suitable for simulators intended for wideband use.

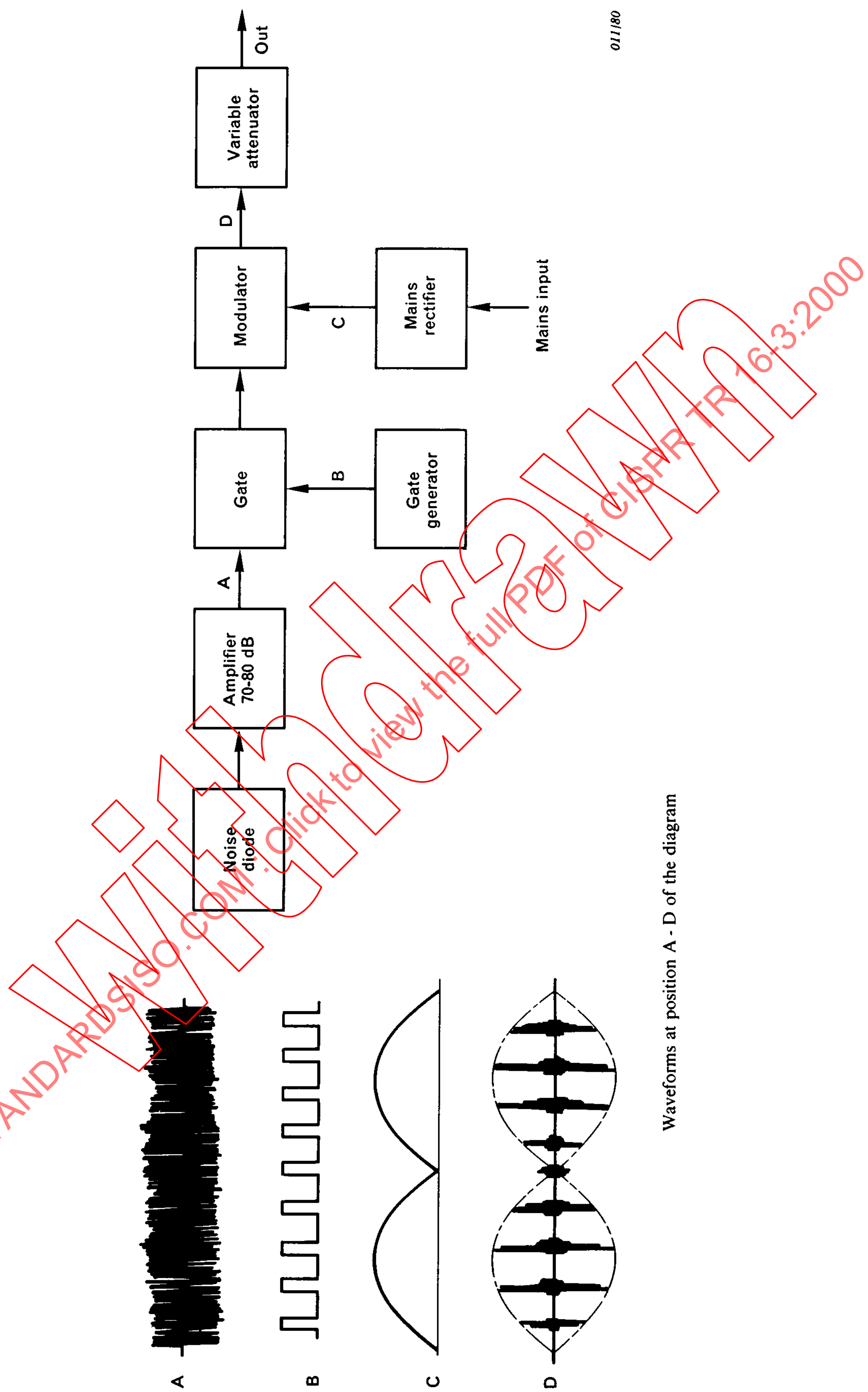

Figure 4.2-1 – Block diagram and waveforms of a simulator generating noise bursts

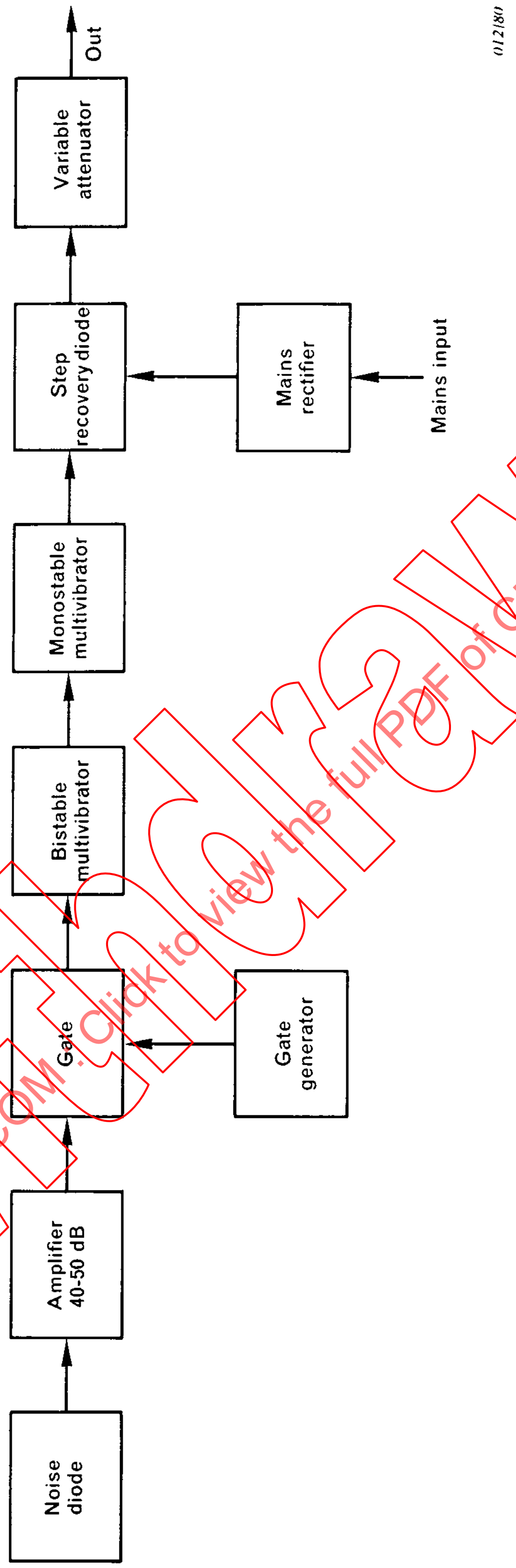

Figure 4.2-2 – Block diagram of a simulator generating noise bursts according to the pulse principle

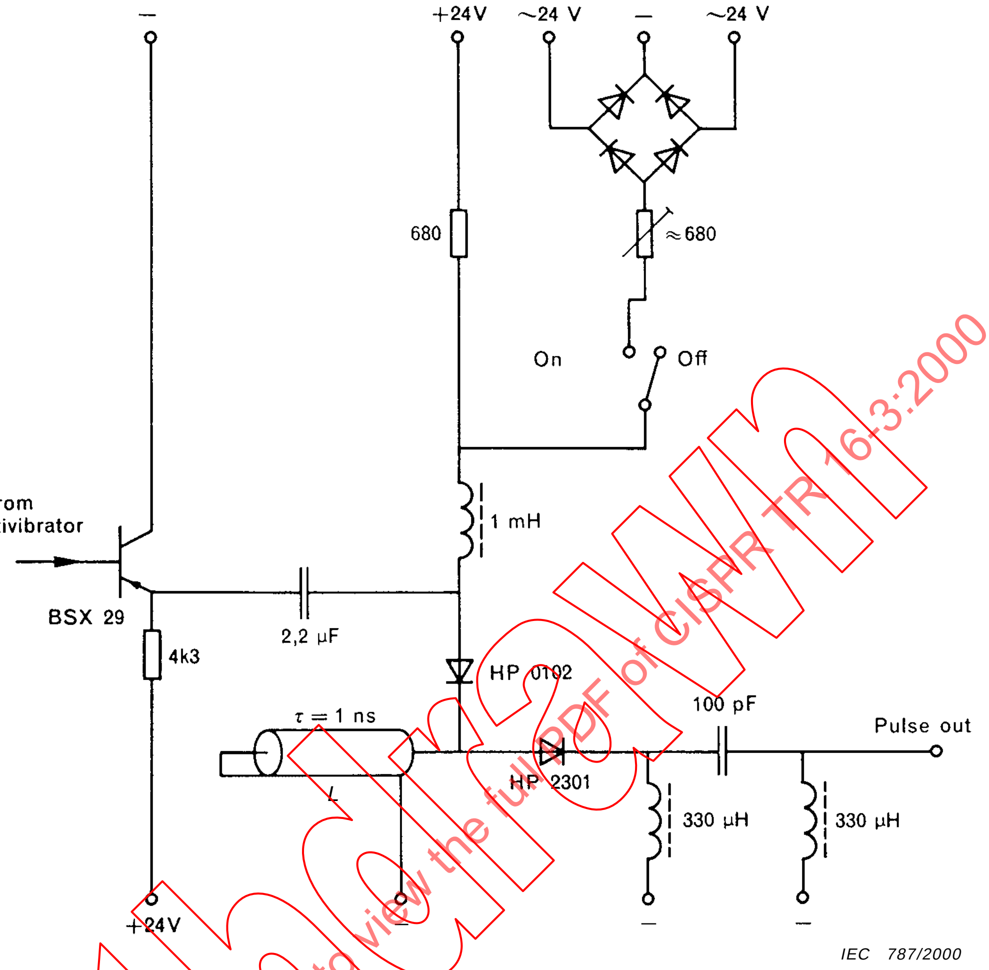

Figure 4.2-3 – Details of a typical output stage

4.3 Relationship between limits for open-area test site and the reverberating chamber

4.3.1 Introduction

At present there are limits for use with the open-area test site method of measurement specified in several CISPR publications. For equipment which can be measured using the reverberating chamber method, a procedure is required to relate the limit to be used with the open-area test site limit. The procedure is described in this report.

4.3.2 Correlation between measurements of the reverberating chamber and the open-area test site

The open-area test site measurement sets out to find the maximum level of radiation of the EUT (equipment under test). Whether the measurement is of the field strength or of power density at the measurement antenna, or of the power into an antenna in substitution of the EUT, the measured results can be expressed in the equivalent, radiated power from a half-wave dipole. Let this equivalent radiated power be P_q dB(pW).

The reverberating chamber measures the total radiated power of the EUT. Let the measured power be P_t dB(pW).

The two measurements are related to each other by the gain of the EUT as a radiator with respect to an isotropic radiator. Let this EUT gain be G dB. The relationship is given by equation (4.3-1). The equation is derived in the appendix.

$$P_t + G = P_q + 2 \tag{4.3-1}$$

4.3.3 Limits for use with the reverberating chamber method

Consider the case of an EUT which is exactly on the limit, L_o, when measured in the open area test site, i.e. $P_q = L_o$.

This EUT should also be exactly on the corresponding limit, L_r, when it is measured in the reverberating chamber, i.e. $P_t = L_r$.

From equation (4.3-1), we can relate the two limits as in equation (4.3-2).

$$L_r = L_o + 2 - G \tag{4.3-2}$$

The value of L_r is dependent not only on L_o, but also on G. Since G will not be the same for EUTs, it is not possible to set L_r to treat EUTs in a manner identical to the effect of L_o. If say $L_r = L_o$, then it is correct only for EUTs with $G = 2$. EUTs with a G greater than 2 will find it easier to pass the reverberating limit, and vice versa.

It is necessary to determine the value of G. This can be done from measurements of P_q and P_t. Figure 1 shows the lines of P_w versus P_t for various values of G. The shaded region is for negative values of G. (Experimental points appearing in this region are caused by failure to locate the maximum open-site radiation, probably due to the maximum radiation lying outside of the horizontal plane.)

An example is given in figure 4.3-2. A number of microwave ovens were measured for P_q and P_t. It can be seen that

– for points lying in the positive G region, the majority have values around 2;

– more points lying in the positive G region as the frequency goes up, indicating that the radiation pattern is becoming more directional in the vertical direction.

On this evidence, the reverberating chamber can be related to the open site. It appears, in fact, to be a more effective method in the ability to measure a quantity representative of the maximum radiation.

4.3.4 Procedure for the determination of the reverberating chamber limit

The procedure is as follows.

i) Measure a sample of equipment for the maximum radiation on the open-area site. Convert the measured quantities to the equivalent power from a half-wave dipole. Call this quantity P_q, in dB (pW).

ii) Measure the same sample in the reverberating chamber for total radiated power. Call this quantity P_t, in dB (pW).

iii) This relationship between the reverberating chamber limit and the open area test site limit can be found by the graphical method of figure 1, or by calculating the gain of each equipment, obtaining a representative value of G for the equivalent type using statistical methods, and applying equation (4.3-2).

Annex 4.3-A

Derivation of the formula

Consider the general case of a lossless antenna with gain g and input power p. At distance d in the direction of maximum radiation, the field strength e is given by the well-known formula:

$$e = (30 \times p \times g)^{1/2} / d$$

Thus, for two antennas, with gains g_1 and g_2 and input powers p_1 and p_2 producing the same field strength at a point at the same distance in the direction of maximum radiation

$$p_1 \times g_1 = p_2 \times g_2 \text{, or, in log form, } P_1 + G_1 = P_2 + G_2$$

and, in the case given in 4.3.2, $P_1 = P_t$ and $G_1 = G$; $P_2 = P_q$ and $G_2 = 2$ therefore the relationship is

$$P_t + G = P_q + 2$$

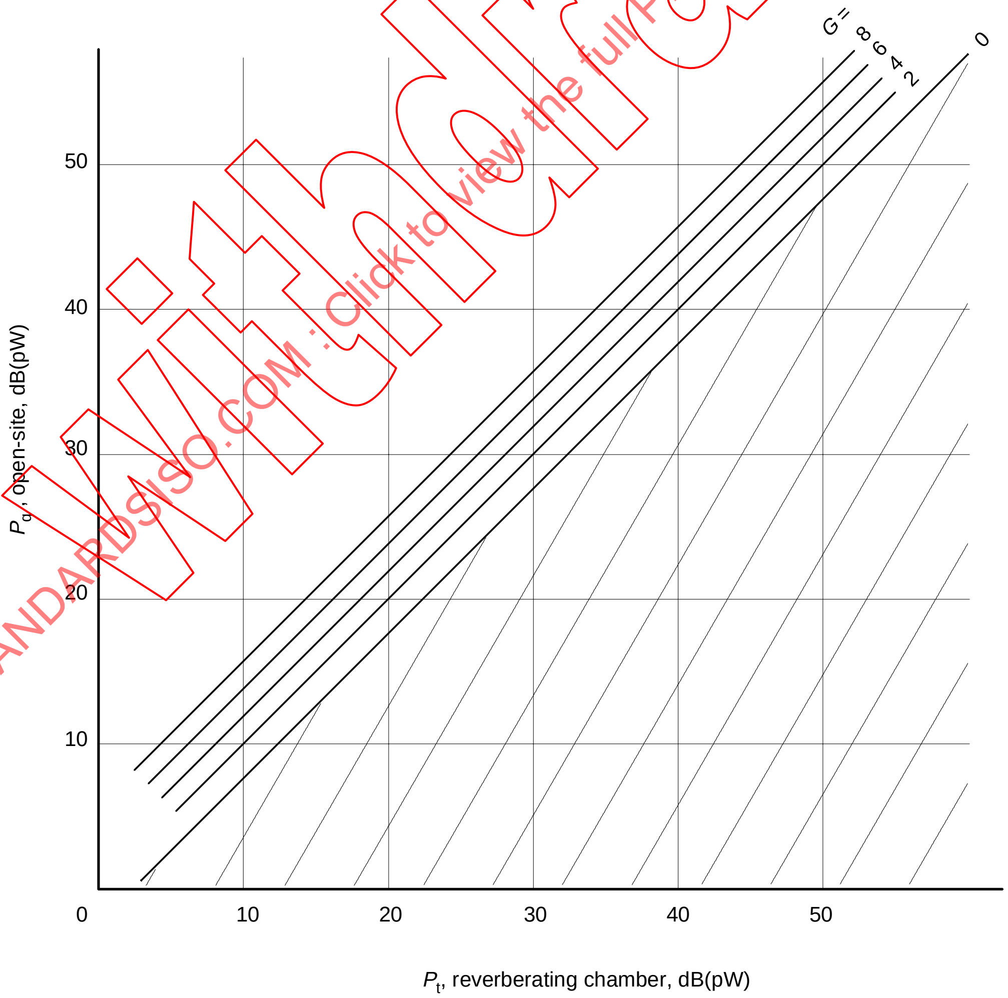

Figure 4.3-1

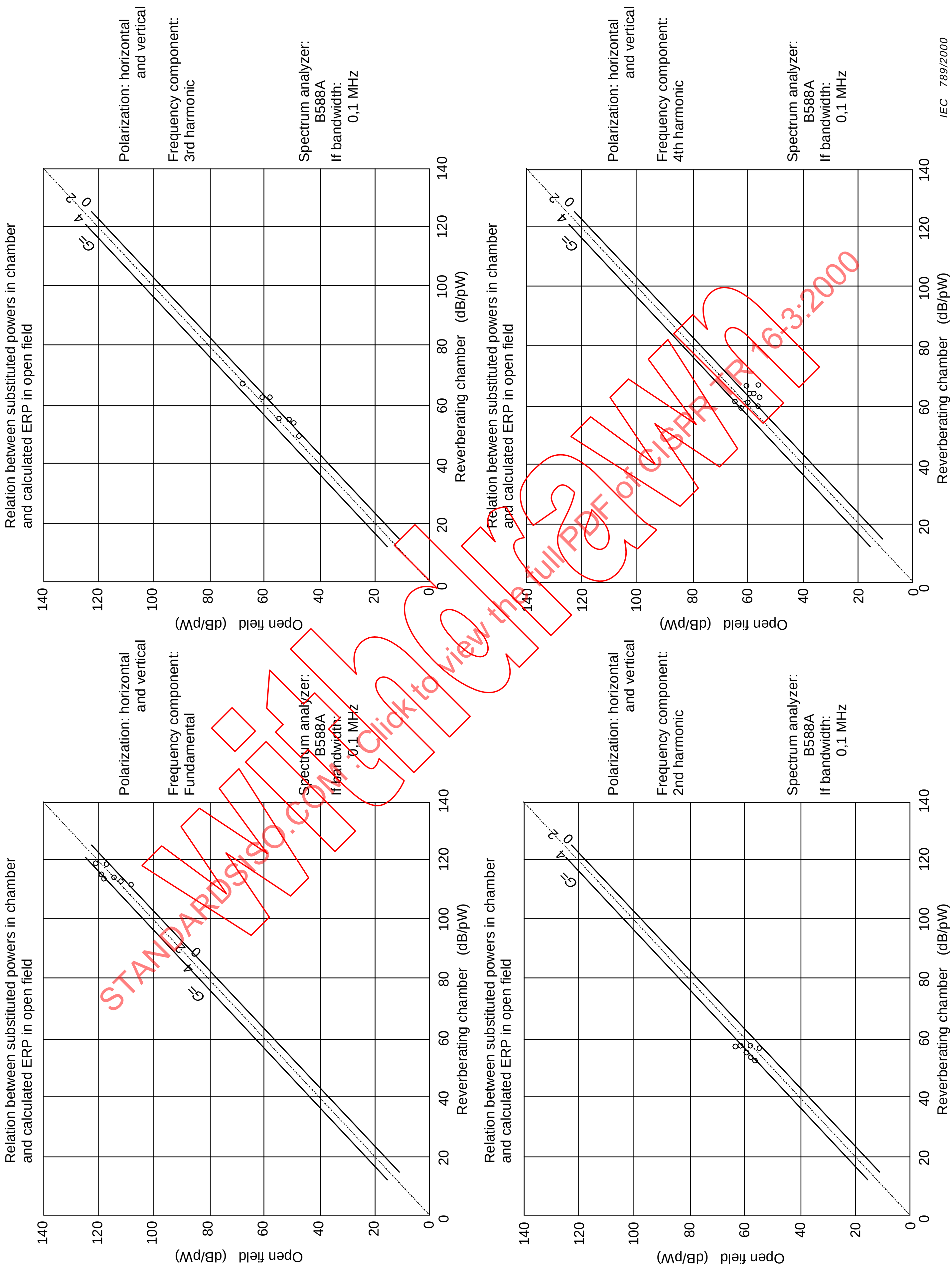
Relation between substituted powers in chamber and calculated ERP in open field
Polarization: horizontal and vertical
Frequency component: Fundamental
Spectrum analyzer: B588A
If bandwidth: 0,1 MHz
Reverberating chamber (dB/pW)
Open field (dB/pW)
Relation between substituted powers in chamber and calculated ERP in open field
Polarization: horizontal and vertical
Frequency component: 3rd harmonic
Spectrum analyzer: B588A
If bandwidth: 0,1 MHz
Reverberating chamber (dB/pW)
Open field (dB/pW)
Relation between substituted powers in chamber and calculated ERP in open field
Polarization: horizontal and vertical
Frequency component: 2nd harmonic
Spectrum analyzer: B588A
If bandwidth: 0,1 MHz
Reverberating chamber (dB/pW)
Open field (dB/pW)
Relation between substituted powers in chamber and calculated ERP in open field
Polarization: horizontal and vertical
Frequency component: 4th harmonic
Spectrum analyzer: B588A
If bandwidth: 0,1 MHz
Reverberating chamber (dB/pW)
Open field (dB/pW)
IEC 789/2000

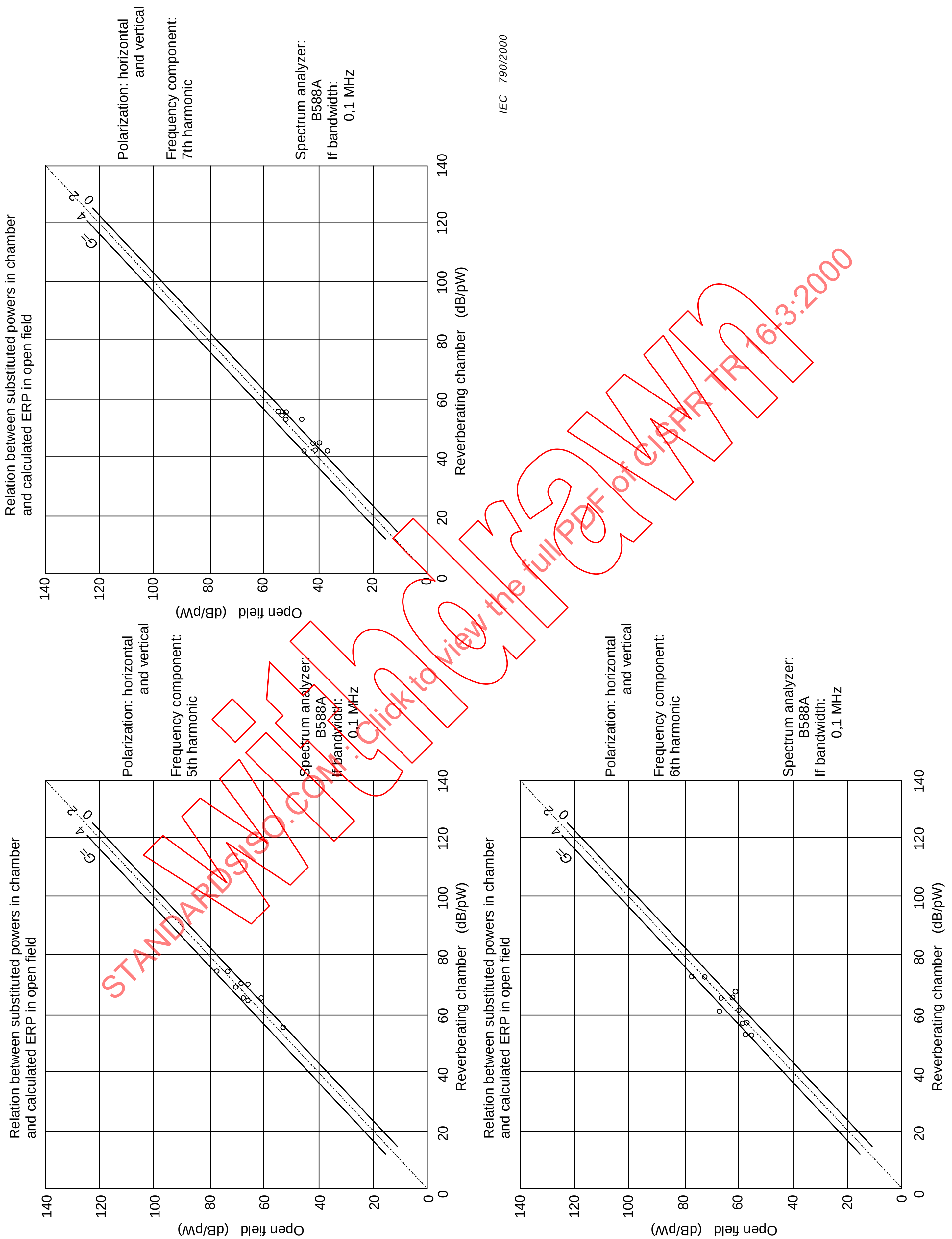

Figure 4.3-2 – Examples of a number of microwave measured for P_q and P_t

4.4 Characterization and classification of the asymmetrical disturbance source induced in telephone subscriber lines by AM broadcasting transmitters in the LW, MW and SW bands

4.4.1 Introduction

The use of semiconductor devices in telephone terminal equipment (TTE) has created the need to verify the immunity to RF fields of this equipment, as non-linear semiconductor devices demodulate the induced RF signals [1-5]. The latter effect gives rise to a d.c. shift which may alter the operating point of such a device, thus, for example, reducing the noise margin of digital devices. In the case of amplitude-modulated RF fields, the non-linearity gives rise to a base-band signal which may become audible in the telephony system. An important class of RF-field sources is formed by AM broadcasting transmitters in the LW, MW and SW bands.

Because of the relatively small dimensions of TTE (compared to the wavelength of the disturbance signal) the asymmetrical (common-mode) source induced in telecommunication lines is expected to be the dominant disturbance source. Therefore, a conducted-immunity test (current-injection test) is relevant for this equipment. In this test, the disturbance signal is applied via the telecommunication lines. As a consequence, this report deals with the characterization of the unwanted antenna properties of telecommunication lines and with prediction models supplying information about the probability that certain parameter values will be met in practice. Moreover, it discusses the parameters which are of relevance when specifying the disturbance source used in the immunity test. The various considerations will be limited to parameters relevant at the subscriber end of the telephone lines.

In 4.4.2 the antenna properties will be expressed in terms of an antenna factor of the subscriber lines i.e. the induced asymmetrical open-circuit voltage normalized to the RF field strength, and an equivalent resistance of the induced asymmetrical source. The prediction models are needed in the classification of the RF fields and the induced asymmetrical disturbances, 4.4.3, and when setting immunity limits, 4.4.4. This report takes the view that the disturbance source in the immunity test is to be specified by an open-circuit voltage and a source impedance.

All mathematical relations associated with the derivation of the models and those needed by the user of this report when applying the models to the respective geographical area are given in annex 4.4-A through 4.4-D.

This report is based on results of experimental investigations carried out on buried telephone-subscriber lines in Germany [6] [7] and in the Netherlands [8]. In these investigations induced-voltage and current data and magnetic-field-strength data were recorded at a large number of locations, permitting a statistical evaluation of the parameter values. A statistical approach was needed, as the telephone lines have random routing in the buildings and, consequently, random orientation with respect to the RF field have random coupling with nearby metal objects, while the buildings cause a random scattering of the RF fields.

It is to be expected that the contents of this report will also be applicable to other types of lines running through buildings in a similar manner to telephone-subscriber lines, for example, bus-system lines and signal and control lines.

4.4.2 Experimental characterization

A full description of the experimental characterization has been presented in [7] [8]. Therefore, this section contains only a summary of this method with regard to the parameters needed in this report.

The induced asymmetrical voltage was measured at the outlet of a telephone-subscriber line using a modified T-network [9] [10]. As a result of this modification, a voltage U_h could be measured across a 10 kΩ resistor and a voltage U_l across a 150 Ω resistor. The investigations showed that U_h can be considered as the induced open-circuit voltage. In practice, the reference for this voltage is generally unknown. During the measurements that reference was a special metal measuring cart connected via a copper strap to the central heating system (CH). The equivalent resistance R_a of the induced source is estimated from data pairs $\{U_h, U_l\}$.

At each location two magnetic-field-strength data of the broadcasting transmitter were measured using a loop antenna positioned in a vertical plane and rotated about its vertical axis to find the maximum reading. One datum, H_i, was measured near the outlet under investigation inside the building, and one datum, H_o, was measured outside the building at a distance of about 10 m from that building. In order to obtain a sufficiently high induced-signal-to-ambient-noise ratio, the measurements were carried out in areas with a relatively high value of the RF field strength. This is not expected to influence the applicability of the results, as the presence of a broadcasting transmitter is not taken into account in the layout of telephone-subscriber lines. Moreover, as mentioned in 4.4.1, the induced voltage will be normalized to the field strength and the resulting "antenna factor" will represent a property of the subscriber lines measured.

4.4.2.1 Field strength and building effect

Although the RF field is not a characteristic of the subscriber lines, it forms the origin of the induced disturbances. Two aspects of the RF field will be considered in this section:

a) The measured field strength H_o outside the buildings compared to the field strength H_c calculated from the simple far-field relation for a half-wave dipole (in its main direction)

$$H_c = \frac{7\sqrt{P}}{Z_0 r} \tag{4.4.2-1}$$

where P is the transmitter power, Z_0 is free-space wave impedance (377 Ω) and r the distance between the transmitter and the point of observation. In the calculations, the values of P as given in [13] will be used.

NOTE Although broadcast transmitter antennas usually are monopoles (in the frequencies of interest), the half-wave dipole formula (4.4.2-1) has been used for convenience.

b) The effect of the building on the field strength, which can be expressed in a building-effect parameter A_b defined by

$$A_b = H_o\ (\text{dB}\mu\text{A/m}) - H_i\ (\text{dB}\mu\text{A/m}) \tag{4.4.2-2}$$

This factor is often called the building attenuation. However, this factor not only depends on the attenuation properties of the building material itself, but also on the reradiation properties of metallic structures in and near the building, and, on the height above ground, H_o and H_i were measured. Therefore the term building effect is used in this report.

A consideration of these two aspects is needed in view of the antenna factors to be discussed in 4.4.2.2 and in view of the prediction models to be discussed in 4.4.2.3.

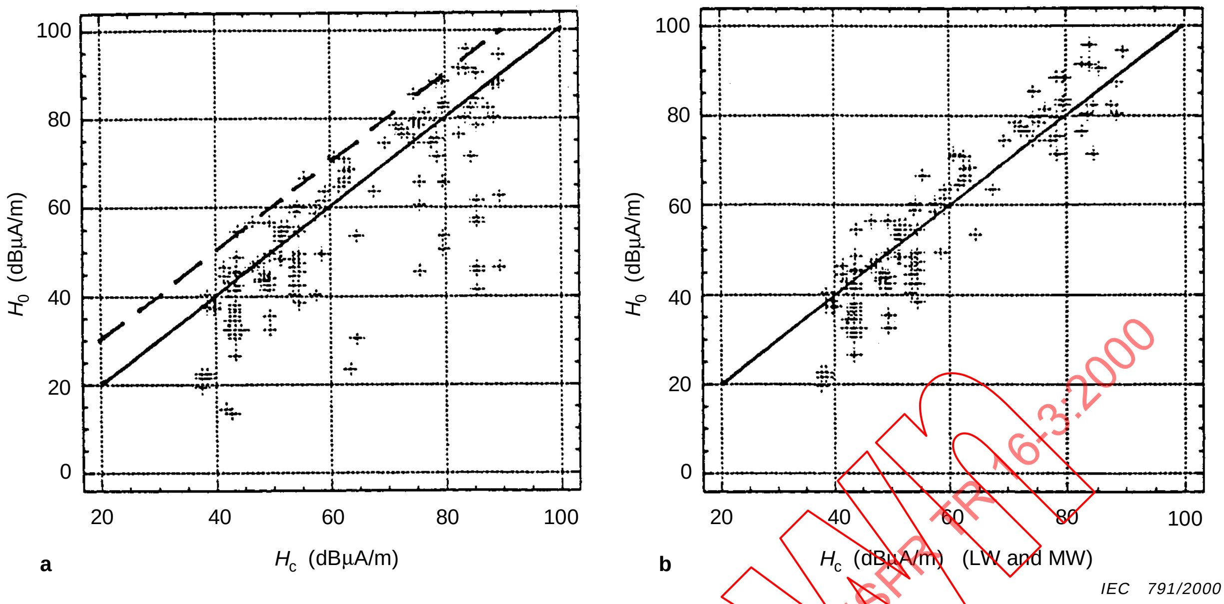

Figure 4.4.2-1 – Scatter plot of the measured outdoor magnetic field strength H_0 (dBµA/m) versus the calculated outdoor magnetic field strength H_c (dBµA/m) a) all data; b) data of SW transmitters rejected

The results of $H_0(H_c)$ given in figure 4.4.2-1a show that large deviations from $H_0 = H_c$ are possible (drawn line), but that $H_0 \leq (H_c + 10)$ dBµA/m (broken line), hence the measured value is at most a factor of 3 higher than the value calculated from equation 4.4.2-1. The largest deviations concern data of SW transmitters. This is understandable, as SW transmitters normally have a beamed antenna pattern, whereas the antenna patterns of the LW and MW transmitters are generally close to circular. Figure 4.4.2-1b gives the scatter plot $H_0(H_c)$ after rejection of the SW transmitter data.

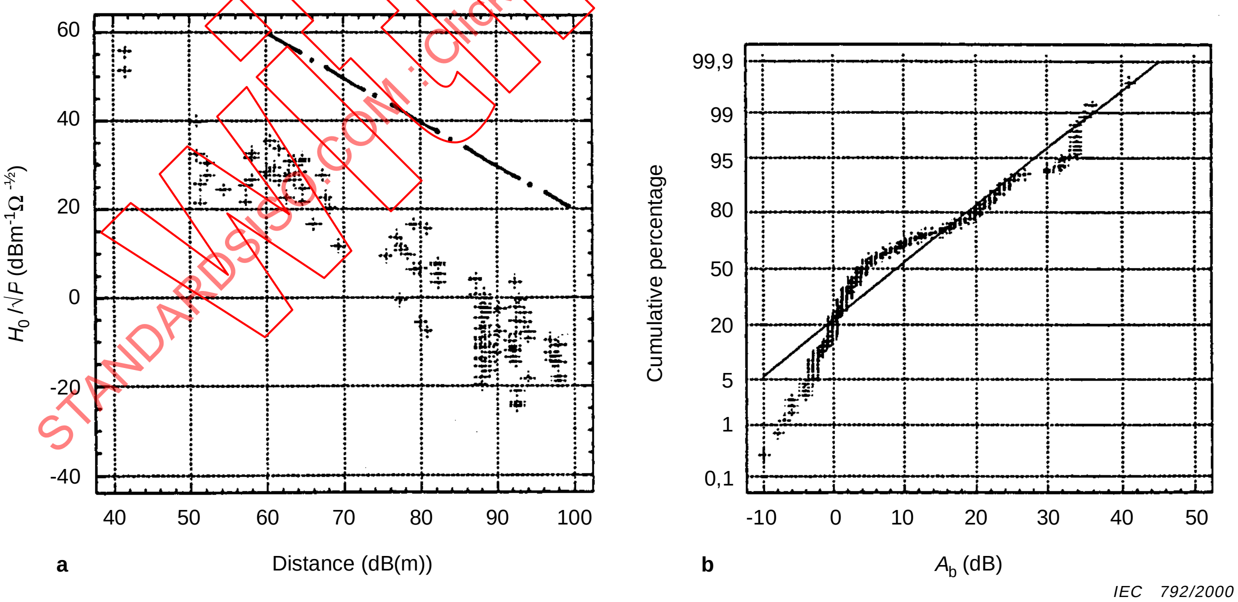

Figure 4.4.2-2 –
a) Scatter plot of the measured outdoor magnetic field strength H_0 normalized to the square root of the reported power [11] versus the distance d (m) to the transmitter,
b) Normal probability plot of the building-effect parameter A_b (dB), all data

Figure 4.4.2-2a shows the ratio $H_0/\sqrt{P}$ versus the distance between the point of observation and the transmitter, and the dash-dot line indicates a slope –1. It can be concluded that, on average, the data follow this slope fairly well. The associated intercept is higher than that expected from equation 4.4.2-1, which is in agreement with the (H_c + 10) dBµA/m limit observed in figure 4.4.2-1.

Figure 4.4.2-2b shows the normal probability plot of all building-effect data. If these data were normally distributed, a straight line would have resulted. This is not the case, and the data suggest that, in first-order approximation, two distributions are superimposed. The two distributions are found when distinguishing between data associated with buildings constructed from brick and/or wood (B/W) and data associated with buildings constructed from reinforced concrete (C). The normal probability plots of these distributions are given in figure 4.4.2-3a and b. The negative values of A_b predominantly stem from measurements where H_i was measured on an upper floor of the building, whereas H_o was already measured at about 1,5 m above ground level outside the building. Effects of reradiation also influence the actual field-strength data.

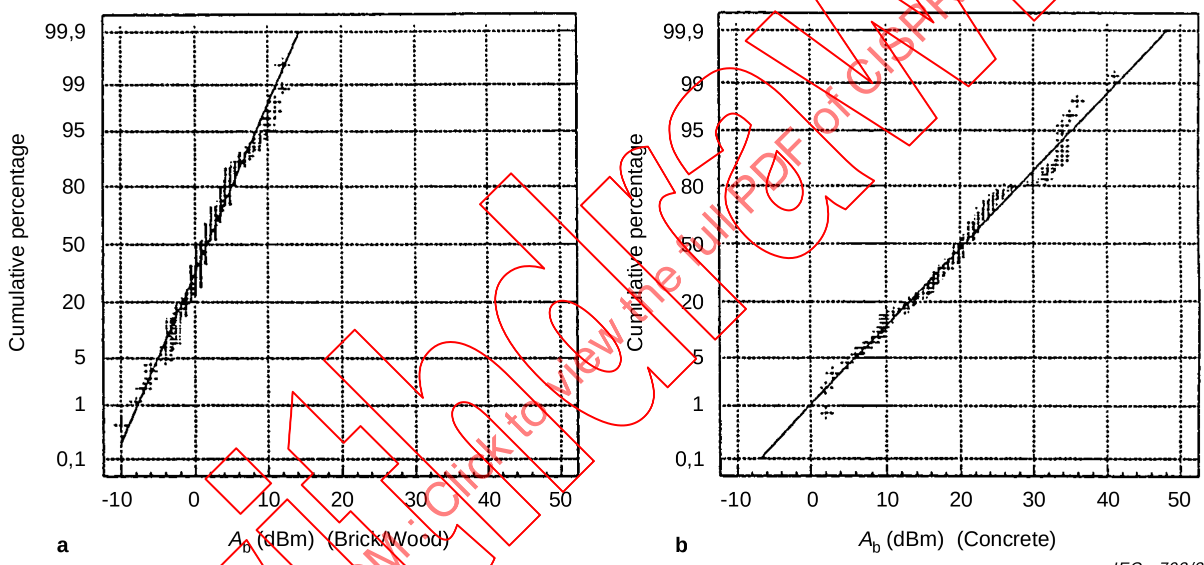

Figure 4.4.2-3 – Normal probability plot of the building-effect parameter A_b (dB)
a) Buildings constructed from brick and/or wood;
b) Buildings constructed from reinforced concrete

The numerical results have been summarized in table 4.4.2-1. No clear frequency dependence of the A_b data could be observed (see 4.4.2.4).

Table 4.4.2-1 – Summary results of building-effect, A_b, analysis

Building material	Average dB	Standard deviation dB	Median dB	Number of data
Brick and/or wood	1,6	4,0	1,0	138
Reinforced concrete	20,6	8,7	20,1	84

4.4.2.2 The asymmetrical open-circuit voltage normalized to the field strength

The interface for the voltage measurements was the outlet to which the telephone set was connected during the measurements. The investigations showed that the influence of the telephone set and its standard lead (4 m long) on the measured voltages could be neglected.

The measured voltage will be normalized to the measured magnetic field strength in 4.4.2.2.1 and, assuming far-field conditions, to the electric field strength in 4.4.2.2.2. After that, 4.4.2.2.3 deals with truncation of the distributions found in 4.4.2.2.1 and 4.4.2.2.2.

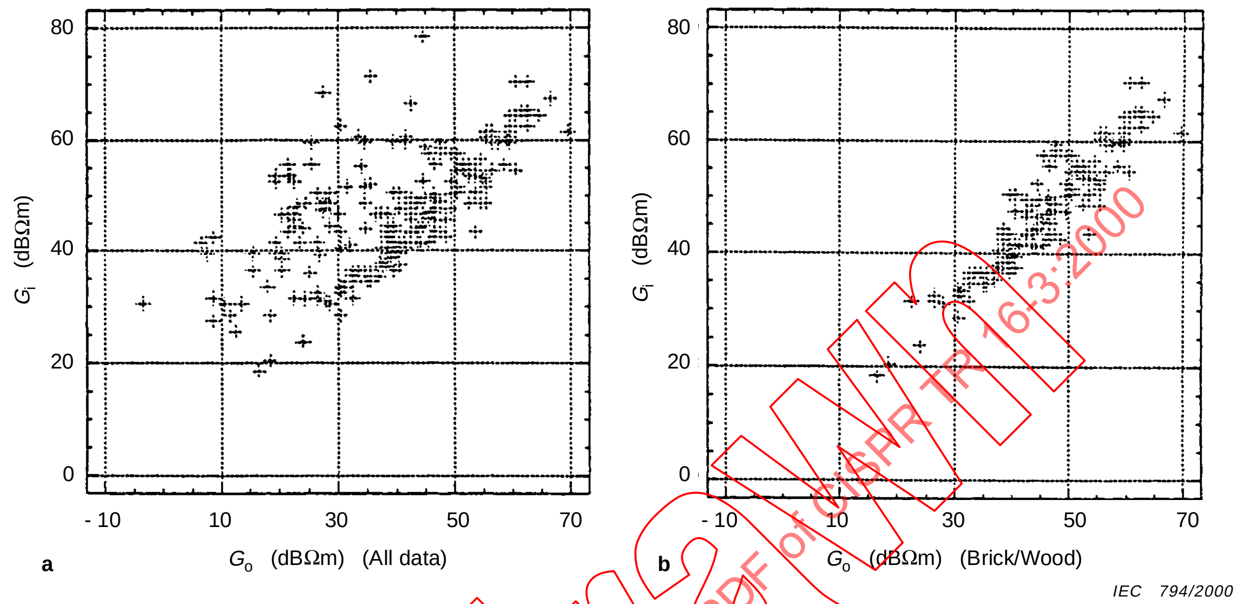

Figure 4.4.2-4 – Scatter plot of the outdoor antenna factor G_o (dBΩm) versus the indoor antenna factor G_j:
a) all data; b) data associated with buildings constructed from brick and/or wood

4.4.2.2.1 *G* factors

To obtain an antenna property of the subscriber lines, the open-circuit voltage U_h is normalized to the field strength (H_i or H_o), yielding the antenna factors G_j and G_o defined by

$$G_{i,o}\,(\Omega\text{m}) = \frac{U_h\ (\mu\text{V})}{H_{ino}\ (\mu\text{A/m})} \qquad (4.4.2\text{-}3)$$

Figure 4.4.2-4a shows the scatter plot $G_i(G_o)$ using all data. The plot suggests that there is one dominant "cloud" of data with a limited scattering and a second "cloud" with much more scattering. Further investigation revealed that the first cloud stems from data measured in buildings constructed from brick and/or wood, see figure 4.4.2-4b, while the other cloud is associated with buildings constructed (predominantly) from reinforced concrete. Consequently, the building effect discussed in 4.4.2.1 is of importance.

The normal probability plots of G_j (dBΩm) and G_o (dBΩm) associated with the two types of building material considered, are given in figure 4.4.2-5. It can be concluded that the data follow a normal distribution, which means lognormal distributions of the *G* factors in Ωm. The numerical results have been summarized in table 4.4.2-2, where G_U and G_L are the upper and lower limit of the range of experimental G data (see 4.4.2.2.3). The differences between G_i and G_o of the two classes of building material considered are in line with the building-effect data for these buildings (see table 4.4.2-1). No clear frequency dependence could be observed (see 4.4.2.4).

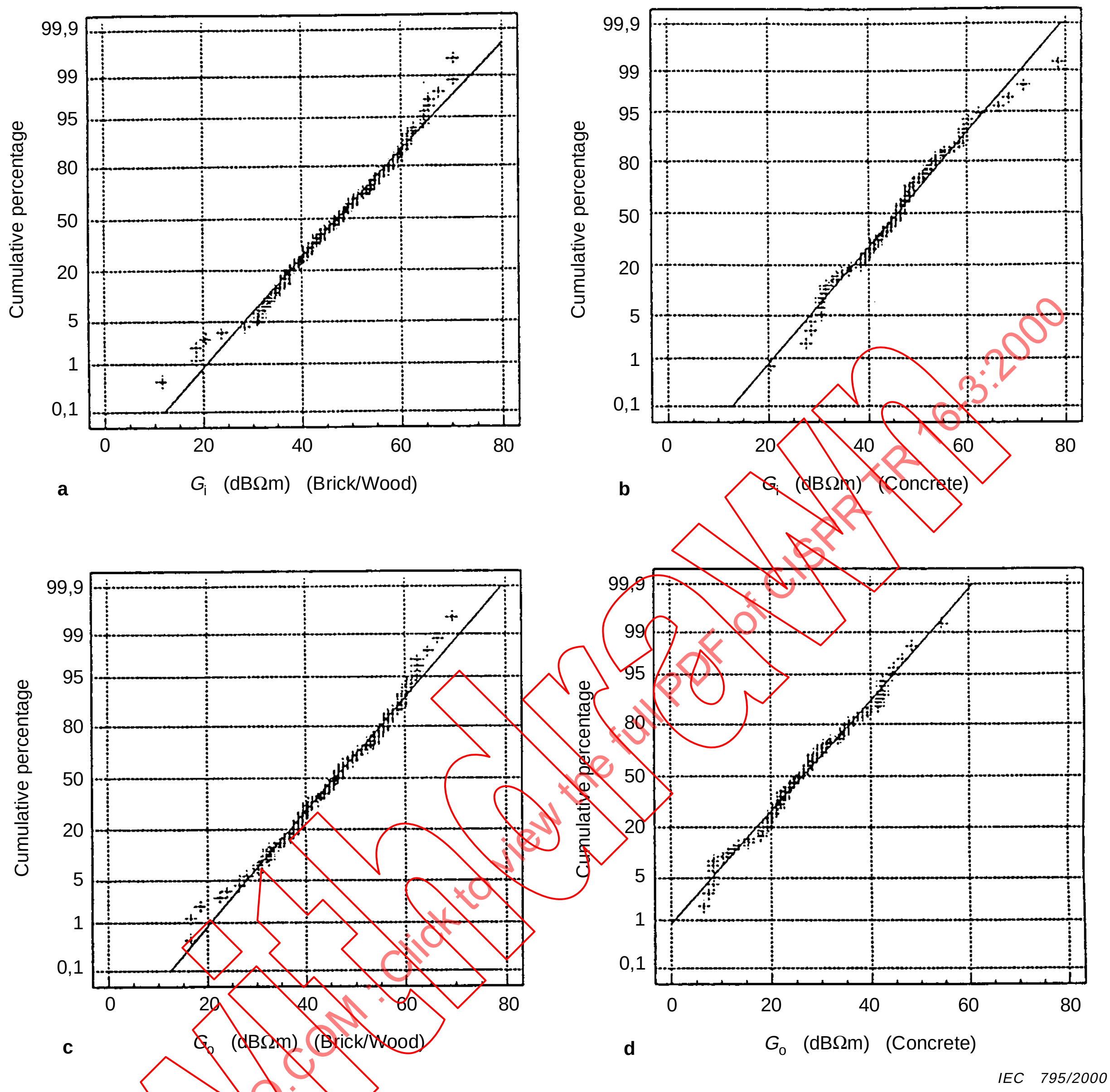

Figure 4.4.2-5 – Normal probability plots of the antenna factors:
a) G_i (dBΩm) and c) G_o (dBΩm) associated with buildings constructed from brick and/or wood;
b) G_i (dBΩm) and d) G_o (dBΩm) associated with buildings constructed from reinforced concrete

Table 4.4.2-2 – Summary of results of *G*-factor analysis

G factor	Building material	Average dBΩm	Standard deviation dB	Median dBΩm	Number of data
G_i	B/W	47,3	11,2	47,5	135
G_i	C	45,9	10,5	46,5	88
G_o	B/W	45,8	10,6	46,4	134
G_o	C	26,5	10,9	26,0	90

4.4.2.2.2 *L* factors

In 4.4.2.2.1, U_h was normalized to the measured magnetic field strength, thus yielding the *G* factors. Assuming far-field conditions, the electric field strength follows from $E = H \cdot Z_0$ with $Z_0 = 377\ \Omega$. If the outdoor field strength is considered, this assumption seems to be reasonable and the G_o factor can be converted into an L_o factor defined by

$$L_o = \frac{G_o}{Z_0} = \frac{U_h}{H_o Z_0} = \frac{U_h\ (\mu\text{V})}{E_o\ (\mu\text{V/m})} \qquad (4.4.2\text{-}4)$$

The *L* factor can be considered as the effective length or effective height of the subscriber line acting as an antenna. The results for L_o have been summarized in table 4.4.2-3, where L_U and L_L are the upper and lower limit of the range of experimental *L* factors (see 4.4.2.2.3).

Table 4.4.2-3 – Summary of L_o factors (far-field)

L factor	Building material	Average* dBm	Standard deviation dB	L_U dBm	L_L dBm
L_o	B/W	–5,7	10,6	18,0	–35,0
L_o	C	–25,0	10,9	3,0	–55,0
* Note that dBm refers to dB with respect to 1 m.					

In the literature an *L* factor of –3,0 dBm average (standard deviation 10 dB, number of data 10) has been reported [12] for a cable running 1 300 m underground and 1 000 m to 3 000 m overhead (aerial cable) towards the subscriber. Broadcasting frequencies were 594 kHz and 1 242 kHz. No details were given about the field-strength measurements, the reference for the asymmetrical voltage and the properties of the building material. The results reported in [12] are in line with the results for L_o (B/W), as given in table 4.4.2-3. However, more recent investigations by the same team [15] indicate an average *L*-factor of 0 dBm.

L_i factors might be derived from the G_i factors in a similar way as the L_o factors. However, it is to be expected that inside the buildings the far-field conditions are not satisfied and it has to be decided which wave impedance has to be taken. Therefore, no L_i data have been presented in table 4.4.2-3. See also note 2 at the end of 4.1.

4.4.2.2.3 Truncation

In 4.4.2.2.1 it was concluded that the distribution $f(G)$ of the *G* factors (antenna factors) is lognormal or in mathematical form

$$f(g)dG = \frac{1}{G\sigma\sqrt{2\pi}}\, e^{\frac{(\ln G - \mu)}{2\sigma^2}}\, dG \qquad (4.4.2\text{-}5)$$

However, by adopting this lognormal distribution it is automatically assumed that a *G* factor may range from zero to infinitely large. In practice, infinitely large will never occur as wavelength effects and effects of coupling with nearby structures create an upper limit (G_U or L_U) of the antenna factors [13]. Consequently, for correct use in the prediction models (4.4.3 and 4.4.4) $f(G)$ has to be truncated. Similarly, truncation has to be applied to the distribution of the building-effect parameters.

Unfortunately, no theoretical study is known which predicts the upper limit of *G* (or *L*) of an actual telephone-subscriber line taking into account the length and the routing of a line inside the building and, buried, outside the building. However, it has to be expected that such a limit exists and the best approach is to use the experimental upper limit (G_U or L_U).

In addition to the upper limit, one may also consider a lower limit (G_L or L_L) and truncate $f(G)$ at the lower end. It is found that in the range of parameter values to be considered in 4.4.3 and 4.4.4, the influence of G_L (or L_L) is negligible.

The truncated probability density function reads

$$f_t(G)dG = \frac{f(G)dG}{\int_{G_L}^{G_U} f(G)dG} = \frac{f(G)dG}{F(G_U) - F(G_L)} = \alpha_t f(G)dG \qquad (4.4.2\text{-}6)$$

The mathematical form of the cumulative distributions $F(G_U)$ and $F(G_L)$ is given in annex 4.4-D. Table 4.4.2-4 summarizes the truncation data of the G factors and the building-effect parameter A_b. Note that αt differs very little from 1, that is from the value of αt if $-\infty \le G$ (dBΩm) $\le \infty$ or $-\infty \le a_b$ (dB) $\le \infty$ since $F(\infty) = 0{,}5$ and $F(-\infty) = -0{,}5$. The upper and lower limit in dBm of the L factor range are found by subtracting 51,5 dBΩ from the corresponding G factors in dBΩm.

Table 4.4.2-4 – Summary of truncation parameters of *f*(*G*)

***G* factor or A_b**	**Building material**	**G_U (dBΩm) A_{bu} (dB)**	**G_L (dBΩm) A_{bl} (dB)**	**$F(G_U)$ $F(A_{bu})$**	**$F(G_L)$ $F(A_{bl})$**	**αt_G αt_A**
G_i	B/W	70,5	11,5	0,4805	–0,4993	1,021
G_i	C	78,5	20,5	0,4985	–0,4922	1,009
G_o	B/W	69,5	16,5	0,4873	–0,4971	1,016
G_o	C	54,5	–3,5	0,4950	–0,4971	1,008
A_b	B/W	12,0	–10,0	0,4953	–0,4981	1,007
A_b	C	41,0	2,0	0,4905	–0,4837	1,026

4.4.2.3 The equivalent asymmetrical-source resistance

The equivalent resistance of the induced asymmetrical source can be determined from data pairs $\{U_h, U_l\}$, where U_h is the open-circuit voltage and U_l the voltage measured across 150 Ω, using the simple relation

$$R_a = \frac{U_h - U_l}{U_l} 150 \ (\Omega) \qquad (4.4.2\text{-}7)$$

The normal probability plot of R_a (dBΩ) is given in figure 4.4.2-6. It can be concluded that R_a (dBΩ) follows a normal distribution and, hence, R_a in Ω follows a lognormal distribution. The numerical results have been summarized in table 4.4.2-5. The average value found is close to the value 150 Ω used in existing immunity tests [9] [14]. In table 4.4.2-5, R_{au} and R_{al} are the upper and lower limit of the range of experimental R_a-data. The relatively large and small values of R_{au} and R_{al} compared to the average value of R_a stem from resonances and anti-resonances in the common mode circuit of the subscriber line. No clear-frequency dependence of R_a could be observed (see 4.4.2.4) and no influence of the building material was observed.

Table 4.4.2-5 – Summary results of equivalent-resistance analysis

R_a (average) dBΩ	Standard deviation dB	Median dBΩ	R_a (average) Ω	Number of data	R_{au} dBΩ	R_{al} dBΩ	R_{au} Ω	R_{al} Ω
44,2	6,8	43,5	162	204	63,7	25,2	1 531	18

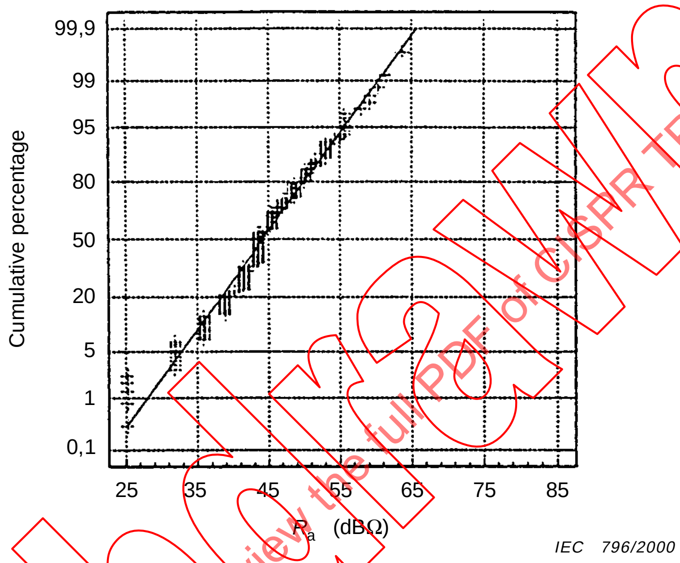

Figure 4.4.2-6 – Normal probability plot of the equivalent asymmetrical resistance R_a (dBΩ)

4.4.2.4 Frequency dependence of the parameters

In the frequency range determined by the measurements in the LW, MW and SW bands, no clear frequency dependence of the building effect A_b, the G factors G_o and G_i, and the equivalent resistance R_a could be observed. This is illustrated in figures 4.4.2-7a and b the A_b data for brick/wood buildings, the R_a data, the G_o data for brick/wood buildings, and for reinforced concrete buildings.

Because no clear frequency dependence of the various quantities could be observed, it will be assumed in 4.4.3 and 4.4.4 that the building effect, the G and the L factors and the equivalent resistance are independent of the frequency in the frequency range of the LW, MW and SW bands. A possible frequency dependence is then incorporated in the standard deviation of the respective distributions.

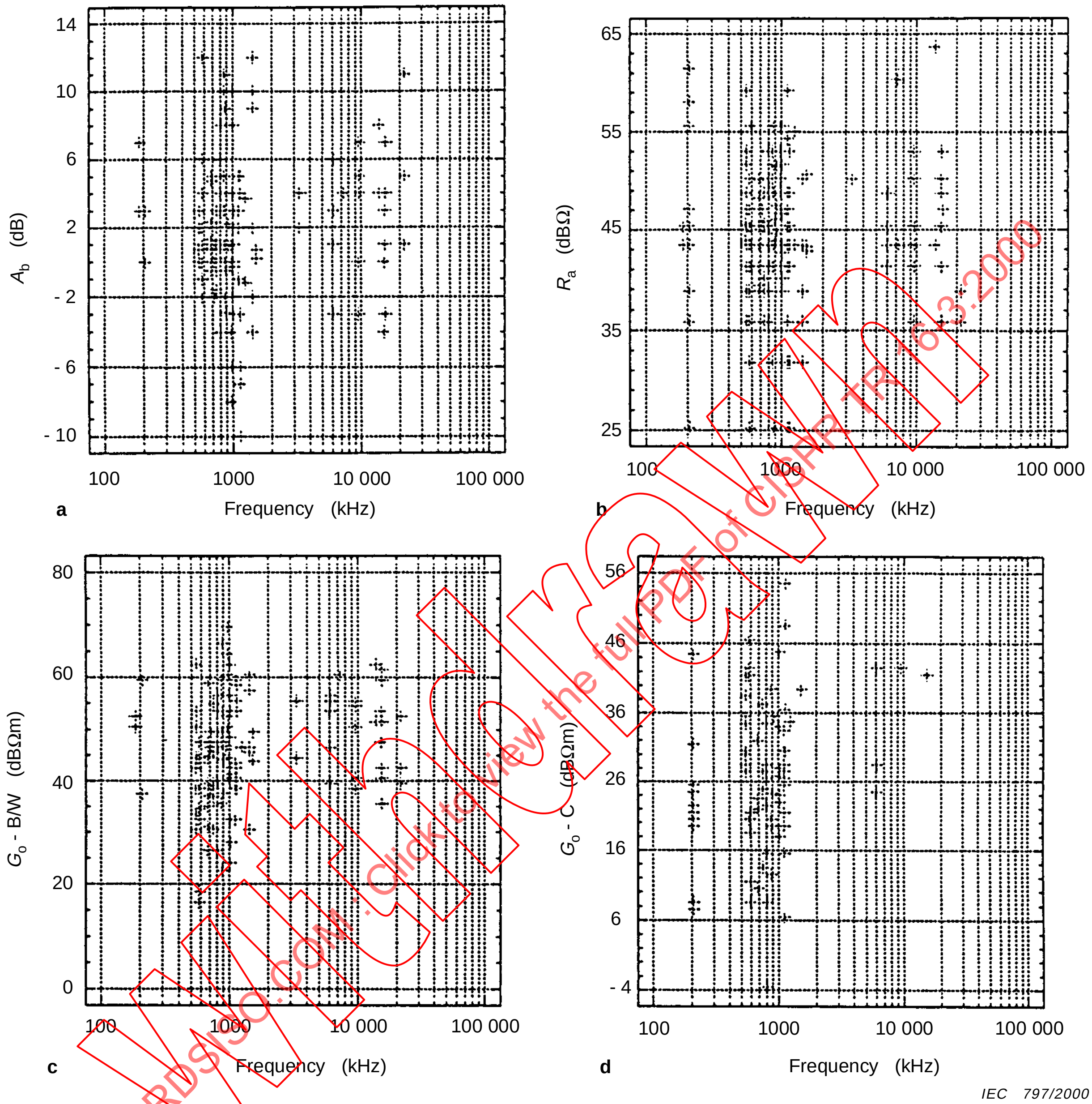

Figure 4.4.2-7 – Examples of the frequency dependence of some parameters

a) the building effect A_b in the case of brick/wood buildings
b) the equivalent resistance R_a
c) the G_o factor for brick/wood buildings, and
d) the G_o factor for reinforced concrete buildings

4.4.3 Prediction models and classification

This section presents some simple prediction models for fields and voltages needed in the process of classification of the electromagnetic environment and when setting immunity limits for the telephone sets to be connected to the subscriber lines.

Because the measuring locations were not chosen randomly in order to obtain a sufficiently high induced signal-to-ambient noise ratio, the basic data from which the parameters reported in 4.4.2 were derived cannot be used directly as they form a non-random sample from their actual distributions. The models to be discussed permit an estimate to be made of the complete distributions of the field strength and induced voltage. In addition, the complete distributions allow for a classification of these quantities. This report gives only the procedure for this classification. The actual class limits are outside its scope.

4.4.3.1 Field-strength classification

As mentioned in 4.4.2.1, the field strength is not a property of the subscriber line. Nevertheless, information about the field strength is needed in order to make a prediction of the induced voltages.

From the results given in 4.4.2.1, it follows that in first-order approximation the outdoor field strength, to be indicated by E_o and H_o for the electric and magnetic field component respectively, is inversely proportional to the distance r between the point of observation and the transmitter, and proportional to the square root of the transmitter power. From the results summarized in 4.4.2.1 it follows that, in the worst case, the constant of proportionality is a factor of 3 (≡ 10 dB) larger than the constant of proportionality in the case of a half-wave dipole.

A classification of the outdoor electric or magnetic field strength may be based on the probability $pr\{E_o \geq E_L\}$ or $pr\{H_o \geq H_L\}$ that the outdoor field strength is equal to or larger than a given limit value, indicated by the subscript L. As explained in annex 4.4-A, this probability can be written as

$$pr\{H_o \geq H_L\} = \int_{H_L}^{H_{max}} f_n(H)dH \text{ or } pr\{E_o \geq E_L\} = \int_{E_L}^{E_{max}} f_n(E)dH \qquad (4.4.3\text{-}1)$$

where $f(H)$ and $f(E)$ represent the normalized field-strength distribution and H_{max} and E_{max} the maximum field strength in the geographical region in which the probability has to be estimated. Under far-field conditions both relations in equation (4.4.3-1) are equivalent.

Considering a ring-shaped area (RSA) around a transmitter having a circular antenna pattern, it follows (see annex 4.4-A) that

$$pr\{E_o \geq E_L\} = \frac{\left(E_{max}^2 - E_L^2\right)E_{min}^2}{\left(E_{max}^2 - E_{min}^2\right)E_L^2} \approx \frac{E_{min}^2}{E_L^2} \qquad (4.4.3\text{-}2)$$

where E_{max} is the field strength at the inner boundary of the RSA and E_{min} the field strength at the outer boundary of the RSA. A similar expression is valid for the magnetic field strength, see annex 4.4-A.

The inner boundary of the RSA has to be specified, as the relation between E_o and r derived from the measuring data will not be valid arbitrarily close to the transmitter, i.e. in the near-field region of the transmitter. A non-zero outer boundary field strength is needed, as $E_{min} = 0$ would mean that $pr\{E_o \geq E_L\} = 0$ for all values of E_L. Note that by definition $pr\{E_o \geq E_L\} = 0$ and that $pr\{E_o \geq E_{min}\} = 1$ (= 100 %). The approximation given in equation (4.4.3-2) is valid if $E_{max} >> \{E_{min}, E_L\}$, which is normally the case. Hence, it can be concluded that in the present model the value of E_{min} to be specified is very important. The choice of E_{min} and E_{max} will be discussed further in 4.4.4.

As an example, table 4.4.3-1 gives the values of E_L for a number of probability values, assuming E_{max} = 60 V/m, which is an example of a radiation-hazard limit in the MW band of frequencies, and E_{min} = 0,01 V/m (= 80 dBμV/m). The latter value is of the order of magnitude of the minimum field strength in the service area of a broadcasting transmitter. Note that the probability values are almost completely determined by E_{min}.

Table 4.4.3-1 – Example of field-strength classification

$pr\{E_o \geq E_L\}$ %	E_L V/m	$\dfrac{E_{min}}{\sqrt{pr\{E_o \geq E_L\}}}$	P = 500 kW	
			k = 7 R_L m	k = 22 R_L m
0	60	–	(80)	(260)
100	0,01	–	495000	1550000
10^{-1}	0,32	0,33	15652	49193
10^{-2}	1,00	1,00	4950	11556
10^{-3}	3,16	3,16	1565	4919
10^{-4}	9,86	10,00	495	1556

By expressing the RSA boundaries in terms of a field strength, and not, for example, in terms of the distance between the transmitter and the point of observation, equation (4.4.3-1) is applicable to any transmitter producing a field strength which is inversely proportional to the distance. However, after the classes have been established, a certain transmitter will have a certain value of the constant of proportionality k. Then class boundaries can be associated with distances R_L = k/P)/E_L between transmitter and point of observation. In table 4.4.3-1 examples of R_L are given, assuming k = 7 (as in the case of a half-wave dipole) and k = 22 (the worst-case value found in 4.4.2.1), while the transmitter power P = 500 kW. The R_L values for E_L = 60 V/m have been put in between brackets, as, in the considered frequency range, the far-field condition is not valid at these distances.

The advantage of choosing the field-strength boundaries first is that the classes are the same for all kinds of transmitter, while the choice of a class is then determined by the probability that victim equipment will be at a certain distance from the chosen class of transmitters. In general, an estimate of the latter probability is easier than an estimate of the field-strength probability.

4.4.3.2 Asymmetrical-voltage classification

A classification of the induced open-circuit common-mode voltage U_h may be based on the probability $pr\{U_h \geq U_L\}$ that U_h is equal to or larger than a given limit value U_L. If $f_t(G)$ describes the truncated distribution of G factors (see 4.4.2.2.3), $f_n(H_o)$ the normalized field-strength distribution and use is made of the relation $U_h = G_o \cdot H_o$, it is shown in annex 4.4-B that this probability can formally be written as

$$pr\{U_h \geq U_L\} = \int_{G_1}^{G_2} dG_o \int_{U_1}^{U_2} dU_h \frac{1}{G_o} f\left(\frac{U_h}{G_o}\right) \cdot f_t(G_o) \qquad (4.4.3\text{-}3)$$

where G_1, G_2, U_1 and U_2 are suitably chosen boundaries (see annex 4.4-B). In this equation the product of the two distributions, i.e. the joint distribution, is needed as $pr\{U_h \geq U_L\}$ depends on simultaneously meeting a certain field-strength value H_o = (=U_h/G_o) and a certain value of G_o. In equation (4.4.3-3) the factor $1/G_o$ stems from the transformation of $f(H_o)$ into $f(U_h/G_o)$.

Note that equation (4.4.3-3) is not an explicit function of the distance between transmitter and point of observation as a consequence of the fact that the boundaries of the RSA have been defined by field-strength values. A similar remark has been made in connection with equation (4.4.3-1) and similar conclusions are possible here.

Considering again the ring-shaped area as introduced in 4.4.3.1, examples of the classification of U_h, i.e. U_L values corresponding with chosen values $pr\{U_h \geq U_L\}$, are given in table 4.4.3-2 classification. The relations used can be found in annex 4.4-B. As in 4.4.3.1, it was assumed that the outdoor field strength E_{max} = 60 V/m (H_{max} = 0,16 A/m) and E_{min} = 0,01 V/m (H_{min} = 27 µA/m) have been specified. When using G_i and specifying the outdoor field strength, the building effect has to be taken into account, as is explained in annex 4.4-B.

Table 4.4.3-2 – Example of voltage classification assuming for the outdoor field strength: E_{max} = 60 V/m and E_{min} = 0,01 V/m

		G_i		G_o	
Building material		**B/W**	**C**	**B/W**	**C**
A_b	dB	1,6	20,6	–	–
S_b	dB	4,0	8,7	–	–
A_{bu}	dB	12,0	41,0	–	–
A_{bl}	dB	–10,0	2,0	–	–
$G_{i,o}$	dBΩm	47,3	45,9	45,8	26,5
S	dB	11,2	10,5	10,6	10,9
G_U	dBΩm	70,5	78,5	69,5	54,5
G_L	dBΩm	11,5	20,5	16,5	–3,5
$pr\{U_h \geq U_L\}$		U_L dBµV	U_L dBµV	U_L dBµV	U_L dBµV
10^{-1}		115	101	114	96
10^{-2}		125	111	124	106
10^{-3}		135	121	134	116
19^{-4}		145	131	143	125

4.4.4 Characterization of the immunity-test disturbance source

The results presented in 4.4.2 and 4.4.3 of this report may be used to specify the open-circuit voltage and the internal impedance of the disturbance source in a conducted-immunity test needed to achieve a sufficiently high probability that TTE to be connected to the subscriber lines will be electromagnetically compatible.

The specification of the open-circuit voltage U_h should be based on the distribution of the voltages over all telephone outlets to be considered. Therefore, this distribution is calculated first, using models and parameter values derived in the preceding sections. Once the distribution is known it is possible to calculate $N_o(U_h \geq U_L)$, i.e. the number of outlets in the respective geographical region showing a voltage $U_h \geq U_L$, where U_L may be considered as the open-circuit voltage in the immunity test. The internal impedance may be chosen directly using the results given in table 4.4.2-3. After that, the relevant parameters for the specification of the disturbance source in the immunity test will be summarized in 4.4.4.2.

This section only gives the procedures to arrive at a specification of the parameters needed. The assignment of actual values is the prerogative of the Product Committees.

4.4.4.1 Outlet-voltage distribution

The derivation of the outlet-voltage distribution is described in detail in annexes 4.4-B and 4.4-C. In this derivation, the following steps have been taken.

1) Determine the total probability density $n(H_o)$ of the telephone outlets experiencing an outdoor magnetic field strength H_o in ring-shaped areas around the N transmitters to be considered, where the inner boundary of the areas is specified by a maximum field strength H_{max} and the outer boundary by a minimum field strength H_{min}.

   (Again, the magnetic field strength is considered first, as this field strength was measured in the experimental characterization procedure. If far-field conditions are valid, so that the magnetic and electric field strength have a constant ratio, the results can be converted directly in terms of the electric field strength.)

2) Determine the joint probability density $f(H_o,G_o) = f(H_o) \cdot f(G_o)$ describing the density of outlets where the field strength has a magnitude H_o and, simultaneously, the antenna factor of the subscriber lines has the magnitude G_o, and convert the result into the joint probability density $f(U_h,G_o)$, by using the relation $U_h = H_o G_o$.

3) Calculate the probability $pr\{U_h \geq U_L\}$. If N_T is the total number of outlets in the respective geographical region and the boundary conditions are taken into account such that $N_o(U_h \geq U_L) = N_T$ (or = 0) if $pf\{U_h \geq U_L\} = 1$ (or = 0), then the number of outlets $N_o(U_h \geq U_L)$ equals $N_T \cdot pr\{U_h \geq U_L\}$.

It is the prerogative of a Product Committee to choose a value of N_o $(U_h \geq U_L)$ from which U_L follows and hence the open-circuit voltage of the disturbance source in the immunity test.

Assuming the field strength to be inversely proportional to the distance between the outlet and the transmitter and assuming constant densities of outlets around the transmitters, it is shown in annex 4.4-C that the field-strength distribution $n(H_o)$ can be written as

$$n(H_o) = \frac{2\pi \sum_{j=1}^{N} \mu_j k_j^2 P_j}{E_o^3} = \frac{-C_{Eo}}{E_o^3} \qquad (4.4.4\text{-}1)$$

where μ_j is the outlet density, k_j the constant of proportionality of the j-th transmitter and N the total number of transmitters considered. If the density μ is the same around all transmitters and all transmitters have the same constant of proportionality k, CH_o is simply a constant times the sum over all transistor powers.

When considering the electric field strength $E_o = (k/P)/r$, the distribution $n(E_o)$ reads

$$n(E_o) = \frac{2\pi \sum_{j=1}^{N} \pi_j k_j^2 P_j}{E_o^3} = \frac{-C_{Eo}}{E_o^3} \qquad (4.4.4\text{-}2)$$

so that $C_{Eo} = C_{Ho} \cdot Z_0^2$. In annexes 4.4-A and 4.4-B it is explained how the various relations change when the indoor field strength H_i or E_i is to be used.

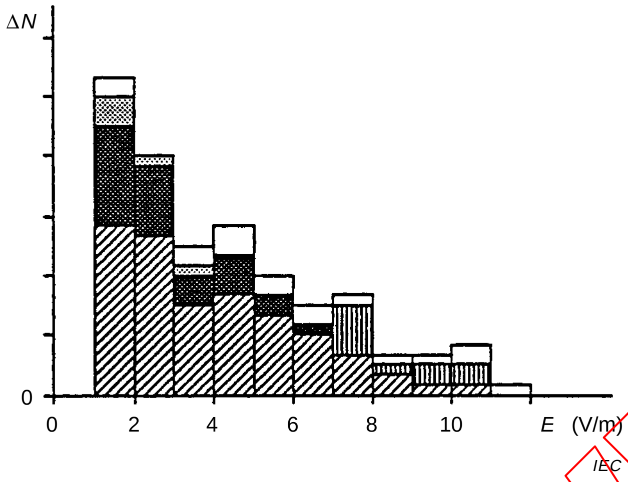

Figure 4.4.4-1 – Example of the frequency histogram $\Delta N(E_0,\Delta E_0)$. The various shadings indicate schematically the contributions from various transmitters and non-homogeneous outlet densities. In this example the field-strength step ΔE_0 = 1 V/m.

The outlet density will, in general, not be homogeneous around a transmitter. To derive $n(H_0)$ in that case, a possible procedure is to determine a frequency histogram $\Delta N(H_0,\Delta H_0)$ so that $n(H_0)$ is approximated by $n(H_0) = \Delta N(H_0,\Delta H_0) / \Delta H_0$.

In practice, the magnitude of the electric field strength is mostly considered, so $n(E_0)$ may be determined first, after which $n(H_0)$ follows after assuming far-field conditions. An example of $\Delta N(E_0,\Delta E_0)$ is given in figure 4.4.4-1, where the different shadings indicate the various contributions resulting from various transmitters and non-homogeneous outlet densities around these transmitters.

A drawback of the method leading to figure 4.4.4-1 and a drawback of the model leading to equations (4.4.4-1) and (4.4.4-2) is that, in particular in the lower field strength regions the fields of the various transmitters overlap. As a result, the same outlets in these regions are counted more than once if no discrimination is made with respect to the broadcast frequency. In 4.4.2.4 it has been explained that no real frequency dependence could be observed, so this discrimination is not possible, which leads to an over-estimate of $\Delta N(E_0,\Delta E_0)$ at the lower field-strength values.

A procedure which might be followed is then to determine $n_m(E_0)$, the distribution of the maximum field strength in the respective geographical region resulting from the N relevant transmitters in (and in the direct vicinity of) that region. An example of such a distribution is given in figure 4.4.4-2. This distribution resulted for a part of Germany (having an area of $2{,}5 \cdot 10^5$ km^2 and $42 \cdot 10^6$ outlets) by calculating the maximum field strength in each node at a 1 km by 1 km grid over this region as caused by one of the 79 actual broadcasting transmitters in the respective frequency range, having a total ERP of 12,2 MW. The resolution of the field strength, i.e. ΔE_0 was taken to be 0,1 dBµV/m. It was assumed that the density μ was a constant ($42 \cdot 10^6/2{,}5 \cdot 10^5 = 168$ km^{-2}) throughout the region. When performing these calculations it was found that $n_m(E_0)$ does not vary much after a certain number (50 in this case, with a total power of 7,5 MW) of transmitters had been taken into account.

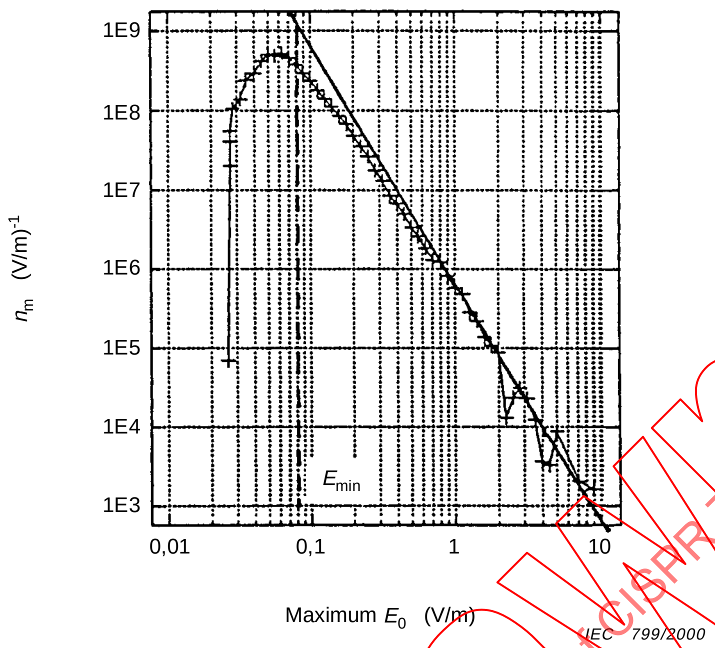

Figure 4.4.4-2 – Example of $n_m(E_o)$ the distribution of the outlets experiencing a maximum field strength E_o resulting from a given number of transmitters in (or near) the respective geographical region. The drawn line represents $n(E_o) = -C_{Eo}/E_o^3$ with $n(E_o = 1\ \text{V/m}) = n_m(E_o = 1\ \text{V/m})$. E_{min} has been chosen such that the integral over the field strength of $n_m(E_o)$ and $n(E_o)$ both yield the total number of outlets in that region

The drawn line in figure 4.4.4-2 represents $n(E_o) = -C_{Eo}/E_o^3$ with C_{Eo} taken such that $n_m(E_o) = n(E_o)$ when $E_o = 1$ V/m. This value is somewhat smaller than C_{Eo} calculated from equation 4.4.4-2 due to the aforementioned fact that $n_m(E_o)$ seems to "saturate" when the number of transmitters is increased.

When integrating the distributions over the whole of the respective region, the total number of outlets N_T must follow, i.e.

$$N_T = \int_{E\,min}^{E\,max} n(E_o)\,dE_{Eo} = \frac{C_{Eo}}{2}\left\{\frac{1}{E_{min}^2} - \frac{1}{E_{max}^2}\right\} \qquad (4.4.4\text{-}3)$$

where the right-hand side of equation (4.4.4-3) follows when equation (4.4.4-2) is used. Equation (4.4.4-3) indicates that for a given or agreed maximum field strength E_{max}, the value of E_{min} follows when C_{Eo} is given or that C_{Eo} follows when E_{min} is given. The former approach has been used to calculate E_{min} = 0,08 V/m as indicated in figure 4.4.4-2, assuming $n_m(E_o = 1\ \text{V/m}) = C_{Eo}/E_o^3 = C_{Eo}$) 5,4 · 10^5 (V^2/m^2).

Table 4.4.4-1 – Summary of the parameters used in the numerical examples presented in figures 4.4.4-3 and 4.4.4-4. Some curves have the same parameter values: Figure 4.4.4-4a) curve 2 and figure 4.4.4-3, and figure 4.4.4-4b curve 1 and figure 4.4.4-4a curve 3

Figure	4.4.4-3	4.4.4-4a			4.4.4-4b		
Curve	–	1	3	4	2	3	4
L-factor	L_o	L_o	L_o	L_o	L_i *	L_o	L_i *
Building material	B/W	B/W	B/W	B/W	B/W	C	C
M_L dBm	–5,7	–5,7	–5,7	–5,7	–4,2	–25,0	–5,6
S_L dB	10,6	10,6	10,6	10,6	11,2	10,9	10,5
L_u dBm	18,0	+∞	18,0	18,0	19,0	3,0	27,0
L_u m	7,9	+∞	7,9	7,9	8,9	1,4	22,4
L_i dBm	–35,0	–∞	–35,0	–35,0	–40,0	–55,0	–31,0
L_i m	0,02	–∞	0,02	0,02	0,01	0,002	0,03
M_A dB	–	–	–	–	1,6	–	20,6
S_A dB	–	–	–	–	4,0	–	8,7
A_{bu} dB	–	–	–	–	12,0	–	41,0
A_{bl} dB	–	–	–	–	–10,0	–	,0
N_T millions	42	42	42	42	42	42	42
C_{Eo} V^2/m^2	$5,4 \cdot 10^5$	$5,4 \cdot 10^5$	$5,4 \cdot 10^5$	$5,4 \cdot 10^5$	–	$5,4 \cdot 10^5$	–
C_{Ei} V^2/m^2	–	–	–	–	$3,3 \cdot 10^4$	–	–
E_{max} V/m	10,0	10,0	3,0	10,0	3,0	3,0	3,0
$E_{i,max}$ V/m	–	–	–	–	9,5	–	2,4
E_{min} V/m	0,08	0,08	0,08	0,008	0,08	0,08	0,08
$E_{i,min}$ V/m	–	–	–	–	0,02	–	0,0007
U_{max} V	79	+∞	24	79	85	42	53
* See note 3 at the end of this subclause.							

This subclause is concluded by giving several numerical examples of $N_0(U_h \geq U_L)$, i.e. of the number of outlets in the respective geographical region showing an induced open-circuit voltage $U_h \geq U_L$, where U_L may be considered as the open-circuit voltage in the immunity test. The region in these examples is the aforementioned part of Germany. The relations used in the calculation of $N_0(U_h \geq U_L)$ can be found in annexes 4.4-B and 4.4-C. The values of the various parameters used in these calculations have been summarized in table 4.4.4-1.

Figure 4.4.4-2 shows an example of $N_0(U_h \geq U_L)$ in the voltage range $U_L \leq U_{max}$ = 79 V, based on L_0 data for buildings constructed from brick and/or wood (B/W) and assuming that all 42 million outlets are in these types of building. U_{max} (see also table 4.4.4-1) is given by $U_{max} = E_{max}L_U$, where E_{max} is the maximum outdoor field strength in the respective geographical region and L_U the upper limit of the range of L_0(B/W) data (see 4.4.2.2.2). U_{max} is quite large in this case. The maximum value measured in the experimental investigations was 22 V.

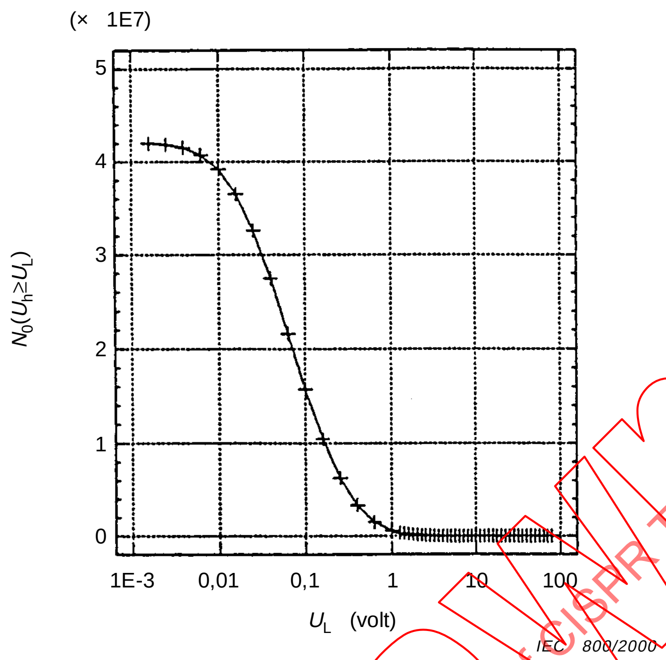

Figure 4.4.4-3 – Example of the number of outlets with an induced asymmetrical open-circuit voltage $U_L \leq U_h \leq U_{max}$ = 79 V, see table 4.4.4-1. Total number of outlets $N_T = 42 \cdot 10^6$

To set the specifications for an immunity test the higher range of U_L values is of interest. Therefore, the results given in figure 4.4.4-3 have been replotted as Curve 2 in figure 4.4.4-4a. Curve 1 in figure 4.4.4-4a gives $N_0(U_h \geq U_L)$ for the same situation as in figure 4.4.4-3 but neglecting the truncation of the *L* factor distribution. In that case U_{max} is infinitely large, which is not very realistic. Curve 3 in figure 4.4.4-4a demonstrates how the results represented by Curve 2 are modified when E_{max} is reduced from 10 V/m to 3 V/m. Then U_{max} = 24 V. Finally, Curve 4 in figure 4.4.4-4a demonstrates how the results represented by Curve 2 are modified when E_{min} is reduced from 0,08 V/m to 0,008 V/m. The latter curve clearly demonstrates the importance of the minimum field strength in the geographical region.

In figure 4.4.4-4b the influence of the building material (B/W or reinforced concrete, C) and the choice of *L* factor (L_o or L_i) on the results can be observed. Curve 1 in that figure is identical to Curve 3 in figure 4.4.4-4a, so it concerns L_o data for B/W-buildings. When using L_i data the building effect has to be taken into account as there is no direct model to predict the indoor field-strength distribution. By doing so, the results represented by Curve 2 are found. As for Curve 1 the maximum outdoor field-strength E_{max} = 3 V/m, but due to the building effect the maximum indoor field strength $E_{i,max} = E_{max}\ A_{bi}$, where A_{bi} is the lowest building effect as determined from the experimental data. In this case A_{bi} = –10 dB, so that $E_{i,max}$ = 9,5 V/m, hence an amplification of the outdoor field strength.

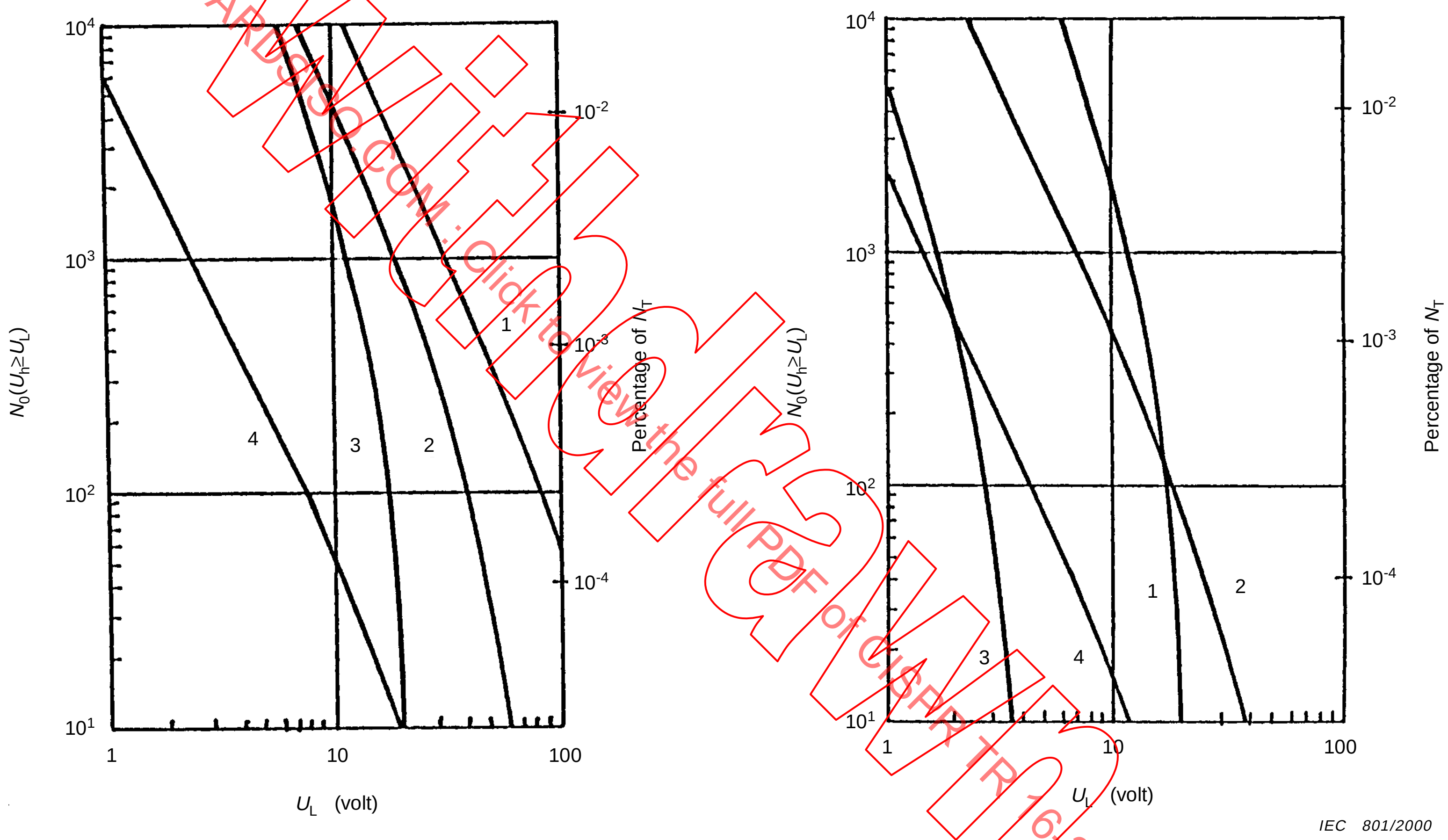

Figure 4.4.4-4 – Examples of number (left-hand scale) and relative number (right-hand scale) of outlets with $U_L \leq U_h \leq U_{max}$. See table 4.4.4-1 for the various parameter values used. Total number of outlets $42 \cdot 10^6$, homogeneous density of the outlets: μ = 168 km^{-2}

a) B/W buildings

Curve 1: nontruncated L_o factor, E_{max} = 10 V/m, E_{min} = 0,08 V/m

Curve 2, truncated L_o factor, E_{max} = 10 V/m; E_{min} = 0,08 V/m

Curve 3, truncated L_o factor, E_{max} = 3 V/m; E_{min} = 0,008 V/m

Curve 4, truncated L_o factor, E_{max} = 10 V/m; E_{min} = 0,08 V/m

b) Truncated *L* factors, maximum outdoor field strength 3 V/m

Curve 1: B/W buildings, L_o factor

Curve 2: B/W buildings, L_i factor

Curve 1: C buildings, L_o factor

Curve 2: C buildings, L_i factor

One might argue that a negative value of A_{bi} is not realistic. As mentioned in 4.4.2.1, the negative values predominantly originated from measurements where the indoor field strength was measured at an upper floor of the building and the outdoor field strength at 1,5 m above ground level. Furthermore, reradiation effects also influenced the actual field-strength data. One may decide to truncate the building-effect distribution at the lower end at 0 dB. In that case $E_{i,max}$ and U_{max} reduces from 85 V to $L_u E_{max}$ = 8,9 × 3 = 27 V.

Assuming that all 42 million outlets are located in reinforced concrete buildings the results represented by Curve 1 in figure 4.4.4-4b are modified into those represented by Curve 3, while Curve 4 follows if the L_i data are used. In practice, the outlets will be distributed over the B/W and C buildings. Then N_T in the calculations is the total number of outlets in a given type of building, and the results for both types of building have to be added.

NOTE 1 Although the number of outlets $N_o(U_h \geq U_L)$ as given in figure 4.4.4-4 may have noticeable values, the relative number is very low. This stresses the importance of the "tails" of the various distributions used and of the applied truncation. In addition, if the analytical expressions given in the annexes are not used, but a full-numerical calculation is made (for example, one starting with $n_m(E_o)$), care has to be taken that the accuracy of the numerical calculations is sufficiently high. The very low values of the relative number $N_o(U_h \geq U_L)/N_T$ form an indication of the accuracy needed. The relative number is identical to $pr\{U_h \geq U_L\}$ in per cent.

NOTE 2 In all calculations the density of the outlets μ was considered to be a constant over the whole respective region. The results can be improved when, for example, the calculations leading to $n_m(E_o)$, see figure 4.4.4-2, take a location-dependent μ into account.

NOTE 3 Curves 2 and 4 in figure 4.4.4-4b are based on L_i and A_b data, and a warning has to be given here. As mentioned in 4.4.2, it is not very likely that inside the buildings the far-field condition will be satisfied and, formally speaking L_i cannot be derived from G_i. In addition A_b has been determined from magnetic field-strength data and A_b for the electric field need not be the same. In the calculations leading to curves 2 and 4, it has tacitly been assumed that $L_i = G_i/Z_0$ (Z_0 = 377 Ω). However, the same curves for $N_o(U_h \geq U_L)$ would have been found when correctly using the G_i and A_b, but quoting on Row 15 and 16 of table 4.4.4-1 the magnetic field quantities $H_{max} = E_{max}/Z_0$ etc. and replacing C_{Ei} by $C_{Hi} = C_{Ei}/Z_0^2$ (see clause 4.4.A-3 in annex 4.4-A).

4.4.4.2 Summary of disturbance source parameters

Assuming that the disturbance source in the conducted-immunity test is sufficiently described by an open-circuit voltage and an internal impedance, the following parameters are of importance.

The internal impedance

The internal impedance may be specified as a purely resistive quantity, of which the magnitude is chosen on the basis of the results for the equivalent asymmetrical resistance R_a, as given in 4.4.2.3. The choice depends on the reference for the asymmetrical disturbance source considered to be relevant in the situations where interference problems have to be prevented. An often used value is R_a = 150 Ω [9] [10] [14] which is not in conflict with R_a results presented in 4.4.2.3.

The open-circuit voltage

Because the induced asymmetrical voltage has been measured at non-random locations in order to have a sufficiently large induced-signal-to-ambient-noise ratio, the bare U_h data cannot be used and the procedure described in 4.4.4.1 has to be followed. From that procedure, described in more detail in annexes 4.4-B and 4.4-C, it can be concluded that the following parameters have to be considered (see also table 4.4.4-1).

a) N_T — The total number of outlets in the geographical region (country) to be considered. N_T is either the grand total of outlets or the total number of outlets in a certain type of building (brick/wood or reinforced concrete).

b) M_G or M_L — The average value of the *G* or *L* factor, in dBΩm or dBm, see tables 4.4.2-2 and 4.4.2-3. If the G_i or L_i factors are used, the following building effect parameters must be known (see tables 4.4.2-1 and 4.4.2-4):

   M_A: the average building effect A_b in dB

   S_A: the standard deviation of A_b in dB

   A_{bu}: the maximum building effect

   A_{bl}: the minimum building effect

c) S_g or S_L — The standard deviation (in dB) associated with M_G or M_L

d) G_U, G_L, L_U, L_L — The upper and lower limit of the *G*-factor range or the *L*-factor range

e) H_{max} or E_{max} — The upper boundary of the outdoor field strength in A/m or V/m which determines the inner boundary of the areas around the transmitters to be considered.

   This value may be chosen after considering radiation hazards. However, in particular in the case of mass-produced appliances the following consideration seems to be relevant. Choose (or agree on) a maximum field strength of *X* (A/m or V/m) such that there is a high probability that all equipment will be electromagnetically compatible when the field strength is equal to or smaller than *X* (A/m or V/m), and agree that special EMC hardening measures are to be taken in that part of the region where the field strength is larger than *X* (A/m or V/m) and (simultaneously) a complaint occurs.

f) H_{min} or E_{min} — The minimum field strength determining the outer boundary of the areas around the transmitters (see 4.4.4.1).

   This value has only to be chosen when the field-strength distribution $n(H)$ or $n(E)$ is unknown. If this distribution is known, H_{min} or E_{min} is calculated from an equation like equation (4.4.4-3).

g) $n(H)$ or $n(E)$ — The field-strength distribution as discussed in 4.4.4.1 and annex 4.4-A.

4.4.5 Bibliography

[1] *Determining EMI in microelectronics – A review of the past decade*, J.J. Whalen, Proc. Intern. Symp. on EMC, pp 337-344, Zurich, Switzerland, March 1995

[2] *A modified Ebers-Moll transistor model for RF interference analysis*, C.E. Larson and J.M. Roe, IEEE Trans. on MEC, vol. EMC-21, pp 283-290, Nov 1979

[3] *The combined effects of internal noise and electromagnetic interference in CMOS VLSI circuits*, K. Liu and J.J. Whalen, Proc. 6th Intern. Symp. on EMC, p 303, York, United Kingdom, Sep 1988

[4] *Interference effects in CMOS and TTL integrated circuits*, B. Demoulin, C. Lardé and P. Degauge, Proc. Intern. Symp. on EMC, pp 543-546, Zurich, Switzerland, March 1989

[5] *EMI problems associated with non-linear device characteristics*, Proc. 1st Intern. Symp. on EMC, Madrid, Spain, Nov 1990

[6] *EMC* Working Group of the ZVEI (Union of Electrotechnical Industries), P.O. Box 700969, 6000 Frankfurt/Main 70, Germany

[7] *RF disturbances on telephone-subscriber lines induced by AM broadcasting transmitters*, J.J. Doedbloed and G. Jeschar, Proc. Intern. Symp. on EMC, pp 537-542, Zurich, Switzerland, March 1989

[8] *Characterization of transient and CW disturbances induced in telephone-subscriber lines*, J.J. Goedbloed and W.A. Pasmooij, Proc. Intern. Symp. on EMC, pp 211-218, York, United Kingdom, Aug 1990

[9] *Funk-Entstörung von Anlagen und Geräten der Fernmelde Technik*, DIN/VDE 0878, Part 1/12.86, Dec 1986

[10] Amendment of Publication 16, Part 1, Clause 20: T-type networks, CISPR/A(Secretariat)98, March 1989

[11] *World Radio and TV Handbook*, 1986

[12] *Radio broadcast induction voltage and pair unbalance in subscriber cable*, M. Hatori, F. Ohtsuki, T. Motomitsu and H. Koga, IEEE Intern. Symp. on EMC, pp 884-889, 1984

[13] *Calculation of voltage induced into telecommunication lines from radio stations broadcasts and method of reducing interference*, CCITT Recommendation K.18

[14] *Measurement of the immunity of sound and television broadcast receivers and associated equipment in the frequency range 1,5 MHz to 30 MHz by the current-injection method*, CISPR Publication 20, 1985

[15] *Electromagnetic interference and countermeasures on metallic lines for ISDN*, M. Hattori and T. Ideguchi, IECEE trans. on Communications, Vol. E75-B, No. 1, Jan 1992

Annex 4.4-A

The field-strength distribution

This annex considers the probability $pr\{H_o \geq T_L\}$ that in a ring-shaped area around a transmitter the outdoor magnetic field strength H_o is equal to or larger than a given field strength H_L. The magnetic field strength has been chosen because the experimental data presented in 4.4.2 are based on magnetic-field-strength measurements. At the end of this annex expressions will be given based on the outdoor electric field strength E_o, assuming that the far-field condition is fulfilled.

4.4-A.1 H_o-field expressions

Recalling the results given in 4.4.2, it is assumed that H_o can be written as

$$H_o = \frac{k\sqrt{P}}{rZ_0} \quad (r \geq R_{min}) \tag{4.4-A1}$$

where k is a constant, r the distance between the transmitter and the point of observation, P the transmitter power and Z_0 the free-space wave impedance. The condition $r \geq R_{min}$ is needed to indicate that equation (4.4-A1) is not valid close to the transmitter, i.e. in the near-field region.

Using equation (4.4-A1), it follows that:

$$pr\{H_o \geq H_L\} = pr\left\{\frac{1}{r} \geq \frac{1}{R_L}\right\} = pr\{r \leq R_L\}, \; (R_L \leq R_{max}) \tag{4.4-A2}$$

where $R_L = (k/P) / (H_L Z_0)$. The latter probability is equal to the area of the ring determined by R_L and R_{min}, see figure 4.4-A1, normalized to the area of the total ring, i.e. the ring determined by R_{min} and R_{max}. A finite outer boundary R_{max} has to be specified, as an infinitely extended region around the transmitter would create an infinitely large region with field strength zero, thus meaning that $pr\{H_o \geq H_L\}$ would be approaching zero for all values of H_L with $R_L > R_{min}$.

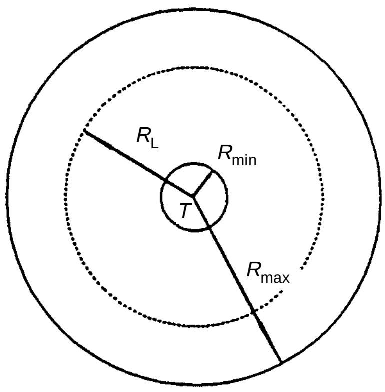

IEC 802/2000

Figure 4.4-A1 – Definition of the ring-shaped area round the transmitter *T*

The probability can now be written as

$$pr\{H_o \geq H_L\} = \frac{\pi\left(R_L^2 - R_{min}^2\right)}{\pi\left(R_{max}^2 - R_{min}^2\right)} = \frac{H_L^{-2} - H_{max}^{-2}}{H_{min}^{-2} - H_{max}^{-2}} \quad (4.4\text{-A3})$$

or as

$$pr\{H_o \geq H_L\} = \frac{\left(H_{max}^2 - H_L^2\right)H_{min}^2}{\left(H_{max}^2 - H_{min}^2\right)H_L^2} \quad (4.4\text{-A4})$$

where H_{min} = (k/P) / ($R_{max}Z_0$) and H_{max} = (k/P)/($R_{min}Z_0$), i.e. H_{max} and H_{min} are the field strength at the inner boundary and the outer boundary of the ring-shaped area. In the case where $H_{max} >> \{H_L, H_{min}\}$ equation (4.4-A4) reduces to

$$pr\{H_o \geq H_L\} \approx \frac{H_{min}^2}{H_L^2} \quad (4.4\text{-A5})$$

which means that $pr\{H_o \geq H_L\}$ is no longer a function of H_{max}. By definition $pr\{H_o \geq H_{max}\} = 0$ and $pr\{H_o \geq H_{min}\} = 1$ so that H_L is not an explicit function of the distance r. Consequently, the choice of H_{min} is very important.

In annex 4.4-B and annex 4.4-C the distribution function $f(H_o)$ has to be known. Since the cumulative distribution $F(H_o) = pr\{H_o \leq H_L\} = 1 - pr\{H_o \geq H_L\}$ and, by definition, $f(H_o)$ is the derivative of $F(H_o)$ with respect to the field strength, the normalized distribution function $f_n(H_o)$ can be calculated using equation (4.4-A4), yielding

$$f_n(H_o) = \frac{\partial}{\partial H} pr\{H_o \leq H\} = \frac{-2}{H_o^3\left(1/H_{max}^2 - 1/H_{min}^2\right)} = \frac{-C_{ho}}{H_o^3} = -C_{Ho} f(H_o) \quad (4.4\text{-A6})$$

Hence the distribution function $f(H_o) = 1/H^3$. The constant of proportionality C_{Ho} n $f_n(H_o) = C_{Ho}f(H_o)$ arose from normalizing $f(H_o)$. The constant C_{Ho} can formally be written as

$$C_{Ho}^{-1} = \int_{H_{min}}^{H_{max}} \frac{dH_o}{H_o^3} \quad (4.4\text{-A7})$$

The relation $f_n(H_o) = -C_{Ho}/H^3$ is applicable in all cases where the field strength varies in inverse proportion to that distance and no specification of the transmitter power P is needed. Of course, H_o is an implicit function of r and P.

Finally, $pr\{H_o \geq H_L\}$ can be written formally as

$$pr\{H_o \geq H_L\} = \frac{\int_{R_L}^{H_{max}} f(H_o)dH_o}{\int_{H_{min}}^{H_{max}} f(H_o)dH_o} \quad (4.4\text{-A8})$$

4.4-A.2 H_i-field expressions

For the indoor field H_i no direct model is available as it is for the outdoor field H_o. Therefore the distribution $f(H_i)$ has to be derived from $f(H_o)$ and the distribution $f(A_b)$ of the building effect.

Assuming $f(H_o)$ and $f(A_b)$ to be independent, the joint distribution $f(H_o,A_b) = f(H_o)f(A_b)$. The latter distribution represents the distribution of locations where the outdoor field strength equals H_o and, simultaneously, the building effect amounts A_b. By carrying out the transformation $H_i = H_o/A_b$ the joint distribution $f(H_i,A_b)$ is known. Since

$$f(H_i, A_b)dH_i = f(A_b)f(H_o)dH_o \qquad \text{or} \qquad f(H_i, A_b) = \frac{f(H_o)f(A_b)}{dH_i\,/\,dH_o} = A_b f(H_o)f(A_b) \tag{4.4-A9}$$

and $f(H_o) = 1/\,H_o^3$ it follows that

$$pf\{H_i \le H_L\} = \int_{H_i} dH_i \int_{A_b} dA_b \frac{f(A_b)}{A_b^2 H_i^3} = E[A_b^{-2}] \int_{H_i} \frac{dH_i}{H_i^3} \tag{4.4-A10}$$

where $E[A_b^{-2}]$ is the expectation of A_b^{-2}. Using the truncated distribution of A_b with truncation factor α_{tA}, see 4.4.2.1 and 4.4.2.2.3, $E[A_b^{-2}]$ is given by

$$E[A_b^{-2}] = \int_{A_{bl}}^{A_{bu}} \frac{f(A_b)dA_b}{A_b^2} = \frac{\alpha_{tA}}{2}\{erf(z_u) - erf(z_i)\}e^{-2\mu_A + 2\sigma_A^2} \tag{4.4-A11}$$

where A_{bu} and A_{bl} are the upper and lower boundary of the range of experimental A_b data, as explained in 4.4.2.2.3, $\mu_A = M_a \ln(10)/20$ and $\sigma_A = S_a \ln(10)/20$ with M_A and S_A being the average value and the standard deviation of the lognormal distribution of A_b. In equation (4.4-A11) "*erf*" denotes the error function, see annex 4.4-D, while z_u and z_i are given by

$$z_u = \frac{\ln(A_{bu}) - \mu_A}{\sigma_A\sqrt{2}} + \sigma_A\sqrt{2}, \qquad z_i = \frac{\ln(A_{bl}) - \mu_A}{\sigma_A\sqrt{2}} + \sigma_A\sqrt{2} \tag{4.4-A12}$$

By definition $f(H_i)$ is the derivative of $F(H_i)$ with respect to the field strength. Hence, the normalized distribution $f_n(H_i)$ reads

$$f_n(H_i) = \frac{C_{Hi}}{H_i^3} \quad \text{with} \quad C_{Hi}^{-1} = E\left\{A_b^{-2}\right\} \int_{H_{i,min}}^{H_{i,max}} \frac{dH_i}{H_i^3} \tag{4.4-A13}$$

where $H_{i,min} = H_{min}/A_u$ and $H_{i,max} = H_{max}/A_t$ and H_{min} and H_{max} are the minimum and maximum outdoor field strength, respectively.

4.4-A.3 E_o-field expressions

Assuming far-field conditions, the outdoor magnetic field component H_o and the outdoor electric field component E_o have a constant ratio, i.e. $E_o = H_o Z_0$. If E_{min} and E_{max} are the field strength at the inner and outer boundary of the ring-shaped area, the probability that $E_o \ge E_L$ can be written as

$$pr\{E_o \geq E_L\} = \frac{\left(E_{max}^2 - E_L^2\right)E_{min}^2}{\left(E_{max}^2 - E_{min}^2\right)E_L^2} \tag{4.4-A14}$$

In the classification of the field strength carried out in 4.4.3.1, use has been made of equation (4.4-A9) to determine the boundaries between the field-strength classes. In that application equation (4.4-A9) was rewritten as

$$E_L = \frac{E_{min}}{\sqrt{pr\{E_o \geq E_L\}\left\{1 - (E_{min} / E_{max})^2\right\} + (E_{min} / E_{max})^2}} \approx \frac{E_{min}}{\sqrt{pr\{E_o \geq E_L\}}} \tag{4.4-A15}$$

which equation follows directly from equation (4.4-A6), while the approximation is valid in the case where $E_{max} >> \{E_{min}, E_L\}$. In the latter case E_L is independent of E_{max}.

Similar to 4.4-A1 in the case of $f(H_o)$, the distribution function $f(E_o)$ is given by

$$f_n(E_o) = \frac{-C_E}{E_o^3} = -C_E f(E_o) \text{ with } C_E^{-1} = \int_{E_{min}}^{E_{max}} \frac{dE_o}{E_o^3} \tag{4.4-A16}$$

and $pr\{E_o \geq E_L\}$ is given by

$$pr\{E_o \geq E_L\} = \frac{\int_{E_L}^{E_{max}} f(E_o)\,dE_o}{\int_{E_{min}}^{E_{max}} f(E_o)\,dE_o} \tag{4.4-A17}$$

The constants C_{Eo} and C_{Ho} are related via $C_{Eo} = C_{Ho} Z_0^2$.

Of course, in a similar way also $f(H_i)$ and $f_n(H_i)$ can be converted into $f(E_i)$ and $f_n(E_i)$.

Annex 4.4-B

The induced asymmetrical open-circuit voltage distribution

In this annex the distribution function $f(U_h)$ of the induced asymmetrical open-circuit voltage U_h will be derived by combining the distribution function of the field strength (see annex 4.4-A) and that of the G factors or the L factors. After that, the probability $pr\{U_h \geq U_L\}$ that U_h is equal to or larger than a given value U_L is calculated. Results of this calculation have been used in 4.4.3.2.

As in annex 4.4-A, it is assumed that the outdoor magnetic field strength H_o can be written as $H_o = (k/P)\ /\ rZ_0)$ or $E_o = (k/P)/r$, where k is a constant, P the transmitter power, Z_0 the free-space wave impedance and r the distance between the transmitter and the point of observation. As in annex 4.4-A, it is also assumed that the transmitter causing the field H_o or E_o is in the centre of a ring-shaped area with an inner radius R_{min} and an outer radius R_{max}. The field strength as the inner boundary is H_{max} or E_{max}, and that at the outer boundary H_{min} or E_{min}. The need for these boundaries has been explained in annex 4.4-A, where it was also explained that the derivation of the relations will start from the magnetic field strength, i.e. use is made of the G factors defined by $U_h = G_o \cdot H$. Electric-field-strength relations using the L factors defined by $U_h = L_E$ will be addressed in clause B.2.

4.4-B.1 *H*-field-based relations

Assuming the field distribution $f_n(H_o)$ and the G factor distribution $f(G_o)$ to be independent, the joint distribution $f(H_o,G_o)$ $f_n(H_o) \cdot f(G_o)$. This joint distribution gives the distribution of the locations where the outdoor field strength equals H_o and, simultaneously, the outdoor G factor equals G_o. Then, by carrying out the transformation $U_h = G_o \cdot H_o$, the distribution is found of the situations where simultaneously the asymmetrical voltage equals U_h and the G factor equals G_o. Since

$$f(U_h)dU_h = f_n(H_o)dH_o \text{ or } f(U_h) = \frac{f_n(H_o)}{dU_h\ /\ dH_o} = \frac{f_n(H_o)}{G_o} \tag{4.4-B1}$$

it follows that

$$f(U_h, G_o) = \frac{f_n\left(\dfrac{U_h}{G_o}\right) f(G_o)}{G_o} = \frac{C_{Ho} G_o^2 f(G_o)}{U_h^3} \tag{4.4-B2}$$

where the right-hand part of this equation is valid if the distribution derived in annex 4.4-A is used, i.e. when it is assumed that $f_n(H_o) = C_{Ho}\ /\ H_o^3$, see equation (4.4-A6). If $f(G_i)$ is used, the building effect A_b has to be taken into account and, hence, $f_n(H_i)$ should be used as discussed in 4.4.A.2 of annex 4.4-A.

By integrating the joint distribution over the permissible ranges of U_h and G_o, the probability $pr\{U_h \geq U_L\}$ can be calculated from

$$pr\{U_h \geq U_L\} = \int_{U_h} dU \int_{G_o} dG \frac{C_{Ho} G_o^2 f(G_o)}{U_h^3} = \frac{C_{Ho}}{2} \int_{G_o} \left\{ \frac{G_o^2}{U_{h1}^2} - \frac{G_o^2}{U_{h2}^2} \right\} f(G_o) dG \tag{4.4-B3}$$

where U_{h1} and U_{h2} are relevant boundaries. To find the relevant ranges and boundaries of U_h and G, consider figure 4.4-B1 showing the U_h-G plane. As the field strength ranges between H_{min} and H_{max} the voltage satisfies the relation $H_{min}G \leq U_h \leq H_{max}G$. Using a truncated lognormal distribution of the G factors (see 4.4.2.2.3), we have $G_L \leq G \leq G_u$.

If U_L has the value indicated in figure 4.4-B1, $pr\{U_h \geq U_L\}$ is found by integrating the joint distribution over the range of U_h and G values indicated by the shaded area in figure 4.4-B1. From that figure it will be clear that U_L can only have values between $U_a = H_{min}G_L$ and $U_d = H_{max}G_U$. The voltages U_b and U_c are defined by $U_b = H_{max}G_L$ and $U_c = H_{min}G_U$, respectively.

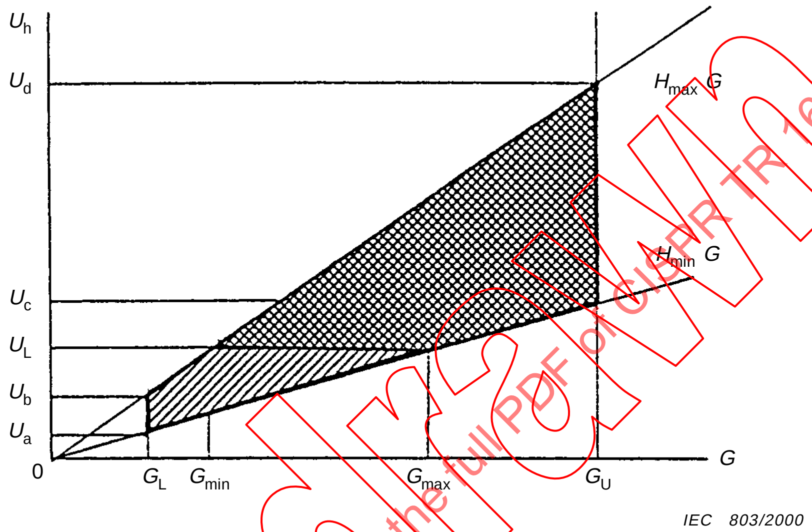

Figure 4.4-B1 – The permissible ranges of U_h and G are within the polygon $\{G_L,U_a\}$, $\{G_L,U_b\}$, $\{G_U,U_d\}$, $\{G_l,U_c\}$ and $\{G_L,U_a\}$. For the given value U_L the double-shaded area represents $pr\{U_h \geq U_L\}$

After straightforward calculations it follows from equation (4.4-B3) that $pr\{U_h,U_L\}$ is given by

$$pr\{I_h \geq U_L\} =$$

$$\frac{\alpha_{tG}C_{Ho}}{4}\left\{\delta_U \frac{erf(x_u) - erf(x_i)}{H_{min}^2} - \frac{erf(y_i) - erf(y_i)}{H_{max}^2} + e^{2\mu_G + 2\sigma_G^2}\frac{erf(z_u) - erf(z_i)}{U_L^2}\right\} \qquad (4.4\text{-B4})$$

where $\mu_G = M_G \cdot \ln(10)/20$ and $\sigma_G = S_G \cdot \ln(10)/20$, M_G and S_G being the average value and the standard deviation of the relevant truncated lognormal G factor distribution with truncation factor α_{tG}. The variables x_u and x_i are given in equation (4.4-B5), while y_u, y_i, z_u, z_i and δ, which depend on the value of U_L, are given by equations (4.4-6) and (4.4-8)

$$x_u = \frac{\ln(G_u) - \mu_G}{\sigma_G\sqrt{2}}, \quad x_i = \frac{\ln(U_L / H_{min}) - \mu_G}{\sigma_G\sqrt{2}} \qquad (4.4\text{-B5})$$

a) $U_a \leq U_L < U_b$: $\delta_U = 1$,

$$y_u = \frac{\ln(G_u) - \mu_G}{\sigma_G\sqrt{2}}, \quad y_i = \frac{\ln(G_L) - \mu_G}{\sigma_G\sqrt{2}} \qquad (4.4\text{-B6(a)})$$

$$z_u = \frac{\ln(U_L / H_{min}) - \mu_G - 2\sigma_G^2}{\sigma_G\sqrt{2}}, \quad z_l = \frac{\ln(G_L) - \mu_G - 2\sigma_G^2}{\sigma_G\sqrt{2}} \tag{4.4-B6(b)}$$

b) $U_b \leq U_L < U_c$: $\delta_U = 1$

$$y_u = \frac{\ln(G_U) - \mu_G}{\sigma_G\sqrt{2}}, \quad y_i = \frac{\ln(U_L / H_{max}) - \mu_G}{\sigma_G\sqrt{2}} \tag{4.4-B7(a)}$$

$$z_u = \frac{\ln(U_L / H_{min}) - \mu_G - 2\sigma_G^2}{\sigma_G\sqrt{2}}, \quad z_i = \frac{\ln(U_L / H_{max}) - \mu_G - 2\sigma_G^2}{\sigma_G\sqrt{2}} \tag{4.4-B7(b)}$$

b) $U_c \leq U_L < U_d$: $\delta_U = 0$

$$y_u = \frac{\ln(G_U) - \mu_G}{\sigma_G\sqrt{2}}, \quad y_i = \frac{\ln(U_L / H_{max}) - \mu_G}{\sigma_G\sqrt{2}} \tag{4.4-B8(a)}$$

$$z_u = \frac{\ln(G_U) - \mu_G - 2\sigma_G^2}{\sigma_G\sqrt{2}}, \quad z_i = \frac{\ln(U_L / H_{max}) - \mu_G - 2\sigma_G^2}{\sigma_G\sqrt{2}} \tag{4.4-B8(b)}$$

In the case where the G_i factors are used, equation (4.4-4) is applicable provided that C_{Ho} is replaced by $E\lfloor A_b^{-2} \rfloor C_{Hi}$, and H_{min} and H_{max} by $H_{i,min}$ and $H_{i,max}$, respectively (see clause 4.4.A.2 in annex 4.4-A).

Equations (4.4-B4) to (4.4-B8) have been used to calculate the data summarized in table 4.4.3-3 and to calculate the results displayed in figures 4.4.4-3 and 4.4.4-4.

4.4-B.2 *E*-field-based relations

Assuming far-field conditions the outdoor electric field strength may be used to calculate $pr\{U_h \geq U_L\}$ in connection with the L_o factors, see 4.4.2.2.2. In that case equations (4.4-B4) to (4.4-B8) can be used, provided that C_{Ho} is replaced by C_{Eo}, H_{max} by E_{max}, H_{min} by E_{min}, G_o by L_o, and M_G and S_G by M_L and S_L. In other words, equations (4.4-B4) to (4.4-B9) can be used, provided that all magnetic-field-related quantities are replaced by the corresponding electric-field quantities.

Similar remarks are valid in the case where L_i factors are to be used, but see note 3 at the end of 4.1.

Annex 4.4-C

The outlet-voltage distribution

This annex considers the number of outlets $N_o(U_h \geq U_L)$ showing an induced open-circuit voltage U_h equal to or larger than a given voltage U_L. This quantity is derived in a number of steps. First, the probability density $n(H_o)$ giving the density of outlets experiencing a certain field strength H_o is considered. Use will be made of the simple models with the ring-shaped area (RSA) already discussed in annex 4.4-A and annex 4.4-B, and of the G_o factors, which give U_h normalized to the magnetic field strength. After that it is possible to calculate the joint distribution $n(H_o,G_o)$ along the lines described in annex 4.4-B, and $N_o(U_h \geq U_L)$ follows after integration of the joint distribution factor over the permissible values of the parameters concerned. When using the G_i factors in combination with the building effect A_b the same procedure can be followed as in annex 4.4-B.

4.4-C.1 *H*-field-based relations

Assuming a homogeneous density of μ outlets per square metre around the transmitter in question, the number $dn(r)$ of outlets in an elementary ring-shaped area between r and $r+dr$ is given by

$$dn(r) = \mu 2\pi r \, dr \tag{4.4-C1}$$

Using $H_o = (k/P)/(rZ_0)$ (see annex 4.4-A), it follows from equation (4.4-C1) that the number of outlets $dn(H_o)$ in the area determined by the field-strength range $H_o(r)$ to $H_o(r+dr)$, is given by

$$dn(H_o) = 2\pi\mu \frac{k^2 P}{H_o^3 Z_0^2} dH_o \tag{4.4-C2}$$

In the case of N transmitters, where the j-th transmitter is characterized by $\{k_j,P_j\}$ and the density of outlets around that transmitter is μ_j, $dn(H_o)$ can be written as

$$dn(H_o) = \sum_{j=1}^{N} 2\pi\mu_j \frac{k_j^2 P_j}{Z_0^2} \frac{d_{Ho}}{H_o^3} = \frac{d_{Ho}}{Z_0^2 H_o^3} = \sum_{j=1}^{N} 2\pi\mu_j k_j^2 P_j = \frac{C_{Ho}}{H_o^3} dH_o \tag{4.4-C3}$$

Hence, in this model the normalized distribution $n(H_o)$ is given by

$$n(H_o) = \frac{dn(H_o)}{dH_o} = \frac{C_{Ho}}{H_o^3} \quad \text{with} \quad C_{Ho} = \frac{2\pi}{Z_0^2} \sum_{j=1}^{N} \mu_j k_j^2 P_j \tag{4.4-C4(a,b)}$$

As had to be expected, the distribution $n(H_o)$ is equal to $f_n(H_o)$ discussed in annex 4.4-A.

If N_T is the total number of outlets in the RSA and if H_{max} and H_{min} determine the boundaries of that RSA, the following relation has to be satisfied

$$N_T = \int_{H_{min}}^{H_{max}} n(H) dH \tag{4.4-C5}$$

or, after substitution of equation (4.4-C4):

$$N_T = \frac{C_{Ho}}{2}\left\{\frac{1}{H_{min}^2} - \frac{1}{H_{max}^2}\right\} \qquad (4.4\text{-C6})$$

If the connection between N_T and C_{Ho} is made via equation (4.4-C4), the expression for the number of outlets $N_o(H_u \geq U_L)$ showing an induced open-circuit voltage $U_h \geq U_L$ is identical to that for $pr\{U_h \geq U_L\}$ as derived in annex 4.4-B, equation (4.4-B4). So $N_o(U_h \geq U_L)$ reads

$$N_o\{U_h \geq U_L\} =$$
$$\frac{\alpha_{tG} C_{Ho}}{4}\left\{\delta_U \frac{erf(x_u) - erf(x_l)}{H_{min}^2} - \frac{erf(y_u) - erf(Y_l)}{H_{max}^2} + e^{2\mu_G + 2\sigma_G^2}\frac{erf(z_u) - erf(z_l)}{U_L^2}\right\} \qquad (4.4\text{-C7})$$

The parameters needed in equation (4.4-C7) have been explained in equations (4.4-B4) to (4.4-B8). In annex 4.4-B it has also been explained how to change equation (4.4-C7) to make a calculation using G_i factors possible.

When it is assumed that N_T is known and H_{max} has been chosen there remain two "unknowns" in equation (4.4-C6): C_{Ho} and H_{min}. If C_{Ho} is calculated for a certain geographical region from equation (4.4-C4b), then H_{min} is known, so that all parameters in equation (4.4-C7) are known. As discussed in 4.4.4, another possibility is to determine H_{min} in that region and C_{Ho} can be calculated by using equation (4.4-C6).

4.4-C.2 *E*-field-based relations

Assuming far-field conditions, the outdoor electric field strength together with the L factors may be used to calculate $N_o\{U_h \geq U_L\}$. In that case equation (4.4-C7) can be used, provided that C_{Ho} is replaced by C_{Eo}, H_{max} by E_{max}, H_{min} by E_{min}, G_o by L_o and M_G and S_G by M_L and S_L. In other words equation (4.4-C7) can be used, provided that all magnetic-field-related quantities are replaced by the corresponding electric-field quantities.

If $E_o = (k/P)/r$ the equivalent of equation (4.4-C4) reads

$$n(E) = \frac{dN(E)}{dE} = -\frac{C_{Eo}}{E^3} \quad \text{with} \quad C_{Eo} = 2\pi\sum_{j=1}^{N}\mu_j k_j^2 P_j \qquad (4.4\text{-C8(a,b)})$$

and the equivalent of equation (4.4-C6) reads

$$N_T = \frac{C_{Eo}}{2}\left\{\frac{1}{E_{min}^2} - \frac{1}{E_{max}^2}\right\} \qquad (4.4\text{-C9})$$

See annex 4.4-B about how to change the various relations to make calculations using L_i factors possible, but see also note 3 at the end of 4.1.

Annex 4.4-D

Some mathematical relations

In this annex a number of mathematical relations involving the so-called Error Function, as used in annexes 4.4-B and 4.4-C, are summarized. In 4.4-D.1 a series expansion of the error function is also given which is sufficiently accurate to be used in computer calculations based on the analytical expressions presented in annexes 4.4-B and 4.4-C. Clause 4.4-D.2 summarizes some mathematical relations involving the lognormal distribution and the error function.

4.4-D.1 The Error Function

By definition *erf*(*x*), the error function of *x*, is given by equation (4.4-D1)

$$erf(x) = \frac{2}{\sqrt{\pi}} \int_0^x e^{-\alpha^2} d\alpha \tag{4.4-D1}$$

The error function has the following properties

$$erf(0) = 0 \tag{4.4-D2(a)}$$

$$erf(\infty) = 1 \tag{4.4-D2(b)}$$

$$erf(-x) = erf(x) \tag{4.4-D2(c)}$$

A useful series expansion of *erf*(*x*) is the following equation (4.4-D2)

$$erf(s) = 1 - \left(a_1 t + a_2 t^2 + a_3 t^3 + a_4 t^4 + a_5 t^5\right) e^{-x^2} + \varepsilon(x) \tag{4.4-D3(a)}$$

$$t = \frac{1}{1 + px}, \left|\varepsilon(x)\right| \le 1{,}5 \times 10^{-7} \tag{4.4-D3(b)}$$

where

p = 0,28449 6736;

a_1 = 0,25482 9592;

a_2 = 0,28449 6736;

a_3 = 1,42141 3741;

a_4 = –1,45315 2027;

a_5 = 1,06140 5429.

4.4-D.2 Application to the lognormal distribution

A quantity x has a lognormal distribution when the logarithm of x has a normal distribution. In mathematical form the lognormal distribution of x reads

$$f(x)dx = \frac{1}{x\sigma\sqrt{2\pi}} e^{-\frac{(\ln(x)-\mu)^2}{2\sigma^2}} dx \qquad (4.4\text{-D4})$$

where μ is the average value of ln(x) and σ the associated standard deviation. If the latter parameters are known in dB and M(dB...) is the average value and S(dB) is the associated standard deviation, $\mu = M \cdot \ln(10)/20$ and $\sigma = S \cdot \ln(10)/20$. The distribution function given in equation (4.4-D4) has the property that the integral of this function over all values of x equals 1 if $-\infty \le x \le \infty$. This means that $f(x)$ given in equation 4.4-D4 is properly normalized. If $f_t(x)$ is the truncated lognormal distribution of x, such that $x_l \le x \le x_u$, the distribution has to be normalized again. In that case $f_t(x)$ can formally be written as $f_t(x) = \alpha_t \cdot f(x)$ with

$$\alpha_t^{-1} = \int_{x_l}^{x_u} \frac{1}{x\sigma\sqrt{2\pi}} e^{-\frac{(\ln(x)-\mu)^2}{2\sigma^2}} dx = \frac{1}{\sqrt{\pi}}\int_{-\infty}^{y_u} e^{-y^2} dy - \frac{1}{\sqrt{\pi}}\int_{-\infty}^{y_l} e^{-y^2} dy \qquad (4.4\text{-D5(a)})$$

so that

$$\alpha_t = \frac{erf(y_u) - erf(y_l)}{2} \qquad (4.4\text{-D5(b)})$$

where

$$y = \frac{\ln(x) - \mu}{\sigma\sqrt{2}}, \quad y_u = \frac{\ln(x_u) - \mu}{\sigma\sqrt{2}}, \quad y_l = \frac{\ln(x_l) - \mu}{\sigma\sqrt{2}} \qquad (4.4\text{-D5(c)})$$

When carrying out the integrations in annex 4.4-B, use has been made of the following integral solutions, which can easily be verified using the above relations.

In the case of equation (4.4-B4) leading to equation (4.4-B7), use was made of

$$\int_{x_l}^{x_u} x^2 f_t(x)dx = \alpha_t \frac{e^{2\mu+2\sigma^2}}{2}\{erf(z_u) - erf(z_l)\} \qquad (4.4\text{-D6(a)})$$

where

$$z_u = y_u - \sigma\sqrt{2}, \quad z_l = y_l - \sigma\sqrt{2} \qquad (4.4\text{-D6(b)})$$

and in the derivation of equation (4.4-B5) use was made of

$$\int_{x_l}^{x_u} x^{-2} f_t(x)dx = \alpha_t \frac{e^{-2\mu+2\sigma^2}}{2}\{erf(z_u) - erf(z_l)\} \qquad (4.4\text{-D7(a)})$$

where

$$z_u = y_u + \sigma\sqrt{2}, \quad z_l = y_l + \sigma\sqrt{2} \qquad (4.4\text{-D7(b)})$$

References

D1 *Handbook of mathematical functions*, M. Abramowitz and I.A. Stegun, Dover Publications Inc., New York, 1972

D2 *Approximations for digital computers*, C. Hastings Jr., Princeton Univ. Press, Princeton, N.J., 1959 (see also Ref. D1)

4.5 The predictability of radiation in vertical directions at frequencies above 30 MHz

Summary

CISPR 11 sets limits for the electromagnetic disturbances emitted *in situ* near the ground from industrial, scientific and medical (ISM) radio-frequency equipment. In CISPR 11, referring to protection of safety of life services, it is stated "Many aeronautical communications require the limitation of vertically radiated electromagnetic disturbances. Work is continuing to determine what provisions may be necessary to provide protection for such systems".

This report considers the calculated vertical radiation patterns of the *E*-field which will be emitted at frequencies above 30 MHz from electrically small sources physically located close to the surface of real homogeneous plane ground. Its purpose is the study of the predictability of radiation in vertical directions based on *in situ* measurements of the strength of the *E*-field near the ground. The sources considered are electrically small balanced electric and magnetic dipoles excited in the frequency range from 30 MHz to 1 000 MHz.

The effects on the vertical radiation patterns caused by a wide range of the electrical properties of the ground, varying from wet ground to very dry ground – and the special case of a ground that behaves like a near-perfect conductor – have also been considered.

These studies show the limitations of the predictability of radiation at elevated angles when based on measurements near the ground. The report identifies some of the factors to be considered when developing and specifying limits of radiated electromagnetic disturbances and methods of measurement which are intended to protect aeronautical radionavigation and communication systems operating at frequencies above 30 MHz. For example, it shows that vertical patterns of the fields over good conductors do not represent the field patterns over real grounds. Moreover, the report shows that for good predictability of the field strengths at elevated angles the *in situ* measurements near the ground must not be made at fixed heights but instead they must use height scans and, in particular, must be made at a known distance from the equipment which is the source of the radiation.

4.5.1 Scope

This report considers the predictability of radiation in vertical directions based on measurements of the strength of the electric (*E*) fields emitted by electrical equipment near the ground. It is intended to give guidance to the predictability of radiation emitted at elevated angles by electrical equipment *in situ*, in particular industrial, scientific, and medical (ISM) radio-frequency equipment. For that purpose, it studies the calculated vertical radiation patterns of the *E*-fields which will be emitted at frequencies above 30 MHz from electrically small sources located close to the surface of real homogeneous plane ground.

The vertical radiation patterns of the horizontally and vertically polarized *E*-fields, including the surface waves, have been calculated at distances of 10 m, 30 m and 300 m from various electrically small sources, so that the field variations with distance can be quantified. In this way, a general knowledge has been obtained of the shapes of the vertical radiation patterns, showing the magnitudes of the *E*-field strengths near ground compared with the magnitudes of the *E*-field components at elevated angles, and the ways in which the relative magnitudes can be expected to vary with distance over a plane ground.

The sources considered were electrically small balanced electric and magnetic dipoles excited in the frequency range from 30 MHz to 1 000 MHz. For the purposes of the study, an electrically small source is defined as one whose largest linear dimension is one-tenth or less of the free-space wavelength at the frequency of interest.

The report also considers the effects on the vertical radiation patterns caused by a range of electrical properties of the ground, varying from electrical conductivities and dielectric constants of wet ground to those of very dry ground [1] [2] and the special case of a ground that behaves like a near-perfect conductor.

The effects on wave propagation near the ground of walls, buildings, terrain irregularities, watercourses, vegetation cover, and so on, are not within the scope of this report. It is important to note, therefore, that the additional uncertainties in wave propagation caused by the presence of such discontinuities, and their effects on predictability based on measurements *in situ*, have not been considered.

4.5.2 Introduction

In CISPR 11 [3], table VI in clause 5.3 provides radiation limits for the protection of specific safety services. The limits apply to ground level measurements of the electromagnetic disturbances emitted by ISM radio-frequency (RF) equipment *in situ*, not on a test site. Above 30 MHz the five frequency bands listed in table VI are all used for aeronautical services, including the instrument landing system or instrument low-approach system (ILS) marker beacon, localizer, and glide path frequencies, as well as a survival frequency and other radionavigation and communication frequencies bands. A note to table VI states: "Many aeronautical communications require the limitation of vertically radiated electromagnetic disturbances. Work is continuing to determine what provisions may be necessary to provide protection for such systems."

The *in situ* measuring distance specified in table VI, for all five frequency bands above 30 MHz, is 10 m "from (the) exterior wall outside the building in which the equipment is situated". It is important to note that the precise measuring distance from the ISM apparatus itself is not specified.

The heights at which measurements of horizontally and vertically polarized *E*-fields are to be made using a balanced dipole are specified in 7.2.4 of CISPR 11. "For Group 2 Class A equipment the centre of the antenna shall be 3,0 m ± 0,2 m above ground. For Group 1 and Group 2 Class B equipment the centre of the antenna shall be adjusted between 1 m and 4 m for maximum indication at each test frequency. The nearest point of the antenna to ground shall be not less than 0,2 m." The height above ground of the measuring antenna when measuring emissions from Group 1 Class A equipment (which might include, for example, large "switched mode power supplies (when not incorporated in an equipment)", see Annex 4.4-A, CISPR 11) is not specified. Generally, CISPR 11 allows Class A ISM equipment to be tested on a test site or *in situ* as preferred by the manufacturer, while requiring Class B ISM equipment to be measured on a test site. However, when providing for protection of specific safety services, CISPR 11 specifies that "...national authorities may require measurements to be made *in situ*...". This presumably includes *in situ* measurements for both Class A and Class B ISM equipment when the need arises, for example under the provisions of 5.3.

After considering the methods of specifying *in situ* measurement distance and measuring antenna height in CISPR 11, it is useful to address the following questions:

1) How well do measurements of the vertically and horizontally polarized *E*-fields, in a height scan of 1 m to 4 m at a horizontal distance of 10 m from the source over real ground, predict the field strengths emitted at elevated angles?
2) How predictable are the field strengths at elevated angles when the horizontal measuring distance is greater than 10 m but, beyond that fact, the actual distance is not known (not specified)?
3) How is the predictability affected when the height above ground to the centre of the measuring antenna is fixed, for example at a nominal 3 m?
4) What errors in judgement of the predictability of the vertical patterns may arise if calculations are made using the common approximation that the influence of the real ground can be simulated by replacing it with a perfect conductor?

To provide some answers in the frequency range 30 MHz to 1 000 MHz a number of vertical polar patterns and linear height scan patterns have been calculated for the *E*-field radiation emitted by four kinds of electrically small sources located close to the surface of real homogeneous plane ground. Predictability has been assessed by judging how well, or how badly, the calculated patterns show that ground-based measurements of the vertically and horizontally polarized *E*-fields emitted from the various sources will correlate with the maximum strengths of either vertically or horizontally polarized *E*-fields (whichever are greater) at elevated angles. The patterns have been calculated for the simplest of sources radiating into the half-space above ground. If these patterns identify problems of predictability, it is unlikely that predictability will be improved when real ISM devices, like plastics welders or RF diathermy machines, are the sources.

Vertical polar patterns and linear height scan patterns have also been calculated for the *E*-field radiation emitted from the small sources over a copper ground plane. A copper ground plane provides boundary conditions which distinguish, in effect, a perfect conductor from a real ground, and allows identification of the differences between the vertical radiation patterns that will exist close to the surface of a real ground when compared with those calculated close to the surface of a perfect conductor. The differences determine how large the errors will be if predictability is judged by considering vertical patterns calculated over a perfectly conducting ground plane.

The four kinds of source considered were electrically small vertical and horizontal balanced electric and magnetic dipoles. There is justification for the use of small dipole sources as models in the study of the predictability of radiation at elevated angles from real ISM equipment. Airborne measurements of the fourth harmonic field radiated from 27 MHz ISM apparatus over real ground reported in [4] have been studied further in [5]. In [5] it is shown that the vertical distribution of horizontally polarized fields at approximately 109 MHz, encountered by an aircraft during any single flight pass over the ISM apparatus, can be well matched with a field distribution produced at elevated angles by a simple small electric or magnetic dipole source. Some of the work in [5] is summarized in appendix 4.5-A.

4.5.3 Method used to calculate field patterns in the vertical plane

The *E*-field vertical polar patterns and linear height scan patterns have been calculated using a double precision version of the Method of Moments computer code known as the Numerical Electromagnetics Code (NEC) [6]. NEC2 with the companion code SOMNEC allows the Sommerfeld integral evaluation of the field interactions at the air-ground interface [7], and so includes the contribution of the Sommerfeld-Norton surface wave when calculating the total *E*-fields above real grounds (discussed in 4.5.4.3). The near fields were also included in the calculations for this report.

The small vertical and horizontal balanced electric dipoles, and vertical and horizontal balanced loops (magnetic dipoles) used as the models for the calculations each had a unit dipole moment (i.e. a dipole [current] moment of a A·m for the electric dipoles and a dipole moment of 1 A·m^2 for the loops). All were positioned with their centres at a height above ground of either 1 m or 2 m in order to show the effects of variations in the source height on the vertical radiation patterns. The effects include the appearance of additional major lobes of radiation – called grating lobes – as the spacing between the source and its image in the ground increases beyond $\lambda/2$ with increasing frequency [8].

The geometries of the models, and the paths of the scans in vertical planes at constant radius about each source for the vertical polar pattern computations, are shown in the top right corner of each polar pattern plot.

The planes in which the linear height scan patterns were calculated are shown in the diagrams accompanying each linear height scan pattern plot.

4.5.3.1 The frequencies of interest and the electrical constants of the ground

The five frequencies of interest at which the models were excited, in the five ITU designated bands [9] listed in table VI of CISPR 11, are shown here in table 4.5-1.

Table 4.5-1

Excitation frequency MHz	**ITU designated bands**
75	74,8-75,2 MHz, Aeronautical Radionavigation (Instrument Landing System (ILS) marker beacons, horizontal polarization)
110	108-137 MHz, Aeronautical Radionavigation and Aeronautical Mobile (R) (including ILS localizers (108-112 MHz), horizontal polarization)
243	243 MHz is for use by survival craft stations and equipment used for survival purposes
330	328,6-335,4 MHz, limited to ILS (glide path, horizontal polarization)
1 000	960-1 215 MHz, reserved on a worldwide basis for the use and development of airborne electronic aids to air navigation

Most attention has been devoted to the small sources placed above a "medium dry ground" [1] (CCIR – medium dry ground; rocks; sand; medium sized towns [2]). The electrical constants, the relative permittivity ε_r and the conductivity σ, mS/m, for "medium dry ground" at 30 MHz and the other five frequencies of interest are listed in table 4.5-2.

Table 4.5-2 – Electrical constants for "medium dry ground" [1] (CCIR – medium dry ground; rocks; sand; medium sized towns [2])

Frequency MHz	ε_r	σ mS/m
30	15	1
75	15	1,5
110	15	2
243	15	4,5
330	15	7,5
1 000	15	35

Near the lower and upper ends of the frequency range, at frequencies of 75 MHz and 1 000 MHz, examples of two other types of grounds have been used with the electrically small vertical loop model (horizontal magnetic dipole) to illustrate the influence of differing values of the ground constants on the vertical radiation patterns (see 4.5.4.1). The electrical constants for "wet ground" and "very dry ground" at 30 MHz, 75 MHz and 1 000 MHz, are listed in table 4.5-3.

Table 4.5-3 – Electrical constants for "wet ground" [1] (CCIR – marshes (fresh water); cultivated land [2]) and "very dry ground" [1] (CCIR – very dry ground; granite mountains in cold regions; industrial areas [2])

Frequency MHz	**"Wet ground"**		**"Very dry ground"**	
	ε_r	σ mS/m	ε_r	σ mS/m
30	30	10	3	0,1
75	30	13	3	0,1
1 000	30	140	3	0,15

4.5.4 Limitations of predictability of radiation at elevated angles

4.5.4.1 Influence of the electrical constants of the ground

It is useful to observe the relatively small influence of widely differing values of the ground constants on the predictability of the field strengths at elevated angles. A small vertical loop (horizontal magnetic dipole) at a centre height of 2 m above ground has been chosen as the source model. The geometry of the model is shown in figure 4.5-1. For this source, the best predictability is obtained when the vertical *Ez* field component is measured near the ground to estimate the maximum strength of either the horizontally oriented *Ex* field or the vertically oriented *Ez* field at elevated angles.

4.5.4.1.1 Influence of the ground constants at 75 MHz

In figure 4.5-1(a), the vertical polar patterns at 75 MHz show the horizontally polarized *Ex* field strengths in the Y-Z plane at scan radii *R* of 10 m, 30 m, and 300 m, over real grounds having the electrical constants in tables 4.5-2 and 4.5-3. It can be seen that at each of the three scan radii, the total *spread* in the maximum *Ex* fields in the vertical direction is less than 3 dB.

In figure 4.5-1(b), the height scan patterns calculated up to a height of 6 m at 75 MHz show the *Ez* field strengths in the Z-X plane at the three corresponding horizontal distances over the same three types of real ground. It can be seen that the *spread* in magnitudes of the *Ez* field strengths at ground level for the three ground types is much greater than 3 dB. However, if measurements of *Ez* are made at heights from 1 m to 4 m, then at a horizontal distance of 10 m the underestimates of the maximum *Ex* field strengths in the vertical direction range from about 3,9 dB to about 4,7 dB (a *spread* of only 0,8 dB), at a horizontal distance of 30 m, the underestimates range from about 5,1 dB to about 5,7 dB (a *spread* of only 0,6 dB), and at 300 m, the underestimates range from about 18,4 dB to about 22,1 dB (a *spread* of 3,7 dB). Thus, for the range of values of the ground constants and measuring distances considered here, the worst case *spread* or *variation* in the underestimates of maximum field strengths in the vertical direction is only 3,7 dB, and this occurs at the largest measuring distance of 300 m.

4.5.4.1.2 Influence of the ground constants at 1 000 MHz

In figure 4.5-2(a), the vertical polar patterns at 1 000 MHz show the horizontally polarized *Ex* field strength in the Y-Z plane at the same three scan radii *R* around the small vertical loop over the same three types of real ground with the electrical constants at 1 000 MHz given in tables 4.5-2 and 4.5-3. It can be seen that for a source height of 2 m at this frequency, multiple grating lobes are established.

Figure 4.5-2(b) shows the vertical polar patterns of the vertically oriented *Ez* field strengths in the Z-X plane, and figure 4.5-2(c) shows the height scan patterns of the *Ez* field strengths calculated up to a height of 6 m in the Z-X plane, at the three scan distances and over the three types of real ground.

Figure 4.5-2(a) shows that the maximum strength of the *Ex* field occurs at an elevation angle between 77° and 78° at all three scan radii. A comparison of figure 4.5-2(b) with figure 4.5-2(a) also shows that, in the case of a "very dry ground", the maximum field strength is contributed by *Ez* at the scan radii of 30 m and 300 m at an elevation angle of 2° (that is, at heights of approximately 1,1 m and 10,5 m at the two radii respectively).

Inspection of figure 4.5-2 reveals the following information. If a vertically polarized antenna measures maximum *Ez* in height scans from 1 m to 4 m, then at 10 m horizontal distance the resulting underestimates of the maximum *Ex* field strengths range from about 1,8 dB to about 3,2 dB, a *spread* of only 1,4 dB. At 30 m horizontal distance, with "medium dry ground" or "wet ground", a 1 m to 4 m *Ez* height scan measurement underestimates the maximum *Ex* field strengths by about 1,4 dB ("medium dry ground") or about 2,9 dB ("wet ground"), a *spread* of only 1,5 dB. Over "very dry ground", the maximum field strength, *Ez*, is reached at a height of about 1,1 m, and will therefore be measured within the height scan from 1 m to 4 m.

At 300 m horizontal distance, over "medium dry ground" and "wet ground", a 1 m to 4 m height scan of *Ez* underestimates the maximum *Ex* field strengths (at about 77° elevation) by about 4,4 dB ("medium dry ground") or about 5,2 dB ("wet ground"), a *spread* of only 0,8 dB. Over "very dry ground" a measurement of *Ez* at a height of 4 m underestimates the maximum field strength (maximum *Ez* at an elevation angle of 2°, height approximately 10,5 m) by about 5,1 dB. The overall *spread* in the underestimates at 300 m distance therefore remains only 0,8 dB.

Thus, at 1 000 MHz, the calculations show that the differing values of the electrical constants of the ground we have considered here produce a worst-case *variation* or *spread* of only 1,5 dB in the underestimates of the maximum *E*-field strengths at elevated angles, when the estimates are based on 1 m to 4 m height scan measurements of *Ez* at horizontal distances ranging from 10 m to 300 m.

4.5.4.1.3 Predictability estimated over a "medium dry ground"

The foregoing shows that in the frequency range from 75 MHz to 1 000 MHz it is justifiable to make general judgements of the predictability of the strength of radiation in vertical directions above ground by considering the *E*-field patterns calculated over a real ground having the electrical constants of a "medium dry ground".

4.5.4.2 Predictability based on height scan measurements near real ground at 10 m distance from the source

Here we can provide an answer to the first question posed in 4.5.2.

In summary, the answer is that the predictability of the maximum *E*-field strengths at elevated angles by means of 1 m to 4 m height scan measurements at a horizontal distance of 10 m, for all four types of sources placed either 1 m or 2 m above a "medium dry ground", is very good. Underestimates at all five of the frequencies used for aeronautical services are less than 6 dB.

At the two lower frequencies of 75 MHz and 110 MHz, the larger underestimates occur when the source is either a small horizontal electric dipole 1 m above the ground or a small vertical loop (horizontal magnetic dipole) with a centre height 2 m above ground.

At the frequencies of 243 MHz and 330 MHz, the larger underestimates occur when the source is either a small vertical electric dipole or a small vertical loop with a centre height 1 m above ground.

At 1 000 MHz, the larger underestimate occurs when the source is a small vertical loop with a centre height 2 m above ground.

4.5.4.2.1 Predictability at 75 MHz

Figure 4.5-3(a) shows polar plots of *Ex* in the Y-Z plane and *Ez* in the Z-X plane, at 75 MHz, around the horizontal electric dipole placed 1 m above ground. At a scan radius of 10 m, *Ex* reaches a maximum field strength of almost 138 dBµV/m at an elevation angle near 73°. The polar plots of *Ez* in the Z-X plane – the vertically polarized radiation emitted from the tips of a horizontal electric dipole over real ground [7] – show that vertically polarized measurements near the ground do not give the best predictions of field strength at high elevation angles. Therefore, figure 4.5-3(b) shows the height scan calculations of horizontally polarized *Ex* in the Y-Z plane, reaching an *Ex* magnitude of almost 133 dBµV/m at a horizontal distance of 10 m and a height of 4 m. In consequence, 1 m to 4 m height scan measurements of *Ex* at a distance of 10 m will underestimate the maximum *Ex* at 73° elevation by almost 5 dB.

The vertical polar plots in figure 4.5-1(a) show that measurement of *Ex* at a distance of 10 m near the ground will not give a good prediction of the maximum field strength emitted at 75 MHz by a small vertical loop placed at a height of 2 m above a "medium dry ground".

Ex field strength reaches a maximum of over 142 dBμV/m in the vertical Y-Z plane. The calculated height scan patterns in figure 4.5-1(b) show that a vertically polarized measurement of *Ez* at a horizontal distance of 10 m in the Z-X plane will reach a maximum of almost 138 dBμV/m at 1,2 m height. This underestimates by less than 5 dB the maximum strength of the radiation in the vertical direction.

Column (4) of table 4.5-4 summarizes the estimated errors to be expected in the predictability of radiation in vertical directions when based on measurements in height scans from 1 m to 4 m at a horizontal distance of 10 m from each of the four sources operating at 75 MHz. Column (1) lists the radiation sources and their heights. Column (2) lists the field components which contribute the maximum field strengths in the vertical polar patterns, and the elevation angles at which the maximum field strengths occur. Column (3) lists the field component which should be measured in a linear height scan at a horizontal distance of 10 m to provide the best estimates of the maximum field strengths.

Table 4.5-4 – Estimates of the errors in prediction of radiation in vertical directions based on a measurement height scan from 1 m to 4 m at known distances, *d*. Frequency = 75 MHz (Adapted from [10])

(1) Source of radiation @ height	(2) Max. *E*, @ angle, in 10 m polar plot	(3) At hor. *d* = 10 m, measure this field	(4) Estimated prediction error, at *d* = 10 m	(5) Max. *E*, @ angle, in 30 m polar plot	(6) At hor. *d* = 30 m, measure this field	(7) Estimated prediction error, at *d* = 30 m	(8) Max. *E*, @ angle, in 300 m polar plot	(9) At hor. *d* = 300 m, measure this field	(10) Estimated prediction error, at *d* = 300 m
Vertical electric dipole @ 1 m	*Ez* @ 15,25°	*Ez*	0 dB	*Ez* @ 17,75°	*Ez*	–2 dB	*Ez* @ 18°	*Ez*	–17,5 dB
Vertical electric dipole @ 2 m	*Ez* @ 8°	*Ez*	0 dB	*Ez* @ 12,75°	*Ez*	–1 dB	*Ez* @ 13°	*Ez*	–16 dB
Horizontal electric dipole @ 1 m	*Ex* @ 72,5° in Y-Z plane	*Ex* in Y-Z plane	–5 dB	*Ex* @ 67,5° in Y-Z plane	*Ex* in Y-Z plane	–12 dB	*Ex* @ 66° in Y-Z plane	*Ex* in Y-Z plane	–31,5 dB
Horizontal electric dipole @ 2 m	*Ex* @ 30° in Y-Z plane	*Ex* in Y-Z plane	–1,5 dB	*Ex* @ 28,75° in Y-Z plane	*Ex* in Y-Z plane	–7 dB	*Ex* @ 28,5° in Y-Z plane	*Ex* in Y-Z plane	–26,5 dB
Vertical loop (horizontal magnetic dipole) @ 1 m	*Ez* @ 17,5° in Z-X plane	*Ez* in Z-X plane	–0,5 dB	*Ez* @ 19,75° in Z-X plane	*Ez* in Z-X plane	–2,5 dB	*Ez* @ 20° in Z-X plane	*Ez* in Z-X plane	–18 dB
Vertical loop (horizontal magnetic dipole @ 2 m	*Ex* @ 90°	*Ez* in Z-X plane	–4,5 dB	*Ex* @ 90°	*Ez* in X-Z plane	–5,5 dB	*Ex* @ 90°	*Ez* in Z-X plane	–20,5 dB
Horizontal loop (vertical magnetic dipole @ 1 m	*Ey* @ 37,5° in Z-X plane	*Ey* in Z-X plane	–2,5 dB	*Ey* @ 36,75° in Z-X plane	*Ey* in Z-X plane	–9 dB	*Ey* @ 36,5° in Z-X plane	*Ey* in Z-X plane	–28,5 dB
Horizontal loop (vertical magnetic dipole) @ 2 m	*Ey* @ 27° in Z-X plane	*Ey* in Z-X plane	–1 dB	*Ey* @ 25,5° in Z-X plane	*Ey* in Z-X plane	–6,5 dB	*Ey* @ 25° in Z-X plane	*Ey* in Z-X plane	–25,5 dB

4.5.4.2.2 Predictability at 110 MHz

Figure 4.5-4(a) shows vertical polar plots of *Ex* in the Y-Z plane and *Ez* in the Z-X plane, at 110 MHz, around a small horizontal electric dipole placed 1 m above the ground. At a scan radius of 10 m, *Ex* reaches a maximum field strength of over 141 dBμV/m at an elevation angle of 41°. The polar plots of *Ez* in the Z-X plane show that vertically polarized measurements near the ground will not give good guidance to high-angle field strength. Figure 4.5-4(b) shows height scan calculations of *Ex* in the Y-Z plane. At a horizontal distance of 10 m the magnitude of *Ex* reaches almost 139 dBμV/m at a height of 4 m, and a height scan measurement of horizontally polarized *Ex* therefore underestimates the maximum strength of *Ex* at 41° elevation by less than 3 dB.

Figure 4.5-5(a) shows vertical polar plots of *Ex* in the Y-Z plane and *Ez* in the Z-X plane, around a small vertical loop (horizontal magnetic dipole) placed at a centre height of 2 m above ground and excited at 110 MHz. The maximum field strength reached at a scan radius of 10 m is the vertical *Ez* component, 146 dBμV/m at an elevation angle of 40°. The height scan plots of *Ez* in figure 4.5-5(b) show that at a horizontal distance of 10 m the magnitude of *Ez* is almost 144 dBμV/m at a height of 1 m, which underestimates the strength of *Ez* at 40° elevation by less than 2,5 dB.

Column (4) of table 4.5-5 summarizes the errors expected in the predictability of radiation in vertical directions based on measurements in height scans from 1 m to 4 m at a horizontal distance of 10 m from each of the four sources operating at 110 MHz.

Table 4.5-5 – Estimates of the errors in prediction of radiation in vertical directions based on a measurement height scan from 1 m to 4 m at known distances, *d*. Frequency = 110 MHz (Adapted from [10])

(1) Source of radiation @ height	(2) Max. *E*, @ angle, in 10 m polar plot	(3) At hor. *d* = 10 m, measure this field	(4) Estimated prediction error, at *d* = 10 m	(5) Max. *E*, @ angle, in 30 m polar plot	(6) At hor. *d* = 30 m, measure this field	(7) Estimated prediction error, at *d* = 30 m	(8) Max. *E*, @ angle, in 300 m polar plot	(9) At hor. *d* = 300 m, measure this field	(10) Estimated prediction error, at *d* = 300 m
Vertical electric dipole @ 1 m	*Ez* @ 13,5°	*Ez*	0 dB	*Ez* @ 15,25°	*Ez*	–1,5 dB	*Ez* @ 15,25°	*Ez*	–17,5 dB
Vertical electric dipole @ 2 m	*Ez* @ 36,5°	*Ez*	–1 dB	*Ez* @ 10,75°	*Ez*	–0,5 dB	*Ez* @ 11°	*Ez*	–15,5 dB
Horizontal electric dipole @ 1 m	*Ex* @ 41° in Y-Z plane	*Ex* in Y-Z plane	–2,5 dB	*Ex* @ 40° in Y-Z plane	*Ex* in Y-Z plane	–9,5 dB	*Ex* @ 39,75° in Y-Z plane	*Ex* in Y-Z plane	–29 dB
Horizontal electric dipole @ 2 m	*Ex* @ 20° in Y-Z plane	*Ex* in Y-Z plane	–0,5 dB	*Ex* @ 19,25° in Y-Z plane	*Ex* in Y-Z plane	–4,5 dB	*Ex* @ 19,25° in Y-z plane	*Ex* in Y-Z plane	–23,5 dB
Vertical loop (horizontal magnetic dipole) @ 1 m	*Ex* @ 90°	*Ez* in Z-X plane	–2 dB	*Ey* @ 90°	*Ez* in Z-X plane	–3,5 dB	*Ey* @ 90°	*Ez* in Z-X plane	–19 dB
Vertical loop (horizontal magnetic dipole) @ 2 m	*Ey* @ 40° in Z-X plane	*Ez* in Z-X plane	–2,5 dB	*Ex* @ 48° in Y-Z plane	*Ez* in Z-X plane	–2,5 dB	*Ex* @ 47,5° in Y-Z plane	*Ez* in Z-X plane	–17,5 dB
Horizontal loop (vertical magnetic dipole) @ 1 m	*Ey* @ 31,75° in Z-X plane	*Ey* in Z-X plane	–1,5 dB	*Ey* @ 31° in Z-X plane	*Ey* in Z-X plane	–8 dB	*Ey* @ 31° in Z-X plane	*Ey* in Z-X plane	–27 dB
Horizontal loop (vertical magnetic dipole) @ 2 m	*Ey* @ 19,25° in Z-X plane	*Ey* in Z-X plane	–0,5 dB	*Ey* @ 18,5° in Z-X plane	*Ey* in Z-X plane	–4 dB	*Ey* @ 18,25° in Z-X plane	*Ey* in Z-X plane	–23 dB

4.5.4.2.3 Predictability at 243 MHz

Figure 4.5-6(a) shows vertical polar plots of *Ez* and *Ex* in the Z-X plane, at 243 MHz, around the small vertical electric dipole placed at a centre height of 1 m above ground. At a scan radius of 10 m the maximum field strength of almost 144 dBµV/m is contributed by *Ez* at an elevation angle of 33,75°. Calculations of the vertical field component *Ez* in a height scan from 1 m to 4 m at a horizontal distance of 10 m produce a peak magnitude of almost 143 dBµV/m at a measuring height of 1,65 m, as shown in figure 4.5-6(b). This under-estimates the maximum field strength by only 1 dB.

Figure 4.5-7(a) shows vertical polar plots of *Ex* in the Y-Z plane and *Ez* in the Z-X plane, around the small vertical loop placed at a centre height of 1 m above a "medium dry ground". It can be seen that, at a scan radius of 10 m, the maximum field strength of more than 159 dBµV/m is reached by *Ez* at an elevation angle of 36,25° in the Z-X plane. The calculated *Ez* height scan patterns shown in figure 4.5-7(b) produce a peak field strength of 157 dBµV/m, at 10 m horizontal distance and a height of 1,65 m. This underestimates the maximum *Ez* by approximately 2,5 dB.

The vertical polar plots of horizontally polarized *E*-field emitted at 243 MHz by a small horizontal loop placed at a height of 1 m above a "medium dry ground" are shown in figure 4.5-8(a). The peak of the major lobe, nearest the ground, occurs at an elevation angle of 17° and is therefore reached at a height of 2,9 m at a horizontal distance of 10 m. The height scan plot at a horizontal distance of 10 m in figure 4.5-8(b), which is of *Ey* in the Z-X plane in this example, underestimates the maximum field strength in a vertical polar scan by less than 0,5 dB.

Column (4) of table 4.5-6 summarizes the errors expected in the predictability of radiation in vertical directions based on measurements in height scans from 1 m to 4 m at a horizontal distance of 10 m from each of the four sources operating at 243 MHz.

Table 4.5-6 – Estimates of the errors in prediction of radiation in vertical directions based on a measurement height scan from 1 m to 4 m at known distances, *d*. Frequency = 243 MHz (Adapted from [10])

(1) Source of radiation @ height	(2) Max. *E*, @ angle, in 10 m polar plot	(3) At hor. *d* = 10 m, measure this field	(4) Estimated prediction error, at *d* = 10 m	(5) Max. *E*, @ angle, in 30 m polar plot	(6) At hor. *d* = 30 m, measure this field	(7) Estimated prediction error, at *d* = 30 m	(8) Max. *E*, @ angle, in 300 m polar plot	(9) At hor. *d* = 300 m, measure this field	(10) Estimated prediction error, at *d* = 300 m
Vertical electric dipole @ 1 m	*Ez* @ 33,75°	*Ez*	–1 dB	*Ez* @ 10,5°	*Ez*	–0,5 dB	*Ez* @ 10,5°	*Ez*	–16 dB
Vertical electric dipole @ 2 m	*Ez* @ 18,25°	*Ez*	–0,5 dB	*Ez* @ 18,25°	*Ez*	–0,5 dB	*Ez* @ 7°	*Ez*	–13 dB
Horizontal electric dipole @ 1 m	*Ex* @ 17,5° in Y-Z plane	*Ex* in Y-Z plane	–0,5 dB	*Ex* @ 17,5° in Y-Z plane	*Ex* in Y-Z plane	–4 dB	*Ex* @ 17,5° in Y-Z plane	*Ex* in Y-Z plane	–22,5 dB
Horizontal electric dipole @ 2 m	*Ex* @ 9° in Y-Z plane	*Ex* in Y-Z plane	0 dB	*Ex* @ 8,75° in Y-Z plane	*Ex* in Y-Z plane	–0,5 dB	*Ex* @ 8,75° in Y-Z plane	*Ex* in Y-Z plane	–17 dB
Vertical loop (horizontal magnetic dipole) @ 1 m	*Ez* @ 36,25° in Z-X plane	*Ez* in Z-X plane	–2,5 dB	*Ez* @ 36,5° in Z-X plane	*Ez* in Z-X plane	–2 dB	*Ez* @ 36,5° in Z-X plane	*Ez* in Z-X plane	–17 dB

Vertical loop (horizontal magnetic dipole @ 2 m	*Ex* @ 70,5° in Y-Z plane	*Ez* in Z-X plane	–2,5 dB	*Ex* @ 69,25° in Y-Z plane	*Ez* in Z-X plane	–3 dB	*Ex* @ 69° in Y-Z plane	*Ez* in Z-X plane	–15 dB
Horizontal loop (vertical magnetic dipole) @ 1 m	*Ey* @ 17° in Z-X plane	*Ey* in Z-X plane	–0,5 dB	*Ey* @ 16,75° in Z-X plane	*Ey* in Z-X plane	–3,5 dB	*Ey* @ 16,75° in Z-X plane	*Ey* in Z-X plane	–22,5 dB
Horizontal loop (vertical magnetic dipole) @ 2 m	*Ey* @ 9° in Z-X plane	*Ey* in Z-X plane	0 dB	*Ey* @ 8,75° in Z-X plane	*Ey* in Z-X plane	0 dB	*Ey* @ 8,75° in Z-X plane	*Ey* in Z-X plane	–17 dB

4.5.4.2.4 Predictability at 330 MHz

Figure 4.5-9(a) shows vertical polar plots of *Ez* and *Ex* in the Z-X plane, at 330 MHz, around the small vertical electric dipole placed at a centre height of 1 m above ground. At a scan radius of 10 m the maximum field strength of almost 148 dBμV/m is contributed by *Ez* at an elevation angle of 26°. Calculations of the vertically oriented *Ez* field in a height scan from 1 m to 4 m at 10 m horizontal distance produce a peak magnitude of almost 146 dBμV/m at a measuring height of 1,45 m, as shown in figure 4.5-9(b). This underestimates the maximum field strength by less than 2 dB.

Figure 4.5-10(a) shows vertical polar plots of *Ex* in the Y-Z plane and *Ez* in the Z-X plane, around the small vertical loop placed at a centre height of 1 m above a "medium dry ground". It can be seen that, at a scan radius of 10 m, the maximum field strength of almost 167 dBμV/m is reached by *Ex* at an elevation angle of 69° in the Y-Z plane. The calculated *Ez* height scan patterns in the Z-X plane shown in figure 4.5-10(b) produce a peak magnitude greater than 162 dBμV/m at 10 m horizontal distance, measured at a height of 1,45 m. A height scan measurement of the vertical *Ez* field therefore underestimates the maximum strength of the radiation in vertical directions, the horizontal polarized *Ex* at an elevation angle of 69°, by approximately 4,5 dB.

It is interesting to observe the vertical polar plots of horizontally polarized *E*-field emitted at 330 MHz by a small horizontal loop placed at a height of 1 m above a "medium dry ground", shown in figure 4.5-11(a). The peak of the major lobe, nearest the ground, occurs at an elevation angle of only 12,75°. It is therefore measured at a height of only 2,2 m at a horizontal distance of 10 m, see figure 4.5-11(b). Thus, there is virtually no error in this example of the estimation of maximum field strength at elevated angles.

Column (4) of table 4.5-7 summarizes the estimated errors in the predictability of radiation in vertical directions based on measurements in height scans from 1 m to 4 m at a horizontal distance of 10 m from each of the four sources operating at 330 MHz.

Table 4.5-7 – Estimates of the errors in prediction of radiation in vertical directions based on a measurement height scan from 1 m to 4 m at known distances, *d*. Frequency = 330 MHz (Adapted from [10])

(1) Source of radiation @ height	(2) Max. *E*, @ angle, in 10 m polar plot	(3) At hor. *d* = 10 m, measure this field	(4) Estimated prediction error, at *d* = 10 m	(5) Max. *E*, @ angle, in 30 m polar plot	(6) At hor. *d* = 30 m, measure this field	(7) Estimated prediction error, at *d* = 30 m	(8) Max. *E*, @ angle, in 300 m polar plot	(9) At hor. *d* = 300 m, measure this field	(10) Estimated prediction error, at *d* = 300 m
Vertical electric dipole @ 1 m	*Ez* @ 26°	*Ez*	–2 dB	*Ez* @ 26°	*Ez*	–0,5 dB	*Ez* @ 9°	*Ez*	–15 dB
Vertical electric dipole @ 2 m	*Ez* @ 27,25°	*Ez*	–0,5 dB	*Ez* @ 5,75°	*Ez*	0 dB	*Ez* @ 5,5°	*Ez*	–11,5 dB
Horizontal electric dipole @ 1 m	*Ex* @ 13° in Y-Z plane	*Ex* in Y-Z plane	0 dB	*Ex* @ 12,75° in Y-Z plane	*Ex* in Y-Z plane	–2 dB	*Ex* @ 12,75° in Y-Z plane	*Ex* in Y-Z plane	–20 dB
Horizontal electric dipole @ 2 m	*Ex* @ 6,5° in Y-Z plane	*Ex* in Y-Z plane	0 dB	*Ex* @ 6,5° in Y-Z plane	*Ex* in Y-Z plane	0 dB	*Ex* @ 6,5° in Y-Z plane	*Ex* in Y-Z plane	–14,5 dB
Vertical loop (horizontal magnetic dipole) @ 1 m	*Ex* @ 69° in Y-Z plane	*Ez* in Z-X plane	–4,5 dB	*Ex* @ 68,25° in Y-Z plane	*Ez* in Z-X plane	–3,5 dB	*Ex* @ 68° in Y-Z plane	*Ez* in Z-X plane	–17,5dB
Vertical loop (horizontal magnetic dipole) @ 2 m	*Ex* @ 66,75° in Y-Z plane	*Ez* in Z-X plane	–2,5 dB	*Ex* @ 66° in Y-Z plane	*Ez* in Z-X plane	–2,5 dB	*Ex* @ 66° in Y-Z plane	*Ez* in Z-X plane	–12,5 dB
Horizontal loop (vertical magnetic dipole) @ 1 m	*Ey* @ 12,75° in Z-X plane	*Ey* in Z-X plane	0 dB	*Ey* @ 12,5° in Z-X plane	*Ey* in Z-X plane	–2 dB	*Ey* @ 12,5° in Z-X plane	*Ey* in Z-X plane	–20 dB
Horizontal loop (vertical magnetic dipole) @ 2 m	*Ey* @ 6,5° in Z-X plane	*Ey* in Z-X plane	0 dB	*Ey* @ 6,5° in Z-X plane	*Ey* in Z-X plane	0 dB	*Ey* @ 6,5° in Z-X plane	*Ey* in Z-X plane	–14,5 dB

4.5.4.2.5 Predictability at 1 000 MHz

Figure 4.5-2 shows vertical polar plots of *Ez* and *Ex*, at 1 000 MHz, around a small vertical loop placed at a centre height of 2 m above ground. At a scan radius of 10 m over a "medium dry ground" the maximum field strength of 187 dBµV/m is contributed by the horizontally polarized *Ex* at an elevation angle of 77,5° in the Y-Z plane. Calculations of the vertically oriented *Ez* field in a height scan from 1 m to 4 m at 10 m horizontal distance in the Z-X plane produce a peak field of almost 184 dBµV/m at a height of 3,2 m, as shown in figure 4.5-2(c). A vertically polarized height scan measurement therefore underestimates the maximum field strength by approximately 3 dB.

It is interesting to observe the vertical polar plots of horizontally polarized *E*-field emitted at 1 000 MHz by a small horizontal loop placed at a height of 1 m above a "medium dry ground", shown in figure 4.5-12(a). The peak of the major lobe, nearest the ground, occurs at an elevation angle of only 4,25°. Shown again in figure 4.5-12(b), it occurs at a height of 0,74 m at a horizontal distance of 10 m, and therefore will *not* be measured in a 1 m to 4 m height scan measurement. The next grating lobe is encountered at a height of 2,3 m, and its measurement contributes an underestimate of less than 0,5 dB to the prediction of maximum field strength of the major (lower) lobe.

Column (4) of table 4.5-8 summarizes the errors estimated for the predictability of radiation in vertical directions based on measurements in height scans from 1 m to 4 m at a horizontal distance of 10 m from each of the four sources operating at 1 000 MHz.

Table 4.5-8 – Estimates of the errors in prediction of radiation in vertical directions based on a measurement height scan from 1 m to 4 m at known distances, *d*. Frequency = 1 000 MHz (Adapted from [10])

(1) Source of radiation @ height	(2) Max. *E*, @ angle, in 10 m polar plot	(3) At hor. *d* = 10 m, measure this field	(4) Estimated prediction error, at *d* = 10 m	(5) Max. *E*, @ angle, in 30 m polar plot	(6) At hor. *d* = 30 m, measure this field	(7) Estimated prediction error, at *d* = 30 m	(8) Max. *E*, @ angle, in 300 m polar plot	(9) At hor. *d* = 300 m, measure this field	(10) Estimated prediction error, at *d* = 300 m
Vertical electric dipole @ 1 m	*Ez* @ 17,5°	*Ez*	–0,5 dB	*Ez* @ 4°	*Ez*	0 dB	*Ez* @ 3,75°	*Ez*	–9,5 dB
Vertical electric dipole @ 2 m	*Ez* @ 17,75°	*Ez*	–0,5 dB	*Ez* @ 2°	*Ez*	0 dB	*Ez* @ 2°	*Ez*	–5 dB
Horizontal electric dipole @ 1 m	*Ex* @ 4,25° in Y-Z plane	*Ex* in Y-Z plane	–0,5 dB	*Ex* @ 4,25° in Y-Z plane	*Ex* in Y-Z plane	0 dB	*Ex* @ 4,25° in Y-Z plane	*Ex* in Y-Z plane	–11 dB
Horizontal electric dipole @ 2 m	*Ex* @ 2,25° in Y-Z plane	*Ex* in Y-Z plane	0 dB	*Ex* @ 2,25° in Y-Z plane	*Ex* in Y-Z plane	0 dB	*Ex* @ 2,25° in Y-Z plane	*Ex* in Y-Z plane	–5,5 dB
Vertical loop (horizontal magnetic dipole) @ 1 m	*Ex* @ 64,5° in Y-Z plane	*Ez* in Z-X plane	–2,5 dB	*Ex* @ 64,25° in Y-Z plane	*Ez* in Z-X plane	–1 dB	*Ez* @ 4° in Z-X plane	*Ez* in Z-X plane	–9,5 dB
Vertical loop (horizontal magnetic dipole) @ 2 m	*Ex* @ 77,5° in Y-Z plane	*Ez* in Z-X plane	–3 dB	*Ex* @ 77,25° in Y-Z plane	*Ez* in Z-X plane	–1,5 dB	*Ez* @ 2° in Z-X plane	*Ez* in Z-X plane	–5 dB
Horizontal loop (vertical magnetic dipole) @ 1 m	*Ey* @ 4,25° in Z-X plane	*Ey* in Z-X plane	–0,5 dB	*Ey* @ 4,25° in Z-X plane	*Ey* in Z-X plane	0 dB	*Ey* @ 4,25° in Z-X plane	*Ey* in Z-X plane	–11 dB
Horizontal loop (vertical magnetic dipole) @ 2 m	*Ey* @ 2,25° in Z-X plane	*Ey* in Z-X plane	0 dB	*Ey* @ 2,25° in Z-X plane	*Ey* in Z-X plane	0 dB	*Ey* @ 2,25° in Z-X plane	*Ey* in Z-X plane	–5,5 dB

4.5.4.3 Predictability based on height scan measurements near real ground at an unknown distance, greater than 10 m, from the radiation source

Here we can answer the second question posed in 4.5.2. This measurement situation is analogous to making measurements *in situ* at a distance of 10 m from the wall outside a building containing ISM equipment which is located at an unknown distance inside the building. As mentioned earlier, we do not consider here the attenuation which may be introduced by intervening building materials.

Calculations have been made of vertical polar patterns and linear height scan patterns at distances of 30 m and 300 m. The reader will have already seen that patterns for those distances have also been included in the figures.

The figures, together with the comprehensive summaries presented in columns (7) and (10) of tables 4.5-4 to 4.5-8, show that the predictability of fields at elevated angles based on height scan measurements near real ground becomes more prone to underestimation as the horizontal measuring distance increases beyond 10 m, especially at the lower frequencies. Underestimation can become very large at a distance of 300 m. At the lower frequencies underestimates can reach more than 30 dB at that distance when the source behaves as a small horizontal electric dipole. The underestimates for both horizontally and vertically polarized fields occur in spite of the significant contributions which can be made by surface waves at the lower frequencies near 30 MHz [11]. Predictability improves as the frequency increases, primarily because at higher frequencies the surface wave contributions decrease and the maximum field strength measured in the height scan is created by the sum of the direct and reflected space wave components (the sum is sometimes called, somewhat misleadingly, the "ground wave"). The contributions of the space wave signals increase at lower elevation angles as more grating lobes form with increasing frequency.

It is particularly important to recognize that, at horizontal distances of 30 m and more, the worst-case underestimations of the maximum levels of field strengths at elevated angles will generally occur when the fields are horizontally polarized. This is very unfortunate, because the signals for the ILS (marker beacons, localizer, and glide path, see table 4.5-1) are all horizontally polarized transmissions and therefore require the maximum protection from horizontally polarized disturbances.

The figures also provide guidance to the rates of change of the fields with distance. Calculations and measurements made at a constant height, avoiding nulls, show that the maximum rate of change of the fields with distance can approach a rate that is inversely proportional to distance squared. When surface wave contributions are negligible, then a grazing incidence in the far field a field strength inversely proportional to distance squared is to be expected at a constant measuring height [11] [12]. However, the space wave field strengths along radial paths at constant elevation angles vary in simple proportion with inverse distance, which is to be expected of such far fields propagating freely in space. Therefore it is to be expected that the fields measured near the ground (the so-called "ground waves") will, in general, attenuate more rapidly with increasing distance than do the fields from the same source which are propagating radially up into space.

If the horizontal distances at which height scan measurements are made *in situ* are not known, very large errors can arise – all of them underestimates – in the predictability of the strength of radiation in vertical directions from all four types of source and at all frequencies from 75 MHz to 1 000 MHz.

4.5.4.4 Predictability based on measurement at a fixed height

In its measurement procedures relating to the ways in which measuring antennas are to be used, CISPR 11 does not distinguish between measurements made *in situ* for the protection of specific safety services and those made for the protection of other services. Thus, if a measurement of emissions is made *in situ* from a Group 2 Class A ISM equipment in accordance with the specification, the measuring antenna is placed at a height of 3 m ± 0,2 m (7.2.4); no height scan is specified.

The obvious risk with fixed height measurements is that a measurement will be made at a null in the field strength pattern. The risk of this happening is increased if the electrical height above ground of the radiation centre of the source increases – for example with increasing frequency – which contributes to the formation of an increasing number of grating lobes, and hence nulls. A few examples of the effects these nulls can have on a measurement made at a height near 3 m (or any other *fixed* height) are shown in several of the figures.

For example, figure 4.5-2(c) shows that, depending on the type of ground over which the measurements are made, at a horizontal distance of 10 m from a small vertical loop source located at a height of 2 m the measured vertically polarized field strength at 1 000 MHz might vary by more than 6 dB for measurements made somewhere in the height tolerance range of 2,8 m to 3,2 m, and that at 30 m horizontal distance a measurement made at 3 m height is also close to a null.

Figure 4.5-12(b) shows that a horizontal distance of 10 m from a small horizontal loop source located 1 m above ground with the measured horizontally polarized field strength at 1 000 MHz might vary by more than 12 dB in the CISPR measurement height tolerance range from 2,8 m to 3,2 m. It also shows how the field strength can vary with distance in an apparently anomalous manner when measurements are made at a fixed height. Note that at a height of 3 m the field strength at 30 m distance is the same as the field strength at 10 m distance. At other heights, the field strength at 30 m distance becomes greater than that at 10 m distance.

Comparison of the height scan curves in figure 4.5-13 with those in figure 4.5-12(b) shows that, at 1 000 MHz, as the small horizontal loop source height varies between 1 m and 2 m, deep nulls will pass through the measuring height of 3 m at horizontal measuring distance of 10 m and 30 m. These effects can be encountered at *greater horizontal measuring distances* and *lower frequencies* if the height of the radiating source is increased.

We are now in a position to answer the third question posed in 4.5.2. The answer is that predictability is degraded by fixed height measurements. Measurements at a fixed height should not be permitted, especially if they are being made to determine protection for specific safety services.

Height scans must be specified or, for measuring convenience, the measuring height *in situ* could be specified in the manner of [13], so that at a horizontal distance of 10 m, the measuring height would be specified as 4 m above the immediate terrain *or at such lower height at which the field strengths may exceed that at 4 m*.

4.5.5 Differences between the fields over a real ground and the fields over a perfect conductor

There are significant differences between the field distributions above a real earth plane and over a perfect conductor. There are several reasons for the differences, not the least being that the reflection factors for both polarizations over a perfect conductor always have a magnitude of unity at all angles of incidence, whereas over real ground they have a magnitude less than unity except at grazing incidence. In addition, for vertically polarized waves over a perfect conductor there is no Brewster's angle or, expressed in another way, at all reflection angles a vertically polarized image in a perfect conductor is always in phase with the vertically polarized source above the conductor. This contrasts with the situation of vertically polarized waves meeting a lossy dielectric like real ground, where reflections taking place below Brewster's angle experience a large phase change and the image can be visualized as being in approximate anti-phase with the source. It should also be observed that the reflection factor for a vertically polarized wave reflecting at Brewster's angle has a very small magnitude for most types of real ground encountered in practice.

The behaviour of the fields above a metal ground plane compared with the fields over an earthen ground plane is discussed at length in [11]. The brief discussion below, derived from [11], serves to provide an answer to the fourth question posed in 4.5.2.

4.5.5.1 Vertically polarized fields over a perfect conductor

The contribution of the vertically polarized surface wave over real ground can be significant. However, it cannot increase the total field strength created by a small vertical electric dipole over real ground to equal the strength of the fields created by the same vertical dipole moment over a perfect conductor. Figure 4.5-14 displays the vertical components of the fields emitted at 30 MHz from a small vertical electric dipole situated 1 m above a "medium dry ground", calculated using NEC and SOMNEC to include the surface wave, compared with the fields calculated over an almost perfect conductor (in this case annealed copper).

Comparisons of the fields over real ground with those over the good conductor show why vertically polarized measurements at 30 MHz on a measuring site with a metal ground plane are not comparable with measurements made on sites with earthen ground planes. Specifically, they show why measurements of vertically polarized disturbances made on a metal ground place for comparison with field strength disturbance limits developed for earth sites may penalize the equipment under test (EUT). The fields measured over a metal ground plane can exceed the limits, even when the fields from the same EUT over an earthen ground plane are comfortably below the limits. The comparisons also show why calculations of the vertically polarized fields created at 30 MHz over a perfect conductor or a metal ground plane, for a given dipole moment, are a bad guide to the predictability achievable for the fields created at elevated angles by that dipole moment over a real ground. If the fields over the good conductor are mistakenly believed to resemble those over a real ground, they will encourage a false sense of confidence that ground based measurements over real ground will give good guidance to the field strengths to be expected at elevated angles.

In figure 4.5-15, the height scan patterns of the vertical components of the *E*-fields emitted from the small vertical dipole show that at 1 000 MHz, just as was the case at 30 MHz, the vertically polarized fields developed near a metal ground plane at 1 000 MHz are much stronger than those developed near a "medium dry ground". The same conclusions which were reached at a frequency of 30 MHz regarding the possible penalties imposed on an EUT, when the disturbances measured on a metal ground plane site are compared with field strength disturbance limits developed for earth sites, also apply at a frequency of 1 000 MHz. Similarly, it can be seen in figure 4.5-15 that at 1 000 MHz the patterns of the vertically polarized fields over a metal ground plane are a bad guide to the predictability of the fields created at elevated angles by the same dipole moment over a real ground.

The height scan patterns in figure 4.5-15 also clearly illustrate the effect of the phase reversal of the vertical dipole image in a lossy dielectric when reflection take place below Brewster's angle. The dashed horizontal line across the height scan pattern for 10 m distance shows the height, approximately 1,6 m, to the field point which corresponds with a reflection taking place at Brewster's angle when the source is 1 m above the "medium dry ground".

It is quite clear in figure 4.5-15 that at 10 m distance the field nulls and maxima at heights greater than 1,6 m above both the copper ground plane and the "medium dry ground" are in phase, signifying that the images in the two kinds of ground planes have similar phases when reflection from the real ground takes place at elevation angles above Brewster's angle. However, it is also quite clear that vertically polarized waves reflected below Brewster's angle over the "medium dry ground" are reversed in phase with respect to the corresponding reflected waves over the copper ground plane. In other words, the vertical image in the lossy dielectric is reversed, producing destructive interference (a null) at the surface of the "medium dry ground" whereas constructive interference (a maximum) occurs at the surface of the copper ground plane (the direct and reflected path lengths being the same in both cases). With the vertical dipole source at a height of 1 m, a maximum occurs in the field at 10 m distance at a height of 0,75 m above the "medium dry ground", whereas a very deep null occurs at that height over the copper ground plane (the direct and reflected path lengths differ by $\lambda/2$ in both cases).

The height scans at 30 m and 300 m, up to a height of 6 m, take place below Brewster's angle. Maxima in the height scanned fields over the metal ground plane therefore coincide with minima in the fields over real ground in both those height scans. This is largely the reason why it must not be believed that the height scanned vertically polarized fields calculated over a good conductor will resemble those over real ground, especially at the larger horizontal distances. Such a belief will create false confidence that measurements made near real ground, without regard for the horizontal distance from the source, can give good guidance to the field strengths to be expected at elevated angles.

4.5.5.2 Horizontally polarized fields over a perfect conductor

Although the contribution of the horizontally polarized surface wave over real ground at 30 MHz is small, nevertheless the height scan patterns in figure 4.5-16 show that the horizontally polarized fields near the "medium dry ground" are stronger in this case than the corresponding fields near the copper ground plane.

In both cases a null is required in the vertical field pattern at the ground, to satisfy the boundary conditions, and the null is deeper in the copper ground plane example. This example shows that, in contrast with vertically polarized measurements, it is possible that measurements of horizontally polarized fields made on a metal ground plane for comparison with radiated disturbance limits developed for earth sites may slightly favour the EUT when measuring for compliance with the limits.

In figure 4.5-17, the height scan patterns of the horizontally polarized *E*-fields emitted at 1 000 MHz from the small horizontal electric dipole show that at height scan distance of 30 m and more, with no useful contribution from the surface wave, the maximum horizontally polarized fields over a "medium dry ground" are very similar to those over a copper ground plane. The similarity of magnitude in regions of constructive interference is caused by the similar reflection factors (magnitudes close to unity) over both surfaces at low angles of reflection. At higher reflection angles, and a shorter measurement distance of 10 m, the maximum horizontally polarized fields over a metal ground plane exceed those over an earthen ground plane because the magnitude of the reflection factor over the earth plane becomes significantly less than unity. The reflected wave then contributes less to the constructive interference occurring at the field maxima.

The behaviour of the horizontally polarized fields over an earthen ground plane is not complicated by a Brewster's angle phenomenon. In general, at frequencies of 30 MHz and above, the horizontally polarized field patterns over a real ground resemble the shapes of the corresponding patterns over a metal ground plane. Some small differences in field strengths are created over real ground compared with those over a metal ground plane at the lower frequencies by the presence of the surface wave over a real ground. Differences are also created at short horizontal distances, and higher frequencies at which the surface wave is insignificant, because the magnitude of the horizontal reflection factor decreases below unity as the waves reflect at higher angles from the earth plane.

4.5.5.3 Fields over a perfect conductor as guides to the fields over real ground

We can now answer the fourth question posed in 4.5.2.

In summary, the horizontal polarized field patterns created over real ground at frequencies of 30 MHz and above resemble the corresponding patterns over a metal ground plane. There are some differences of a few decibels in field magnitudes. At the lower frequencies some small differences are also created by the existence of the surface wave over a real ground. At the higher frequencies the field strength differences at short measuring distances are caused by the decrease below unity of the magnitude of the horizontal reflection factor for real ground when reflection takes place at angles significantly above grazing incidence. Constructive interference of direct and reflected waves over real ground then produces field strength maxima of somewhat smaller magnitudes than those produced over a good conductor which has a reflection factor close to unity at all reflection angles.

However, very large differences are found when comparing the patterns of vertically polarized fields over a metal ground plane with those over a real ground. The differences are primarily created by the existence of Brewster's angle for the reflections of vertically polarized waves from a lossy dielectric like real ground. When reflections from real ground take place below Brewster's angle the minima in the fields occur at the same heights at which the maxima are produced with the same measuring geometry over the metal ground plane, most notably at the surface of the ground plane. This contrapositioning of minima and maxima is the main reason why the height scanned vertically polarized fields calculated over a good conductor must not be assumed to resemble those over real ground, especially at the larger horizontal distances when reflection take place near grazing incidence. An assumption that there is a resemblance encourages false confidence that measurements near real ground, without regard for the horizontal distance from the source, can give good guidance to the field strengths to be expected at elevated angles.

Vertically polarized field patterns over a metal ground plane do not resemble the shapes and magnitudes of the vertically polarized field patterns to be expected from the same sources over a real ground.

4.5.6 Uncertainty ranges

The information summarized in tables 4.5-4 to 4.5-8 can also be used to show pictorially the ranges of uncertainties in the predictability of the radiation emitted at elevated angles at frequencies above 30 MHz. The information has been used to construct bar charts illustrating the uncertainties for electrically small sources located 1 m or 2 m above ground when predictions of the field strengths at elevated angles are based on *E*-field measurements in 1 m to 4 m height scans at horizontal distances of 10 m, 30 m and 300 m.

Figure 4.5-18 illustrates the uncertainties in predictability based on measurements made at a horizontal distance of 10 m. The bar for the uncertainty range at 330 MHz shows that the best predictability at 330 MHz is obtained when the source behaves as either a small horizontal dipole (dh) or as a small horizontal loop (lh). There is nominally zero error predicting the maximum strength of the horizontally polarized *Eh* fields. The poorest predictability at 330 MHz results in an underestimate of approximately 4,5 dB for the maximum horizontally polarized field *Eh* emitted at elevated angles from a small vertical loop (lv).

When measurements are made in a height scan at a horizontal distance of 30 m, the bar for the uncertainty range at 110 MHz in figure 4.5-19 shows that the best predictability at 110 MHz occurs when the source behaves as a small vertical dipole (dv). There is a negligible underestimate, by 0,5 dB, predicting the *Ez* vertical component of the vertically polarized field. The poorest predictability at 110 MHz produces a greater underestimate, by 9,5 dB, of the horizontally polarized *Eh* field emitted at elevated angles from a small horizontal dipole source (dh).

Figure 4.5-20 graphically illustrates the very large uncertainties in predictability that occur if the horizontal measuring distance is as great as 300 m. At 243 MHz, the bar illustrating the uncertainty range shows that the poorest predictability at 243 MHz introduces a very large underestimate by 22,5 dB for the horizontally polarized *Eh* fields emitted at elevated angles from a small horizontal dipole (dh) and from a small horizontal loop (lh). The best predictability at 243 MHz also produces a large underestimate, by 13 dB, of the vertical *Ez* component of the vertically polarized field emitted at elevated angles from a small vertical dipole (dv). Figures 4.5-19 and 4.5-20, in particular, graphically illustrate the very large underestimates which can occur when attempts are made to predict the strength of radiation in vertical directions based on measurements near the ground at unknown horizontal distances greater than 10 m from the sources.

4.5.7 Conclusions

The *in situ* measurement procedures at frequencies above 30 MHz which are specified in CISPR 11 can lead to significant underestimates of the field strengths emitted at elevated angles from ISM equipment. The underestimates can arise due to the ill-defined measurement distance; the measuring distance from the radiating ISM equipment is not defined.

The largest underestimates of the fields at elevated angles will generally occur for horizontally polarized fields. This is a cause for concern, because the aeronautical safety of life services requiring greatest protection from disturbances originating at the ground are those provided by the horizontally polarized marker beacon, localizer, and glide path signals of the aeronautical ILS.

Under some conditions, measurements are specified in CISPR 11 at a fixed height of 3 m. Measurements at a fixed height should not be specified if they are being made to determine protection for specific safety services. There is a risk that fixed height measurements will be made in, or close to, a null. The risk increases at the higher frequencies and when the height to the radiation centre of the source is unknown. Fixed height measurements can seriously underestimate the true field strength near the ground and, in consequence, the maximum field strength at elevated angles.

Calculations or measurements of the field strength patterns of vertically polarized fields over a perfect conductor or metal ground plane do not provide good guidance to the fields to be expected over a real ground. At reflection angles below Brewster's angle over real ground the field minima and maxima are contraposed with those created by the same source over a metal ground plane.

To provide protection for aeronautical safety of life services, and other communication systems, height scan measurements and limits for radiated disturbances from *in situ* ISM equipment located near the ground must be *specified at a known horizontal distance from the equipment*. Height scan measurements at a horizontal distance of 10 m from an ISM equipment *in situ* allow accurate estimates to be made of the fields emitted at elevated angles. If for practical reasons the *in situ* measurements must be made at a distance greater than 10 m from the equipment which is the source of the radiation then the limits at the larger distance, particularly if it is more than 30 m, must be derived from the 10 m limits by adjusting them in inverse proportion with increasing distance squared. This must be so in order to prevent relaxation of the protection the limits are intended to provide for communication or radionavigation systems that are operated high above ground.

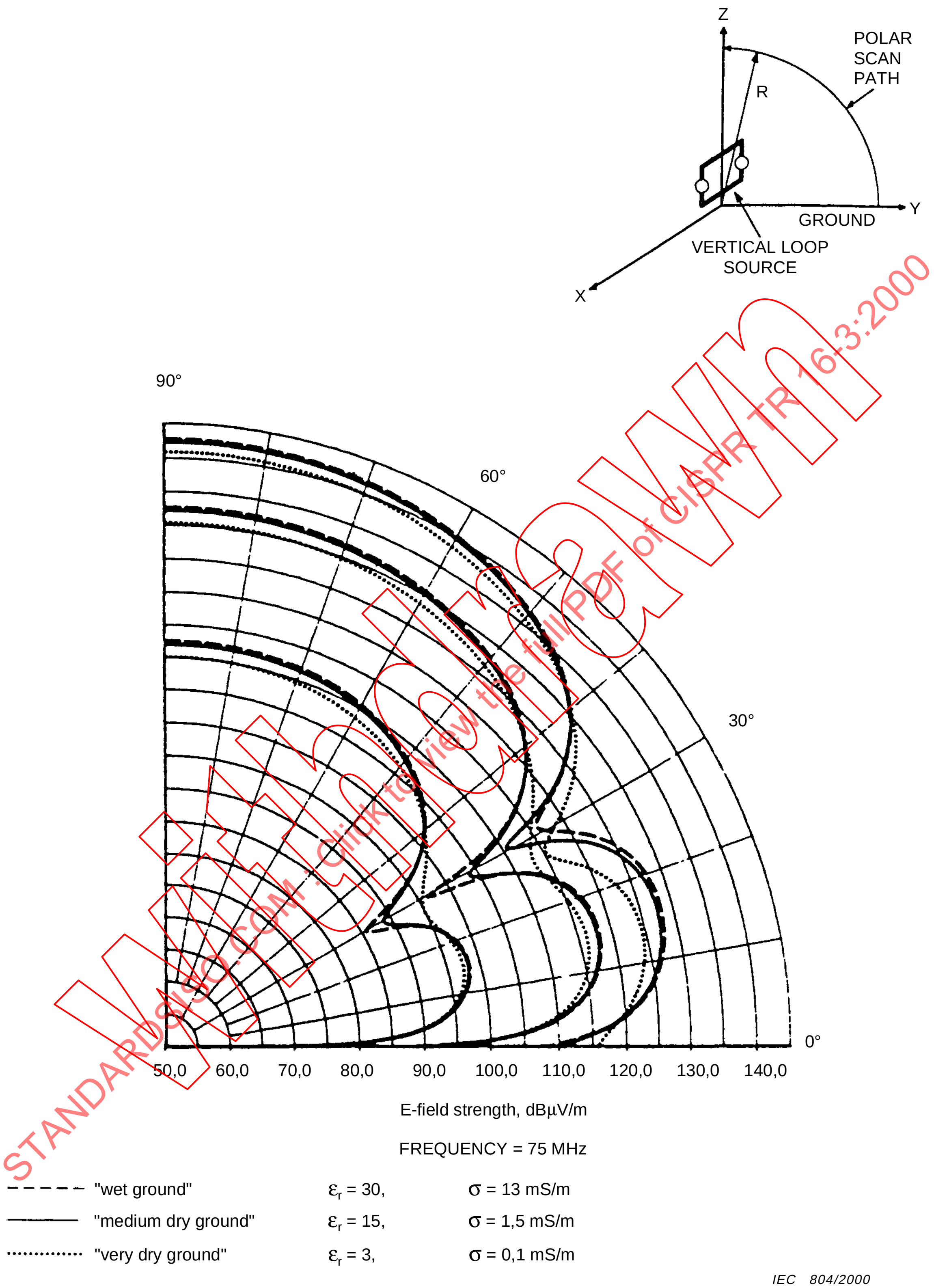

Figure 4.5-1(a) – Vertical polar patterns of horizontally polarized *Ex* field strengths emitted at 75 MHz around the small vertical loop (horizontal magnetic dipole), at scan radii of 10 m, 30 m and 300 m in the Y-Z plane over three different types of real ground. Loop dimensions 0,1 m × 0,1 m. Loop centre height 2 m. Dipole moment 1 A·m^2. (Reproduced from [10])

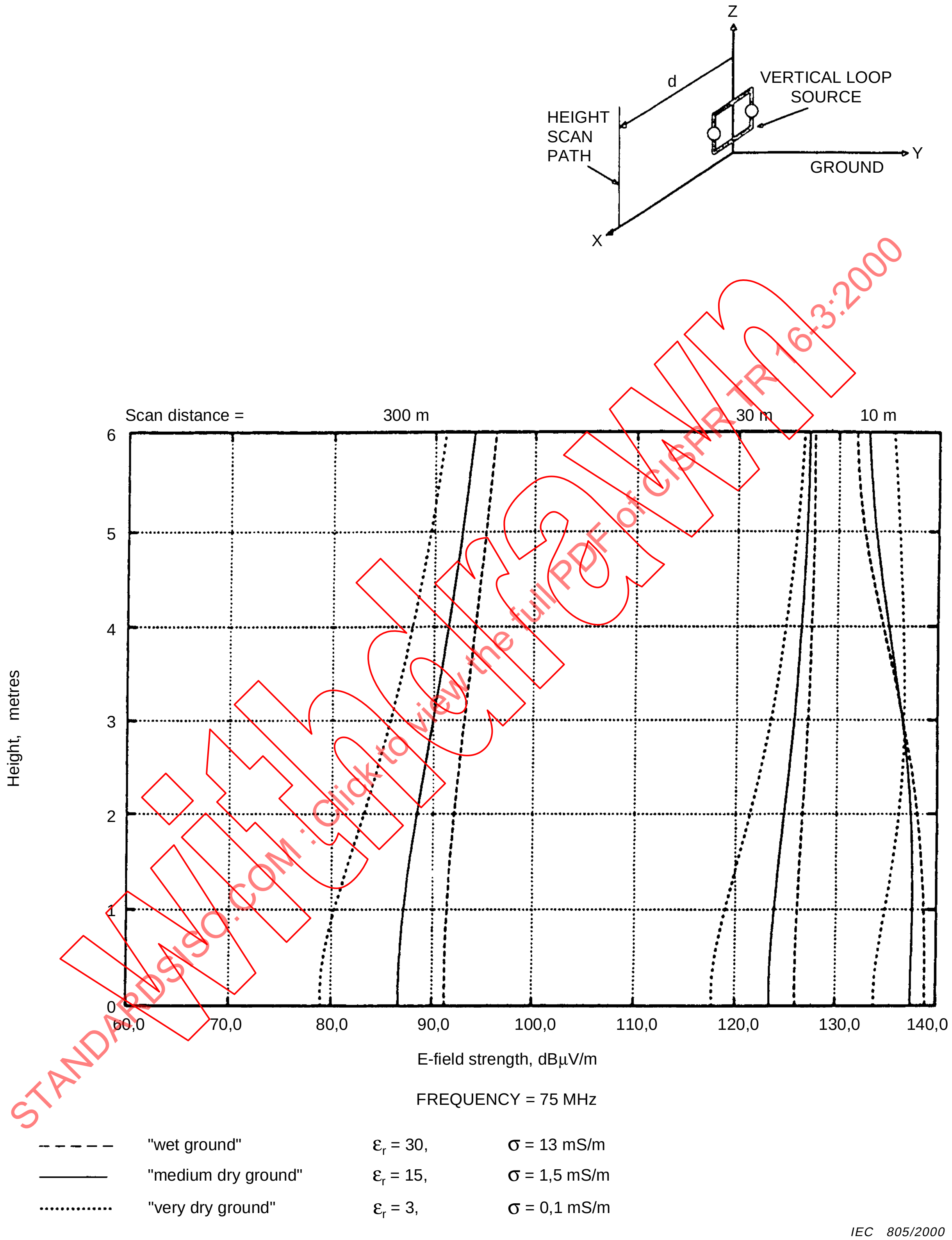

Figure 4.5-1(b) Height scan patterns of vertically oriented *Ez* field strengths emitted at 75 MHz from the small vertical loop (horizontal magnetic dipole), at horizontal distances of 10 m, 30 m and 300 m in the Z-X plane over three different types of real ground.
Loop dimensions 0,1 m × 0,1 m. Loop centre height 2 m. Dipole moment 1 A·m^2.
(Reproduced from [10])

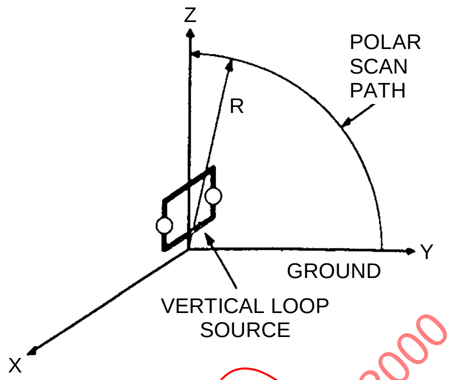

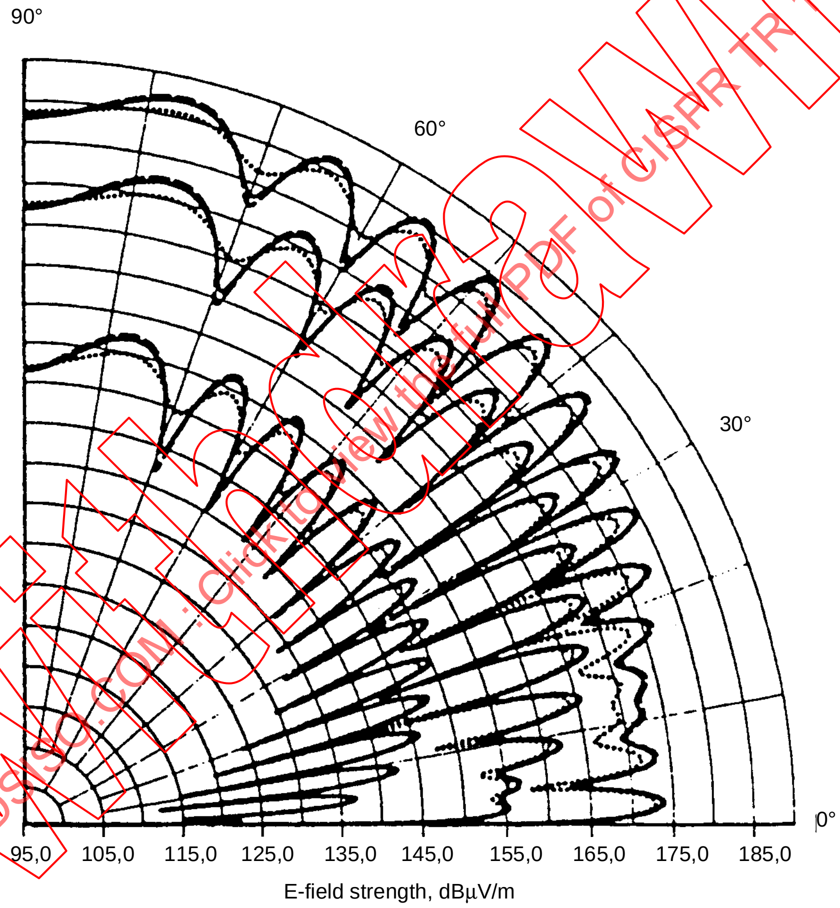

FREQUENCY = 1 000 MHz

– – – – –	"wet ground"	ε_r = 30,	σ = 140 mS/m
————	"medium dry ground"	ε_r = 15,	σ = 35 mS/m
··············	"very dry ground"	ε_r = 3,	σ = 0,15 mS/m

IEC 806/2000

Figure 4.5-2(a) – Vertical polar patterns of horizontally polarized *Ex* field strengths emitted at 1 000 MHz around the small vertical loop (horizontal magnetic dipole), at scan radii of 10 m, 30 m and 300 m in the Y-Z plane over three different types of real ground. Loop dimensions 0,02 m × 0,02 m. Loop centre height 2 m. Dipole moment 1 A·m².
(Reproduced from [10])

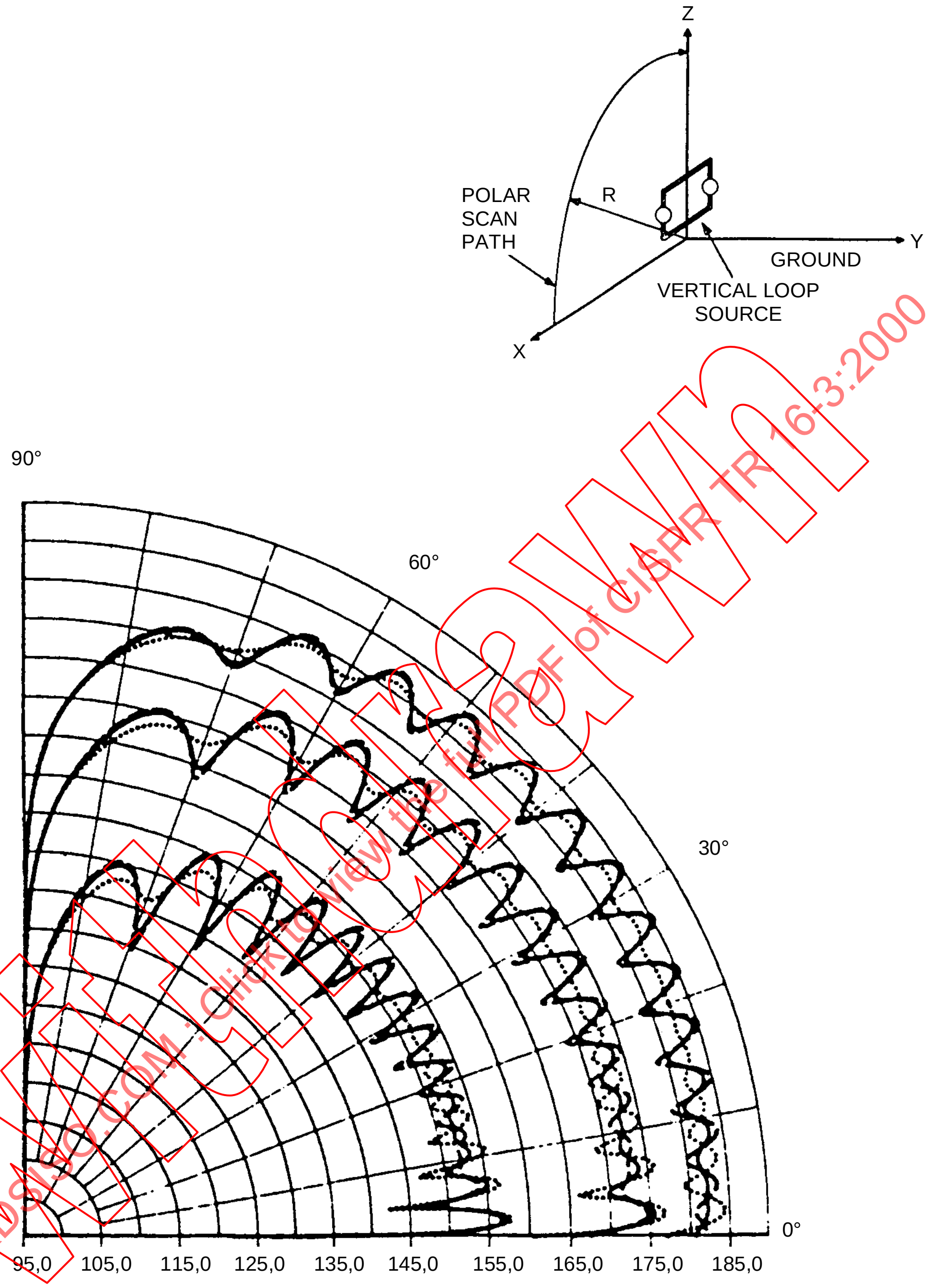

E-field strength, dBμV/m

FREQUENCY = 1 000 MHz

– – – – –	"wet ground"	ε_r = 30,	σ = 140 mS/m
————	"medium dry ground"	ε_r = 15,	σ = 35 mS/m
··············	"very dry ground"	ε_r = 3,	σ = 0,15 mS/m

IEC 807/2000

Figure 4.5-2(b) – Vertical polar patterns of vertically oriented *Ez* field strengths emitted at 1 000 MHz around the small vertical loop (horizontal magnetic dipole), at scan radii of 10 m, 30 m and 300 m in the Z-X plane over three different types of real ground. Loop dimensions 0,02 m × 0,02 m. Loop centre height 2 m. Dipole moment 1 A·m^2. (Reproduced from [10])

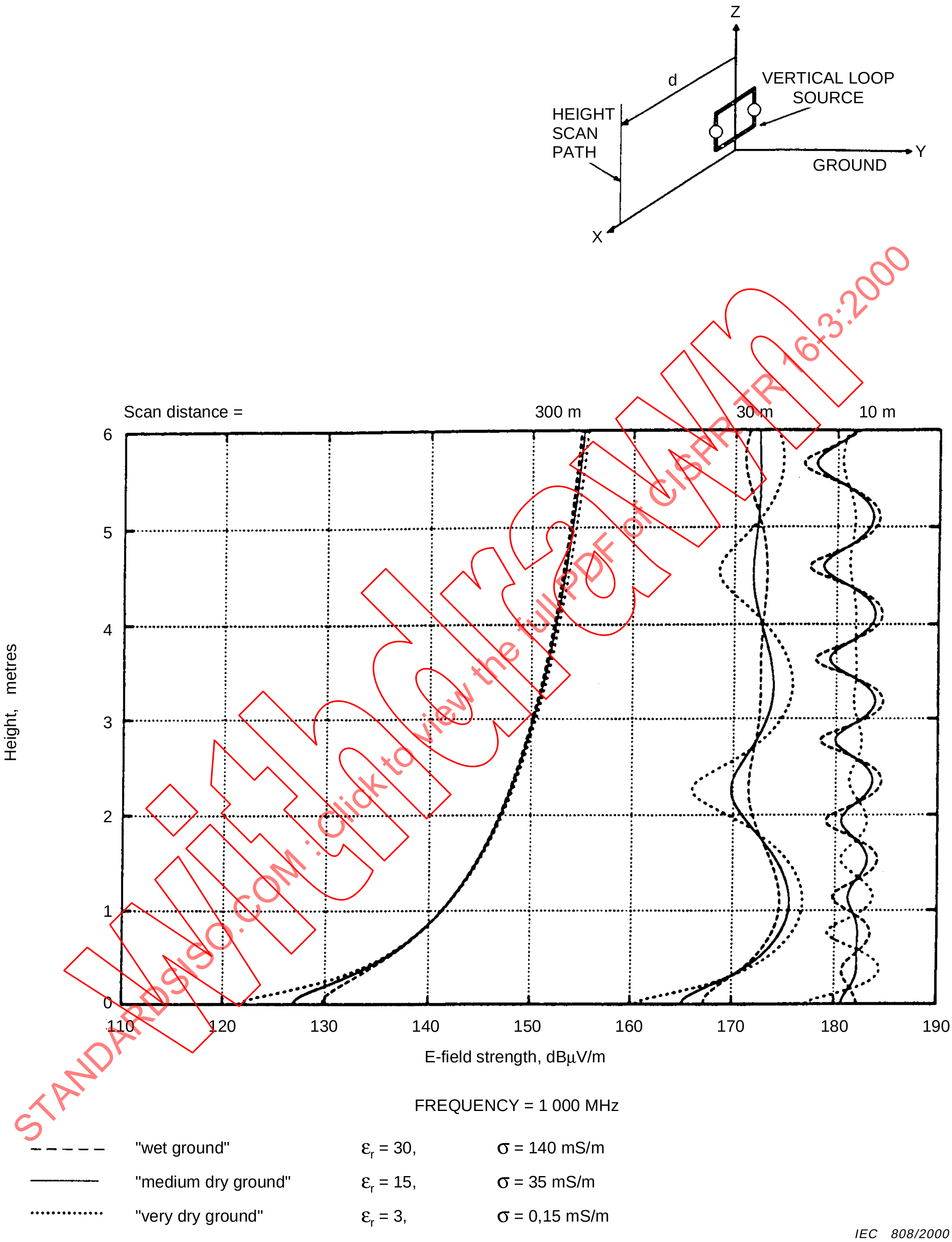

Figure 4.5-2(c) – Height scan patterns of vertically oriented *Ez* field strengths emitted at 1 000 MHz from the small vertical loop (horizontal magnetic dipole), at horizontal distance of 10 m, 30 m and 300 m in the Z-X plane over three different types of real ground.
Loop dimensions 0,02 m × 0,02 m. Loop centre height 2 m. Dipole moment 1 A·m^2.
(Reproduced from [10])

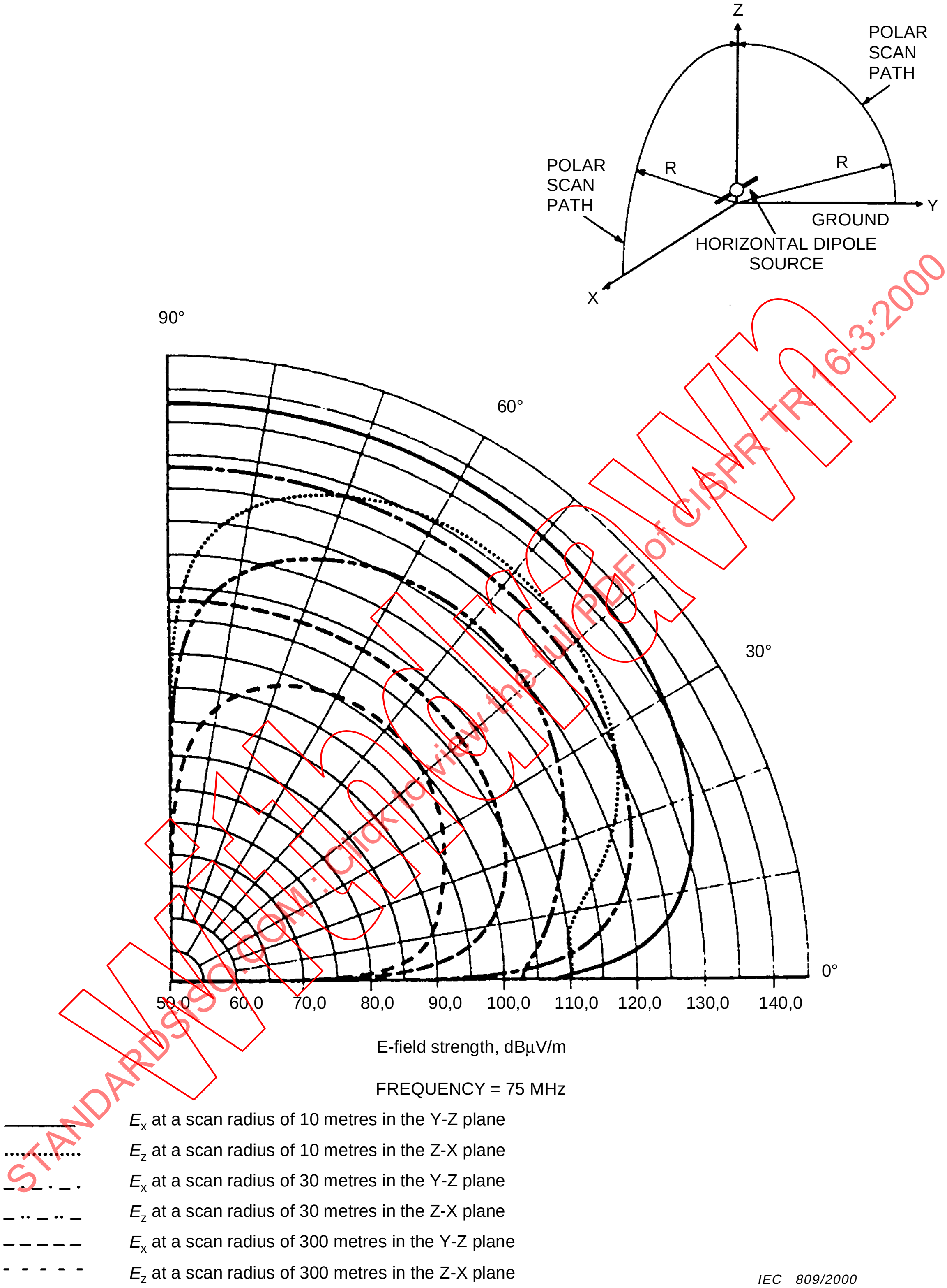

Figure 4.5-3(a) – Vertical polar patterns of horizontally polarized *Ex* and vertically oriented *Ez* field strengths emitted at 75 MHz around the small horizontal electric dipole, at scan radii of 10 m, 30 m and 300 m in the Y-Z plane and the Z-X plane respectively. Dipole length 0,2 m. Dipole height 1 m. Dipole moment 1 A·m. Ground constants: ε_r = 15, σ = 1,5 mS/m. (Reproduced from [10])

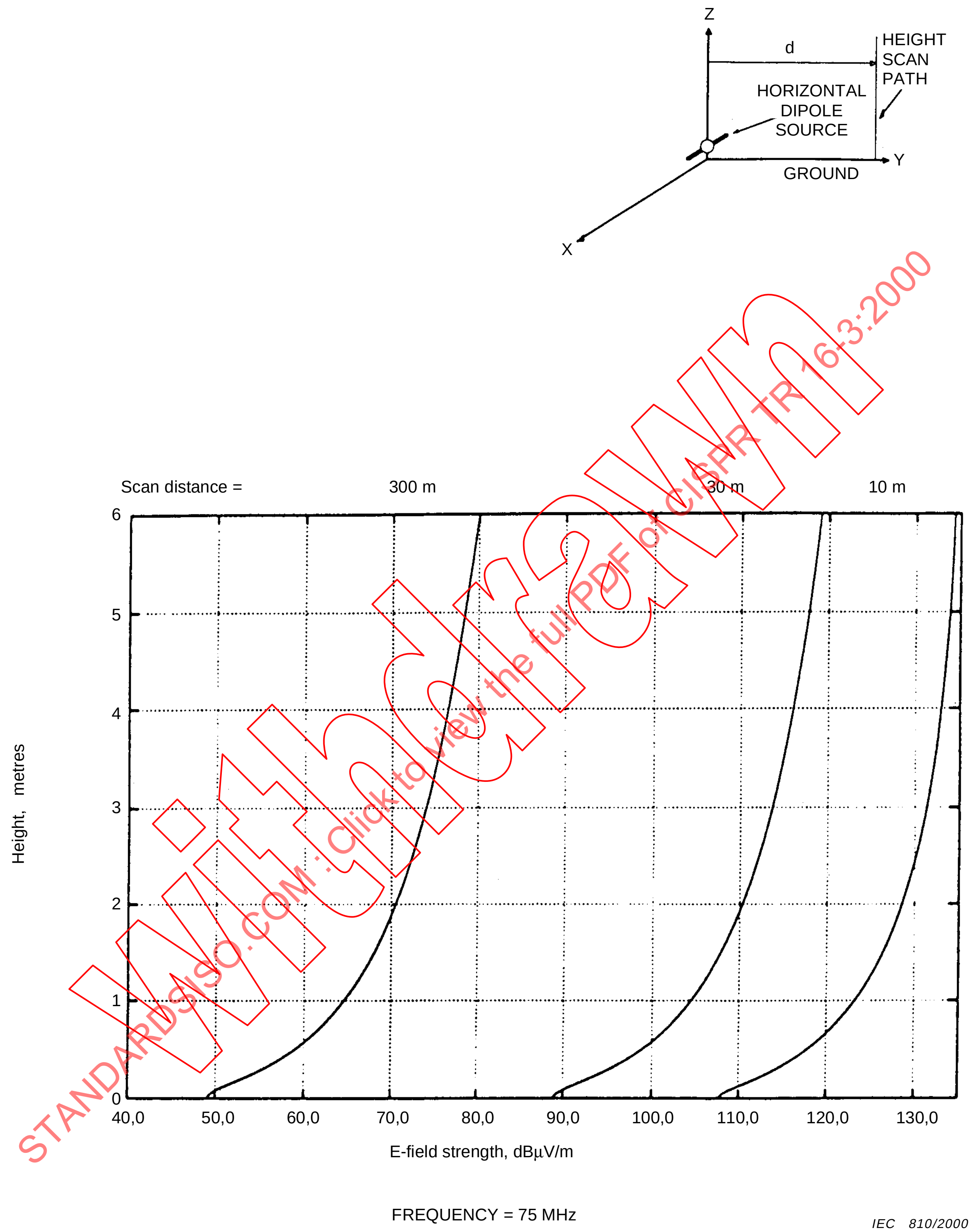

Figure 4.5-3(b) – Height scan patterns of horizontally polarized *Ex* field strengths emitted at 75 MHz from the small horizontal electric dipole, at horizontal distances of 10 m, 30 m and 300 m in the Y-Z plane. Dipole length 0,2 m. Dipole height 1 m. Dipole moment 1 A·m. Ground constants: ε_r = 15, σ = 1,5 mS/m. (Reproduced from [10])

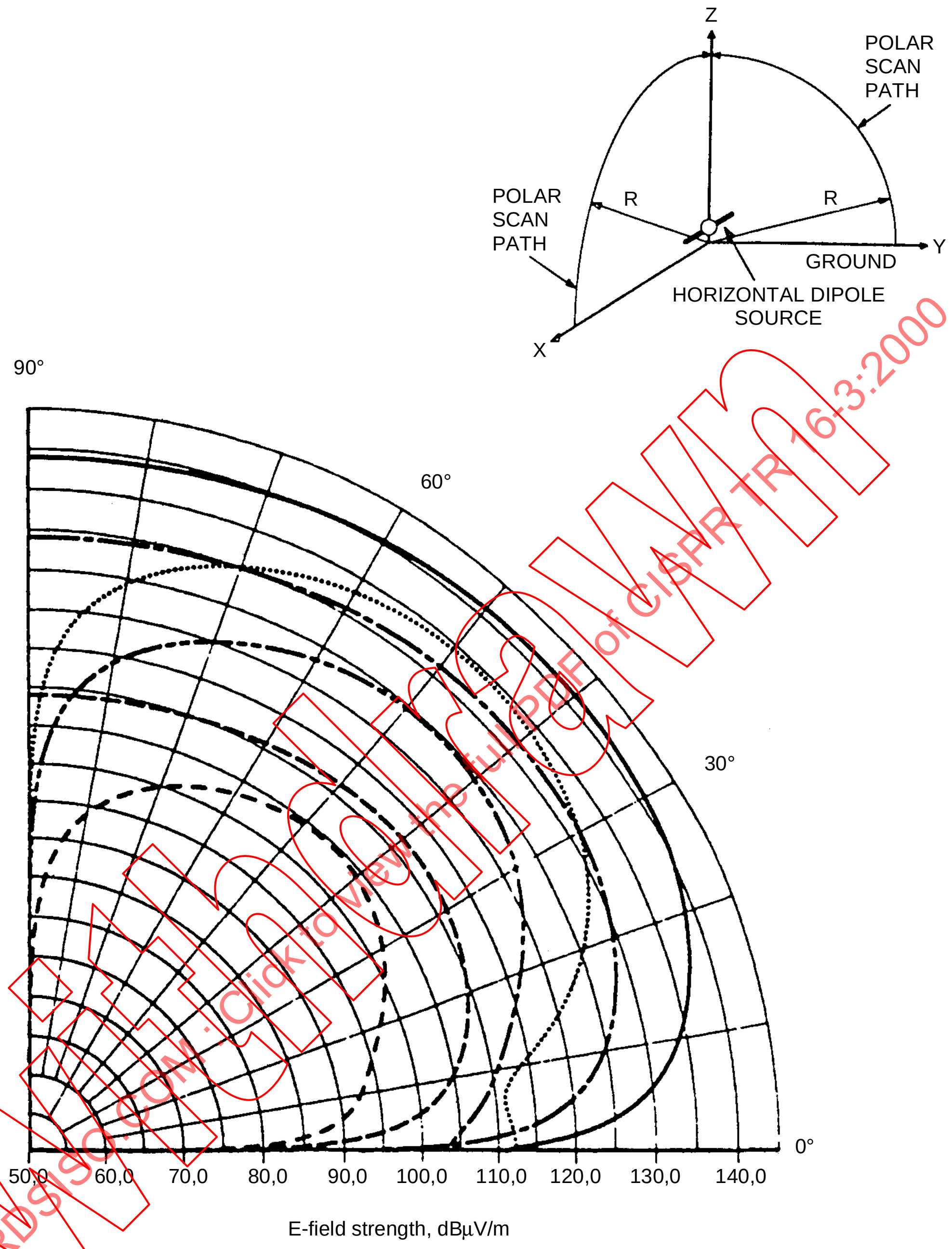

———— E_x at a scan radius of 10 metres in the Y-Z plane

·········· E_z at a scan radius of 10 metres in the Z-X plane

_ . _ . _ E_x at a scan radius of 30 metres in the Y-Z plane

_ .. _ .. _ E_z at a scan radius of 30 metres in the Z-X plane

– – – – – E_x at a scan radius of 300 metres in the Y-Z plane

- - - - - E_z at a scan radius of 300 metres in the Z-X plane

IEC 811/2000

Figure 4.5-4(a) – Vertical polar patterns of horizontally polarized *Ex* and vertically oriented *Ez* field strengths emitted at 110 MHz around the small horizontal electric dipole, at scan radii of 10 m, 30 m and 300 m, in the Y-Z plane and the Z-X plane respectively. Dipole length 0,2 m. Dipole height 1 m. Dipole moment 1 A·m. Ground constants: ε_r = 15, σ = 2 mS/m. (Reproduced from [10])

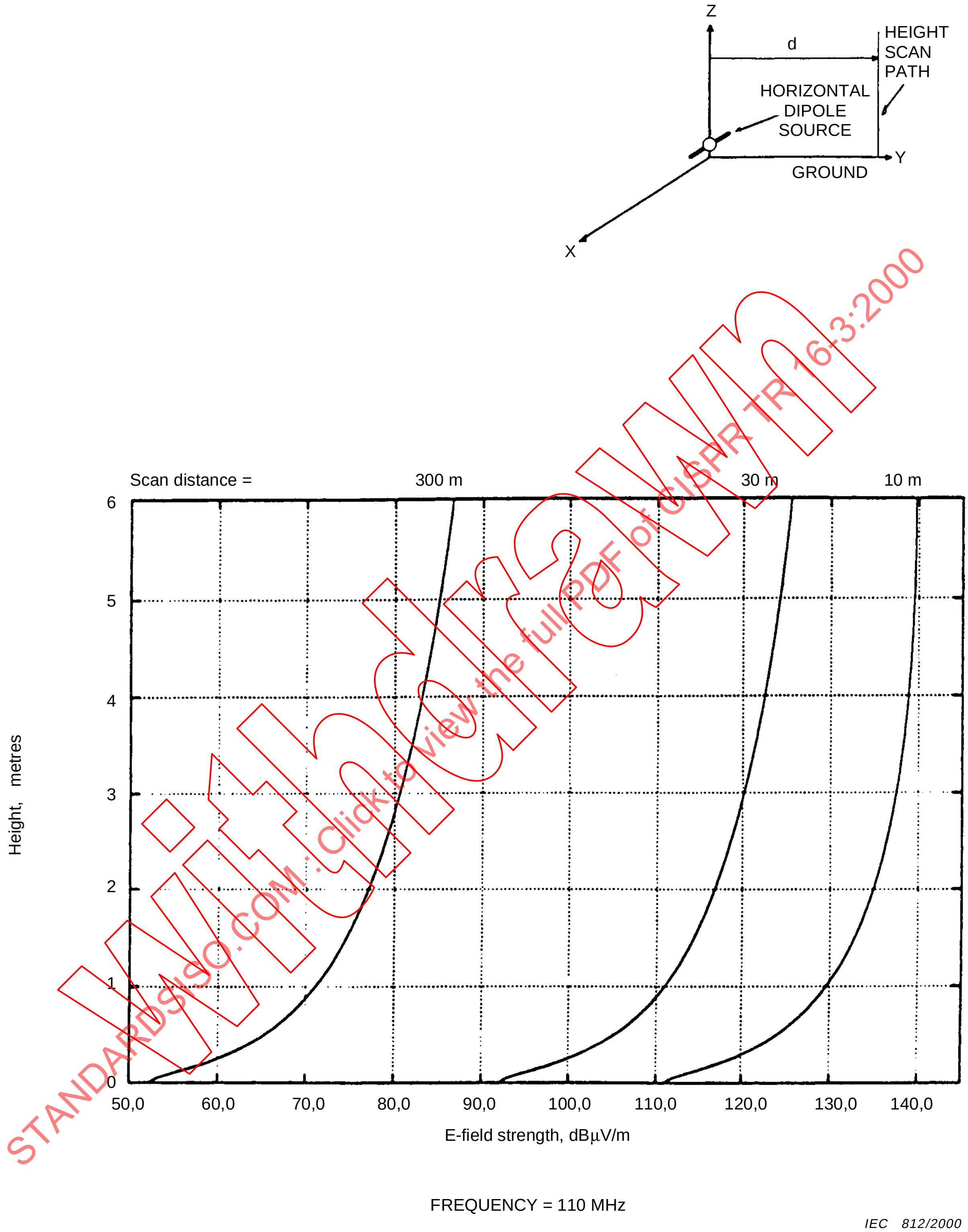

Figure 4.5-4(b) – Height scan patterns of horizontally polarized *Ex* field strengths emitted at 110 MHz from the small horizontal electric dipole, at horizontal distances of 10 m, 30 m and 300 m, in the Y-Z plane. Dipole length 0,2 m. Dipole height 1 m. Dipole moment 1 A·m. Ground constants: ε_r = 15, σ = 2 mS/m. (Reproduced from [10])

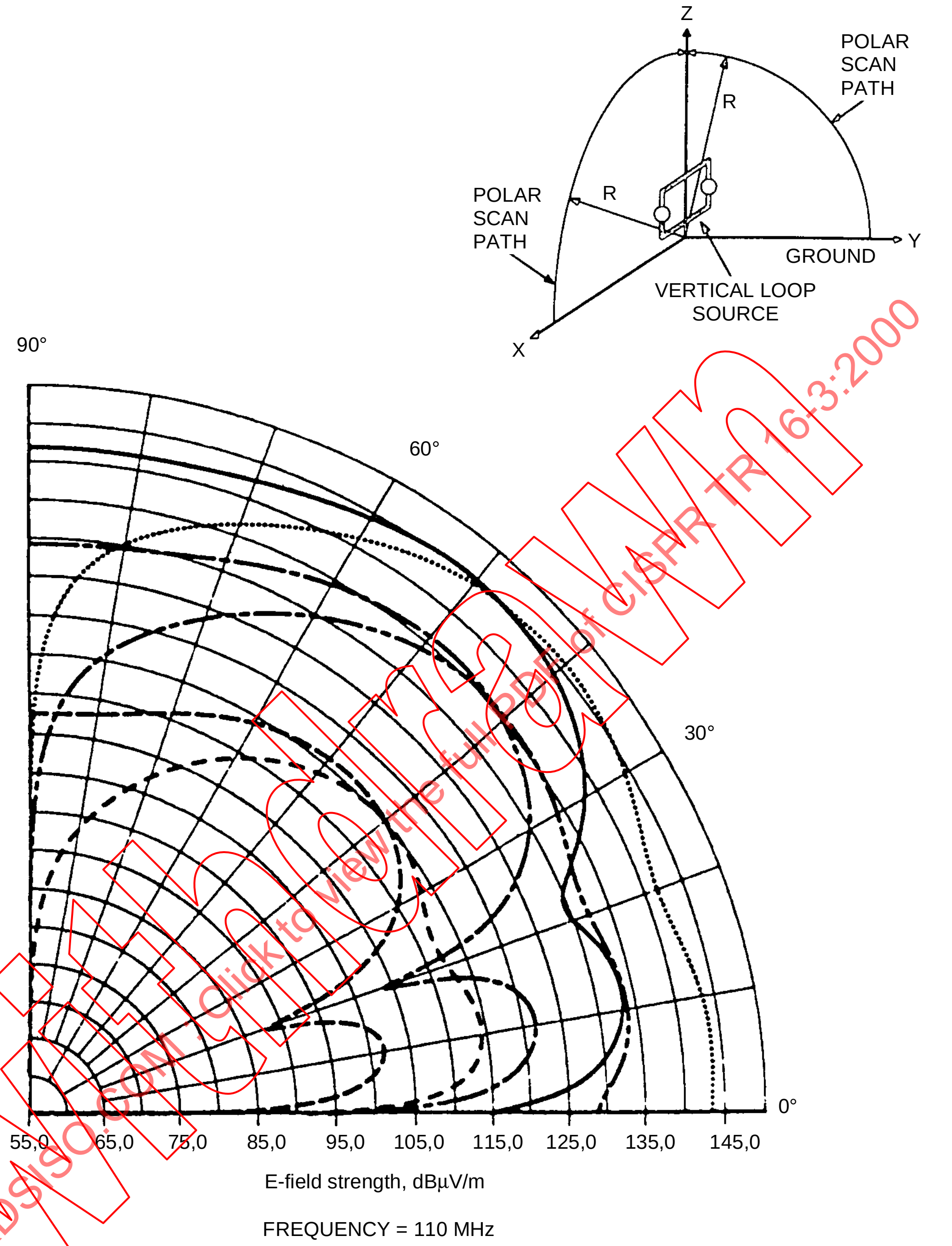

E_x at a scan radius of 10 metres in the Y-Z plane

E_z at a scan radius of 10 metres in the Z-X plane

E_x at a scan radius of 30 metres in the Y-Z plane

E_z at a scan radius of 30 metres in the Z-X plane

E_x at a scan radius of 300 metres in the Y-Z plane

E_z at a scan radius of 300 metres in the Z-X plane

IEC 813/2000

Figure 4.5-5(a) – Vertical polar patterns of horizontally polarized *Ex* and vertically oriented *Ez* field strengths emitted at 110 MHz around the small vertical loop (horizontal magnetic dipole), at scan radii of 10 m, 30 m and 300 m, in the Y-Z plane and the Z-X plane respectively. Loop dimensions 0,1 m × 0,1 m. Loop centre height 2 m. Dipole moment 1 A·m^2. Ground constants: ε_r = 15, σ = 2 mS/m. (Reproduced from [10])

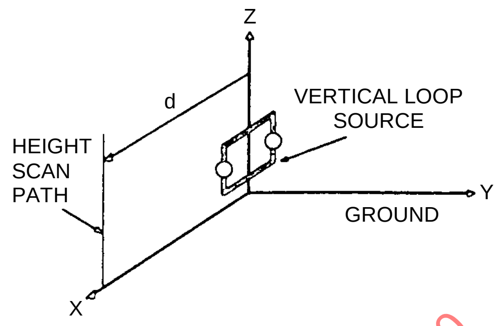

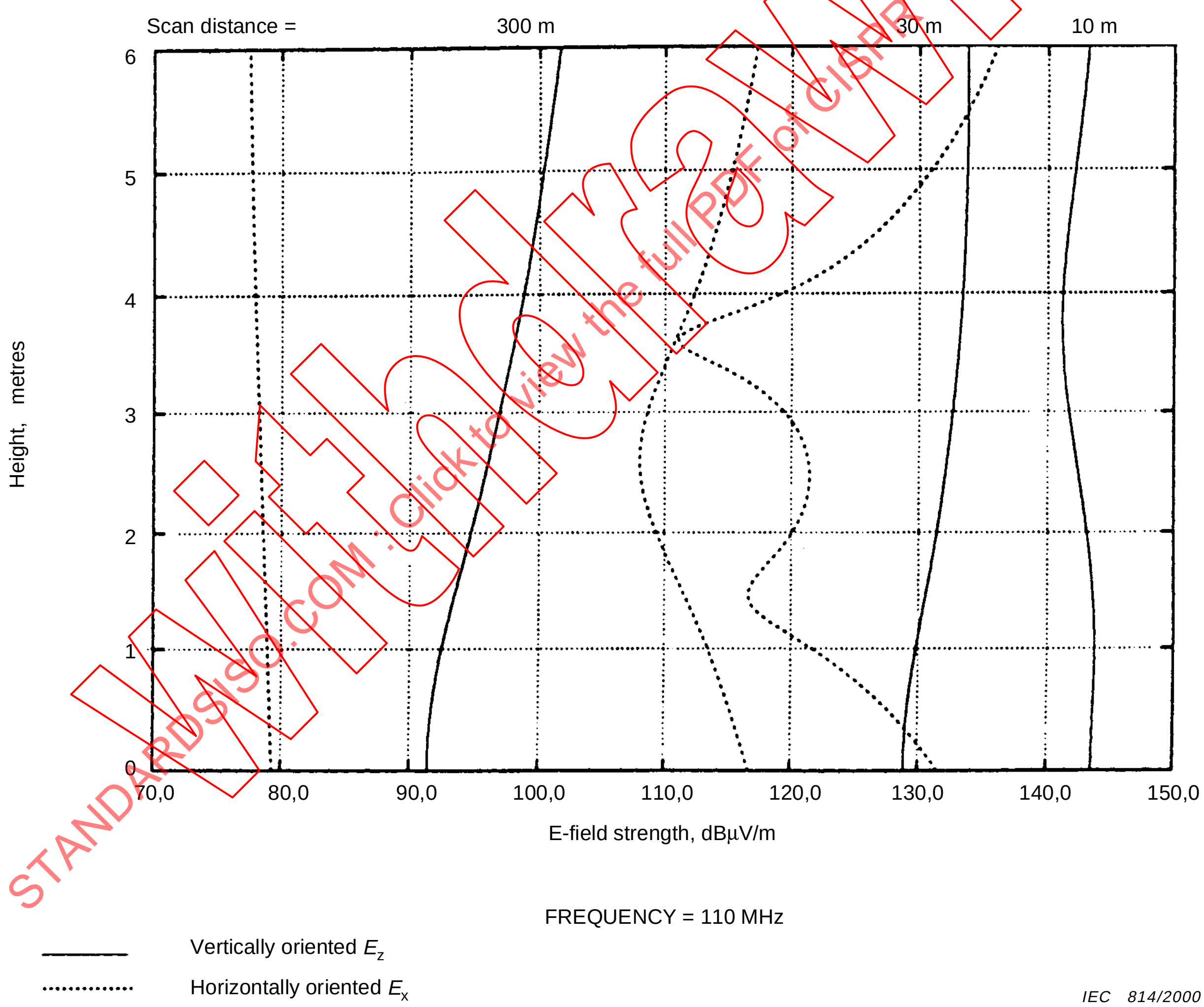

Figure 4.5-5(b) – Height scan patterns of vertically oriented *Ez* and horizontally oriented *Ex* field strengths emitted at 110 MHz from the small vertical loop (horizontal magnetic dipole), at horizontal distances of 10 m, 30 m and 300 m, in the Z-X plane. Loop dimensions 0,1 m × 0,1 m. Loop centre height 2 m. Dipole moment 1 A·m^2. Ground constants: ε_r = 15, σ = 2 mS/m. (Reproduced from [10])

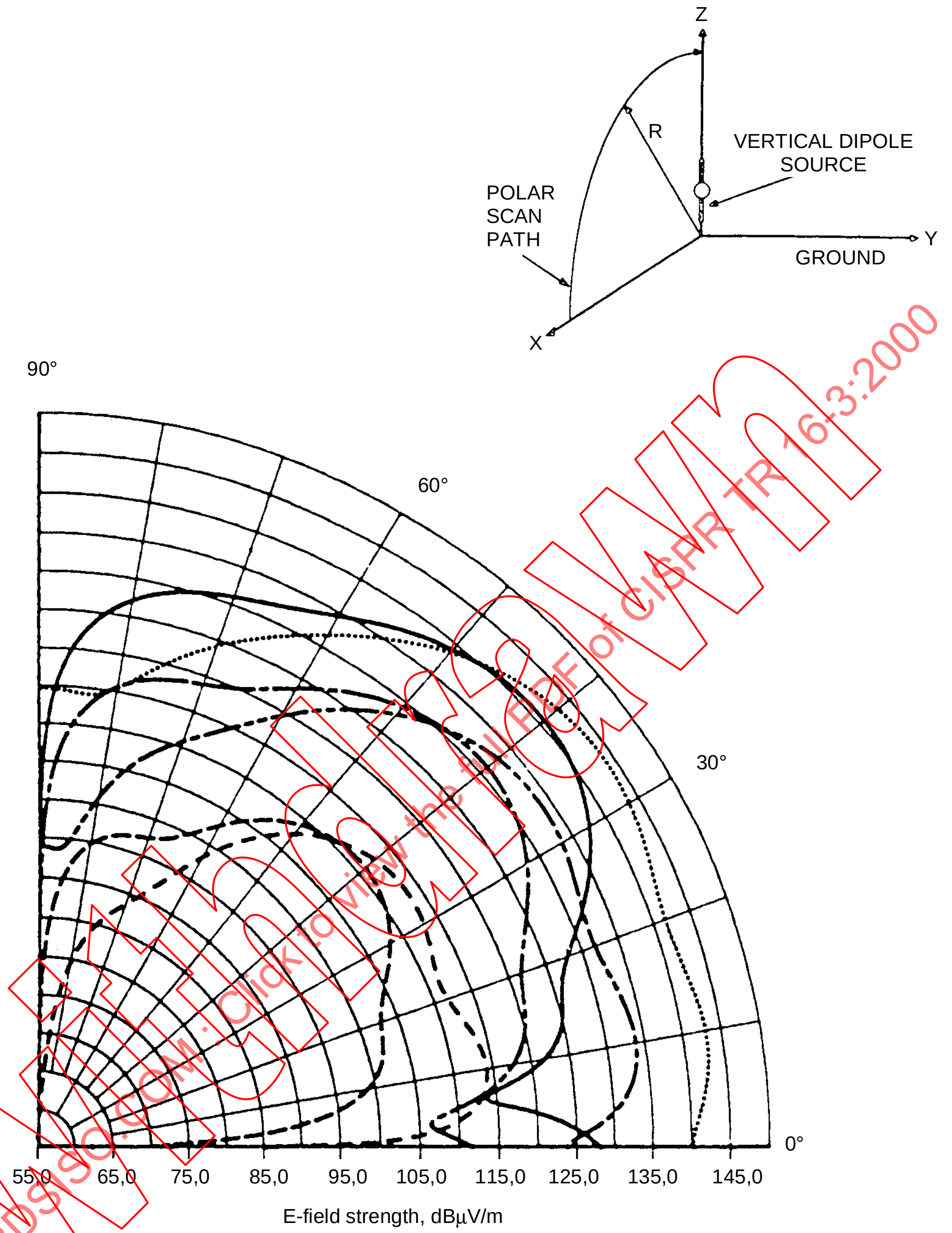

FREQUENCY = 243 MHz

E_x at a scan radius of 10 metre

E_z at a scan radius of 10 metres

E_x at a scan radius of 30 metres

E_z at a scan radius of 30 metres

E_x at a scan radius of 300 metres

E_z at a scan radius of 300 metres

IEC 815/2000

Figure 4.5-6(a) – Vertical polar patterns of vertically oriented *Ez* and horizontally oriented *Ex* field strengths emitted at 243 MHz around the small vertical electric dipole, at scan radii of 10 m, 30 m and 300 m in the Z-X plane. Dipole length 0,05 m. Dipole centre height 1 m. Dipole moment 1 A·m. Ground constants: ε_r = 15, σ = 4,5 mS/m. (Reproduced from [10])

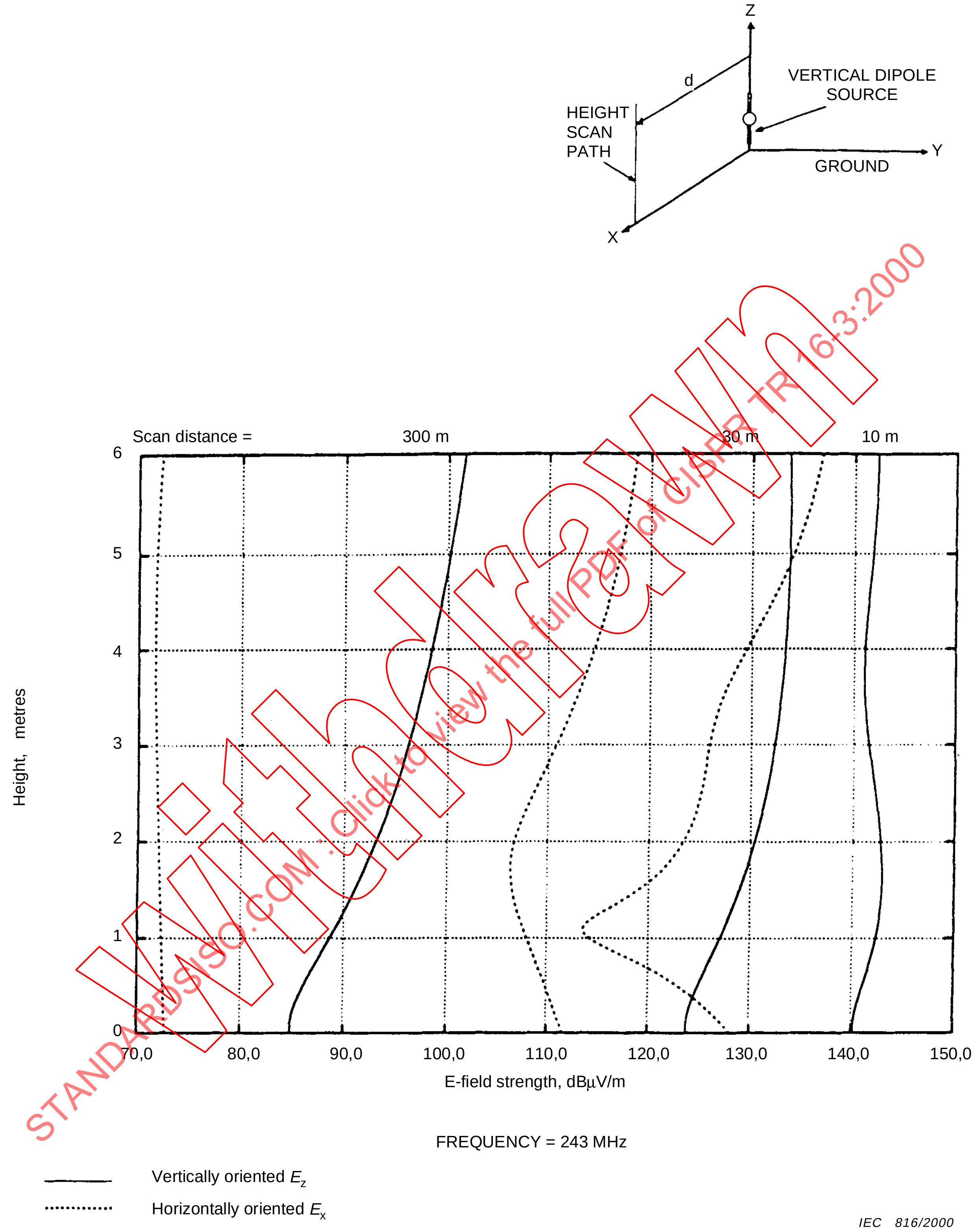

Figure 4.5-6(b) – Height scan patterns of vertically oriented *Ez* and horizontally oriented *Ex* field strengths emitted at 243 MHz from the small vertical electric dipole, at horizontal distances of 10 m, 30 m and 300 m in the Z-X plane. Dipole length 0,05 m. Dipole centre height 1 m. Dipole moment 1 A·m. Ground constants: ε_r = 15, σ = 4,5 mS/m. (Reproduced from [10])

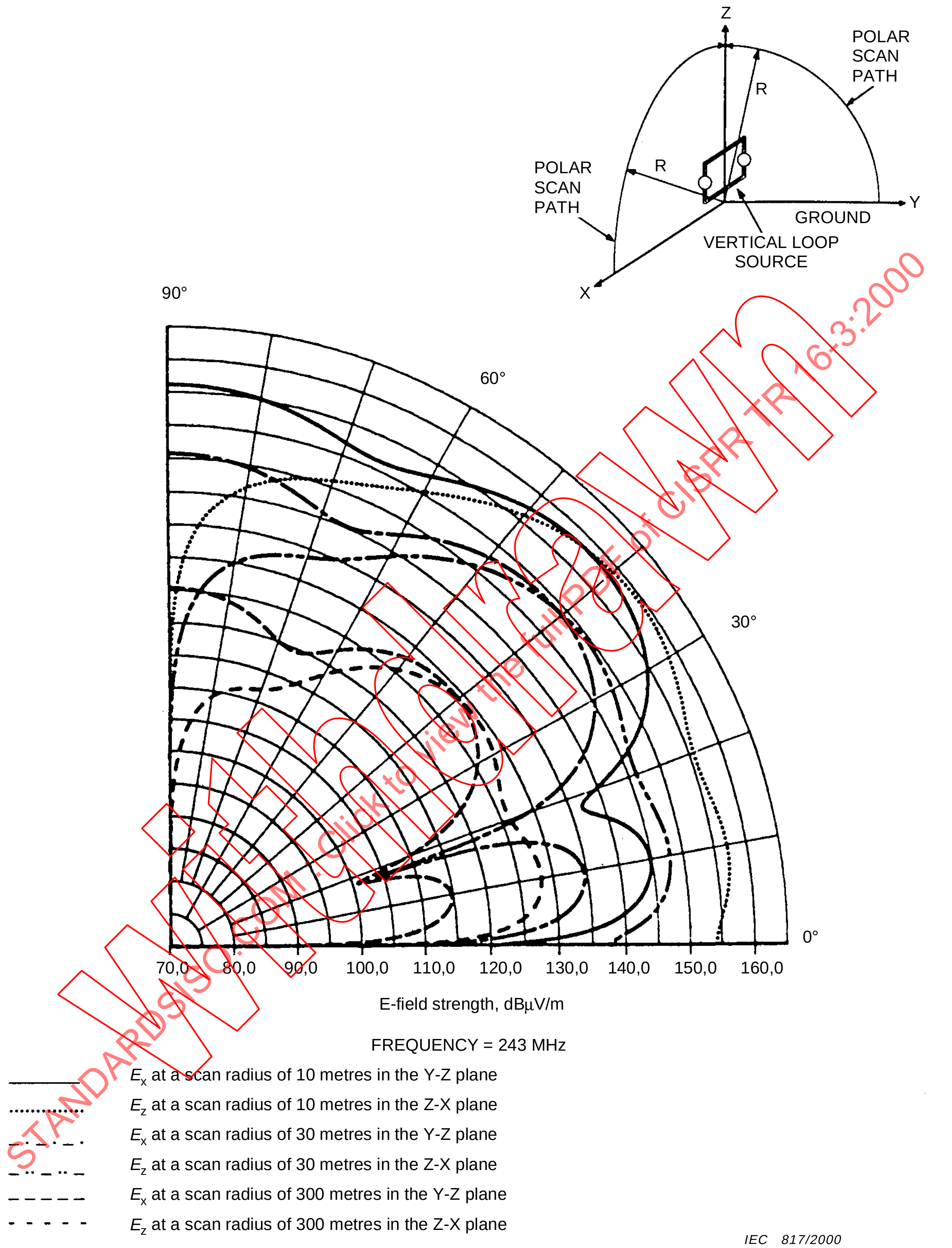

Figure 4.5-7(a) – Vertical polar patterns of horizontally polarized *Ex* and vertically oriented *Ez* field strengths emitted at 243 MHz around the small vertical loop (horizontal magnetic dipole), at scan radii of 10 m, 30 m and 300 m in the Y-Z plane and the Z-X plane respectively. Loop dimensions 0,05 m × 0,05 m. Loop centre height 1 m. Dipole moment 1 A·m^2. Ground constants: ε_r = 15, σ = 4,5 mS/m. (Reproduced from [10])

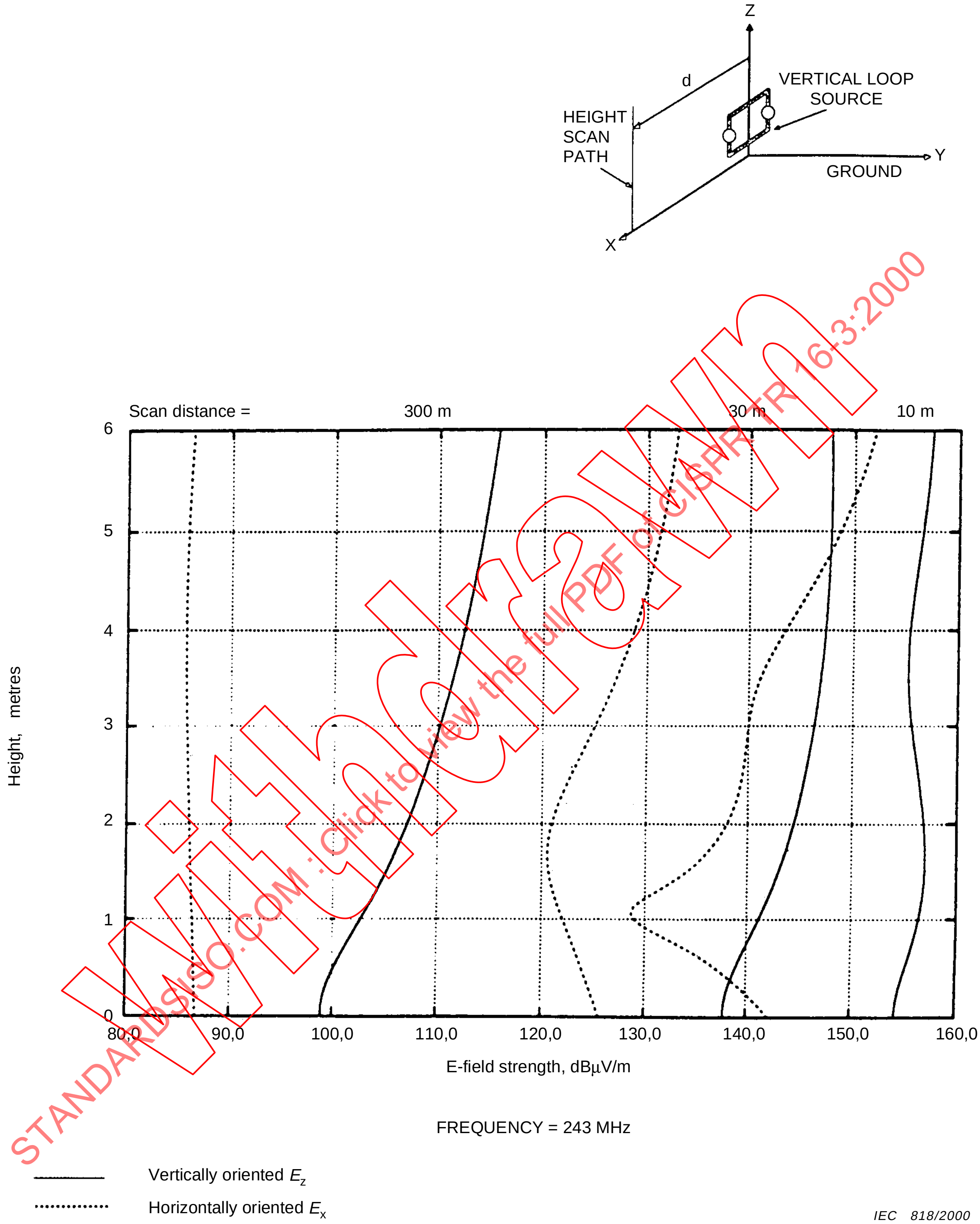

Figure 4.5-7(b) – Height scan patterns of vertically oriented *Ez* and horizontally oriented *Ex* field strengths emitted at 243 MHz from the small vertical loop (horizontal magnetic dipole), at horizontal distances of 10 m, 30 m and 300 m, in the Z-X plane. Loop dimensions 0,05 m × 0,05 m. Loop centre height 1 m. Dipole moment 1 A·m^2.
Ground constants: ε_r = 15, σ = 4,5 mS/m.
(Reproduced from [10])

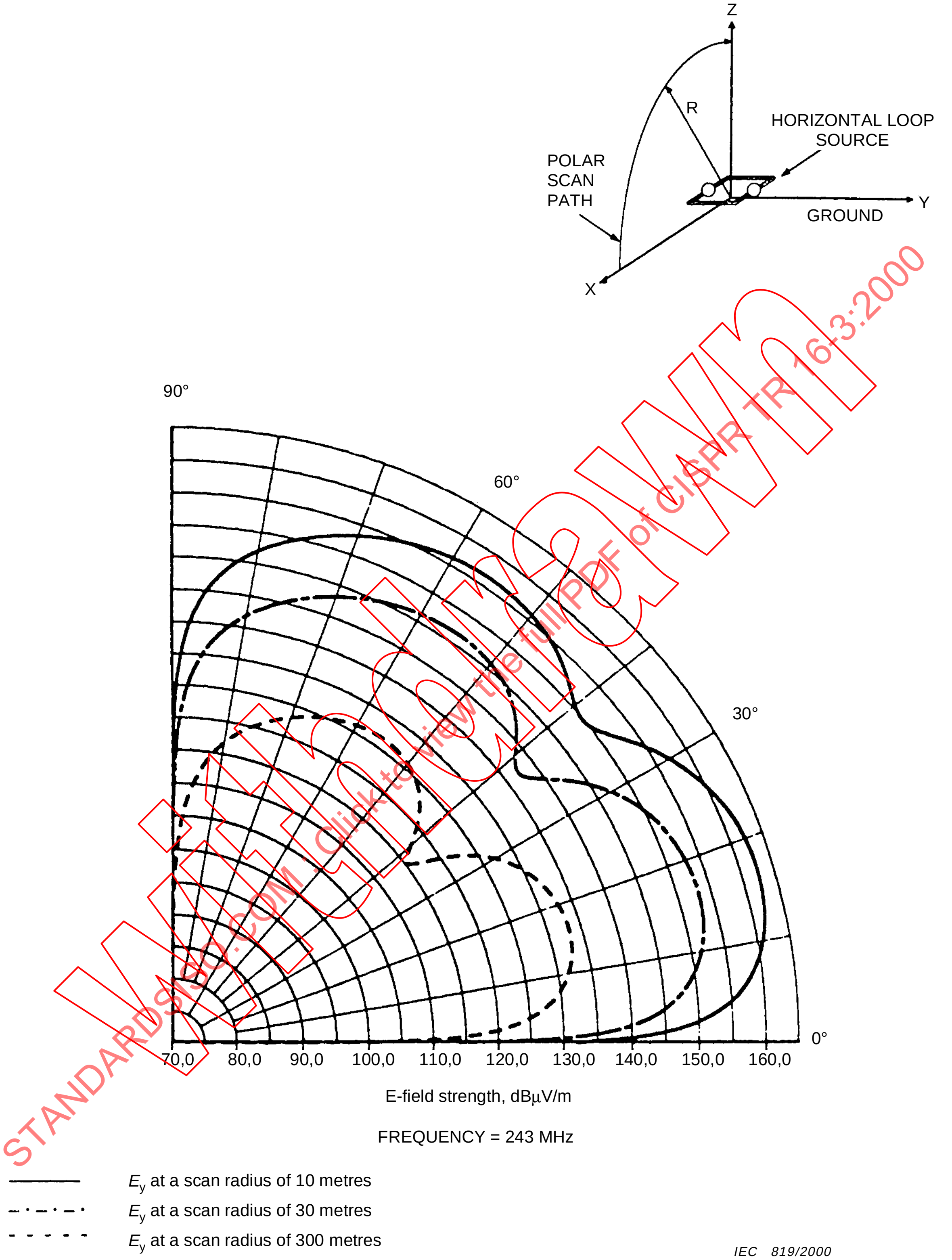

Figure 4.5-8(a) – Vertical polar patterns of horizontally polarized *E*-field strength emitted at 243 MHz around the small horizontal loop (vertical magnetic dipole), at scan radii of 10 m, 30 and 300 m in the Z-X plane. Loop dimensions 0,05 m × 0,05 m. Loop height 1 m. Dipole moment 1 A·m^2. Ground constants: ε_r = 15, σ = 4,5 mS/m. (Reproduced from [10])

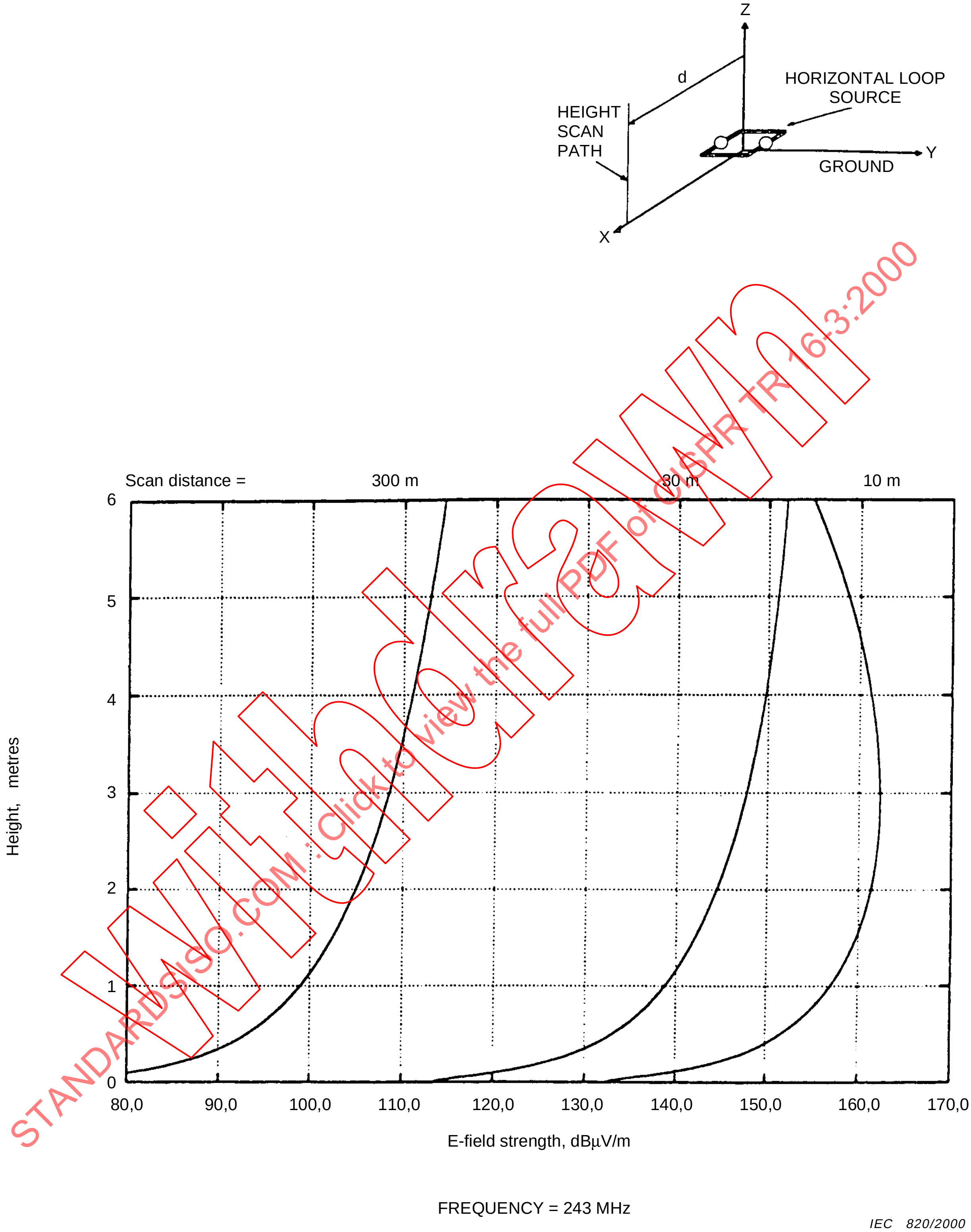

Figure 4.5-8(b) – Height scan patterns of horizontally polarized *E*-field strength emitted at 243 MHz from the small horizontal loop (vertical magnetic dipole), at horizontal distances of 10 m, 30 m and 300 m in the Z-X plane. Loop dimensions 0,05 m × 0,05 m. Loop height 1 m. Dipole moment 1 A·m^2. Ground constants: ε_r = 15, σ = 4,5 mS/m. (Reproduced from [10])

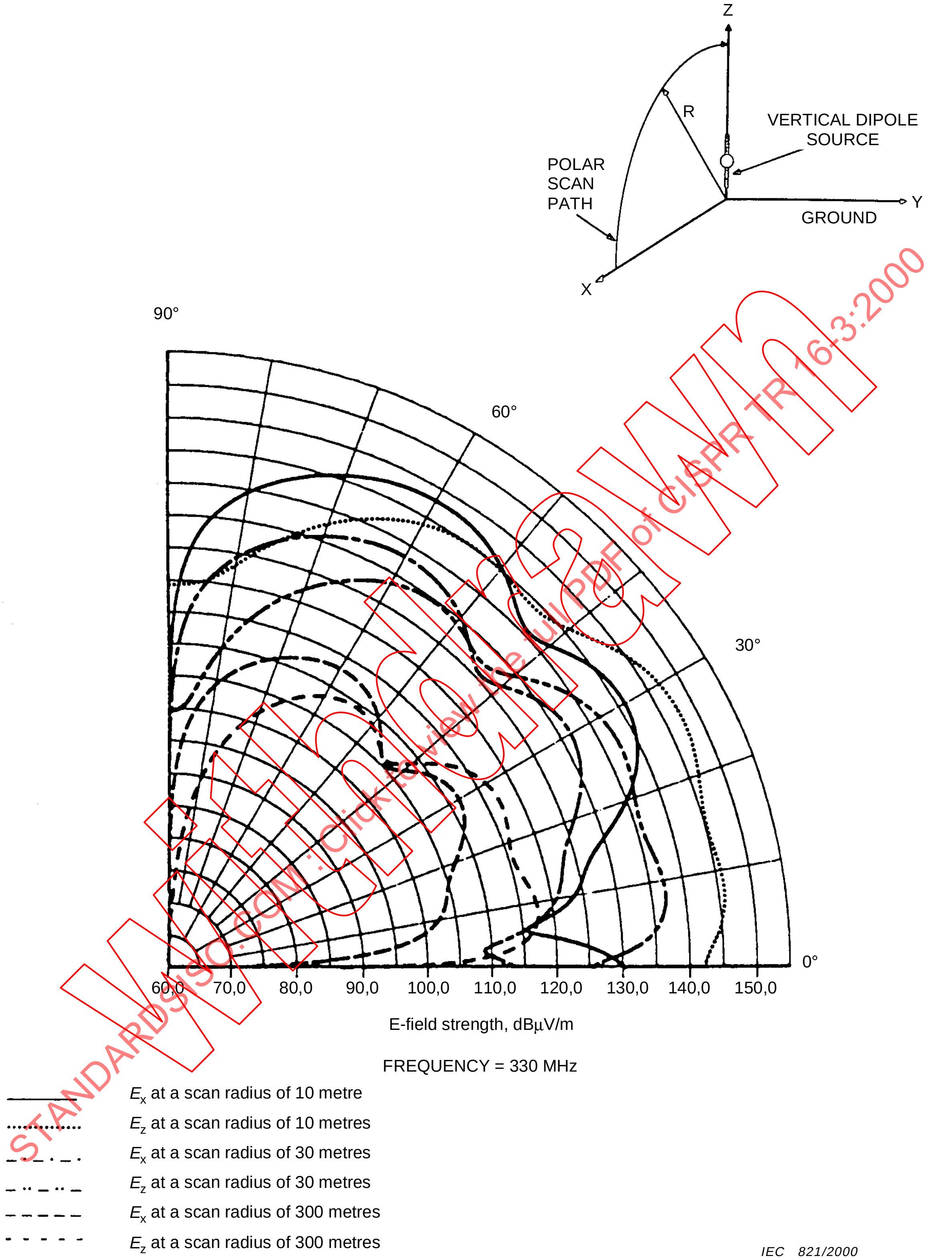

Figure 4.5-9(a) – Vertical polar patterns of vertically oriented *Ez* and horizontally oriented *Ex* field strengths emitted at 330 MHz around the small vertical electric dipole, at scan radii of 10 m, 30 m and 300 m in the Z-X plane. Dipole length 0,05 m. Dipole centre height 1 m. Dipole moment 1 A·m. Ground constants: ε_r = 15, σ = 7,5 mS/m. (Reproduced from [10])

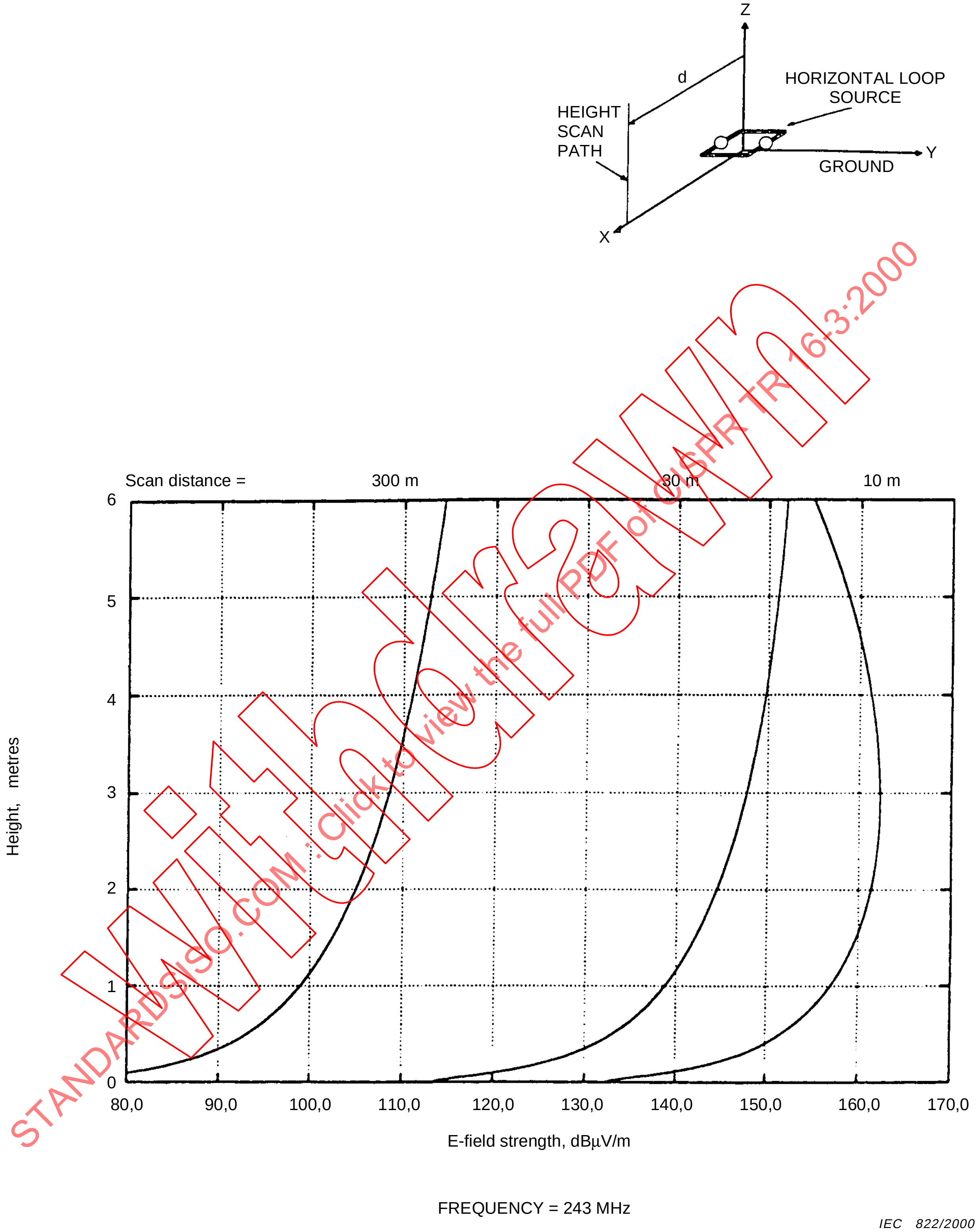

Figure 4.5-9(b) – Height scan patterns of vertically oriented *Ez* and horizontally oriented *Ex* field strengths emitted at 330 MHz from the small vertical electric dipole, at horizontal distances of 10 m, 30 m and 300 m in the Z-X plane. Dipole length 0,05 m. Dipole centre height 1 m. Dipole moment 1 A·m. Ground constants: ε_r = 15, σ = 7,5 mS/m. (Reproduced from [10])

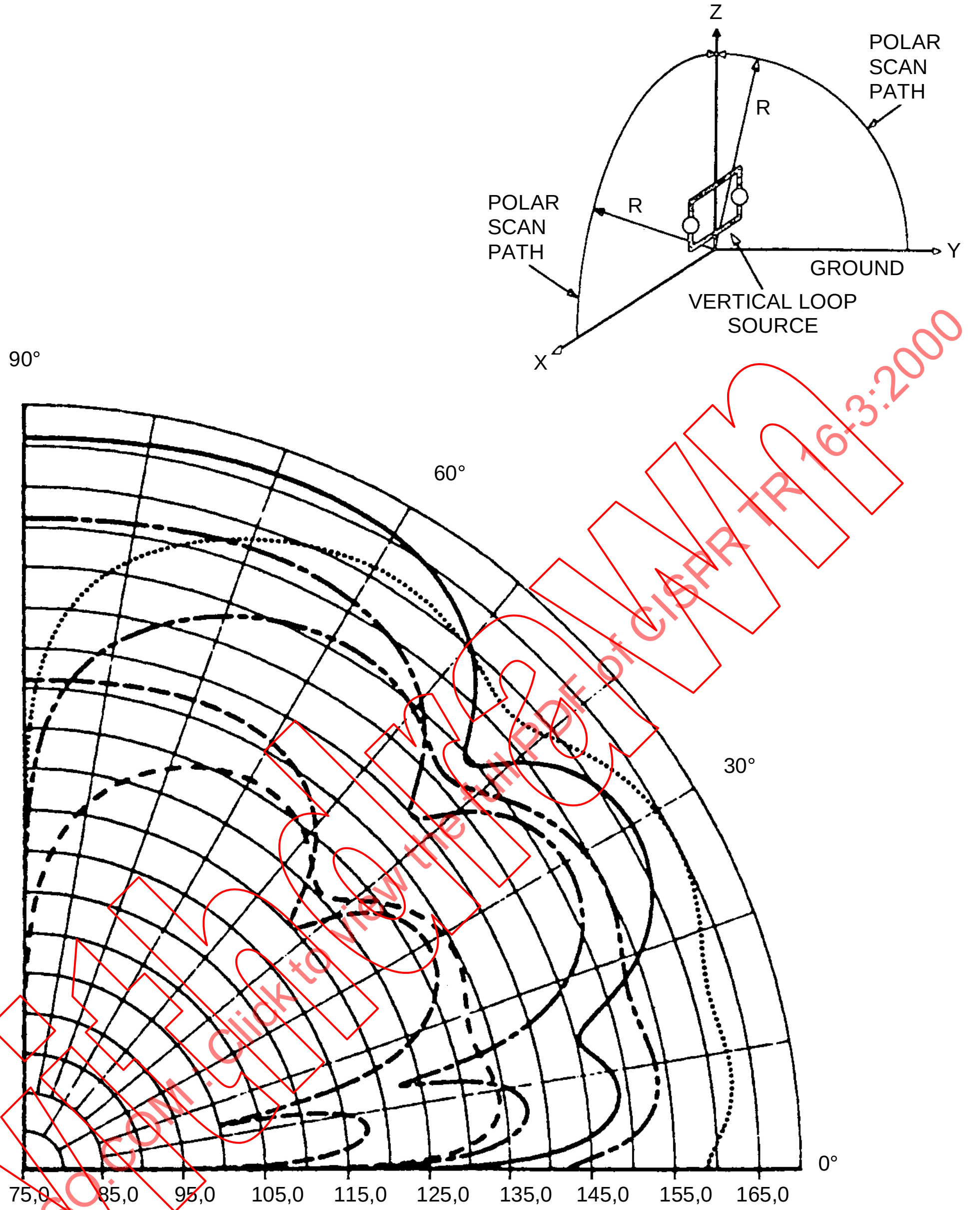

E-field strength, dBµV/m

FREQUENCY = 330 MHz

E_x at a scan radius of 10 metres in the Y-Z plane
E_z at a scan radius of 10 metres in the Z-X plane
E_x at a scan radius of 30 metres in the Y-Z plane
E_z at a scan radius of 30 metres in the Z-X plane
E_x at a scan radius of 300 metres in the Y-Z plane
E_z at a scan radius of 300 metres in the Z-X plane

IEC 823/2000

Figure 4.5-10(a) – Vertical polar patterns of horizontally polarized *Ex* and vertically oriented *Ez* field strengths emitted at 330 MHz around the small vertical loop (horizontal magnetic dipole), at scan radii of 10 m, 30 m and 300 m, in the Y-Z plane and the Z-X plane respectively. Loop dimensions 0,05 m × 0,05 m. Loop centre height 1 m. Dipole moment 1 A·m^2. Ground constants: ε_r = 15, σ = 7,5 mS/m. (Reproduced from [10])

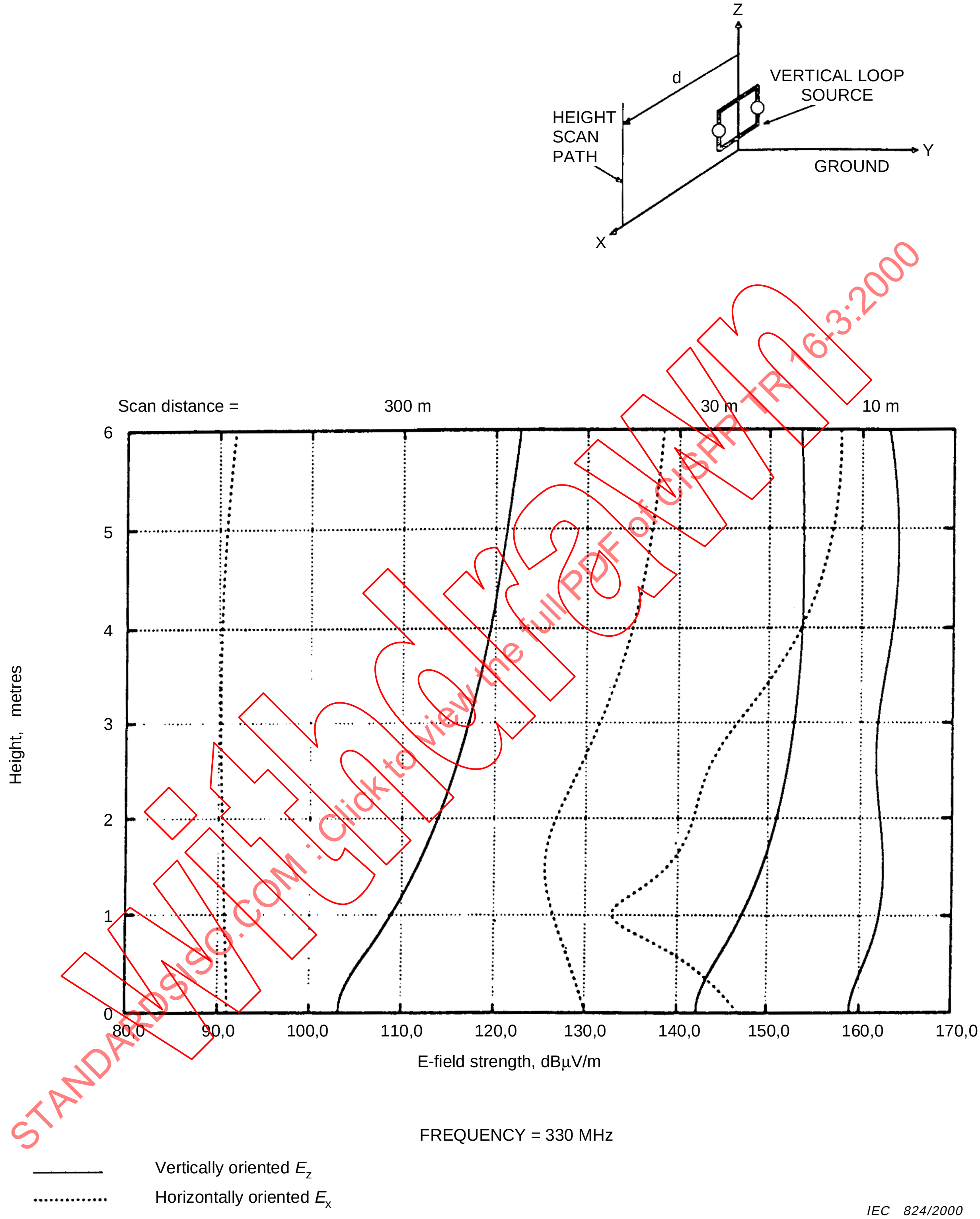

Figure 4.5-10(b) – Height scan patterns of vertically oriented *Ez* and horizontally oriented *Ex* field strengths emitted at 330 MHz from the small vertical loop (horizontal magnetic dipole), at horizontal distances of 10 m, 30 m and 300 m in the Z-X plane. Loop dimensions 0,05 m × 0,05 m. Loop centre height 1 m. Dipole moment 1 A·m^2. Ground constants: ε_r = 15, σ = 7,5 mS/m. (Reproduced from [10])

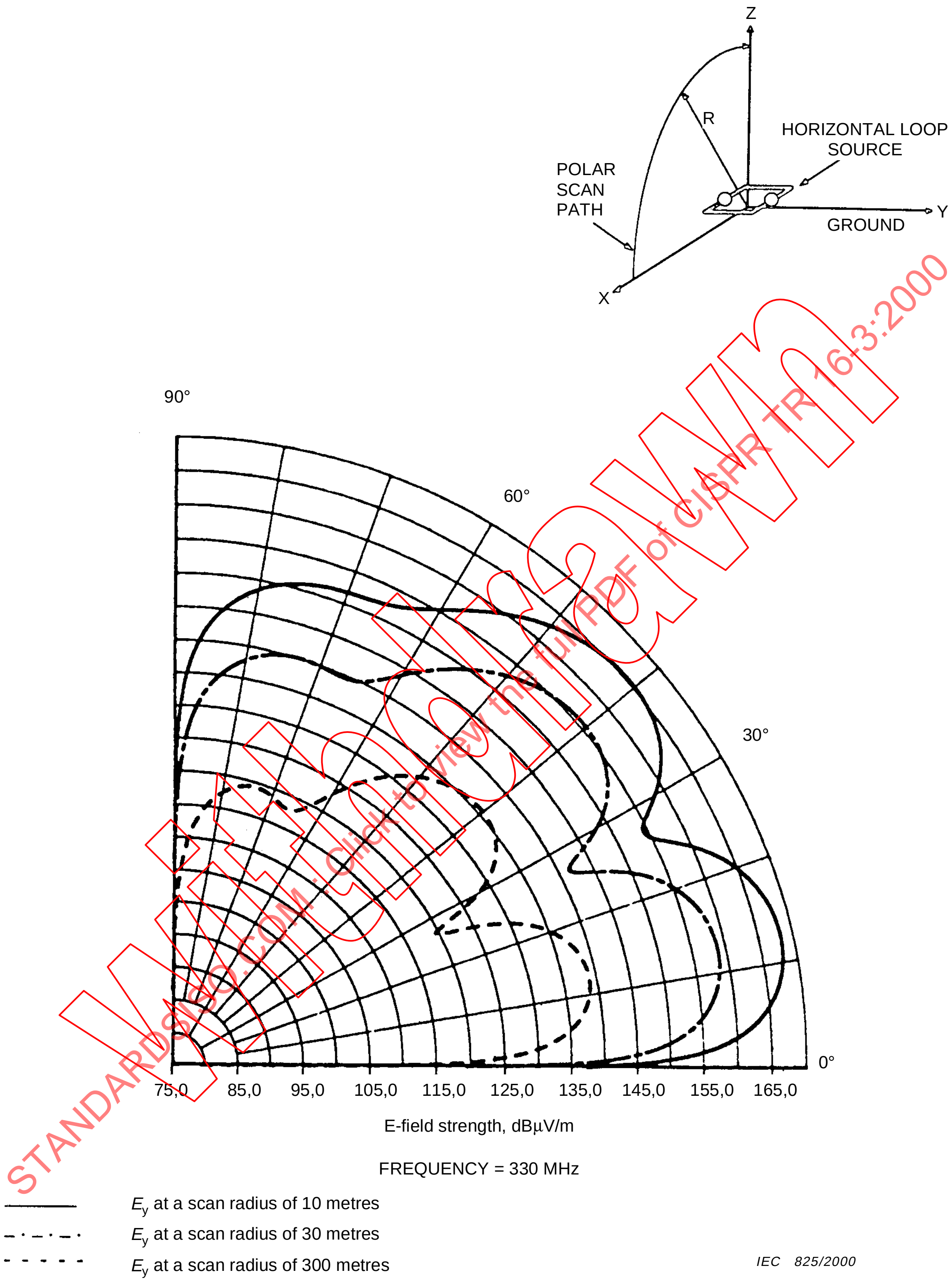

Figure 4.5-11(a) – Vertical polar patterns of horizontally polarized *E*-field strength emitted at 330 MHz around the small horizontal loop (vertical magnetic dipole), at scan radii of 10 m, 30 m and 300 m in the Z-X plane. Loop dimensions 0,05 m × 0,05 m. Loop height 1 m. Dipole moment 1 A·m^2. Ground constants: ε_r = 15, σ = 7,5 mS/m. (Reproduced from [10])

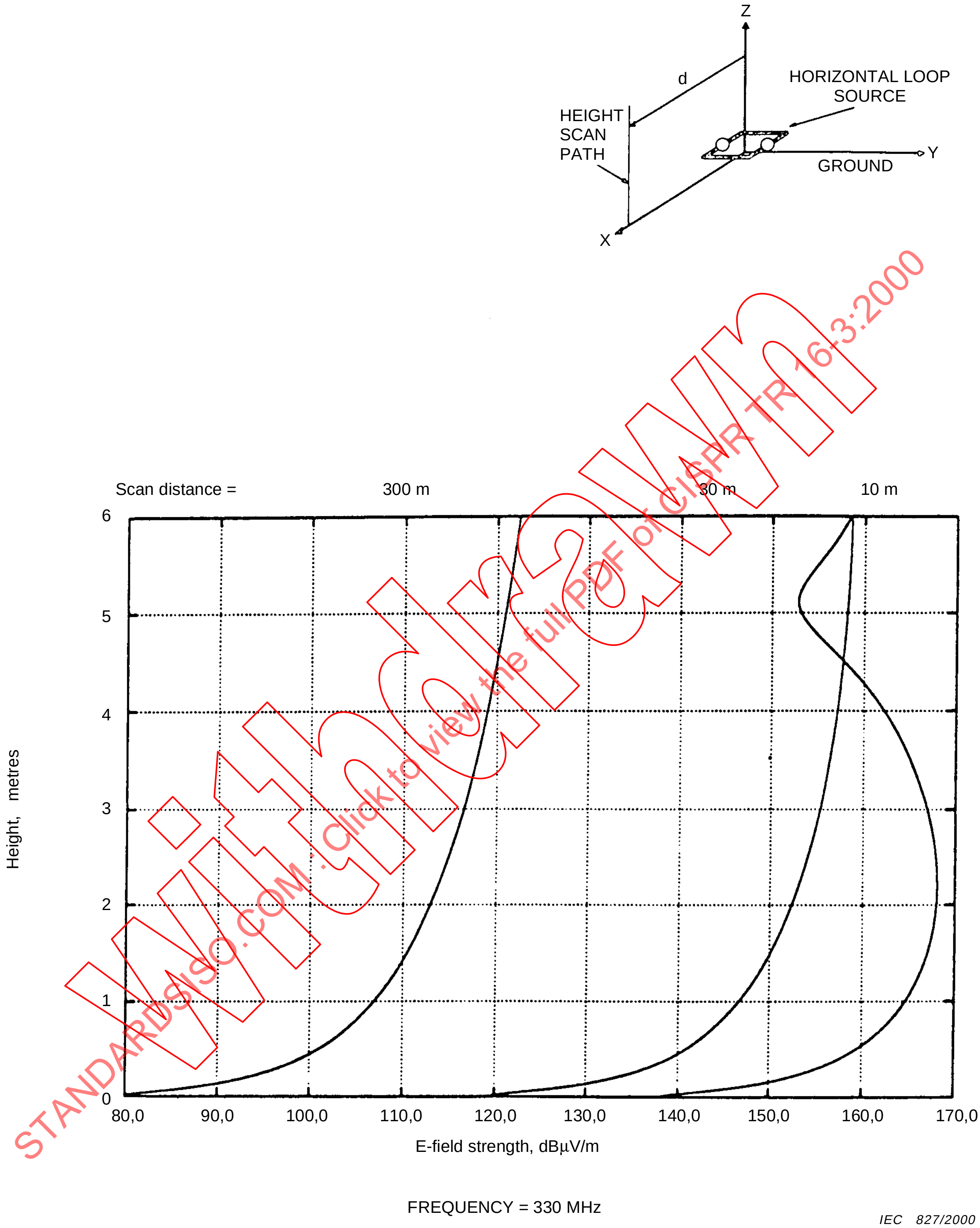

Figure 4.5-11(b) – Height scan patterns of horizontally polarized *E*-field strength emitted at 330 MHz from the small horizontal loop (vertical magnetic dipole), at horizontal distances of 10 m, 30 m and 300 m in the Z-X plane. Loop dimensions 0,05 m × 0,05 m. Loop height 1 m. Dipole moment 1 A·m^2. Ground constants: ε_r = 15, σ = 4,5 mS/m. (Reproduced from [10])

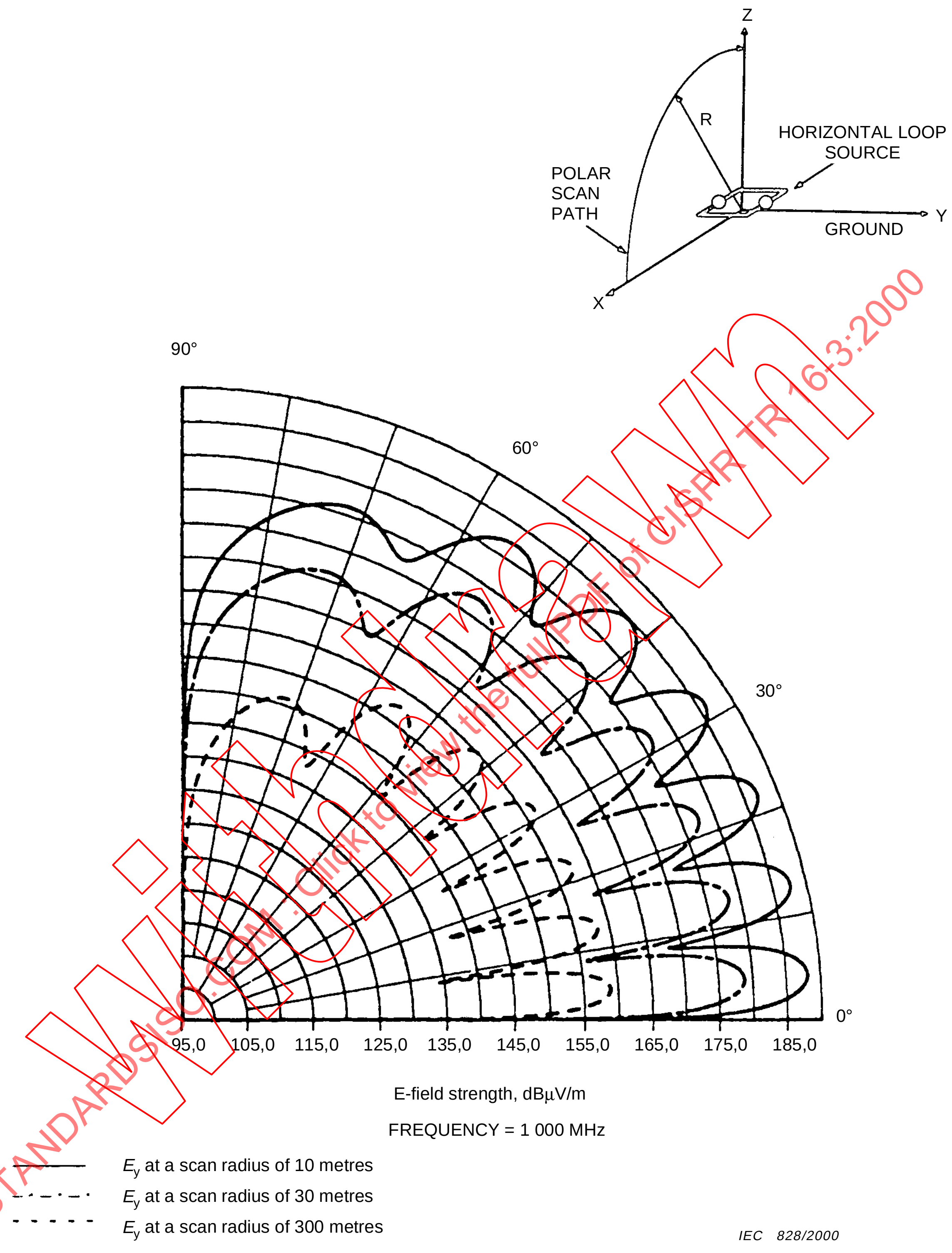

Figure 4.5-12(a) – Vertical polar patterns of horizontally polarized *E*-field strength emitted at 1 000 MHz around the small horizontal loop (vertical magnetic dipole), at scan radii of 10 m, 30 m and 300 m in the Z-X plane. Loop dimensions 0,02 m × 0,02 m. Loop height 1 m. Dipole moment 1 A·m^2. Ground constants: ε_r = 15, σ = 35 mS/m. (Reproduced from [10])

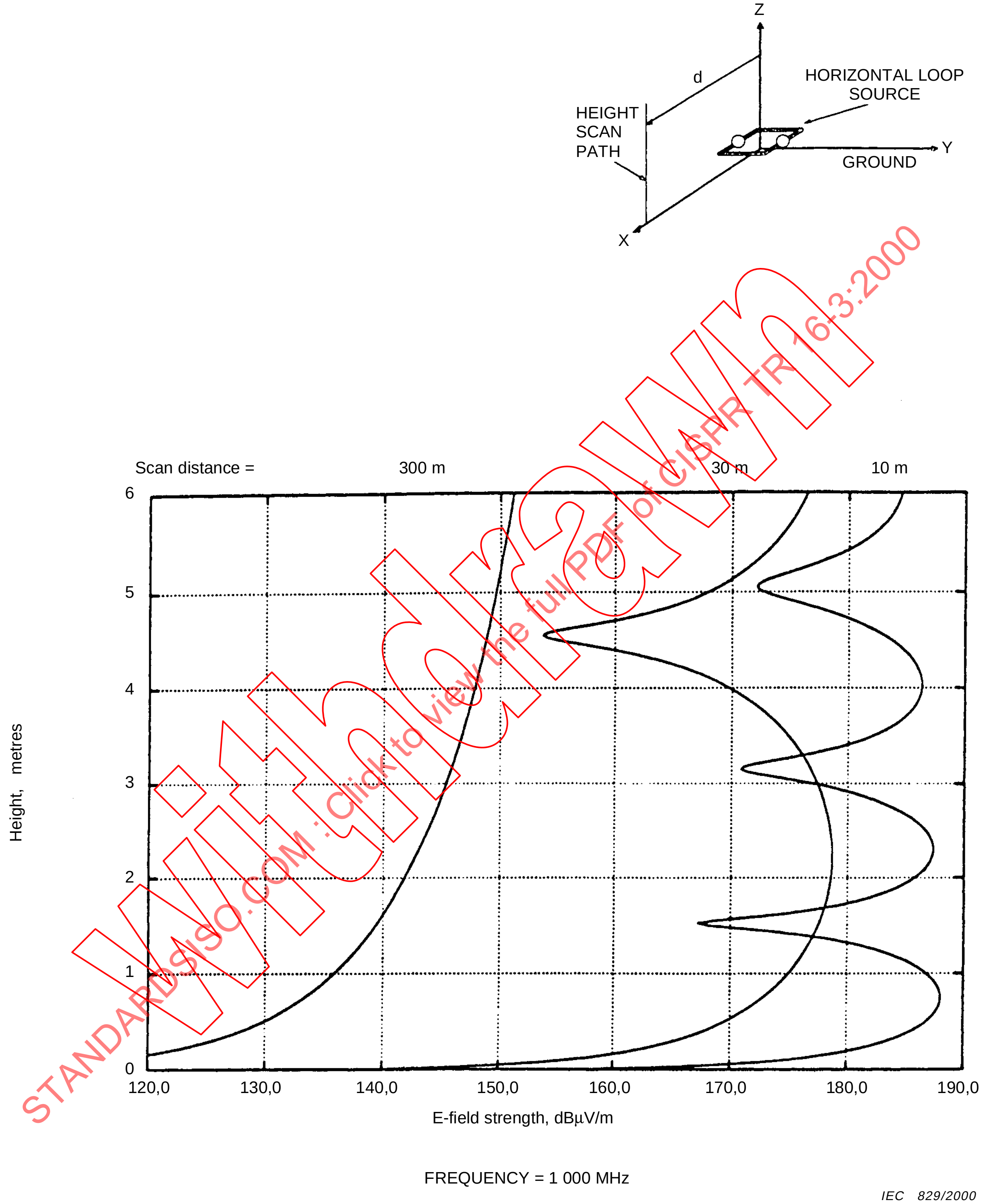

Figure 4.5-12(b) – Height scan patterns of horizontally polarized *E*-field strength emitted at 1 000 MHz from the small horizontal loop (vertical magnetic dipole) at horizontal distances of 10 m, 30 m and 300 m in the Z-X plane. Loop dimensions 0,02 m × 0,02 m. Loop height 1 m. Dipole moment 1 A·m^2. Ground constants: ε_r = 15, σ = 35 mS/m. (Reproduced from [10])

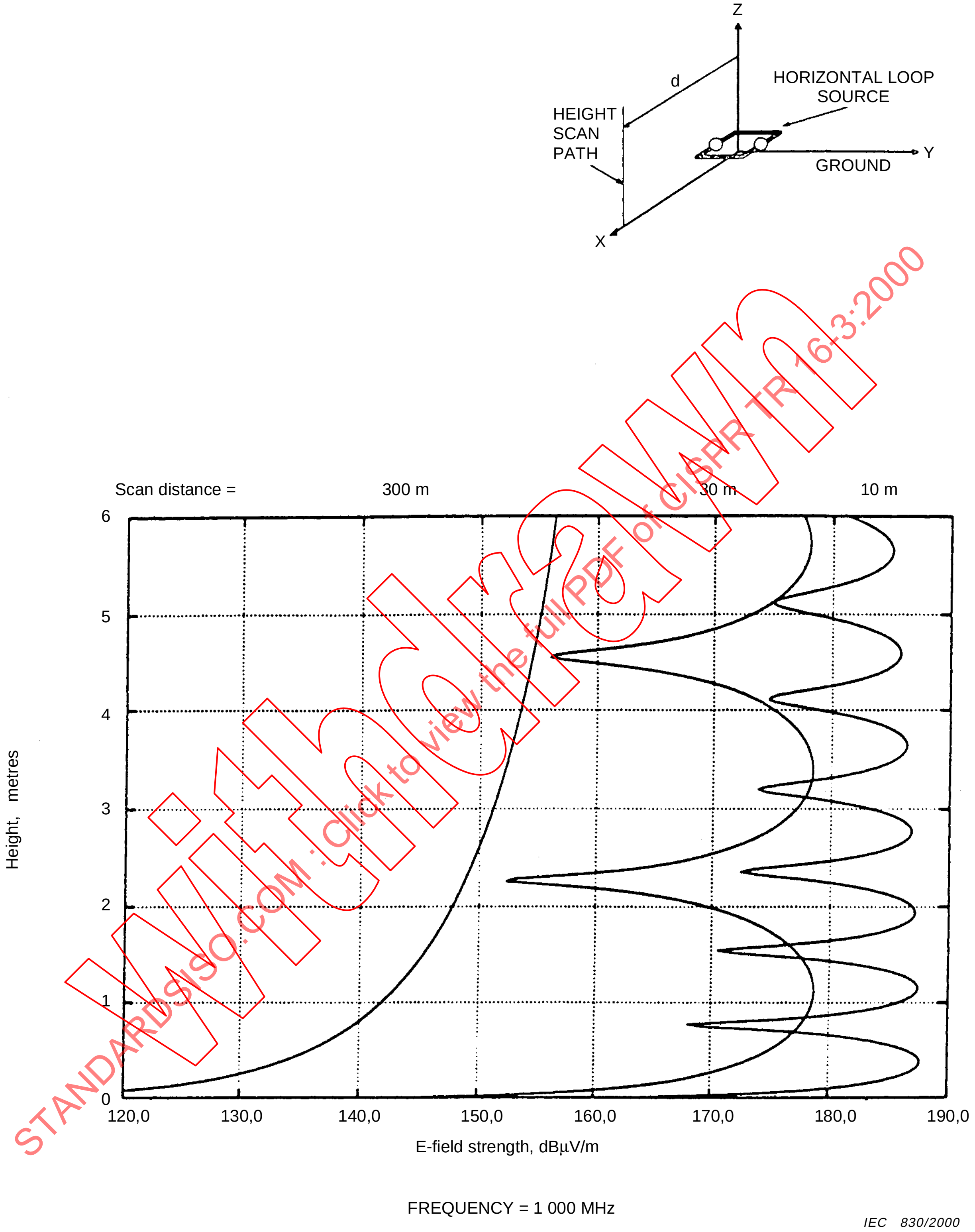

Figure 4.5-13 – Height scan patterns of horizontally polarized *E*-field strength emitted at 1 000 MHz from the small horizontal loop (vertical magnetic dipole), at horizontal distances of 10 m, 30 m and 300 m in the Z-X plane. Loop dimensions 0,02 m × 0,02 m. Loop height 2 m. Dipole moment 1 A·m^2. Ground constants: ε_r = 15, σ = 35 mS/m. (Reproduced from [10])

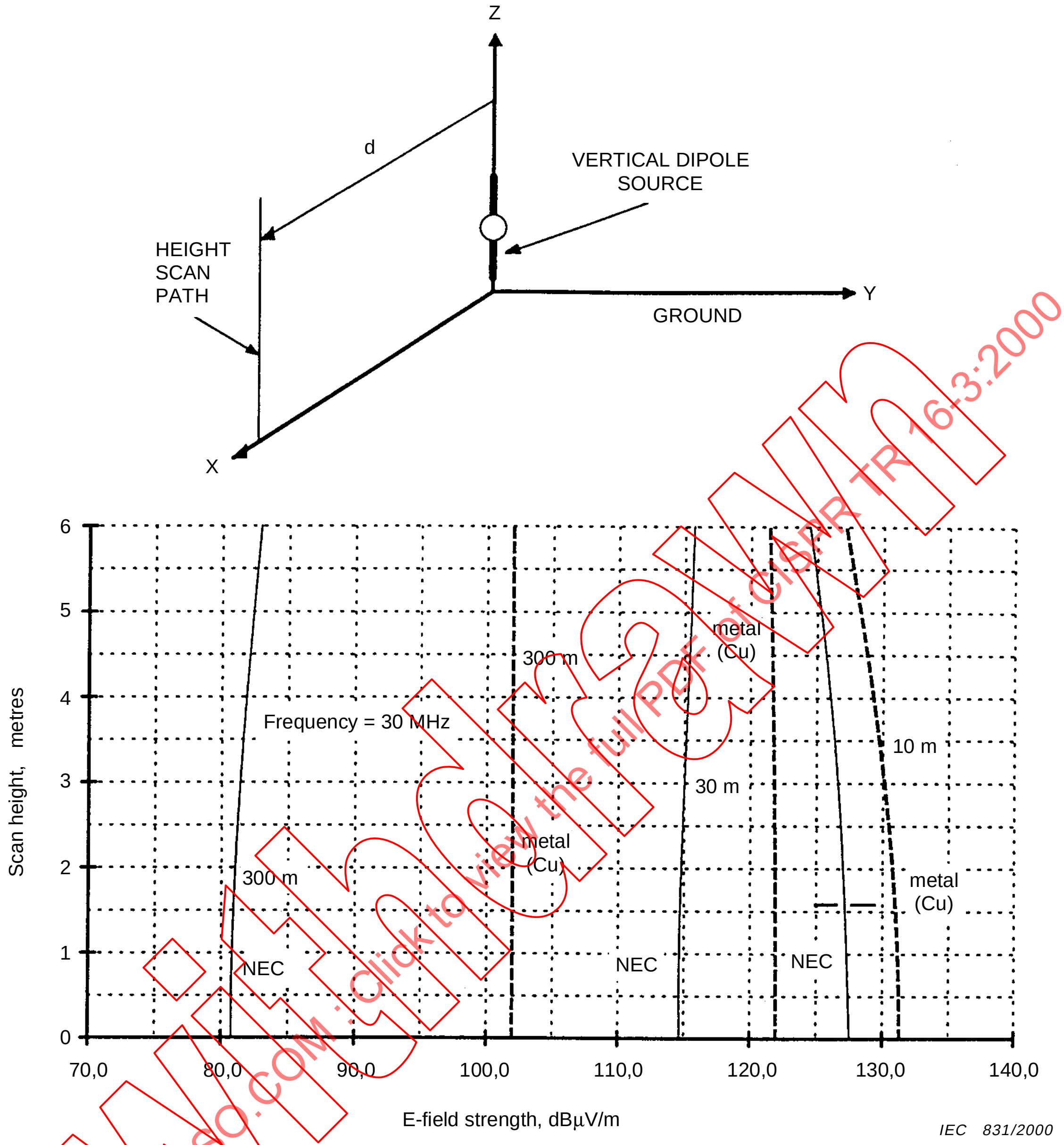

Figure 4.5-14 – Height scan patterns of the vertical component of the *E*-fields emitted at 30 MHz from a small vertical electric dipole, at horizontal distances of 10 m, 30 m and 300 m. Fields calculated in NEC (solid lines) include the surface wave over real ground. Electrical constants used for the real ground plane were $\varepsilon_r = 15$, $\sigma = 1$ mS/m ("medium dry ground"). The dashed curves were calculated geometrically to include the direct and reflected space waves from an infinitesimal vertical electric dipole over a metal ground plane. For the metal ground plane the electrical constants of copper were used, with $\varepsilon_r = 1$, $\sigma = 5{,}81 \times 10^7$ S/m. Dipole moment = 1 A·m. Dipole centre height above ground = 1 m. In NEC the dipole length is 0,2 m. (Adapted from [11])

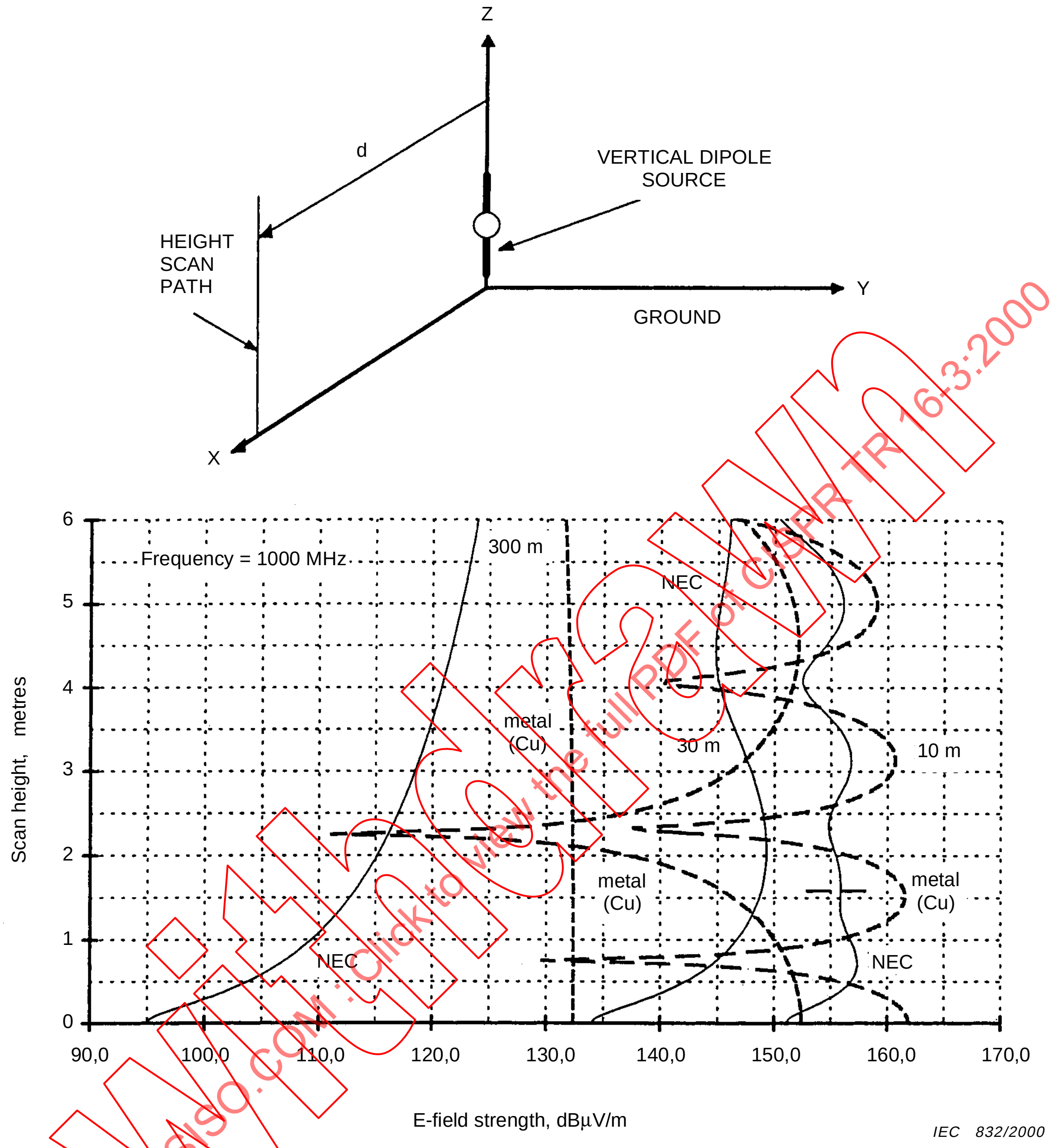

Figure 4.5-15 – Height scan patterns of the vertical component of the *E*-fields emitted at 1 000 MHz from a small vertical electric dipole, at horizontal distances of 10 m, 30 m and 300 m. Fields calculated in NEC (solid lines) include the surface wave over real ground. Electrical constants used for the real ground plane were ε_r = 15, σ = 35 mS/m. The dashed curves were calculated geometrically to include the direct and reflected space waves from an infinitesimal vertical electric dipole over a metal ground plane. For the metal ground plane the electrical constants of copper were used, with ε_r = 1, σ = 5,81 $\times$ 10^7 S/m. Dipole moment = 1 A·m. Dipole centre height above ground = 1 m. In NEC the dipole length is 0,02 m. (Adapted from [11])

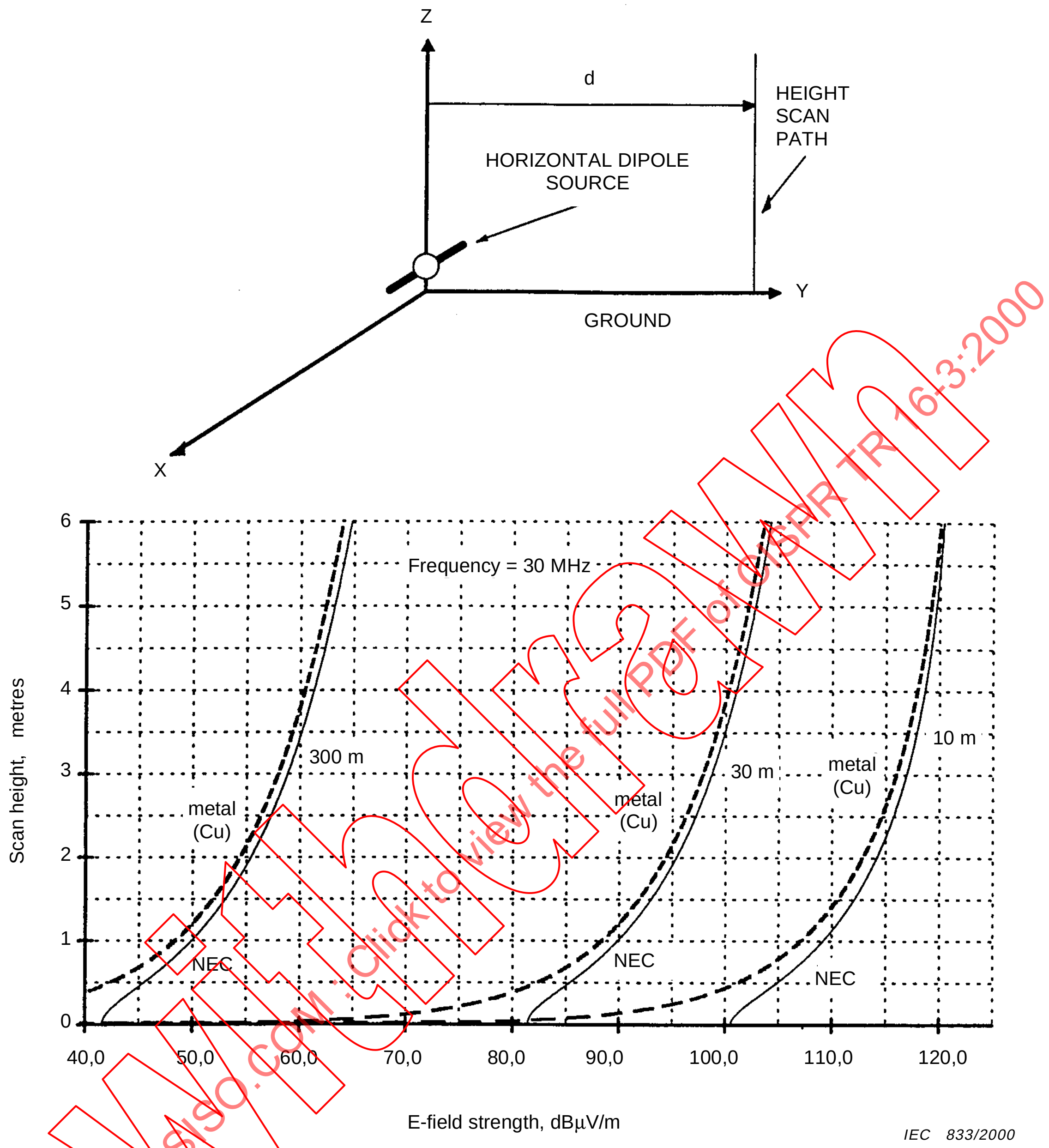

Figure 4.5-16 – Height scan patterns of the horizontally polarized *E*-fields emitted at 30 MHz in the vertical plane normal to the axis of a small horizontal electric dipole, at horizontal distances of 10 m, 30 m and 300 m. Fields calculated in NEC (solid lines) include the surface wave over real ground. Electrical constants used for the real ground plane were ε_r = 15, σ = 1 mS/m ("medium dry ground"). The dashed curves were calculated geometrically to sum the direct and reflected waves from an infinitesimal horizontal electric dipole over a metal ground plane. The electrical constants of copper were used for the metal ground plane, ε_r = 1, σ = 5,81 × 10^7 S/m. Dipole moment = 1 A·m. Dipole height above ground plane = 1 m. In NEC the dipole length is 0,2 m. (Adapted from [11])

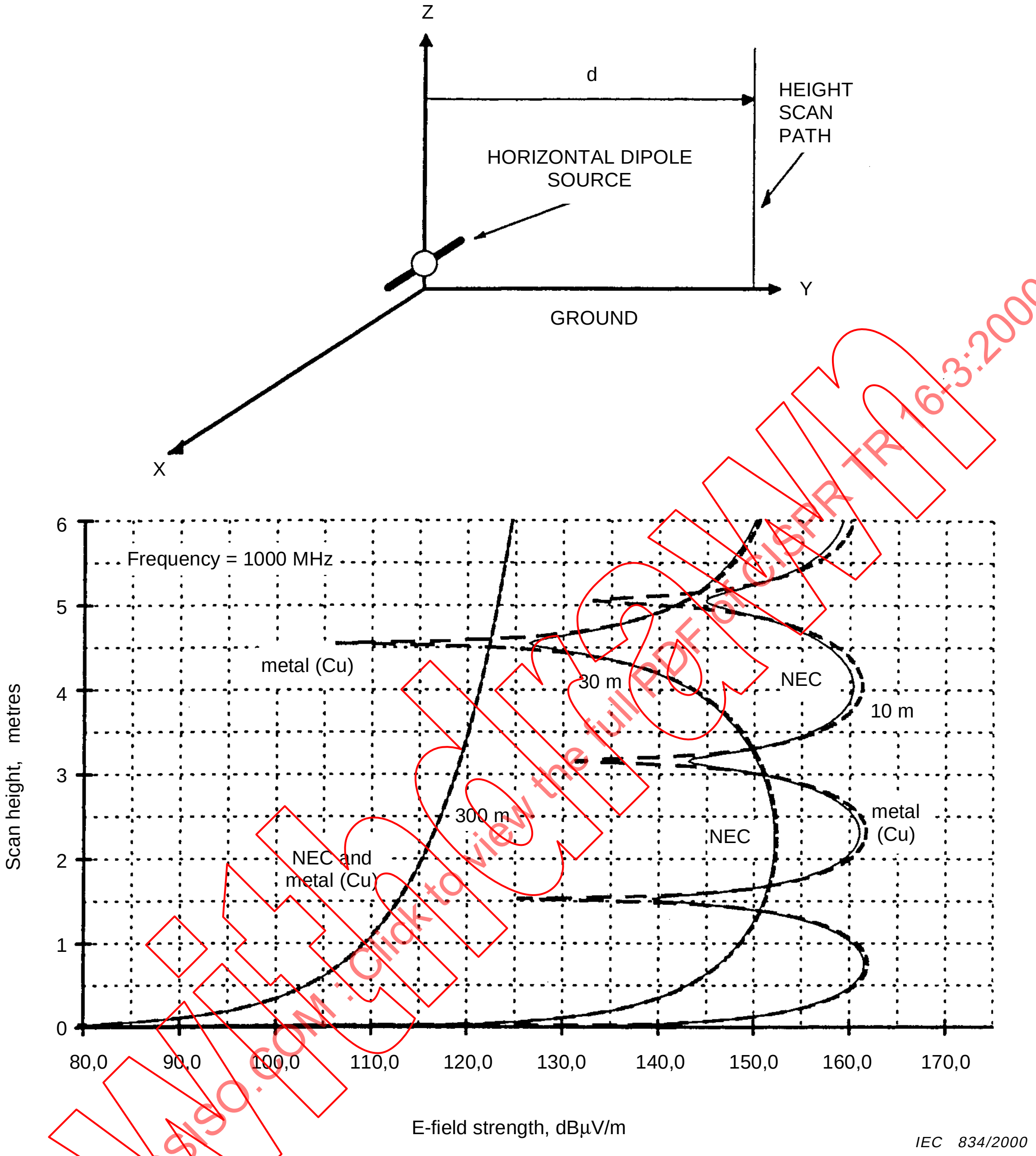

Figure 4.5-17 – Height scan patterns of the horizontally polarized *E*-fields emitted at 1 000 MHz in the vertical plane normal to the axis of a small horizontal electric dipole, at horizontal distances of 10 m, 30 m and 300 m. Fields calculated in NEC (solid lines) include the surface wave over real ground. Electrical constants used for the real ground plane were ε_r = 15, σ = 35 mS/m ("medium dry ground"). The dashed curves were calculated geometrically to sum the direct and reflected space waves from an infinitesimal horizontal electric dipole over a metal ground plane. The electrical constants of annealed copper were used for the metal ground plane, ε_r = 1, σ = 5,81 × 10^7 S/m. Dipole moment = 1 A·m. Dipole height above ground plane = 1 m. In NEC the dipole length is 0,02 m. (Adapted from [11])

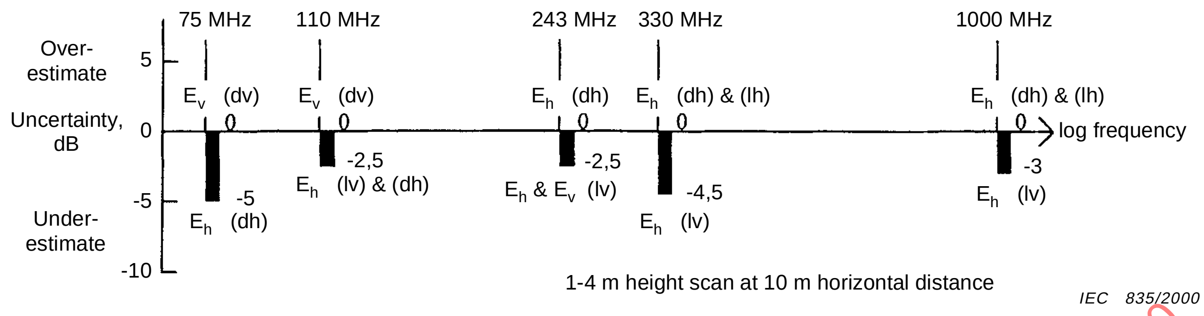

Figure 4.5-18 – Ranges of uncertainties in the predictability of radiation in vertical directions from electrically small sources located at a height of 1 m or 2 m above ground. The predictability is based on measurements of the horizontally and vertically polarized *E*-fields in a height scan from 1 m to 4 m at a horizontal distance of 10 m from the sources. The following example shows how the bar chart can be interpreted. At 243 MHz, the bar shows that the best predictability, with nominally zero error, is obtained when estimating the maximum strength of the horizontally polarized *Eh* field emitted at elevated angles from a source behaving as a small horizontal dipole (dh). The poorest predictability at 243 MHz, an underestimate by as much as 2,5 dB, can occur when predicting the maximum strengths of the horizontally polarized *Eh* fields and the *Ez* vertical component of the vertically polarized fields emitted at elevated angles from a source behaving as a small vertical loop (lv). (Reproduced from [10])

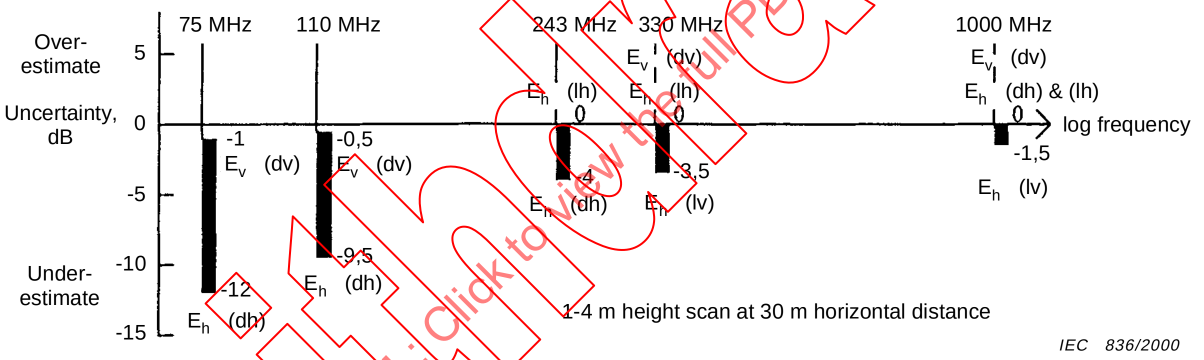

Figure 4.5-19 – Ranges of uncertainties in the predictability of radiation in vertical directions from electrically small sources located at a height of 1 m or 2 m above ground. The predictability is based on measurements of the horizontally and vertically polarized *E*-fields in a height scan from 1 m to 4 m at a horizontal distance of 30 m from the sources. The following example shows how the bar chart can be interpreted. At 330 MHz, the bar shows that the best predictability, with nominally zero error, is obtained when estimating the maximum strength of either the horizontally polarized *Eh* field emitted at elevated angles from a small horizontal loop (lh) or the *Ez* vertical component of the vertically polarized field emitted at elevated angles from a small vertical dipole (dv). But at 330 MHz the height scan measurements may provide an underestimate by as much as 3,5 dB when predicting the strength of the horizontally polarized *Eh* field, which is the maximum field emitted at elevated angles from a source behaving as a small vertical loop (lv) (Reproduced from [10])

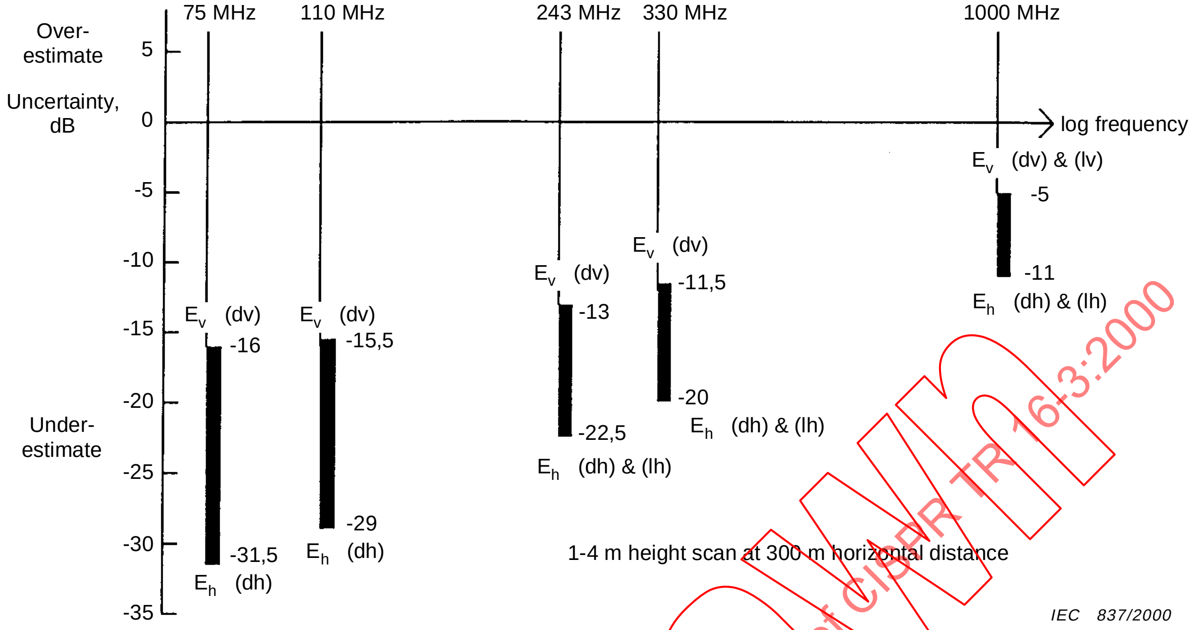

Figure 4.5-20 – Ranges of uncertainties in the predictability of radiation in vertical directions from electrically small sources located at a height of 1 m or 2 m above ground. The predictability is based on measurements of the horizontally and vertically polarized *E*-fields in a height scan from 1 m to 4 m at a horizontal distance of 300 m from the sources. The following example shows how the bar chart can be interpreted. The bar at 1 000 MHz shows that the best predictability at that frequency, which is an underestimate by as much as 5 dB, will be obtained when predicting the maximum strength of the *Ez* vertical component of the vertically polarized field emitted at elevated angles from a source behaving as a small vertical loop (lv) or a small vertical dipole (dv). However, an underestimate by as much as 11 dB can occur at 1 000 MHz when predicting the maximum strength of the horizontally polarized *Eh* field emitted at elevated angles from a source behaving as a small horizontal loop (lh) or a small horizontal dipole (dh). (Reproduced from[10])

Annex 4.5-A

Harmonic fields radiated at elevated angles from 27 MHz ISM equipment over real ground

A close match can be achieved between vertical radiation patterns calculated for simple electrically small electric dipoles and loops over real ground and the vertical radiation patterns created by real ISM equipment. This can be shown using airborne data, measured by Ohio University, of the harmonic field strengths from four different 27 MHz ISM machines positioned at ground level on an earthen open field site [4]. Each ISM machine was a RF plastics sealer, identified by a letter symbol A, B, C or D. Fundamental operating powers ranged from 2 kW to 27 kW. In [5], the horizontally polarized fourth harmonic field-strength data at approximately 109 MHz, collected by an aircraft flying at constant height and varying slant range, were converted to field strengths in vertical polar radiation patterns at a constant radial distance of 300 m, at elevation angles varying from approximately 4° up to 90°. The resultant far-field vertical radiation patterns were then compared with vertical radiation patterns calculated at the same distance from small electric dipoles and loops over real ground. The objective was to meet a tolerance of fit which was arbitrarily chosen as ±10 dB. The comparisons show that the vertical radiation patterns of harmonic radiation from ISM equipment, at 109 MHz in the aeronautical ILS localizer band, closely resemble the patterns calculated for simple dipoles and loops.

The in-flight field strength data gathered at varying slant distances from the ISM equipment were converted to vertical radiation patterns using the simple inverse distance law of attenuation in equation (4.5-A1)

$$E_{300}\ (\mathrm{dB\mu V/m}) = E_{\mathrm{d}}\ (\mathrm{dB\mu V/m}) + 20\log_{10}\left(\frac{d_{\mathrm{s}}}{300}\right) \tag{4.5-A1}$$

where

E_{d} is the field strength measured at the aircraft at a particular elevation angle;

d_{s} is the slant distance to the aircraft at that elevation angle;

E_{300} is the calculated field strength at 300 m radial distance at the same elevation angle.

The values of E_{300} have been plotted against elevation angle to create two vertical radiation patterns for each flight. One vertical radiation pattern has been created for that part of the flight which took place to the south of the ISM device and another for that part of the flight which took place to the north of the ISM device. Each pattern therefore extends up to an elevation angle of 90°, which locates the common field point between the two patterns.

Sommerfeld-Norton surface wave contributions to the horizontally polarized fields at very low elevation angles have also been considered inasmuch as their presence might have complicated the adjustment with distance of the measured field strengths at those low angles. Surface waves at frequencies above 30 MHz have been studied in [11]. In [11] it is shown that at the distances and heights over ground at which the in-flight data were gathered, the contributions of surface waves are insignificant.

Figure 4.5-A1 illustrates vertical patterns of horizontally polarized fourth harmonic radiation from ISM Machine A (a 25 kW RF plastic sealer) with its RF shields removed, calculated from the data in [4] using equation (4.5-A1) and shown as solid line curves, compared with vertical patterns of horizontally polarized radiation calculated at 109 MHz for two electrically small horizontal electric dipoles (dashed curves). The in-flight field strength data were obtained at a flight altitude of 152 m (500 feet) and plotted in figure A-4, page 54 of reference [4].

The sharp step in the field strength from Machine A close to the elevation angle of 5° in figure 4.5-A1(b) corresponds with the switch-on of the ISM equipment. Note that, to match the patterns of the fields measured to the south of the ISM equipment, the dipole current moment *I.dl*, the dipole height above ground, and the radiated power required from the small electric dipole, are all different from those required to match the fields measured to the north.

Figure 4.5-A2 uses in-flight data for ISM Machine B operated with RF shields in place, collected at an altitude of 152 m. In figure 4.5-A2(b) the noise floor of the measurements is visible in the solid curve for elevation angles between 12° and 20°. Switch-on of the ISM equipment occurred near the elevation angle of 20°. Note that the horizontally polarized vertical field patterns created broadside to two electrically small vertical loops were used to provide the matching patterns in figure 4.5-A2. The dipole moments required were the same, but the source height and therefore the radiated power required to match the patterns to the north were different from those required to match the patterns to the south.

Figure 4.5-A3 compares the radiation at 109 MHz emitted from Machine C (a 3 kW RF plastics sealer), derived from in-flight data measured at an altitude of 152 m, with the calculated horizontally polarized field patterns for two small horizontal electric dipoles. Machine C was operated with its RF shields in place. The sharp step in the Machine C field strength close to the elevation angle of 20° in figure 4.5-A3(b) corresponds with the switch-on of the ISM equipment. The match in figure 4.5-A3(a) was obtained with a small horizontal electric dipole at a height of 2,7 m, slightly higher than the 2 m maximum source height considered elsewhere in this report.

Examples of pattern matching for ISM Machine D (a 2 kW RF plastic sealer), with its RF shields in place, are shown in figure 4.5-A4. In this example the horizontally polarized fields emitted broadside from two small vertical loops were used to provide the matching patterns. The match in figure 4.5-A4(a) was obtained using an electrically small vertical loop at a centre height of 0,85 m, slightly lower than the 1 m minimum source height considered elsewhere in this paper. Switch-off of the ISM equipment is shown by the field strength step near the elevation angle of 5° in figure 4.5-A4(a).

The figures all show how variable the field strengths of the disturbances radiated from ISM equipment can be during short periods of time. Each data gathering flight took place at an air speed of approximately 135 knots [5], from north to south over the ISM equipment. Only one ISM equipment operating cycle of approximately 1 min duration occurred during each flight.

However, after examination of the vertical radiation patterns, it can be concluded that – in spite of the field strength fluctuations – the horizontally polarized field distribution encountered by an aircraft at elevated angles, during any single flight pass over the ISM equipment, can be reasonably well matched (within ≈ ±10 dB) with field distributions created at elevated angles by simple electric or magnetic dipole sources. Given the relatively good match of the simple model patterns with the measured fields at angles above about 4°, and the boundary conditions which reduce the strength of the horizontally polarized fields near the ground, the patterns of the fields of the simple models calculated near the ground will be similar to the patterns of the real fields if they were measured at elevation angles below 4° (see [11]). These results support the belief that the predictability of far field radiation emitted at elevated angles by ISM equipment *in situ* can be judged by considering the vertical patterns of radiation emitted by simple electric and magnetic dipoles near the ground.

Moreover, there seems to be no obvious reason why vertically polarized fields emitted by typical ISM equipment should behave differently from the vertically polarized fields emitted over ground by small dipoles. Such small dipole models should also serve to indicate the predictability of vertically polarized fields.

More detailed studies of the measurements reported by the Avionics Engineering Center at Ohio University [4], and many more examples of matching the measured data with vertical patterns calculated for electrically small electric or magnetic dipole sources, have been described in [5]. Figures 4.5-A1 to 4.5-A4 are adapted from figures in [5].

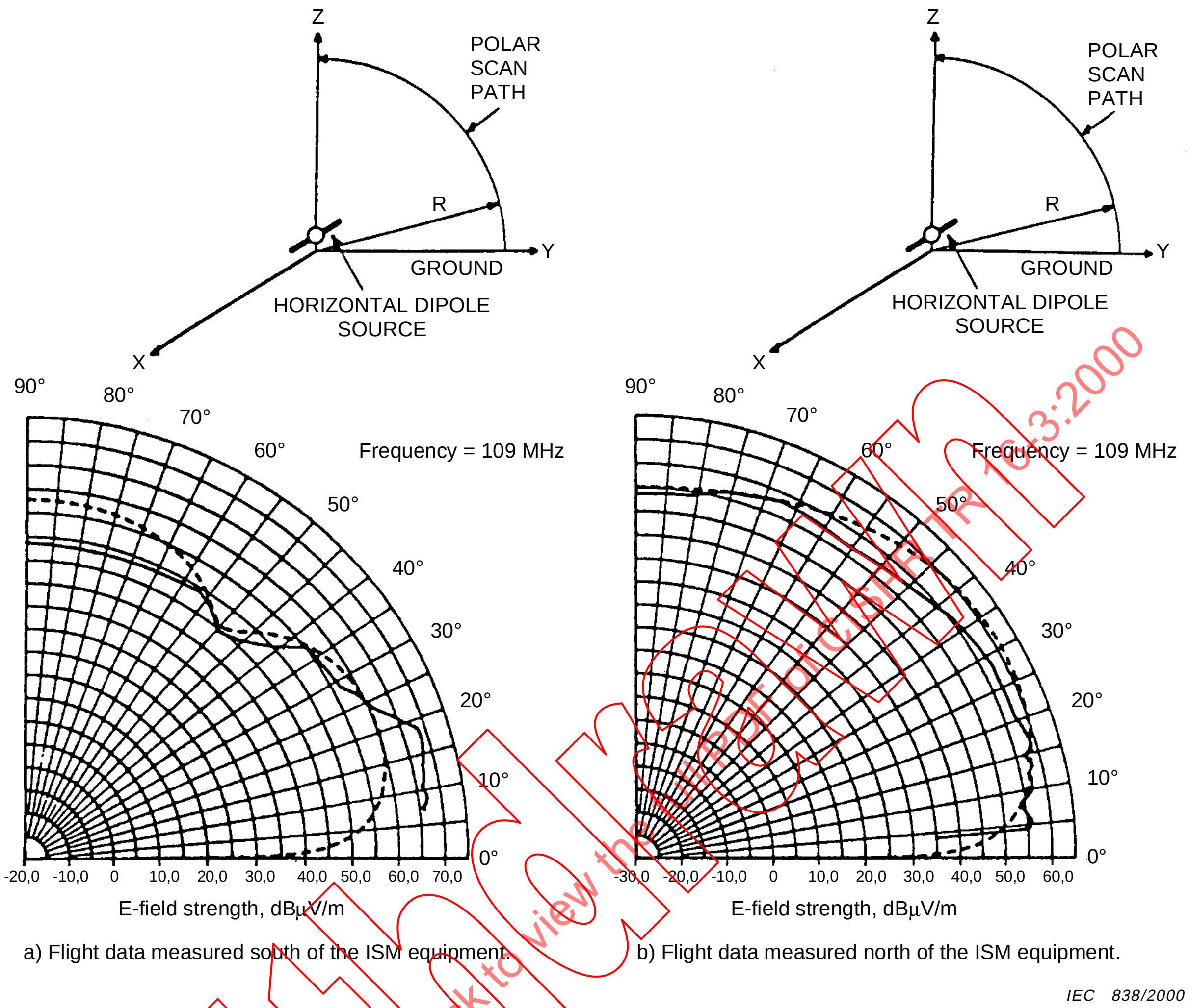

Figure 4.5-A1 – Vertical radiation patterns of horizontally polarized fields, 109 MHz, 300 m scan radius (Adapted from [5])

Solid curves: Machine A (fundamental RF power 25 kW), 180° azimuth, flight altitude 152 m, RF shields removed, derived from in-flight field strength data in figure A-4 at page 54 in [4].

a) Dashed curve: Source = horizontal electric dipole, centre height above ground 1,8 m, dipole (current) moment *I.dl* ≈ 2,51 mA·m, radiated power ≈ 704 µW.

b) Dashed curve Source = horizontal electric dipole, centre height above ground 1,3 m, dipole (current) moment *I.dl* ≈ 2,82 mA·m, radiated power ≈ 996 µW.

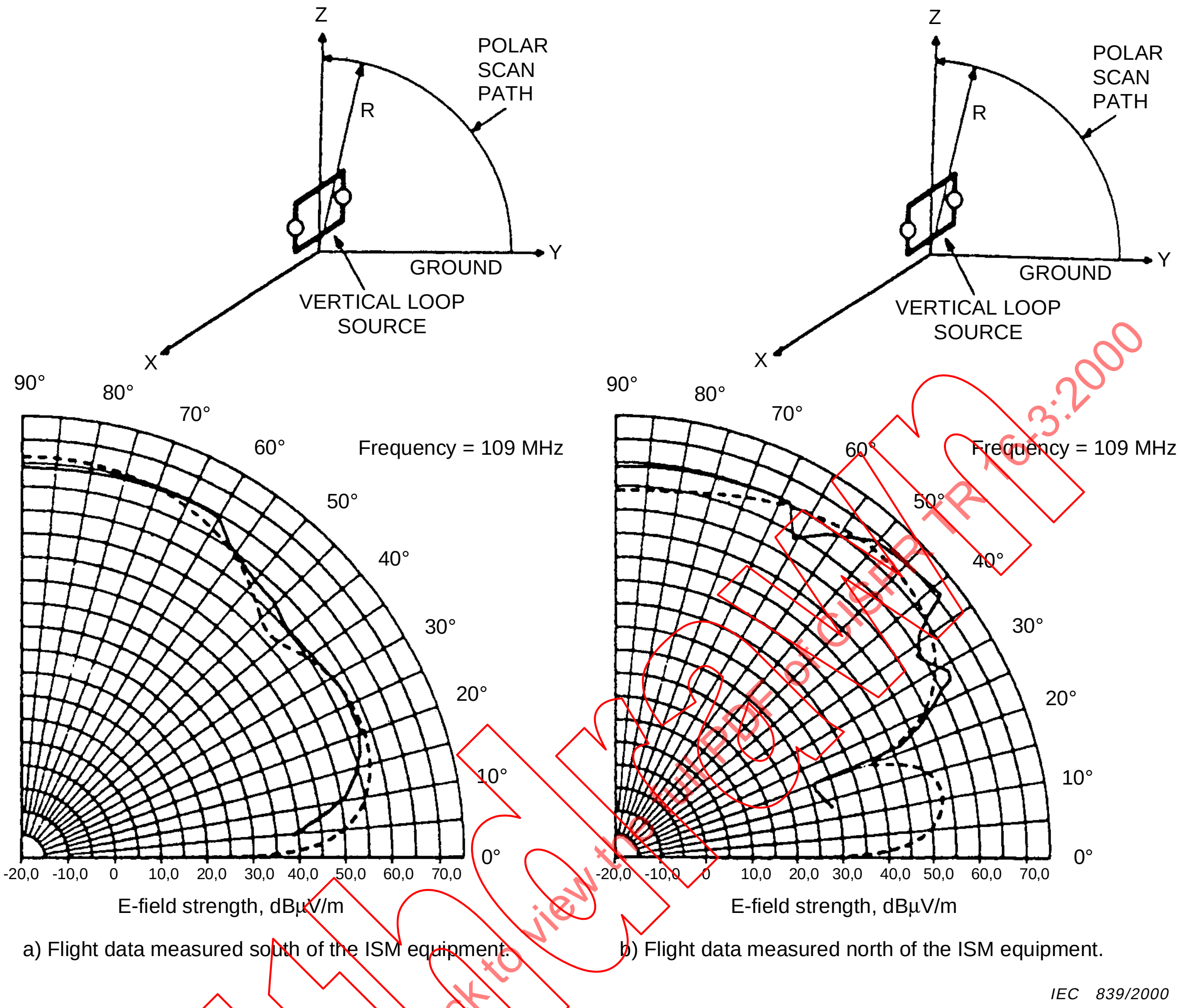

Figure 4.5-A2 – Vertical radiation patterns of horizontally polarized fields, 109 MHz, 300 m scan radius (Adapted from [5])

Solid curves: Machine B (fundamental RF power 2 kW), 0° azimuth, flight altitude 152 m, RF shields in place, derived from in-flight field strength data in figure A-11 at page 62 in [4].

a) Dashed curve: Source = small vertical loop, centre height above ground 1 m, dipole moment $I.dA \approx 3,6$ mA·m^2, radiated power ≈ 6,56 mW.

b) Dashed curve: Source = small vertical loop, centre height above ground 2 m, dipole moment $I.dA \approx 3,6$ mA·m^2, radiated power ≈ 8,33 mW.

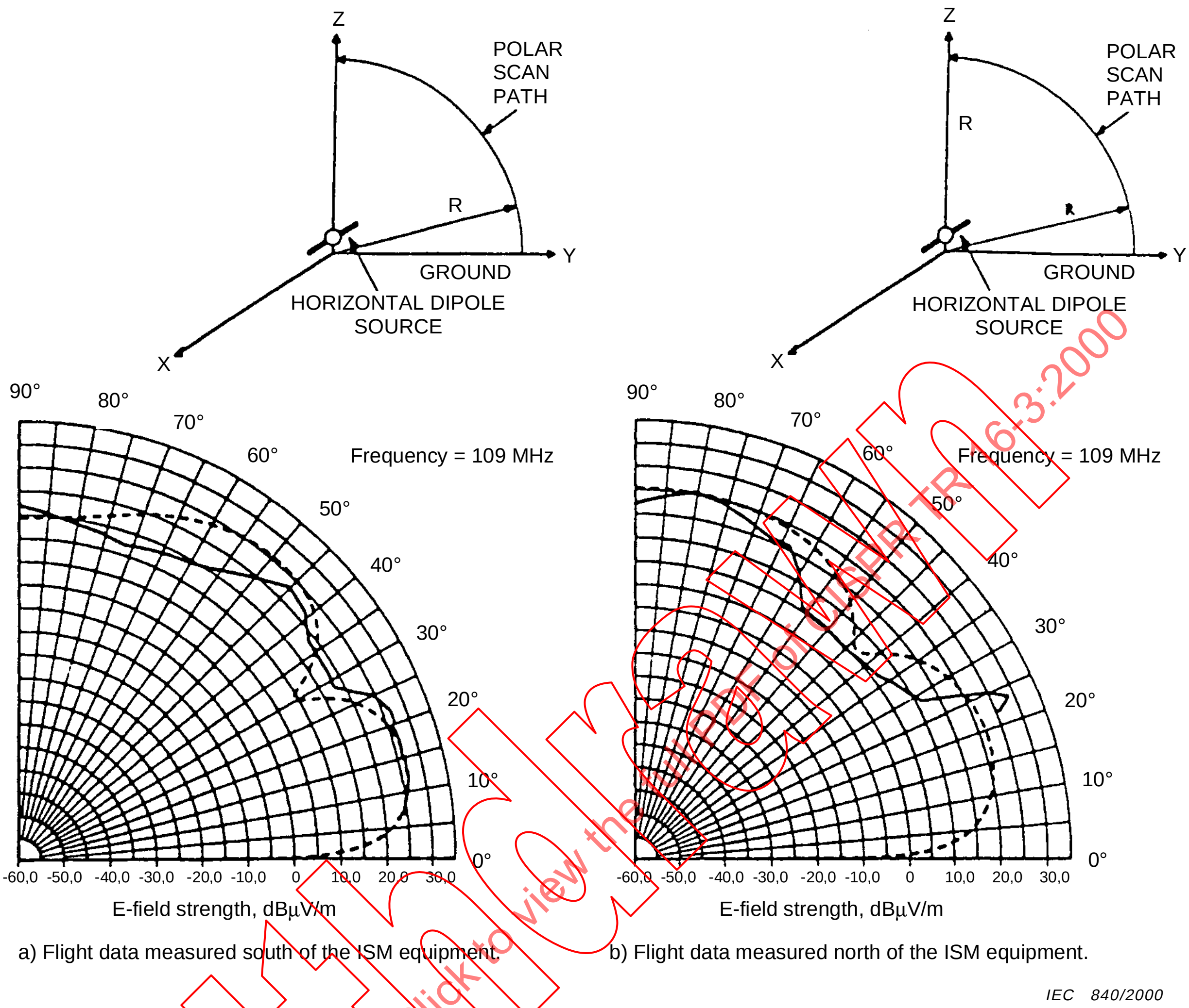

Figure 4.5-A3 – Vertical radiation patterns of horizontally polarized fields, 109 MHz, 300 m scan radius (Adapted from [5])

Solid curves:	Machine C (fundamental RF power 3 kW), 20° azimuth, flight altitude 152 m, RF shields in place, derived from in-flight field strength data in figure A-13 at page 65 in [4].
a) Dashed curve:	Source = horizontal electric dipole, centre height above ground 2,7 m, dipole (current) moment *I.dl* ≈ 50,1 µA·m, radiated power ≈ 0,31 µW.
b) Dashed curve	Source = horizontal electric dipole, centre height above ground 2 m, dipole (current) moment *I.dl* ≈ 28,2 µA·m, radiated power ≈ 0,096 µW.

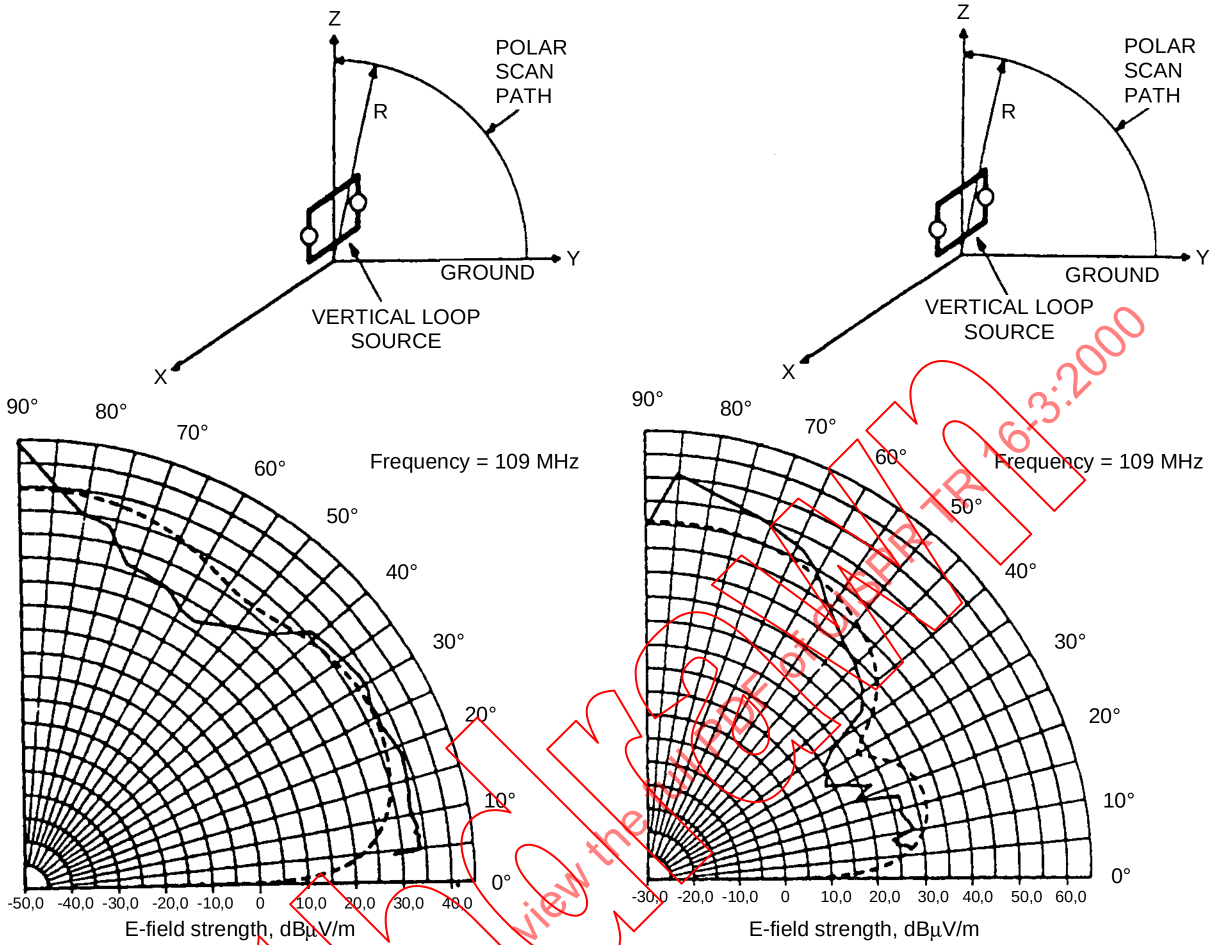

a) Flight data measured south of the ISM equipment. b) Flight data measured north of the ISM equipment.

IEC 841/2000

Figure 4.5-A4 – Vertical radiation patterns of horizontally polarized fields, 109 MHz, 300 m scan radius (Adapted from [5])

Solid curves:	Machine D (fundamental RF power 2 kW), 20° azimuth, flight altitude 152 m, RF shields in place, derived from in-flight field strength data in figure A-19 at page 72 in [4].
a) Dashed curve:	Source = small vertical loop, centre height above ground 0,85 m, dipole moment $I.dA \approx 0{,}14$ mA·m^2, radiated power ≈ 10,4 µW.
b) Dashed curve	Source = small vertical loop, centre height above ground 2 m, dipole moment $I.dA \approx 0{,}23$ mA·m^2, radiated power ≈ 42,0 µW.

4.5.8 References

[1] ITU-R Recommendation 527-1, *Electrical Characteristics of the Surface of the Earth*, International Consultative Committee on Radio (CCIR), International Telecommunication Union, Geneva, 1982

[2] ITU-R Report 879-1, *Methods for Estimating Effective Electrical Characteristics of the Surface of the Earth*, International Consultative Committee on Radio (CCIR), International Telecommunication Union, Geneva, 1986

[3] CISPR 11:1990, *Limits and methods of measurement of electromagnetic disturbance characteristics of industrial, scientific and medical (ISM) radio-frequency equipment*, Second Edition, International Special Committee on Radio Interference (CISPR), International Electrotechnical Commission, Geneva, 1990

[4] J.D. Nickum and W. Drury, *Measurement of RF Fields Associated With ISM Equipment as it Relates to Aeronautical Services*, Report No. OU/AEC/EER 67-1, Avionics Engineering Center, Department of Electrical and Computer Engineering, Ohio University, Athens, Ohio 45701, USA. Final report to the US Federal Aviation Administration, Systems Engineering Service, Washington, DC 20591, Report No. DOT/FAA/ES-84/2, May 1985. Document disseminated under sponsorship of the US Department of Transportation, publicly available through the National Technical Information Service, Springfield, Virginia 22161, USA

[5] I.P. Macfarlane, *Harmonic Fields Radiated at Elevated Angles from 27 MHz ISM Apparatus Over Real Ground*, Telstra Research Laboratories Report 8347, Telstra Research Laboratories, 770 Blackburn Road, Clayton, Victoria 3168, Australia, 1995

[6] G.J. Burke and A.J. Poggio, *Numerical electromagnetics code (NEC) – Method of Moments*, Naval Ocean Systems Center, San Diego, CA 92152,USA, NOSC Technical Document 116, 1981. (Numerical Electromagnetics Code (NEC2) developed at Lawrence Livermore National Laboratory, Livermore, California, File Created 4/11/80, Double Precision 6/4/85).

[7] A. Sommerfeld, translated by Straus, "Partial Differential Equations in Physics", *Lectures on Theoretical Physics*, Volume VI, Academic Press, New York, 1964, Chapter VI

[8] W.L. Stutzman and G.A. Thiele, *Antenna Theory and Design*, John Wiley & Sons, New York, 1981, p.123

[9] **Radio Regulations**. Edition of 1990, International Telecommunication Union (ITU), General Secretariat, Geneva, 1990

[10] I.P. Macfarlane, *Predictability of Electromagnetic Radiation in the Vertical Plane Over Real Ground at Frequencies Above 30 MHz*, Telstra Research Laboratories Report 8331, Telstra Research Laboratories, 770 Blackburn Road, Clayton, Victoria 3168, Australia, 1995

[11] I.P. Macfarlane, *Surface Waves and Near Fields Over Ground Planes at Frequencies Above 30 MHz*, Telstra Research Laboratories Report 8329, Telstra Research Laboratories, 770 Blackburn Road, Clayton, Victoria 3168, Australia, 1995

[12] E.C. Jordon and K.G. Balmain, *Electromagnetic Waves and Radiating Systems*, Prentice-Hall, Inc., Second Edition, 1968, Chapter 16

[13] US Code of Federal Regulations (CFR), Chapter I – *Federal Communications Commission (FCC), Title 47, Part 18, Industrial, scientific and medical equipment*, US Government Printing Office, issue of October 1992. Measurement techniques to determine compliance are set out in FCC/OST Measurement Procedure MP-5 (1986), *Methods of Measurement of Radio Noise Emissions from Industrial, Scientific and Medical Equipment*, US Department of Commerce, National Technical Information Service, Springfield, VA 22161, February 1986

4.6 The predictability of radiation in vertical directions at frequencies up to 30 MHz

4.6.1 Scope

This report considers the vertical radiation patterns of the magnetic (*H*) fields and electric (*E*) fields emitted at frequencies up to 30 MHz from electrically small sources located close to the surface of real homogeneous plane ground, for the purpose of studying the predictability of radiation in vertical directions based on measurements of the strength of the *H*-field near the ground.

The vertical radiation patterns of the fields have been calculated at a distance of 30 m from various electrically small sources, and then the patterns of the fields at greater distances have been calculated so that the field variations with distance can be quantified. In this way, a general knowledge has been obtained of the shapes of the vertical radiation patterns, showing the magnitudes of the field strengths near ground compared with the magnitudes of the field components at elevated angles, and the ways in which the relative magnitudes can be expected to vary with distance over a plane ground.

The sources considered are electrically small balanced electric and magnetic dipoles excited in the frequency range 100 kHz to 30 MHz. For the purposes of the report, an electrically small source is defined as one whose largest linear dimension is one-tenth or less of the free space wavelength at the frequency of interest.

The report also considers the effects on the vertical radiation patterns of locating the electrically small sources close to real grounds having several different values of electrical conductivity and dielectric constants [1] [2], and includes the special case of a ground that behaves as a perfect conductor.

The possible effects on the vertical radiation patterns produced by walls, buildings, reinforced concrete structures, and the like, in the vicinity of the sources, and the effects on wave propagation near the ground that could be produced by changes with distance of the electrical constants of the ground, caused by intervening roads, watercourses, buried metallic pipes, and so on, are not within the scope of this report. It is important to note, therefore, that the errors in predictability that may be produced by such effects have not been considered.

4.6.2 Introduction

CISPR 11 [3] sets limits for the electromagnetic disturbances emitted near the ground from industrial, scientific and medical (ISM) radio-frequency equipment. The limits are intended to provide protection of the reception of radio services. At frequencies below 30 MHz the limits apply to the horizontally oriented components of the *H*-fields emitted by the ISM apparatus. For measurements on a test site, the limits apply at a distance of 30 m from the source. When measurements are made *in situ* the distance to the measurement point is defined as 30 m from the exterior wall outside the building in which the ISM equipment is situated; the distance from the source is not defined. Measurements are to be made with a vertically oriented loop, the base of which must be 1 m above the ground.

It is acknowledged in CISPR 11 that many aeronautical communications require the limitation of vertically radiated electromagnetic disturbances, and that work is necessary to determine what provisions may be required to provide protection of such systems.

The aeronautical radio services to be protected may be either horizontally or vertically polarized transmissions. Thus, the field components at elevated angles, emitted from potential interference sources located near the ground, that are of interest in a study of field strength predictability include the vertically and horizontally oriented *H*- and *E*-field components.

In this report the judgements of predictability of radiation in vertical directions are based on the accuracy with which ground-based measurements of the horizontally oriented *H*-fields emitted from a variety of sources will indicate the maximum strengths of the horizontally or vertically oriented *H*-fields at elevated angles.

As might be expected, at a distance of 30 m from an electrically small source there are significant changes in the field behaviour with changing wavelength as the frequency is varied from 100 kHz to 30 MHz. The report, therefore, concentrates attention at four frequencies, namely 100 kHz, 1 MHz, 10 MHz and 30 MHz. At 100 kHz the distance of 30 m lies well within the electrostatic or inductive near-field region close to the source. At 1 MHz the distance of 30 m is within $\lambda/10$ of an electrically small source and places the measurement position in what might be called the radiating near-field region. At 10 MHz, a distance of 30 m represents approximately one wavelength from the source, a region where the far-field has become established. At 30 MHz, a distance of 30 m represents approximately three wavelengths from the source and places the measurement position well into the far-field.

In addition to the variations in field behaviour produced by changes from near-field to far-field conditions as the wavelength is varied, in the frequency range 100 kHz to 30 MHz the electrical behaviour of real ground varies. In general, real ground has the characteristics of a lossy conductor at low frequencies and the characteristics of a lossy dielectric at the higher frequencies. Moreover, the values of the electrical constants of real ground can vary widely; they may range typically from a conductivity of 10^{-4} S/m and relative permittivity of 3 to a conductivity of 10^{-2} S/m and relative permittivity of 30 [1] [2]. Even this wide range of values of the ground constants does not encompass all of the values that may be encountered in some localities.

The report shows the limitations of the predictability of radiation in vertical directions. In particular, it identifies the critical importance of a knowledge of the precise measurement distance – the actual distance between the source and the field measuring point near the ground – if it is to be possible to make predictions of the radiated field strengths at elevated angles with a known margin of error.

The report indicates the ranges of magnitude of the significant errors in predictability that can still occur when the precise measurement distance over real ground is 30 m from the sources, and the large errors that can arise from the approximation that the influence of real ground can be determined by assuming it behaves like a perfect conductor. It also shows how magnitudes of the errors in predictability above real ground may be reduced, although they remain significant, by supplementing measurements of horizontally oriented *H*-fields near ground with height scan measurements of vertically oriented *H*-fields at heights up to 6 m, when the measurements are made at a distance of 30 m from the sources.

4.6.3 Method of calculation of the vertical radiation patterns

The *H*- and *E*-field vertical radiation patterns in this report were calculated using a Method of Moments computer code known as the Numerical Electromagnetics Code (NEC) [4]. A double precision version, NEC2D, with the companion code SOMNEC2D, was used. NEC with SOMNEC allows the Sommerfeld integral evaluation of the field interactions at the air-ground interface [5] to be included in the determination of the *E*-fields above real grounds.

In the version of the NEC codes that were first released for public use, a section of code for calculation of the near *H*-field in the presence of real ground was omitted, which can lead to large errors in the *H*-field calculations [6] [7]. In the version of NEC2D used to calculate the radiation patterns in this report the missing code has been restored, allowing calculation *f* all the *H*-field components close to the surface of a real ground. The restored section of code calculates the *H*-field components by using a six-point finite-difference approximation of the curl of the *E*-field obtained by the Sommerfeld method.

The spatial sampling interval used in the finite-difference calculation of *H*-field in NEC is normally fixed at $10^{-3}\,\lambda$. For the *H*-field radiation patterns calculated at the frequencies of 100 kHz and 1 MHz the spatial sampling interval has to be altered to $10^{-5}\,\lambda$ and $10^{-4}\,\lambda$ respectively in order to obtain accurate calculations of the near *H*-fields [7] [8].

Some remaining problems of numerical stability, arising from the finite-difference approximation of the *H*-fields from *E*-fields which in some cases have components whose curl is mathematically zero but which have become numerically non-zero due to small numerical inaccuracies [9], have required smoothing of some of the calculated *H*-field radiation patterns.

4.6.4 The source models

The electrically small sources that form the basis of this report consist of small vertical and horizontal balanced electric dipoles, and vertical and horizontal balanced magnetic dipoles (horizontally and vertically oriented loops respectively), each having a unit dipole moment (i.e. a dipole [current] moment of 1 A·m for the electric dipoles and a dipole moment of 1 $A \cdot m^2$ for the magnetic dipoles). All were located very close electrically to the air-ground interface (within a small fraction of a wavelength); the height above ground of the base of each dipole was varied between either 7 cm or 15 cm and a maximum of 1 m to determine the sensitivity of the shape of the field-strength patterns to changes in the source height. The patterns considered in this report are those that exhibited the greatest variation in shape with height.

The geometries of the models used for the field-pattern computations are shown in figures 4.6-1 to 4.6-4, including the paths of the radial scans about each source; advantage has been taken of the verified azimuthal symmetry of the fields around the vertical magnetic and vertical electric dipoles to confine attention to the radial scans around those sources in only the Z-X plane.

It will be seen in figures 4.6-3 and 4.6-4 that each loop is driven by two generators. Although the loops used in the models were electrically small it was found that, when driven by one generator only, each displayed sufficient current asymmetry to produce a significant electric dipole contribution to the electromagnetic fields – because of their finite size the small loops did not behave as electrically infinitesimal magnetic dipole sources. Therefore, in the models used here, each loop was driven by two identical aiding generators located as shown, and the electric dipole contribution produced by current asymmetry arising from the use of a single generator was reduced to insignificance. Of course, in the case of the horizontal magnetic dipole (vertical loop), there is always a loop current asymmetry (and a resultant electric dipole moment) caused by proximity to the ground and this effect also occurs in the models used in this report.

4.6.5 Electrical constants of the ground

Most attention in this report has been devoted to radiation sources located close to a ground having a conductivity, σ, of 10^{-3} S/m and a relative dielectric constant, ε_r of 15; these electrical constants are in the CCIR category of a medium dry ground [1] [2].

At the upper and lower extremes of the frequency range, 30 MHz and 100 kHz, examples of two other sets of values of ground constants have been used with the small horizontal electric dipole model to illustrate the influence of differing values of the ground constants on the vertical radiation patterns. The electrical constants mentioned in 4.6.2, with the numerical values of $\sigma = 10^{-2}$ S/m and $\varepsilon_r = 30$ (ITU-R – cultivated land and fresh water marshes) and $\sigma = 10^{-4}$ S/m and $\varepsilon_r = 3$ (ITU-R – very dry ground and granite mountains in cold regions), were chosen as the examples [1] [2].

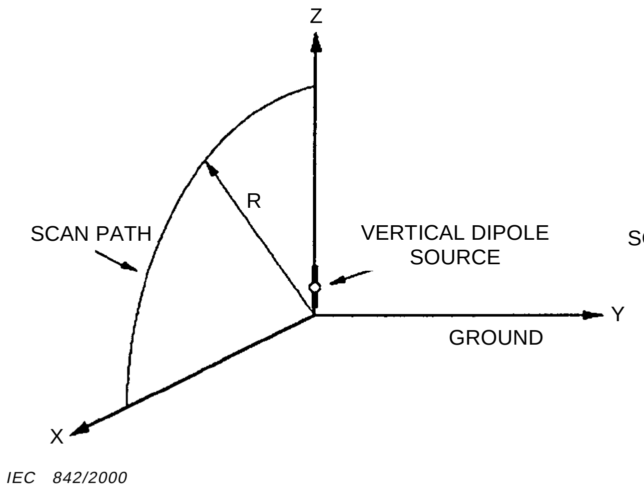

Figure 4.6-1 – Geometry of the small vertical electric dipole model

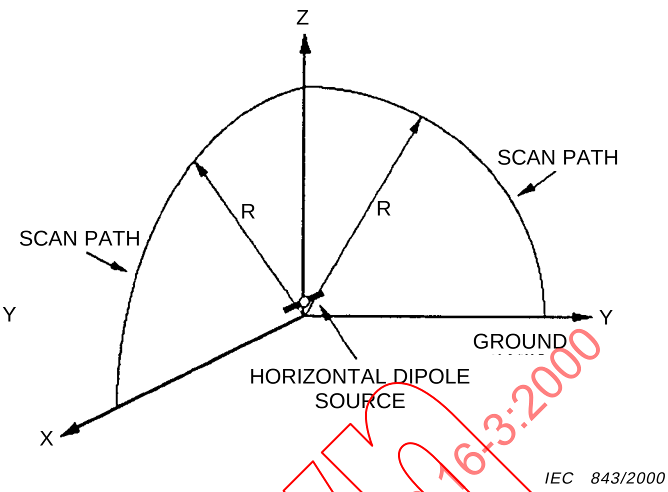

Figure 4.6-2 – Geometry of the small horizontal electrical dipole model

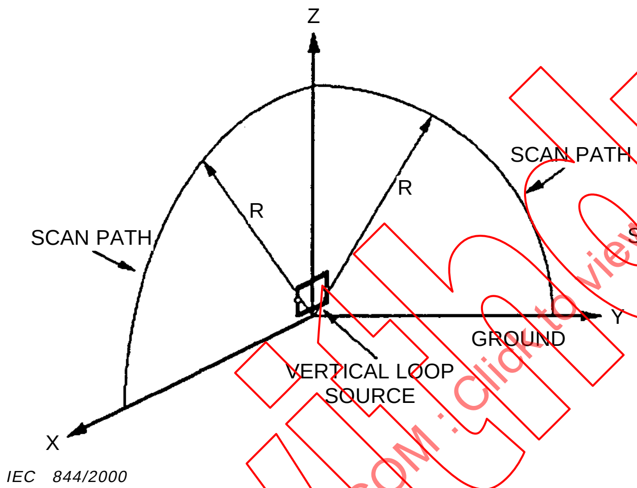

Figure 4.6-3 – Geometry of the small horizontal magnetic dipole model (small vertical loop)

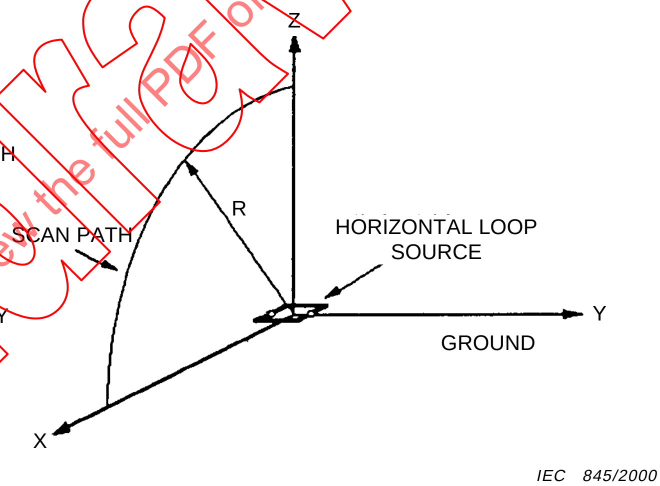

Figure 4.6-4 – Geometry of the small vertical magnetic dipole model (small horizontal loop)

For each type of source, the field patterns above a perfectly conducting ground have also been compared with the patterns generated above real grounds, to identify the errors that can arise from the approximation which is sometimes made that the influence of real ground can be determined by assuming it behaves as a perfect conductor.

In general, it is necessary to recall that specific boundary conditions apply to the fields at the surface of a perfect conductor that do not necessarily apply at the surface of a real ground. In particular, the *H*-field component normal to the surface of a perfect conductor must go to zero at the surface, as must the tangential *E*-field component at the surface, and it will be recalled that this is why a horizontally polarized surface wave cannot exist at the surface of a perfect conductor. Further, a vertically polarized surface wave travelling on a perfectly conducting ground plane experiences no ohmic loss, it merely attenuates with distance at the free space rate. Those boundary conditions, however, certainly do not apply at the surface of a real ground – thus the boundary conditions identify the most general set of differences between the vertical radiation patterns that will exist close to the surface of a real ground when compared with those calculated close to the surface of a perfectly conducting ground.

4.6.6 Predictability of radiation in vertical directions

4.6.6.1 Tabular summaries of predictability

The vertical radiation patterns on which the judgements of predictability are based are presented in figures 4.6-7 to 4.6-62, polar patterns showing field strength plotted against elevation angle above the ground. To summarize the information presented in those figures, four tables of summary information have been prepared, one for each frequency considered in this report.

Table 4.6-1 – Predictability of radiation in vertical directions at 100 kHz, using ground-based measurements of horizontally oriented *H*-field at distances up to 3 km from the source

Type of source	Predictability based on measurements near real ground at 30 m distance from the source	Predictability based on *in situ* measurements near real ground when the measurement distance from the source is not precisely known	Predictability based on vertical radiation patterns calculated at a known distance from the source, assuming the ground behaves as a perfect conductor
Electrically small vertical electric dipole	Excellent (see figures 4.6-7, 4.6-9)	Excellent (see figures 4.6-7, 4.6-8, 4.6-9, 4.6-10)	Excellent (see figure 4.6-7)
Electrically small horizontal electric dipole	Excellent (see figures 4.6-11, 4.6-12, 4.6-13) Notes 1, 2	Very good (see figures 4.6-11, 4.6-13, 4.6-14, 4.6-15)	Poor (see figure 4.6-11) Note 3
Electrically small horizontal magnetic dipole (vertical loop)	Excellent (see figures 4.6-16, 4.6-18) Note 4	Very good (see figures 4.6-16, 4.6-18, 4.6-19, 4.6-20)	Very good (see figures 4.6-16, 4.6-17) Note 5
Electrically small vertical magnetic dipole (horizontal loop)	Poor (see figures 4.6-21, 4.6-25) Note 6	Impossible (see figures 4.6-21, 4.6-23 to 4.6-26) Note 7	Impossible (see figures 4.6-21, 4.6-22) Note 8

NOTE 1 The measurement of horizontally oriented *H*-field emitted by the small horizontal electric dipole near the ground can overestimate the maximum vertically oriented *H*-field strength emitted at an elevated angle by approximately 1 dB, see figure 4.6-11. Note, however, that the measurement overestimates the strength of the horizontally oriented *H*-field emitted in the vertical direction by 5 dB.

NOTE 2 The small influence exerted on the small horizontal electric dipole's vertical radiation patterns at 100 kHz by a wide range of the electrical constants of the ground is shown in figure 4.6-12.

NOTE 3 The horizontal electric dipole's *H*-field pattern calculated assuming a perfectly conducting ground shows that such an assumption causes an underestimate of more than 20 dB in the absolute field strength, and falsely indicates that the ground-based measurement underestimates the maximum field strength by 6 dB (refer to Note 1). See figure 4.6-11.

NOTE 4 Measurement of horizontally oriented *H*-field emitted by the small horizontal magnetic dipole (vertical loop) near the ground can overestimate the maximum vertically oriented *H*-field strength at elevated angles by less than 1 dB, see figure 4.6-16. Note, however, that the measurement overestimates the strength of the horizontally oriented *H*-field emitted in the vertical direction by more than 3 dB.

NOTE 5 Vertical patterns of the horizontally oriented *H*-fields emitted by the small horizontal magnetic dipole (vertical loop), calculated assuming a perfectly conducting ground, can overestimate absolute values of field strength over real ground by 6 dB, but the shapes of the patterns are a good guide to those over real ground. However, boundary conditions require that the vertically oriented *H*-field must go to zero at the surface of the perfectly conducting ground which is not the case at the surface of a real ground. See figures 4.6-16 and 4.6-17.

NOTE 6 Measurement of horizontally oriented *H*-field emitted by the small vertical magnetic dipole (horizontal loop) near the ground at a distance of 30 m underestimates the *H*-field strengths at elevated angles by more than 16 dB, see figure 4.6-21. However, measurement of the vertically oriented *H*-field, *Hz*, near the ground improves predictability; it provides an underestimate of the vertically oriented *H*-field emitted in the vertical direction by approximately 6 dB, and an underestimate of the maximum horizontally oriented *H*-field emitted at elevated angles by about 3 dB.

NOTE 7 The relative magnitudes of the *H*-field components near the ground and at elevated angles are strongly dependent on the actual distance from the small horizontal loop. See figures 4.6-21, 4.6-23 and 4.6-24.

NOTE 8 The small horizontal loop's field patterns calculated close to the ground assuming a perfectly conducting ground have no resemblance, in shape and absolute magnitude, to the field patterns calculated close to a real ground. See figures 4.6-21 and 4.6-22.

Table 4.6-2 – Predictability of radiation in vertical directions at 1 MHz, using ground-based measurements of horizontally oriented *H*-field at distances up to 300 m from the source

Type of source	Predictability based on measurements near real ground at 30 m distance from the source	Predictability based on *in situ* measurements near real ground when the measurement distance from the source is not precisely known	Predictability based on vertical radiation patterns calculated at a known distance from the source, assuming the ground behaves as a perfect conductor
Electrically small vertical electric dipole	Excellent (see figures 4.6-27, 4.6-28)	Excellent (see figures 4.6-27, 4.6-28, 4.6-29)	Excellent (see figure 4.6-27)
Electrically small horizontal electric dipole	Very good (see figures 4.6-30, 4.6-32) Note 9	Good (see figures 4.6-30, 4.6-31, 4.6-32, 4.6-33)	Poor (see figure 4.6-30) Note 10
Electrically small horizontal magnetic dipole (vertical loop)	Excellent (see figures 4.6-34, 4.6-37) Note 11	Good (see figures 4.6-34, 4.6-36, 4.6-37, 4.6-38)	Fair (see figures 4.6-34, 4.6-35) Note 12
Electrically small vertical magnetic dipole (horizontal loop)	Excellent (see figures 4.6-39, 4.6-42) Note 13	Impossible (see figures 4.6-39, 4.6-41 to 4.6-42) Note 14	Poor (see figures 4.6-40) Note 15

NOTE 9 Measurement of the horizontally oriented *H*-field emitted by the horizontal electric dipole near the ground can overestimate the maximum vertically oriented *H*-field strength emitted at elevated angles by approximately 3 dB. See figure 4.6-30. Note, however, that the measurement can overestimate the strength of the horizontally oriented *H*-field emitted in the vertical direction by more than 9 dB.

NOTE 10 The *H*-field patterns calculated at a distance of 30 m from the horizontal electric dipole assuming a perfectly conducting ground show that such an assumption causes an underestimate of 20 dB in the absolute field strength at 1 MHz, and falsely indicates that the ground-based measurement underestimates the maximum field strength emitted in vertical directions by 5 dB. See figure 4.6-30.

NOTE 11 Measurement of the horizontally oriented *H*-field emitted by the small vertical loop near the ground can overestimate the maximum field strength emitted at elevated angles by less than 3 dB, see figure 4.6-34.

NOTE 12 The patterns of horizontally oriented *H*-field calculated at 30 m from the small vertical loop assuming perfectly conducting ground are very similar to the *H*-field patterns over a real ground. See figures 4.6-34 and 4.6-35.

NOTE 13 The measurement of the horizontally oriented *H*-field emitted by the small horizontal loop near the ground at 30 m distance can underestimate the maximum vertically oriented *H*-field strength emitted in the vertical direction by more than 2 dB, and the maximum horizontally oriented *H*-field emitted at elevated angles by less than 1 dB, see figure 4.6-39. A measurement of the vertically oriented *H*-field, *Hz*, near ground reduces the underestimate of the strength of the vertically oriented *H*-field emitted in the vertical direction to about 1 dB, and overestimates the maximum horizontally oriented *H*-field strength by more than 1 dB.

NOTE 14 The relative magnitudes of the *H*-field components near the ground and at elevated angles are strongly dependent on the actual distance from the horizontal loop source. The horizontally oriented *H*-field near the ground is a radially directed component which attenuates more rapidly with increasing distance than does the horizontally oriented *H*-field at elevated angles. The vertically oriented *H*-field near the ground is a component of the horizontally polarized ground wave launched by the horizontal loop and attenuates very rapidly with increasing distance from the source at 1 MHz. See figures 4.6-39 and 4.6-41.

NOTE 15 At 1 MHz, the vertical radiation pattern of the horizontally oriented *H*-field emitted by the small horizontal loop above a perfectly conducting ground has an absolute value more than 15 dB less than the field strength calculated above a real ground. The shape of the vertical pattern of the vertically oriented *H*-field calculated close to a perfectly conducting ground bears no resemblance to the vertical pattern calculated close to the real ground. Compare figures 4.6-39 and 4.6-40. In general, the boundary condition which requires the vertically oriented *H*-field strength to be zero at the surface of a perfectly conducting ground means that the pattern of vertically oriented *H*-field at the real ground, which is non-zero, does not resemble the corresponding pattern at the perfect ground.

Table 4.6-3 – Predictability of radiation in vertical directions at 10 MHz, using ground-based measurements of horizontally oriented *H*-field at distances up to 300 m from the source

Type of source	Predictability based on measurements near real ground at 30 m distance from the source	Predictability based on *in situ* measurements near real ground when the measurement distance from the source is not precisely known	Predictability based on vertical radiation patterns calculated at a known distance from the source, assuming the ground behaves as a perfect conductor
Electrically small vertical electric dipole	Excellent (see figures 4.6-43, 4.6-44)	Excellent (see figures 4.6-43, 4.6-44, 4.6-45) Note 16	Impossible (see figure 4.6-43) Note 17
Electrically small horizontal electric dipole	Poor (see figures 4.6-46, 4.6-47) Note 18	Good (see figures 4.6-46, 4.6-47, 4.6-48 Note 19	Impossible (see figure 4.6-46) Note 20
Electrically small horizontal magnetic dipole (vertical loop)	Very good (see figures 4.6-49, 4.6-50) Note 21	Impossible (see figures 4.6-49, 4.6-50) Note 22	Impossible (see figure 4.6-49) Note 23
Electrically small vertical magnetic dipole (horizontal loop)	Poor (see figures 4.6-51, 4.6-52) Note 24	Impossible (see figures 4.6-51, 4.6-52) Note 25	Fair (see figures 4.6-51) Note 26

NOTE 16 The horizontally oriented *H*-field near the ground is a component of the vertically polarized ground wave emitted from the vertical electric dipole. At 10 MHz the vertically polarized wave near the ground attenuates rapidly with increasing distance, such that there is an excess 8 dB ground-wave attenuation in addition to the 20 dB sky-wave attenuation over the distance from 30 m to 300 m. See figure 4.6-43.

NOTE 17 At a distance of 30 m from the vertical electric dipole over a perfectly conducting ground the vertical radiation pattern of the horizontally oriented *H*-field is within about 3 dB of the pattern of the *H*-field over a real ground. However, the vertically polarized wave near a perfectly conducting ground attenuates with increasing distance at the free space rate and therefore does not attenuate with distance in the way it does over a real ground at 10 MHz (see Note 16). It is thus misleading as a guide to the vertical radiation patterns over real ground at distances much beyond 30 m.

NOTE 18 The measurement of the horizontally oriented *H*-field near the real ground at 30 m from the small horizontal electric dipole can underestimate the field strength of the horizontally oriented *H*-field emitted in the vertical direction by approximately 8 dB, and the vertically oriented *H*-field strength emitted at elevated angles by about 3 dB. Measurements of vertically oriented *Hz* near ground cannot improve the predictability in this case. See figure 4.6-46.

NOTE 19 At 10 MHz, the horizontally oriented *H*-field components near real ground attenuate more rapidly with increasing distance from the horizontal electric dipole than do the sky-wave components. The excess attenuation is approximately 7 dB over the distance from 30 m to 300 m. See figure 4.6-46.

NOTE 20 The horizontally oriented *H*-field near a perfectly conducting ground attenuates by 40 dB as the distance from the small horizontal electric dipole increases from 30 m to 300 m, an excess attenuation of 20 dB more than the sky-wave attenuation over the same distance. Near a real ground the excess attenuation is about 7 dB over the same distance at 10 MHz. The vertical radiation patterns over real and perfectly conducting grounds therefore differ significantly in that range of measuring distances. See figure 4.6-46.

NOTE 21 Measurement of the horizontally oriented *H*-field near the real ground at 30 m distance from the small vertical loop can underestimate the horizontally oriented *H*-field strength emitted in the vertical direction by less than 3 dB, but it overestimates the strength of the vertically oriented *H*-field emitted at elevated angles by approximately 3 dB. See figure 4.6-49.

NOTE 22 The horizontally oriented *H*-field components near real ground attenuate much more rapidly with increasing distance from the small vertical loop than do the sky-wave components, at 10 MHz. The excess attenuation is approximately 8 dB over the distance from 30 m to 300 m. See figure 4.6-49.

NOTE 23 At a distance of 30 m from the small vertical loop over a perfectly conducting ground the vertical radiation pattern of the horizontally oriented *H*-field is within about 4 dB of the pattern of the *H*-field over a real ground. However, the vertically polarized wave near a perfectly conducting ground attenuates with increasing distance at the free space rate, unlike a vertically polarized wave over a real ground which attenuates more rapidly with distance at 10 MHz – see Note 22 and figures 4.6-49 and 4.6-50. Vertical radiation patterns calculated over a perfectly conducting ground can therefore be very misleading as guidance to the patterns to be expected over real ground at distances much beyond 30 m at 10 MHz.

NOTE 24 Measurement of the horizontally oriented *H*-field components near the real ground at 30 m distance from the small horizontal loop can underestimate the maximum horizontally and vertically oriented *H*-field strengths at elevated angles by more than 6 dB. Note, however, that a measurement of the vertically oriented *H*-field, *Hz*, at a height of 6 m underestimates the maximum *H*-field, the vertically oriented *H*-field, at elevated angles by approximately 5 dB at 10 MHz. See figure 4.6-51.

NOTE 25 The relative magnitudes of the *H*-field components near the ground and at elevated angles are strongly dependent on the actual distance from the horizontal loop source at 10 MHz. The horizontally oriented *H*-field near the ground is a radially directed component which attenuates more rapidly with increasing distance than does the horizontally oriented *H*-field at elevated angles. The vertically oriented *H*-field near the ground is a component of the horizontally polarized ground wave launched by the horizontal loop and attenuates very rapidly with increasing distance from the source. See figure 4.6-51.

NOTE 26 The shape of the vertical radiation pattern of the horizontally oriented *H*-field calculated at a distance of 30 m from the small horizontal loop over perfectly conducting ground is very similar to that calculated over a real ground at 10 MHz. The absolute value of the field strength calculated over perfectly conducting ground is about 5 dB less than the field strength calculated over real ground. Both calculated vertical radiation patterns at 30 m distance indicate that ground-based measurement of horizontally oriented *H*-field underestimates the maximum field strength at elevated angles by more than 6 dB. The measurable horizontally oriented *H*-field components near the ground in both cases are the remnants of radially directed near-field components, not a part of propagating waves, and they attenuate more rapidly with increasing distance from the source than do the fields at elevated angles. See figure 4.6-51. It must also be recalled that, in general, the boundary condition which requires the vertically oriented *H*-field strength to be zero at the surface of a perfectly conducting ground means that at all frequencies up to 30 MHz the patterns of vertically oriented *H*-field which are non-zero at the real ground do not resemble the corresponding vertically oriented *H*-field patterns which go to zero at the perfectly conducting ground.

Table 4.6-4 – Predictability of radiation in vertical directions at 30 MHz, using ground-based measurements of horizontally oriented *H*-field at distances up to 300 m from the source

Type of source	Predictability based on measurements near real ground at 30 m distance from the source	Predictability based on *in situ* measurements near real ground when the measurement distance from the source is not precisely known	Predictability based on vertical radiation patterns calculated at a known distance from the source, assuming the ground behaves as a perfect conductor
Electrically small vertical electric dipole	Very good (see figures 4.6-53, 4.6-54) Note 27	Impossible (see figures 4.6-53, 4.6-54) Note 28	Impossible (see figure 4.6-53) Note 29
Electrically small horizontal electric dipole	Poor (see figures 4.6-55, 4.6-57, 4.6-58) Notes 30, 31	Impossible (see figures 4.6-55, 4.6-56, 4.6-58 Note 32	Impossible (see figures 4.6-55, 4.6-56) Note 33
Electrically small horizontal magnetic dipole (vertical loop)	Good (see figures 4.6-59, 4.6-60) Note 34	Impossible (see figures 4.6-59, 4.6-60) Note 35	Impossible (see figure 4.6-59) Note 36
Electrically small vertical magnetic dipole (horizontal loop)	Poor (see figures 4.6-61, 4.6-62) Note 37	Impossible (see figures 4.6-61, 4.6-62) Note 38	Good (see figure 4.6-61) Note 39

NOTE 27 The measurement of the horizontally oriented *H*-field near the real ground at 30 m distance from the small vertical electric dipole underestimates the maximum field strength at elevated angles by about 3 dB at 30 MHz.

NOTE 28 The horizontally oriented *H*-field near ground is a component of the vertically polarized ground wave emitted from the vertical electric dipole. At 30 MHz the vertically polarized wave attenuates rapidly with increasing distance near ground, such that there is an excess 13 dB attenuation of the ground wave in addition to the 20 dB sky-wave attenuation over the distance from 30 m to 300 m. See figures 4.6-53 an 4.6-54.

NOTE 29 At a distance of 30 m from the small vertical electric dipole over a perfectly conducting ground, the vertical radiation pattern of the horizontally oriented *H*-field is within about 8 dB of the pattern of the *H*-field over real ground. However, the very high rate of attenuation with a distance of a vertically polarized ground wave over real ground at 30 MHz is apparent even at the short range of 30 m (see figure 4.6-53). Moreover, at 30 MHz there is an excess 13 dB attenuation of the ground wave in addition to the 20 dB sky-wave attenuation over the distance from 30 m to 300 m. Over a perfectly conducting ground the excess ground-wave attenuation does not occur, so that the vertical radiation patterns over perfectly conducting ground cannot give guidance to the patterns over real ground at the distances from the small vertical electric dipole that are considered in this report.

NOTE 30 The measurement of horizontally oriented *H*-field emitted by the small horizontal electric dipole near the ground can underestimate the maximum horizontally oriented *H*-field strength in the vertical direction by more than 16 dB at 30 MHz (see figure 4.6-55). Note, however, that a measurement of the vertically oriented *H*-field, *Hz*, at a height of 6 m improves predictability and underestimates the magnitude of the horizontally oriented *H*-field in the vertical direction by approximately 12 dB. The height scan measurement of *Hz* underestimates the magnitude of the vertically oriented *H*-field at elevated angles by approximately 7 dB.

NOTE 31 The small influence exerted by a wide range of the electrical constants of the real ground on the shape and magnitude of the small horizontal electric dipole's vertical radiation pattern at 30 MHz is shown in figure 4.6-57.

NOTE 32 Excess attenuation of the horizontally oriented *H*-field component of the vertically polarized ground wave emitted by the small horizontal electric dipole at the real ground is almost 12 dB more than the sky-wave attenuation over the distance from 30 m to 300 m from the source. If the true measurement distance is not known, the amount of excess attenuation suffered by the ground wave cannot be known when making predictions of the strength of radiation in vertical directions based on measurements at the ground.

NOTE 33 The horizontally oriented *H*-field near a perfectly conducting ground attenuates by 40 dB as the distance from the small horizontal electric dipole increases from 30 m to 300 m, an excess attenuation of 20 dB more than the sky-wave attenuation, as the far-field radiation pattern becomes established over that distance. On the other hand, the excess attenuation of the *H*-field component of the vertically polarized ground wave is about 12 dB near a real ground over the 30 m to 300 m distance. The vertical radiation patterns over real and perfectly conducting grounds therefore differ significantly at 30 MHz in that range of measuring distances. See figures 4.6-55 and 4.6-56.

NOTE 34 Measurement of the horizontally oriented *H*-field near real ground at 30 m distance from the small vertical loop can underestimate the maximum horizontally oriented *H*-field strength emitted in the vertical direction by less than 6 dB. It gives an exact indication of the strength of the vertically oriented *H*-field emitted at elevated angles. See figure 4.6-59.

NOTE 35 The horizontally oriented *H*-field components near real ground attenuate more rapidly with increasing distance from the small vertical loop than do the sky-wave components, at 30 MHz. The excess attenuation is approximately 13 dB over the distance from 30 m to 300 m. See figure 4.6-59.

NOTE 36 At a distance of 30 m from the small vertical loop over a perfectly conducting ground the vertical radiation pattern of the horizontally oriented *H*-field is within about 8 dB of the pattern of the *H*-field over a real ground. However, the vertically polarized wave near a perfectly conducting ground attenuates with distance at the free space rate, unlike the vertically polarized wave over a real ground which attenuates more rapidly with distance at 30 MHz – see figures 4.6-59 and 4.6-60. Vertical radiation patterns calculated over a perfectly conducting ground can therefore be very misleading as guidance to the patterns over real ground at a distance of 30 m and beyond.

NOTE 37 Measurement of the horizontally oriented *H*-field components near the real ground at 30 m distance from the small horizontal loop can underestimate the *H*-field strengths emitted at elevated angles by more than 16 dB. Note, however, that a measurement of the vertically oriented *H*-field, *Hz*, at a height of 6 m underestimates the maximum *H*-field strengths at elevated angles by less than 6 dB. See figure 4.6-61.

NOTE 38 The relative magnitudes of the *H*-field components near the ground and at elevated angles are strongly dependent on the actual distance from the horizontal loop source. The horizontally oriented *H*-field near the ground is a radially directed component which attenuates more rapidly with increasing distance than does the horizontally oriented *H*-field at elevated angles. The vertically oriented *H*-field near the ground is a component of the horizontally polarized ground wave launched by the horizontal loop and at 30 MHz it attenuates very rapidly with increasing distance from the source. See figures 4.6-61 and 4.6-62.

NOTE 39 The shape and magnitude of the vertical radiation pattern of the horizontally oriented *H*-field calculated at a distance of 30 m from the small horizontal loop over perfectly conducting ground at 30 MHz are very similar to the shape and magnitude of the pattern calculated over real ground. Both the calculated patterns indicate that ground-based measurement of horizontally oriented *H*-field will underestimate the maximum field strength at elevated angles by 16 dB or 17 dB. However, the measurable horizontally oriented *H*-field components near the ground in both cases are the remnants of radially directed near-field components, not a part of propagating waves, and they attenuate more rapidly with increasing distance from the small horizontal loop than do the fields at elevated angles. See figure 4.6-61. It must also be recalled that, in general, the boundary condition which requires the vertically oriented *H*-field strength to be zero at the surface of a perfectly conducting ground means that at all frequencies up to 30 MHz the patterns of vertically oriented *H*-field which are non-zero at the real ground do not resemble the corresponding vertically oriented *H*-field patterns which go to zero at the perfectly conducting ground.

4.6.6.2 Error ranges

It is possible to present pictorially the ranges of errors of the predictability of radiation in vertical directions at different frequencies, when the precise horizontal measurement distance from the sources is known to be 30 m.

Figure 4.6-5 and 4.6-6 show in bar chart form the error ranges to be expected, in figure 4.6-5 when measurements are made of the horizontally oriented *H*-field near the ground at 30 m distance from the sources, and in figure 4.6-6 when those measurements of horizontally oriented *H*-field are supplemented with measurements of vertically oriented *H*-field in a 6 m height scan near the ground at 30 m distance from the sources.

The error range bar charts summarize the information presented in the various notes to the tables and in the radiation pattern diagrams.

The following examples serve to illustrate the ways in which the error range bar charts can be interpreted.

In figure 4.6-5, which is used when predictability of radiation in vertical directions is to be based only on measurements near ground of the horizontally oriented *H*-field components at 30 m horizontal distance from the sources, the charts show that at 100 kHz the largest over-estimation of the strength of radiation in vertical directions occurs in the case of a source behaving as a small horizontal electric dipole, and the error is an overestimate by 5 dB of the maximum strength of the horizontally oriented *H*-field. The largest error in overestimating the maximum vertically oriented *H*-field strength at 100 kHz is an overestimate of only 1 dB, as indicated in the chart by the solid bar, again for the case of a source behaving as a small horizontal electric dipole. At 100 kHz, figure 4.6-5 shows that the largest error in prediction of the strength of radiation in vertical directions occurs in the case of a source behaving as a small vertical magnetic dipole (horizontal loop) and the error is an underestimate by 16 dB of the maximum vertically oriented *H*-field. The largest error at 100 kHz in predicting the maximum horizontally oriented *H*-field strength emitted in vertical directions is an under-estimate by 15 dB, again in the case of a source behaving as a small vertical magnetic dipole (horizontal loop).

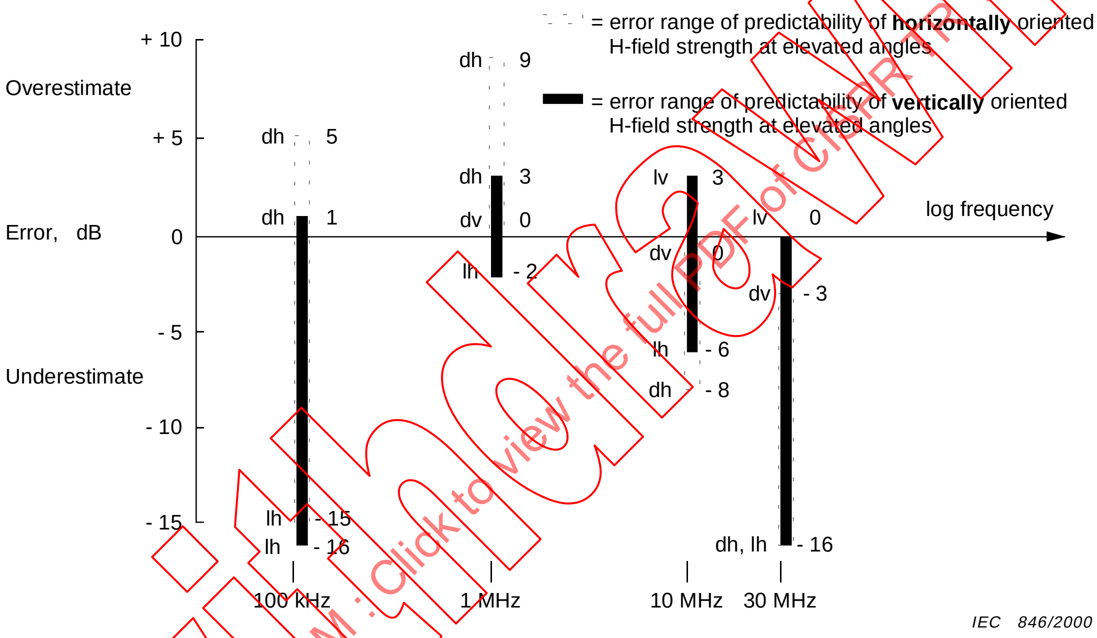

Figure 4.6-5 – Ranges of errors in the predictability of radiation in vertical directions from electrically small sources located close to the ground, based on measurements of the horizontally oriented *H*-field near ground at a distance of 30 m from the sources.

Electrical constants of the ground: σ = 1 mS/m, ε_r = 15.

Source identification:

dh = horizontal electric dipole

lv = horizontal magnetic dipole (vertical loop)

dv = vertical electric dipole

lh = vertical magnetic dipole (horizontal loop)

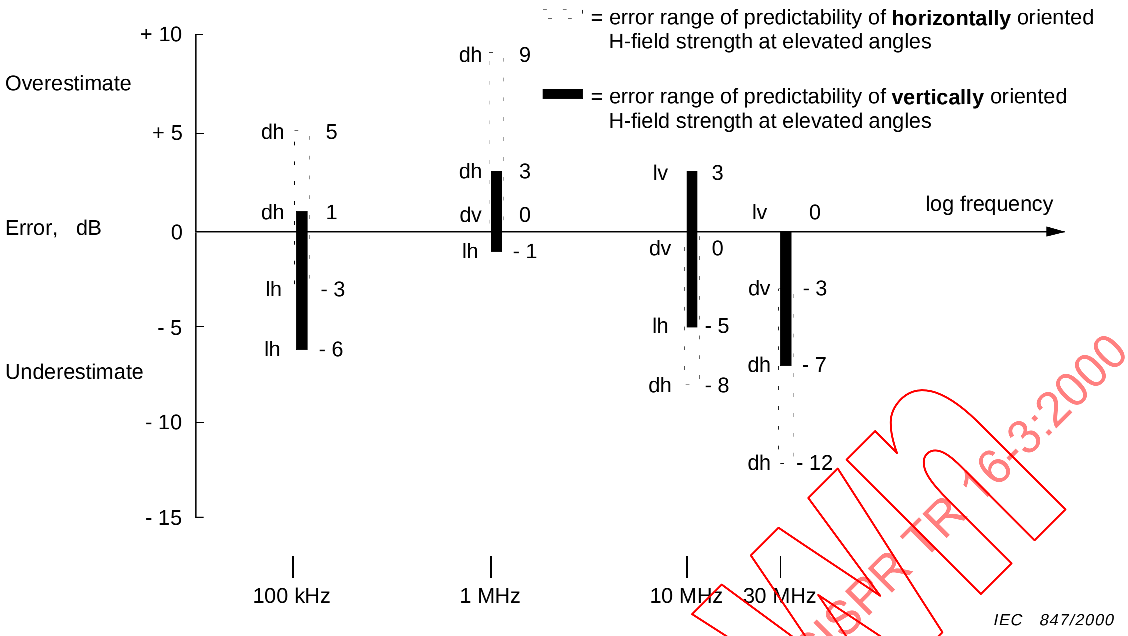

Figure 4.6-6 – Ranges of errors in the predictability of radiation in vertical directions from electrically small sources located close to the ground, based on measurements of the horizontally oriented *H*-field at the ground supplemented with measurements of the vertically oriented *H*-field in a height scan up to 6 m at a distance of 30 m from the sources

Electrical constants of the ground: σ = 1 mS/m, ε_r = 15.

Source identification:

dh = horizontal electric dipole
dv = vertical electric dipole
lv = horizontal magnetic dipole (vertical loop)
lh = vertical magnetic dipole (horizontal loop)

In figure 4.6-6, which is used when predictability of radiation in vertical directions is to be based on measurements near ground of the horizontally oriented *H*-field components supplemented with 6 m height-scan measurements of the vertically oriented *H*-field components at 30 m distance, the charts show that at 100 kHz the worst error in the prediction of the strength of radiation in vertical directions still occurs for the vertically oriented *H*-field components emitted from a source behaving as a small vertical magnetic dipole (horizontal loop), but that the magnitude of the error has been reduced to an under-estimate by 6 dB (solid bar). The magnitude of the largest underestimate at 100 kHz of the maximum strength of the horizontally oriented *H*-fields emitted in vertical directions has been reduced to 3 dB, and this also occurs for the case of a source behaving as a small vertical magnetic dipole (horizontal loop).

4.6.7 Conclusions

Vertical radiation patterns have been calculated for electrically small sources located close to real homogeneous plane ground, ignoring the possible contributions to pattern distortion that might arise from the presence of nearby buildings or other field disturbing objects, or from discontinuities in the electrical constants of the ground. Nevertheless, even with such a simplification, the studies still show that in the case of solitary electrically small sources located close to a plane homogeneous ground the predictability of radiation in vertical directions can be subject to large errors, when the predictions are to be based on measurements of the strength of the horizontally oriented *H*-field at the ground in the manner presently described in CISPR 11.

In particular, the report has identified many examples of the impossibility of making predictions of field strength at elevated angles with a known margin of error, using ground-based measurements, when the measuring distances from the sources are not precisely known. The limits and methods of measurement of radiation *in situ* for which the precise measurement distance from the ISM equipment is not defined in CISPR 11 cannot provide a known level of protection of aeronautical communication services. For example, this limitation applies over the entire frequency range from 100 kHz to 30 MHz if the radiation source behaves like an electrically small vertical magnetic dipole (horizontal loop).

The large errors in calculation of the vertical radiation patterns that can arise from the approximation, which is sometimes made, that the influence of real ground can be determined by assuming it behaves like a perfect conductor have also been indicated. Apart from the more complex interaction between the source and its image in a real ground, two more obvious reasons for the errors are that the boundary condition which requires the vertically oriented *H*-field strength and the horizontally oriented *E*-field strength to be zero at the surface of a perfectly conducting ground does not apply at the surface of a real ground, and the vertically polarized ground wave attenuation with distance over real ground is greater than the attenuation with distance over a perfectly conducting ground, especially at the higher frequencies.

The report has also shown that, even when the measurement distance over real ground is precisely known, predictability of the strength of radiation in vertical directions based on measurements near the ground at a distance of 30 m remains subject to significant errors.

Figure 4.6-5 depicts the error ranges that can apply when predictability is based solely on measurement of the horizontally oriented *H*-field near ground at 30 m distance. It can be seen that over the frequency range from 100 kHz to 30 MHz the margin for error can be as much as +9 dB (overestimate) at 1 MHz, or as much as –16 dB (underestimate) at the extremes of the frequency range, 100 kHz and 30 MHz.

Figure 4.6-6 illustrates the reduced error ranges obtained for predictability of radiation in vertical directions when measurements of horizontally oriented *H*-field near the ground are supplemented with measurements of vertically oriented *H*-field at heights up to 6 m above the ground. It can be seen that the potential overestimate of 9 dB at 1 MHz remains a possibility, but the potential underestimate of 16 dB at 100 kHz and 30 MHz has become a possible underestimate of 6 dB at 100 kHz and of 12 dB at 30 MHz.

The studies in this report have identified some of the factors that must be taken into account when determining limits and methods of measurement of radiated electromagnetic disturbances from ISM apparatus to ensure the protection of aeronautical communication services operating below 30 MHz.

In addition, the comparisons of the vertical radiation patterns over real ground with those over perfectly conducting ground have also shown the large differences that can occur in the assessments of the potential for interference made by measurements on a test site having a conducting metal ground plane compared with assessments using measurements made on a test site having a real ground reference plane.

4.6.8 References

[1] ITU-R Recommendation 527-1, *Electrical Characteristics of the Surface of the Earth*, International Telecommunication Union, Geneva, 1982

[2] ITU-R Report 879-1, *Methods of Estimating Effective Electrical Characteristics of the Surface of the Earth*, International Telecommunication Union, Geneva, 1986

[3] CISPR 11, *Limits and methods of measurement of electromagnetic disturbance characteristics of industrial, scientific and medical (ISM) radio-frequency equipment*, Second edition, International Electrotechnical Commission, Geneva, 1990

[4] Burke, G.J. and Poggio, A.J., *Numerical electromagnetics code (NEC) – Method of Moments*, Naval Ocean System Center, San Diego, CA, NOSC Tech. Document 116, 1981. (Numerical Electromagnetics Code (NEC2) developed at Lawrence Livermore National Laboratory, Livermore, California, File Created 4/11/80, Double precision 6/4/85).

[5] Sommerfeld A, translated by Straus, "Partial Differential Equations in Physics, *Lectures on Theoretical Physics*", Volume VI, Academic Press, New York, 1964, Chapter VI

[6] Macfarlane, I.P., Error in the Numerical Electromagnetic Code (NEC2) Calculation of Magnetic Field Strength Near Ground, Australian telecommunication Research (*ATR*), Vol. 24, No.1, 1990

[7] Macfarlane, I.P., Fleming, A.H.J., Iskra, S. and Haack, G. Pilgrims' Progress – Learning to Use the Numerical Electromagnetics Code (NEC) to Calculate Magnetic Field Strength Close to a Sommerfeld Ground, *Applied Computational Electromagnetics Society (ACES) Journal*, Vol. 5, No. 2, Winter 1990

[8] Macfarlane, I.P., Addendum to: Error in the Numerical Electromagnetics Code (NEC2). Calculation of Magnetic Field Strength Near Ground, Australian Telecommunication Research (*ATR*), Vol. 24, No. 2, 1990

[9] Haack, G.R. and Fleming, A.H.J., Using the Numerical Electromagnetics Code (NEC) to Calculate Magnetic Field Strength Close to a Sommerfeld Ground, Proceedings of the Seventh Annual Review of Progress in *Applied Computational Electromagnetics*, Monterey, California, March 18-22, 1991, pp 493-506, Managing Editor: Richard W. Adler, U.S. Naval Postgraduate School, Code EC/AB, Monterey, CA 93943, USA

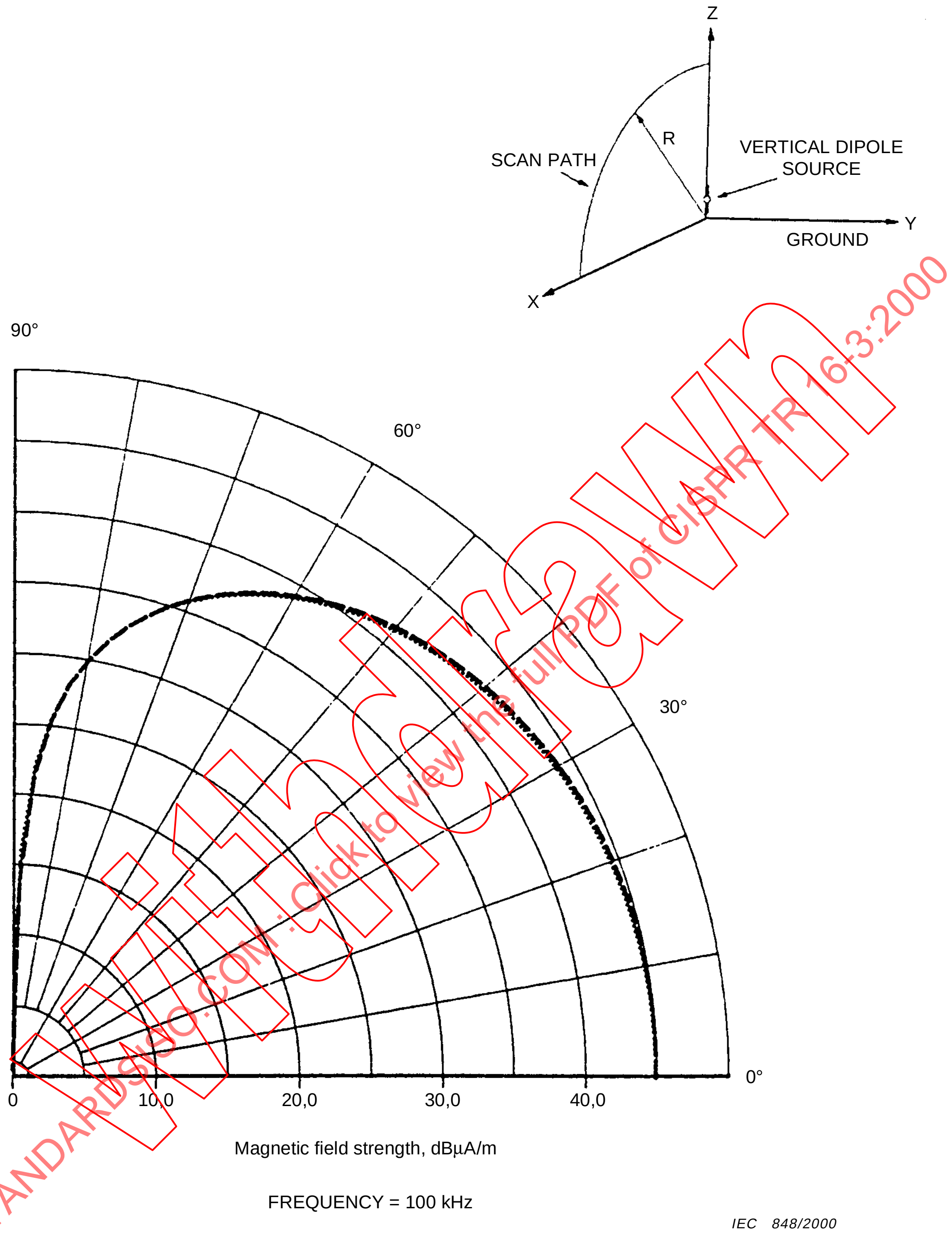

Figure 4.6-7 – Vertical radiation patterns of the horizontally oriented *H*-fields emitted by a small vertical electric dipole located close to the ground

Dipole length 3 m. Dipole base at a height above ground of 0,15 m. Dipole moment 1 A·m.

Dashed line curve – *Hy* at a scan distance of 30 m
Electrical constants of the ground: σ = 1 mS/m, ε_r = 15

Dotted line curve – *Hy* at a scan distance of 30 m
Perfectly conducting ground

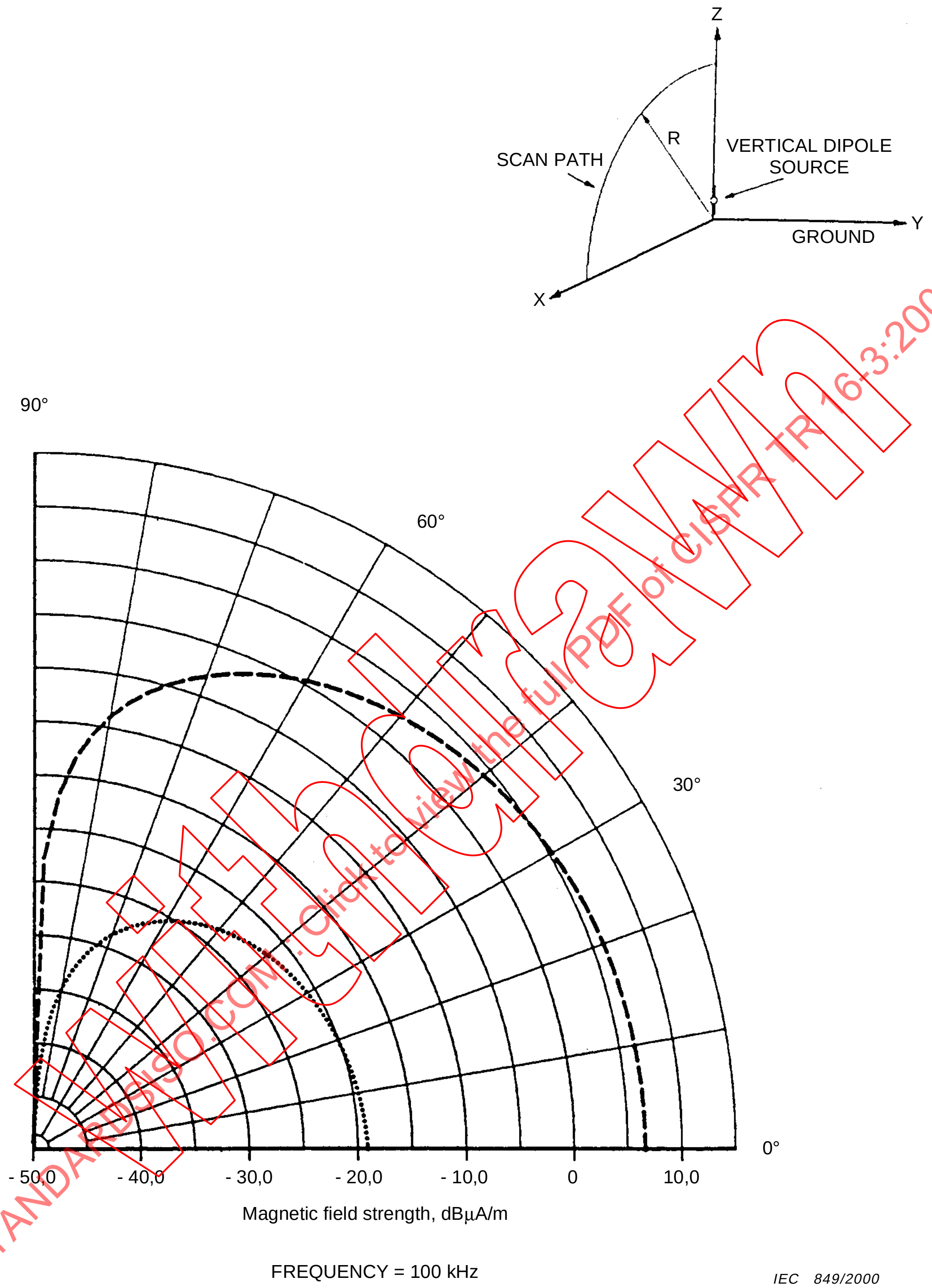

Figure 4.6-8 – Vertical radiation patterns of the horizontally oriented *H*-fields emitted by a small vertical electric dipole located close to the ground

Dipole length 3 m. Dipole base at a height above ground of 0,15 m. Dipole moment 1 A·m.

Dashed line curve – *Hy* at a scan distance of 300 m
Dotted line curve – *Hy* at a scan distance of 3 000 m
Electrical constants of the ground: σ = 1 mS/m, ε_r = 15

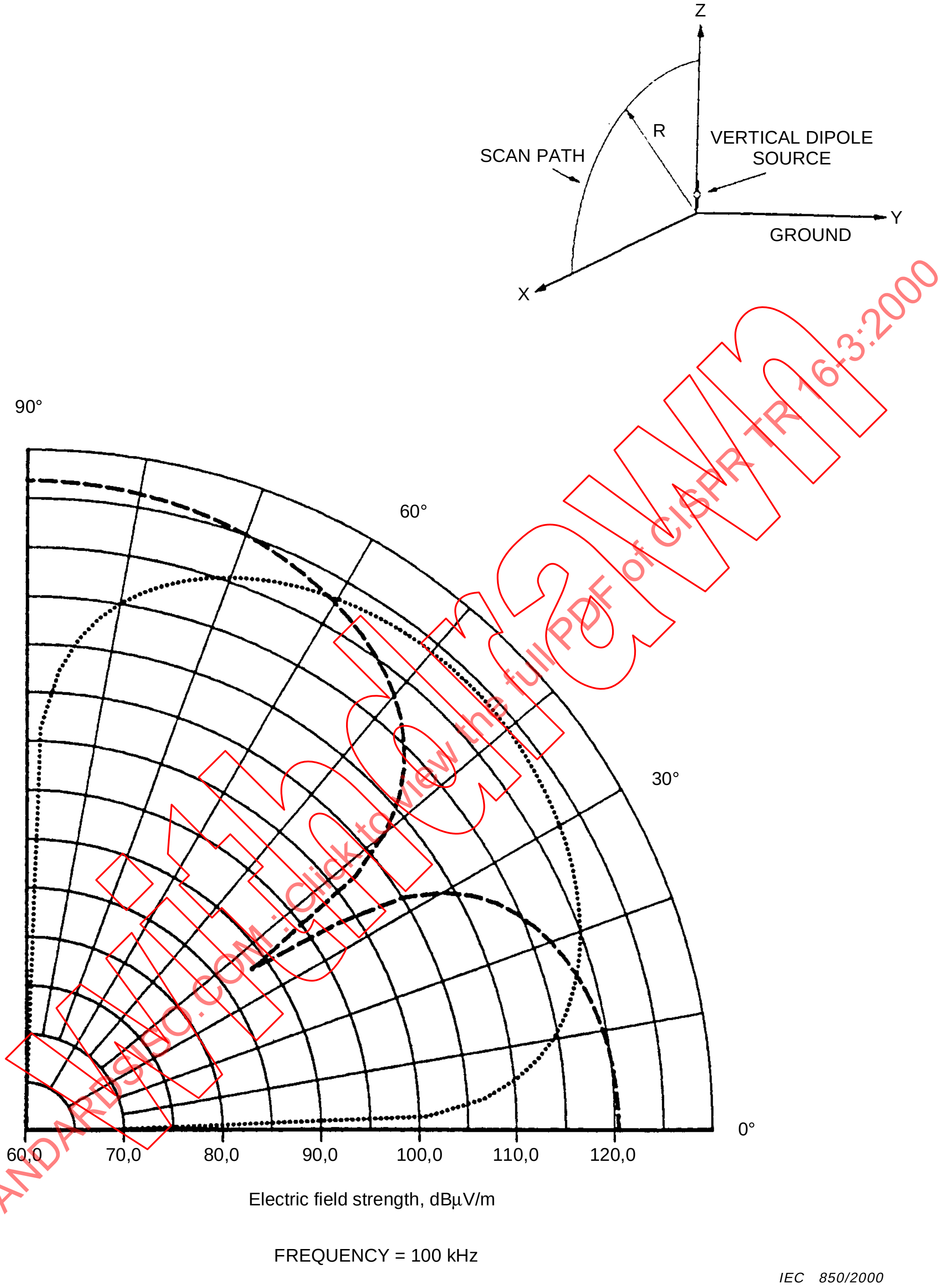

Figure 4.6-9 – Vertical radiation patterns of *E*-fields emitted by a small vertical electric dipole located close to the ground

Dipole length 3 m. Dipole base height above ground 0,15 m. Dipole moment 1 A·m.

Dashed line curve – vertically oriented *Ez* at a scan distance of 30 m
Dotted line curve – horizontally oriented *Ex* at a scan distance of 30 m
Electrical constants of the ground: σ = 1 mS/m, ε_r = 15

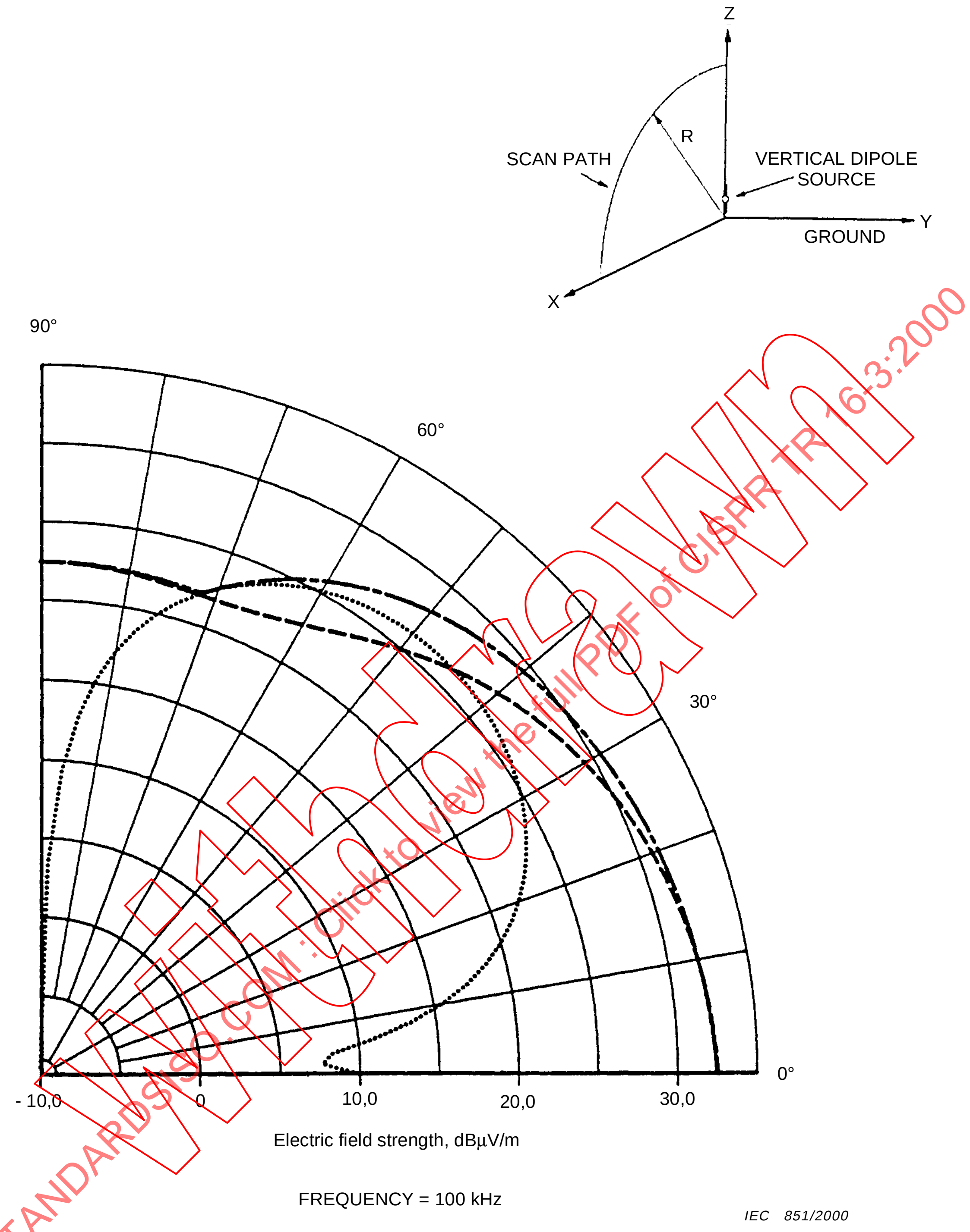

Figure 4.6-10 – Vertical radiation patterns of the *E*-fields emitted by a small vertical electric dipole located close to the ground

Dipole length 3 m. Dipole base height above ground 0,15 m. Dipole moment 1 A·m.

Dashed line curve – vertically oriented *Ez* at a scan distance of 3 000 m
Dotted line curve – horizontally oriented *Ex* at a scan distance of 3 000 m
Dash-dot line curve – total vector/phasor sum of *Ez* and *Ex* at a scan distance of 3 000 m, the vertically polarized *E*-field

Electrical constants of the ground: σ = 1 mS/m, ε_r = 15

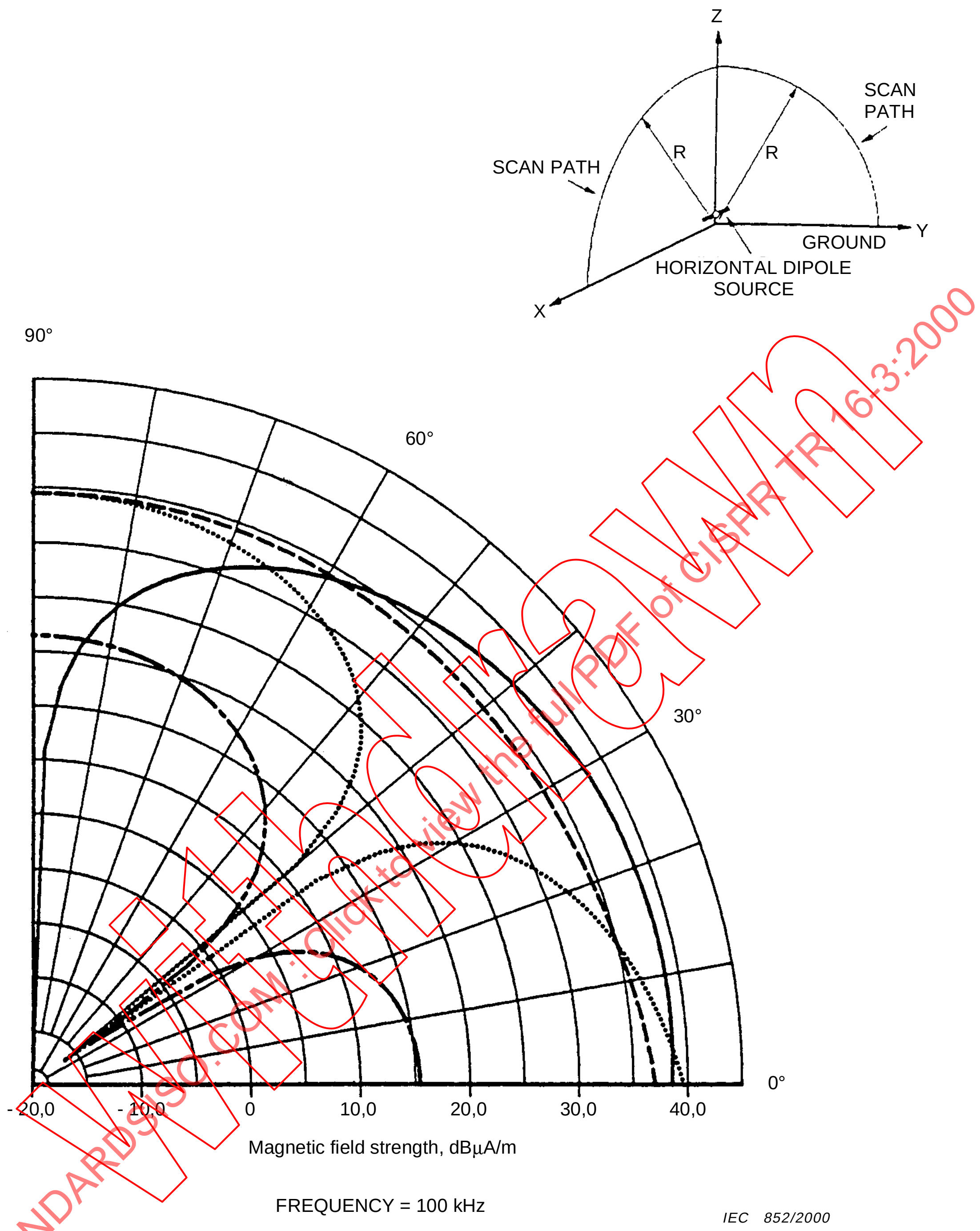

Figure 4.6-11 – Vertical radiation patterns of the *H*-fields emitted by a small horizontal electric dipole located close to the ground

Dipole length 3 m. Dipole height above ground 1 m. Dipole moment 1 A·m.

Dashed line curve – horizontally oriented *Hy* at a scan distance of 30 m in the Z-X plane
Dotted line curve – horizontally oriented *Hy* at a scan distance of 30 m in the Y-Z plane
Solid line curve – vertically oriented *Hz* at a scan distance of 30 m in the Y-Z plane
Electrical constants of the ground: σ = 1 mS/m, ε_r = 15
Dash-dot line curve – horizontally oriented *Hy* at a scan distance of 30 m in the Z-X plane
Perfectly conducting ground

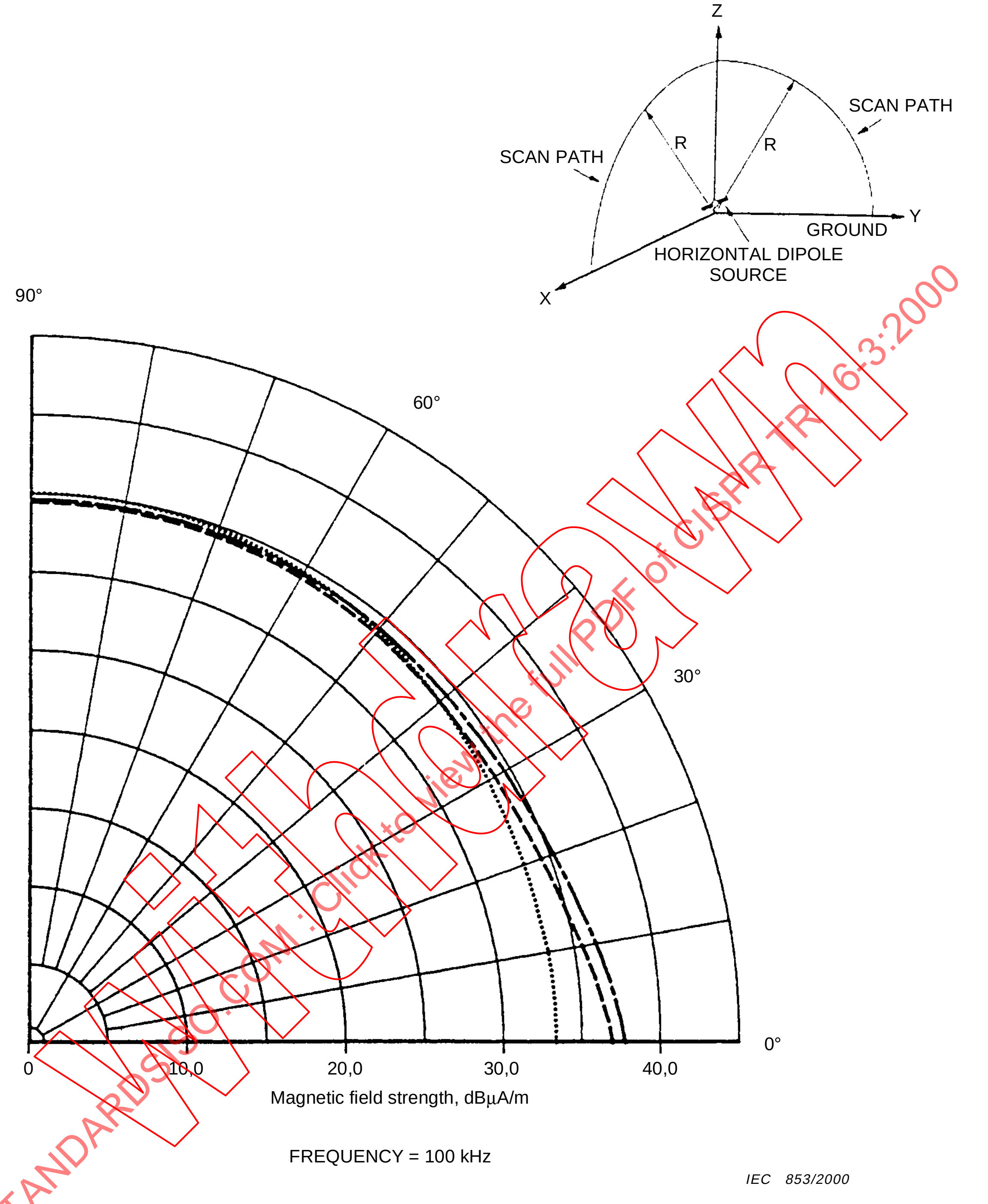

Figure 4.6-12 – Influence of a wide range of values of the electrical constants of the ground on the vertical radiation patterns of the horizontally oriented *H*-fields emitted by a small horizontal electric dipole located close to the ground

Dipole length 3 m. Dipole height above ground 1 m. Dipole moment 1 A·m.

Hy at a scan distance of 30 m in the Z-X plane

Dash-dot line curve –	ground constants are σ = 0,1 mS/m, ε_r = 3
Dashed line curve –	ground constants are σ = 1 mS/m, ε_r = 15
Dotted line curve –	ground constants are σ = 10 mS/m, ε_r = 30

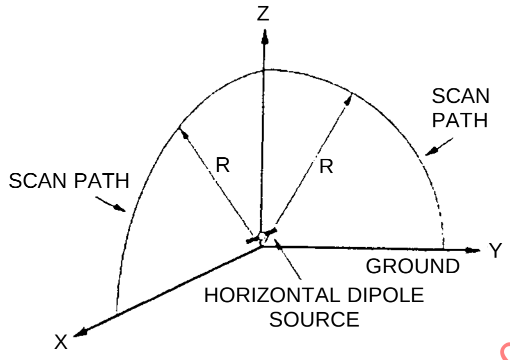

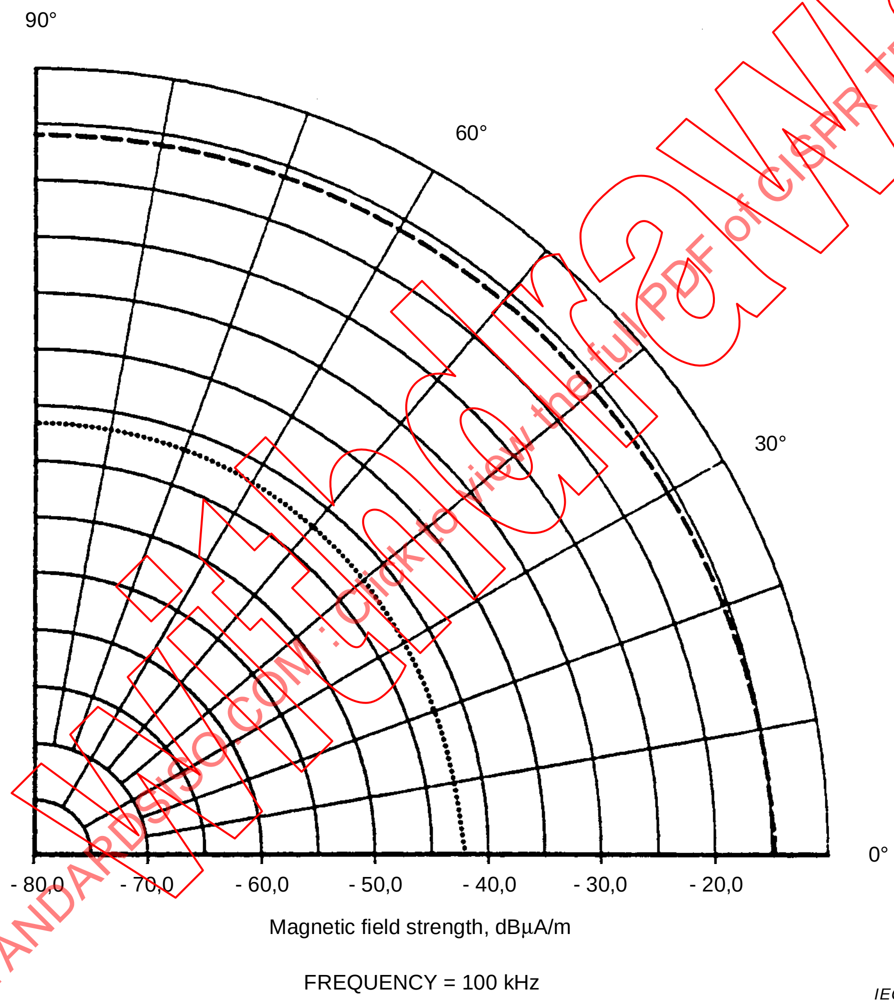

Figure 4.6-13 – Vertical radiation patterns of the horizontally oriented *H*-fields emitted by a small horizontal electric dipole located close to the ground

Dipole length 3 m. Dipole height above ground 1 m. Dipole moment 1 A·m.

Dashed line curve – *Hy* at a scan distance of 300 m in the Z-X plane
Dotted line curve – *Hy* at a scan distance of 3 000 m in the Z-X plane
Electrical constants of the ground σ = 1 mS/m, ε_r = 15

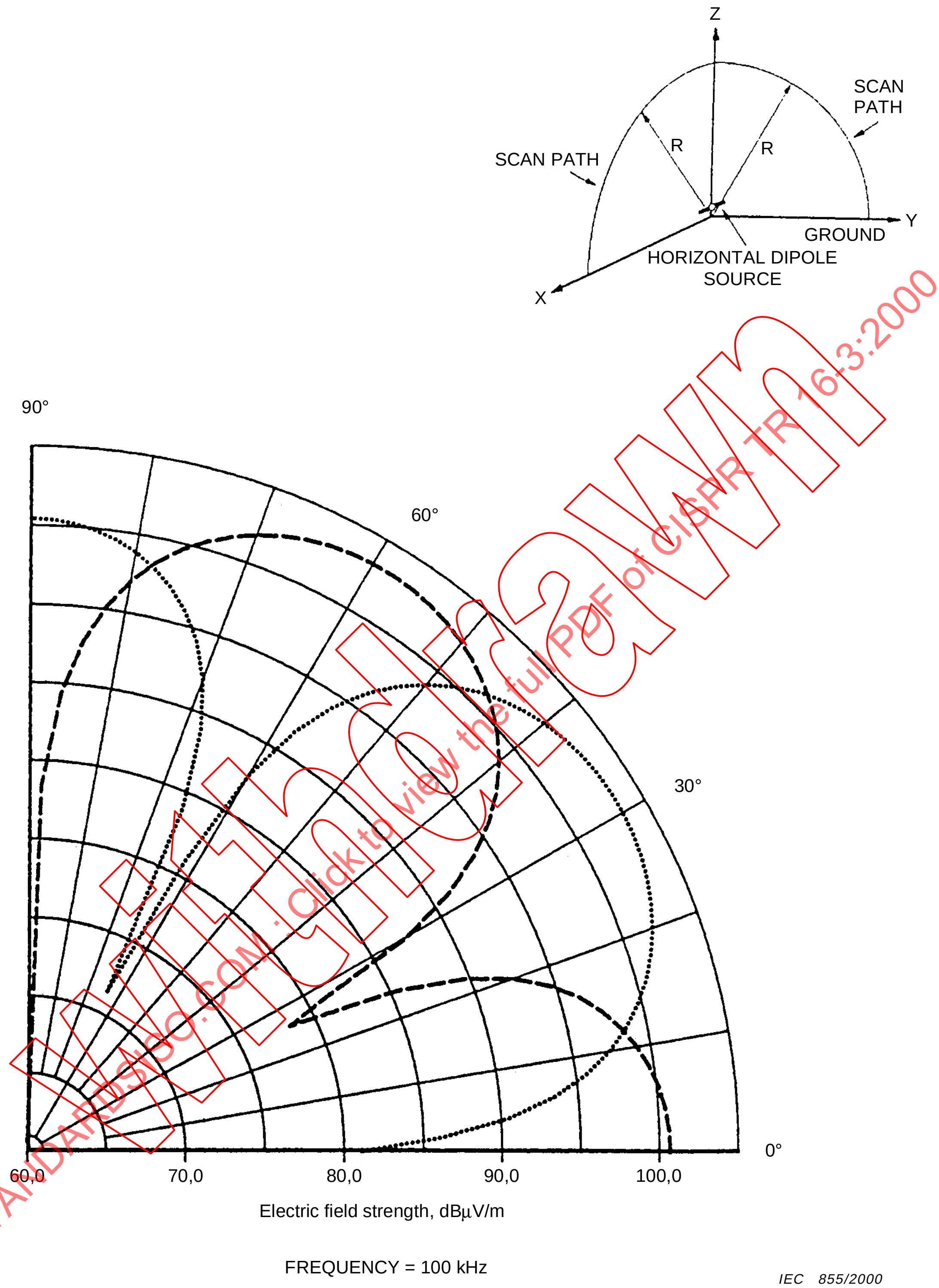

Figure 4.6-14 – Vertical radiation patterns of the *E*-fields emitted by a small horizontal electric dipole located close to the ground

Dipole length 3 m. Dipole height above ground 1 m. Dipole moment 1 A·m.

Dashed line curve – vertically oriented *Ez* at a scan distance of 30 m in the Z-X plane
Dotted line curve – horizontally oriented *Ex* at a scan distance of 30 m in the Z-X plane
Electrical constants of the ground σ = 1 mS/m, ε_r = 15

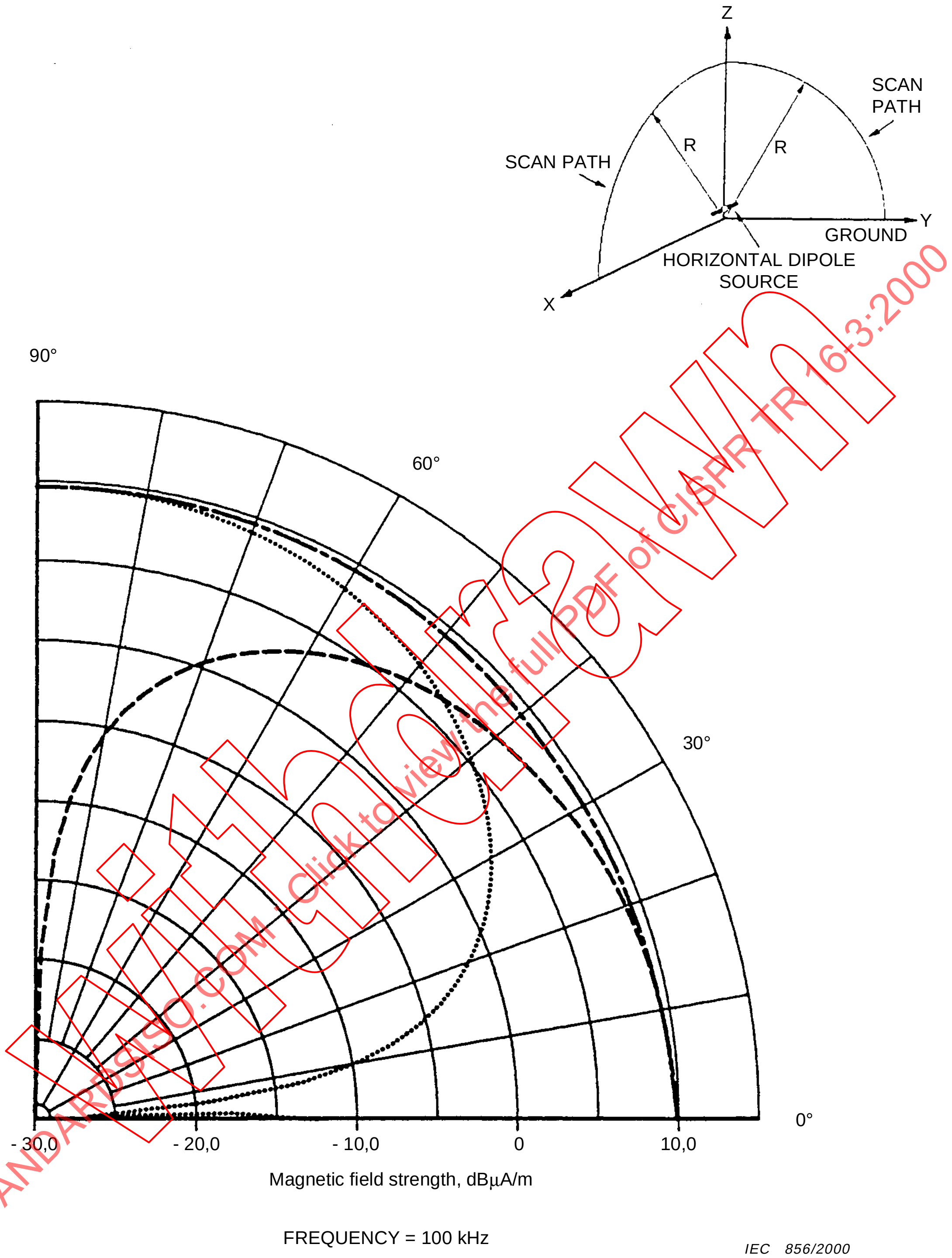

Figure 4.6-15 – Vertical radiation patterns of the *E*-fields emitted by a small horizontal electric dipole located close to the ground

Dipole length 3 m. Dipole height above ground 1 m. Dipole moment 1 A·m.

Dashed line curve – vertically oriented *Ez* at a scan distance of 3 000 m in the Z-X plane
Dotted line curve – horizontally oriented *Ex* at a scan distance of 3 000 m in the Z-X plane
Dash-dot line curve – total vector/phasor sum of *Ez* and *Ex* at a scan distance of 3 000 m in the Z-X plane, the vertically polarized *E*-field

Electrical constants of the ground σ = 1 mS/m, ε_r = 15

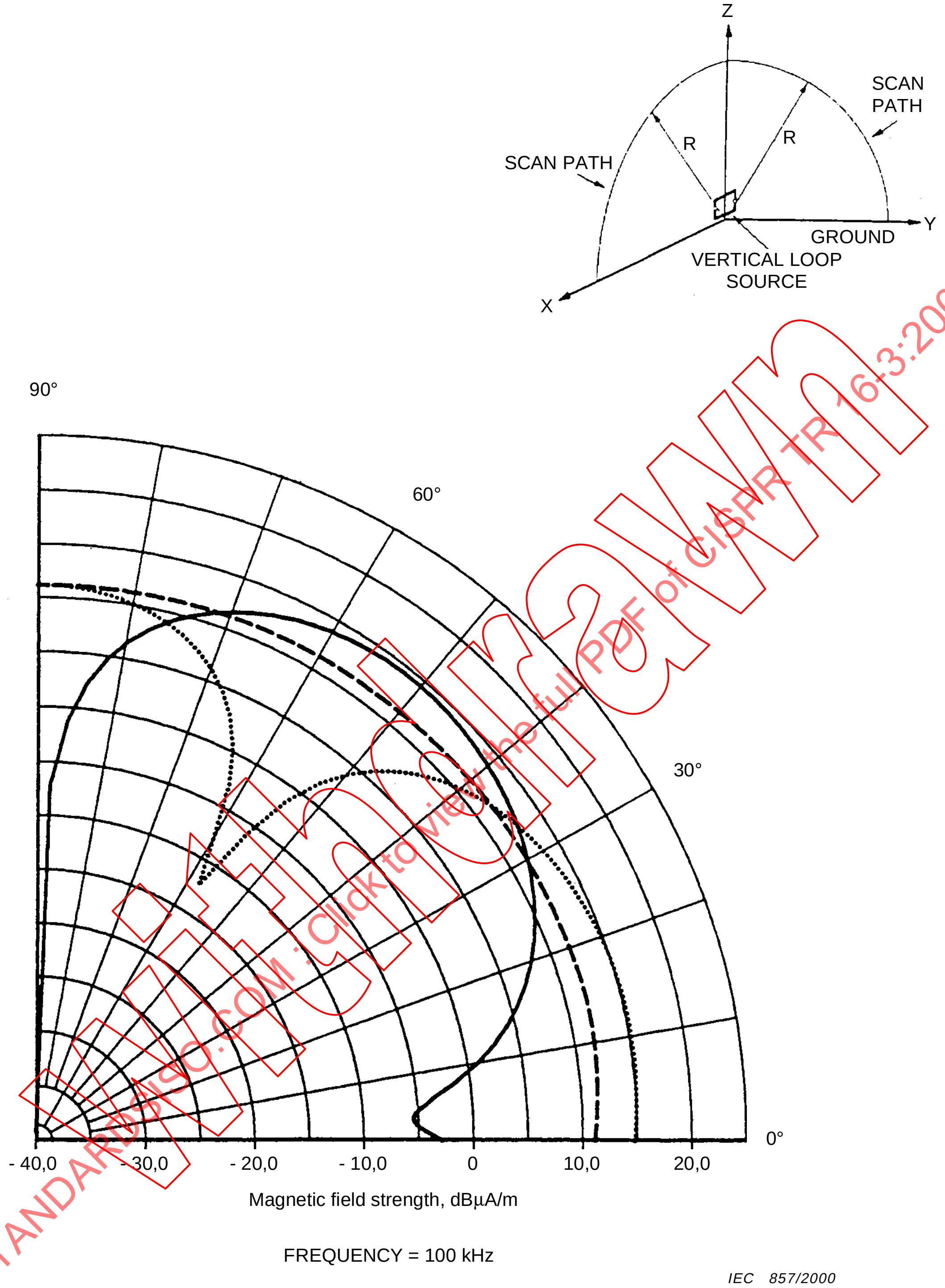

Figure 4.6-16 – Vertical radiation patterns of the *H*-fields emitted by a small horizontal magnetic dipole (vertical loop) located close to the ground

Square loop 3 m × 3 m. Loop base height above the ground 1 m. Dipole moment 1 A·m^2.

Dashed line curve – horizontally oriented *Hy* at a scan distance of 30 m in the Z-X plane
Dotted line curve – horizontally oriented *Hy* at a scan distance of 30 m in the Y-Z plane
Solid line curve – vertically oriented *Hz* at a scan distance of 30 m in the Y-Z plane
Electrical constants of the ground: σ = 1 mS/m, ε_r = 15

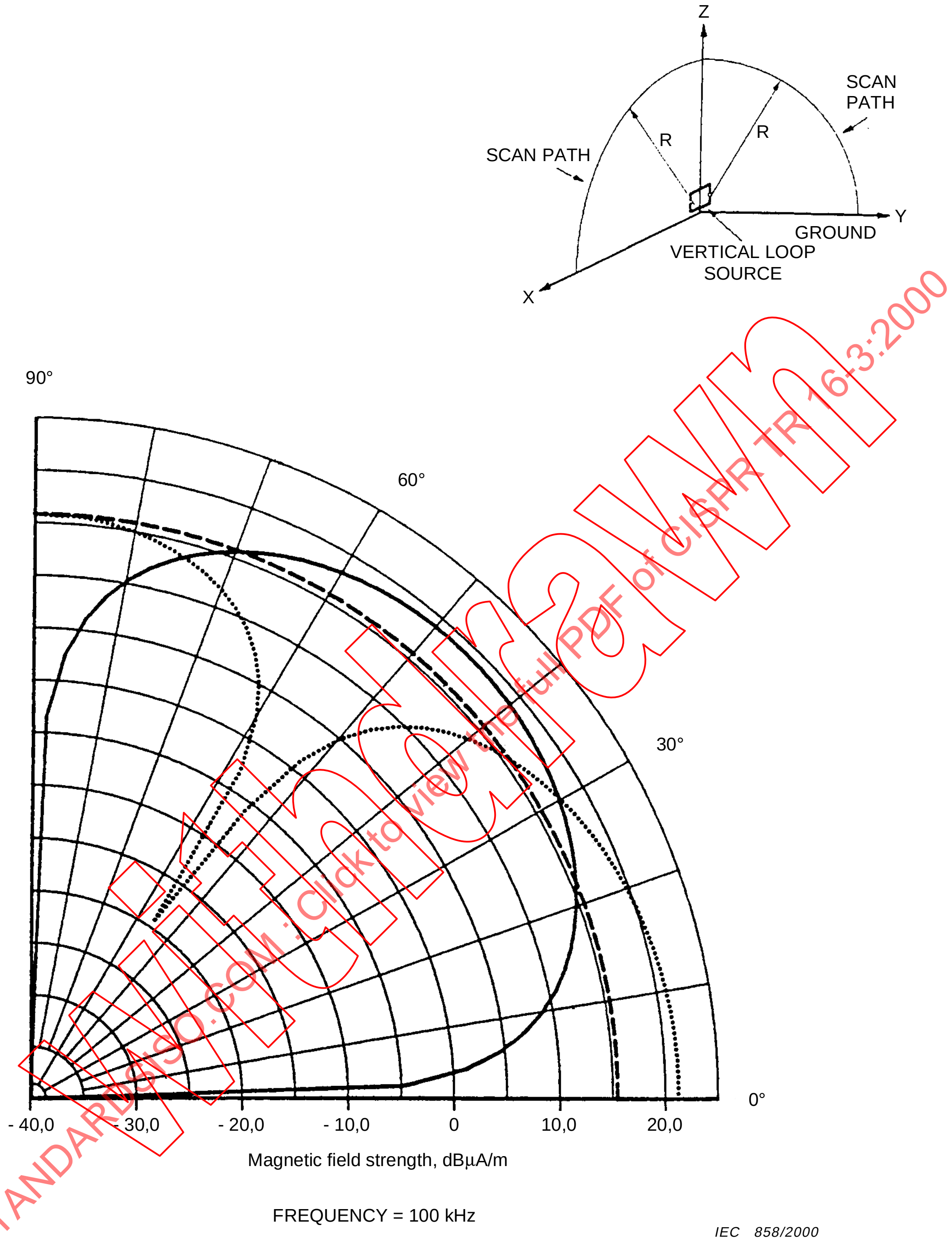

Figure 4.6-17 – Vertical radiation patterns of the horizontally oriented *H*-fields emitted by a small horizontal magnetic dipole (vertical loop) located close to the ground

Square loop 3 m × 3 m. Loop base height above ground 1 m. Dipole moment 1 A·m^2.

Dashed line curve – horizontally oriented *Hy* at a scan distance of 30 m in the Z-X plane
Dotted line curve – horizontally oriented *Hy* at a scan distance of 30 m in the Y-Z plane
Solid line curve – vertically oriented *Hz* at a scan distance of 30 m in the Y-Z plane
Perfectly conducting ground

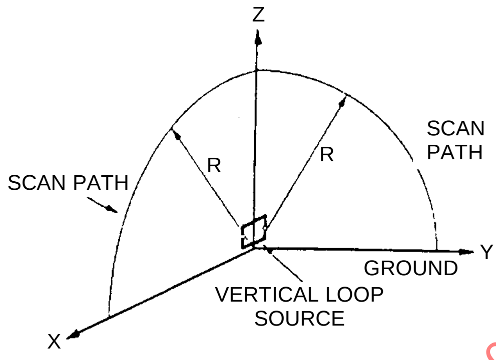

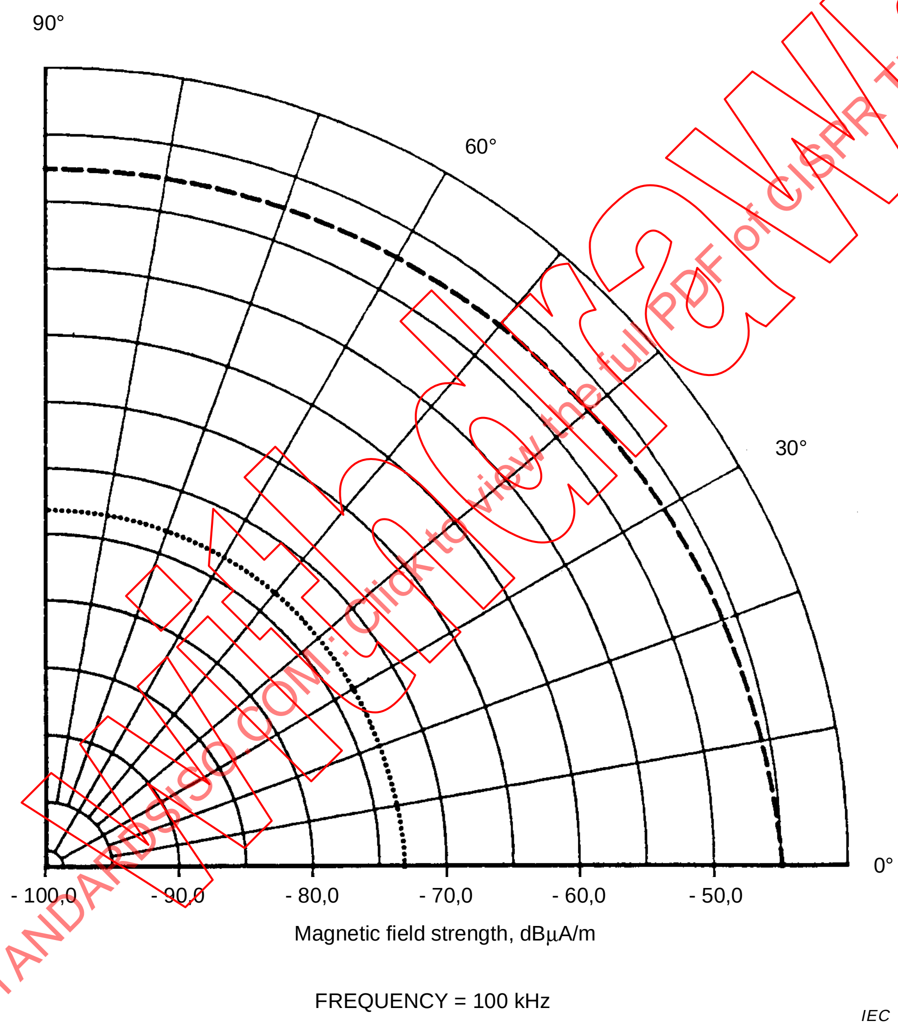

Figure 4.6-18 – Vertical radiation patterns of the horizontally oriented *H*-fields emitted by a small horizontal magnetic dipole (vertical loop) located close to the ground

Square loop 3 m × 3 m. Loop base height above ground 1 m. Dipole moment 1 A·m^2.

Dashed line curve – *Hy* at a scan distance of 300 m in the Z-X plane
Dotted line curve – *Hy* at a scan distance of 3 000 m in the Z-X plane
Electrical constants of the ground σ = 1 mS/m, ε_r = 15

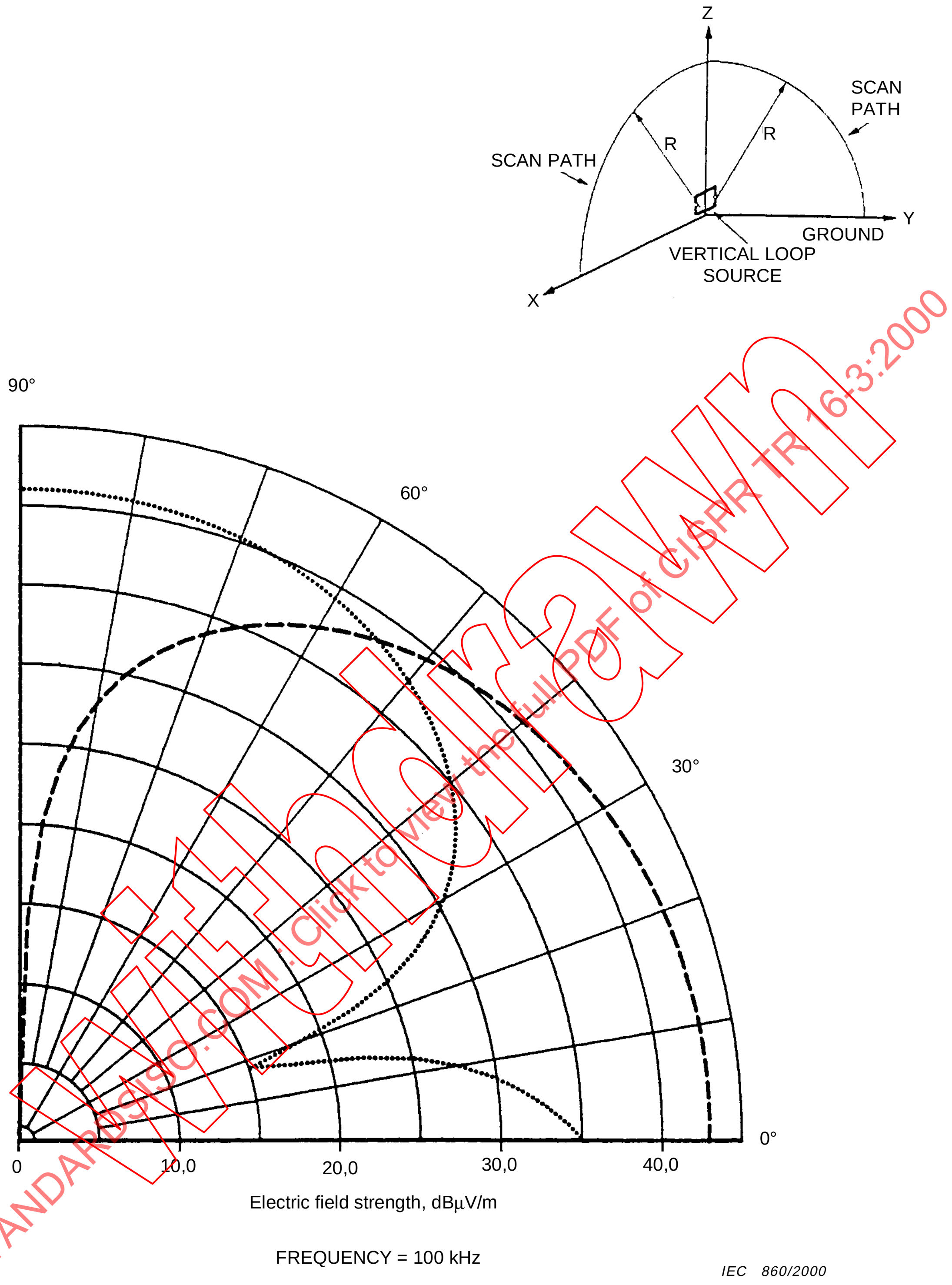

Figure 4.6-19 – Vertical radiation patterns of the *E*-fields emitted by a small horizontal magnetic dipole (vertical loop) located close to the ground

Square loop 3 m × 3 m. Loop base height above ground 1 m. Dipole moment 1 A·m^2.

Dashed line curve – vertically oriented *Ez* at a scan distance of 30 m in the Z-X plane
Dotted line curve – horizontally oriented *Ex* at a scan distance of 30 m in the Z-X plane
Electrical constants of the ground σ = 1 mS/m, ε_r = 15

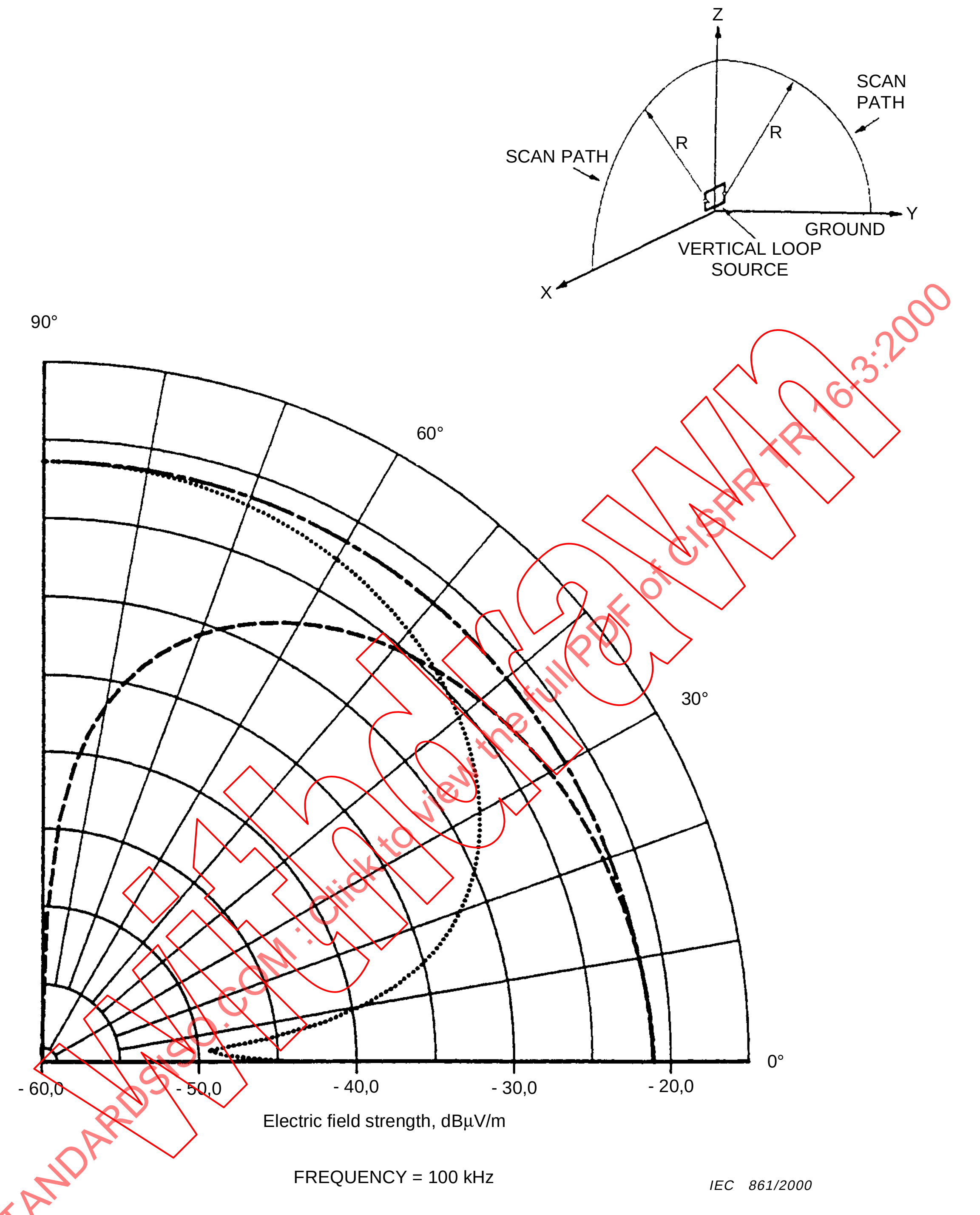

Figure 4.6-20 – Vertical radiation patterns of the *E*-fields emitted by a small horizontal magnetic dipole (vertical loop) located close to the ground

Square loop 3 m × 3 m. Loop base height above ground 1 m. Dipole moment 1 A·m^2.

Dashed line curve –	vertically oriented *Ez* at a scan distance of 3 000 m in the Z-X plane
Dotted line curve –	horizontally oriented *Ex* at a scan distance of 3 000 m in the Z-X plane
Dash-dot line curve –	total vector/phasor sum of *Ez* and *Ex* at a scan distance of 3 000 m in the Z-X plane, the vertically polarized *E*-field

Electrical constants of the ground σ = 1 mS/m, ε_r = 15

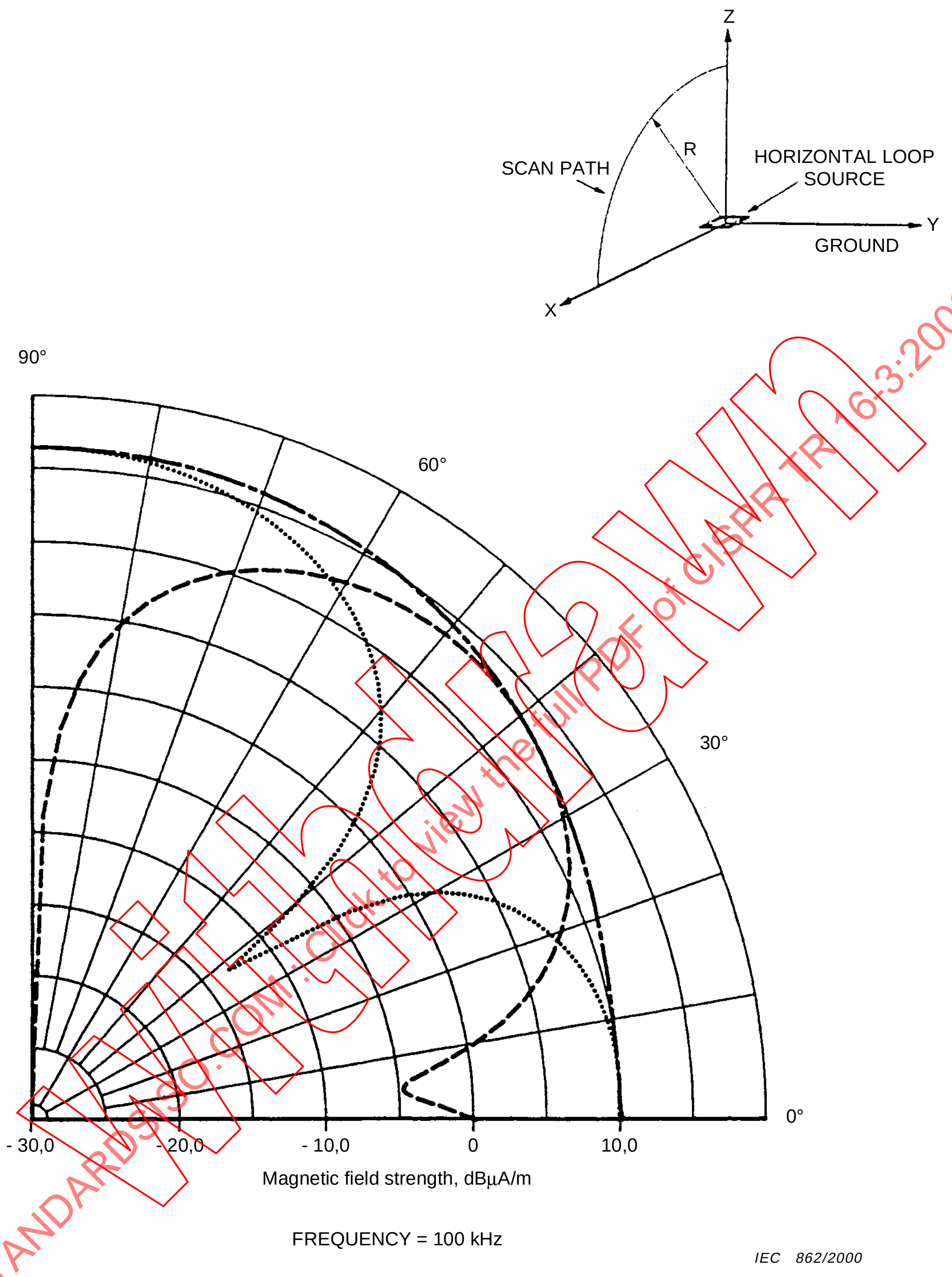

Figure 4.6-21 – Vertical radiation patterns of the *H*-fields emitted by a small vertical magnetic dipole (horizontal loop) located close to the ground

Square loop 3 m × 3 m. Loop height above ground 1 m. Dipole moment 1 A·m^2.

Dashed line curve – horizontally oriented *Hx* at a scan distance of 30 m
Dotted line curve – horizontally oriented *Hz* at a scan distance of 30 m
Dash-dot line curve – total vector/phasor sum of *Hx* and *Hz* at a scan distance of 30 m, the total *H*-field component of the horizontally polarized radiation

Electrical constants of the ground σ = 1 mS/m, ε_r = 15

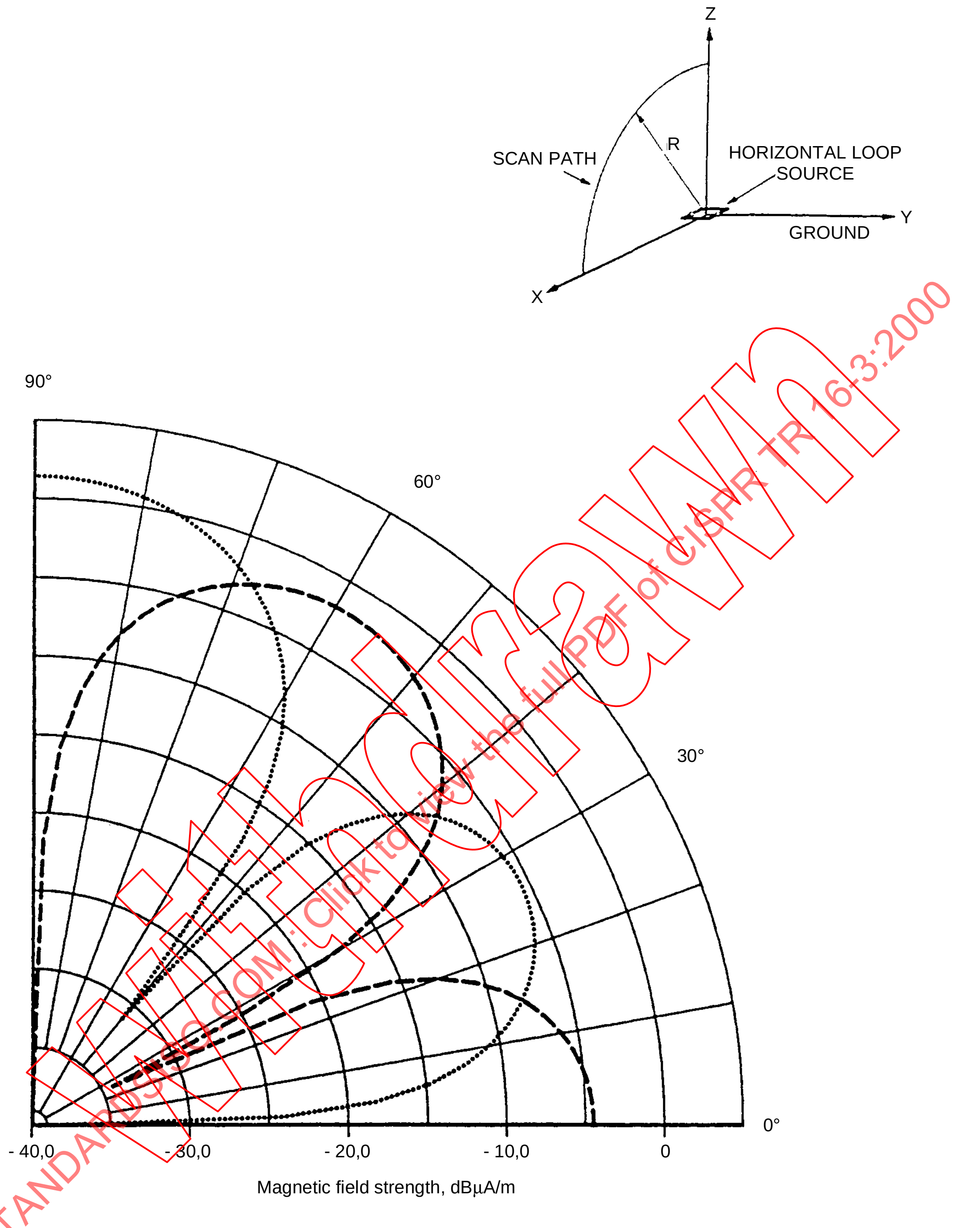

Figure 4.6-22 – Vertical radiation patterns of the *H*-fields emitted by a small vertical magnetic dipole (horizontal loop) located close to the ground

Square loop 3 m × 3 m. Loop height above ground 1 m. Dipole moment 1 A·m^2.

Dashed line curve – horizontally oriented *Hx* at a scan distance of 30 m
Dotted line curve – vertically oriented *Hz* at a scan distance of 30 m
Perfectly conducting ground

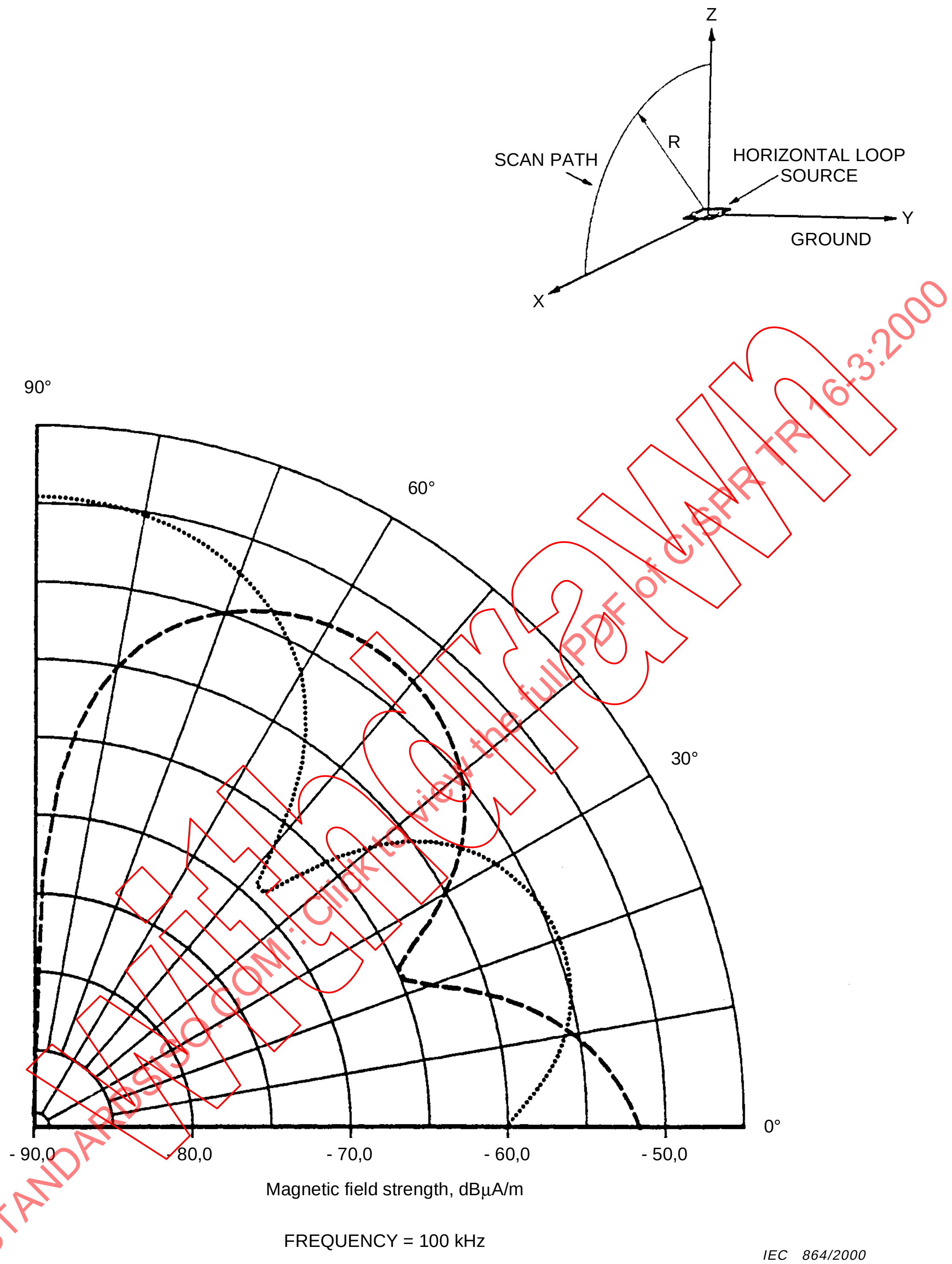

Figure 4.6-23 – Vertical radiation patterns of the *H*-fields emitted by a small vertical magnetic dipole (horizontal loop) located close to the ground

Square loop 3 m × 3 m. Loop height above ground 1 m. Dipole moment 1 A·m^2.

Dashed line curve – horizontally oriented *Hx* at a scan distance of 300 m
Dotted line curve – vertically oriented *Hz* at a scan distance of 300 m
Electrical constants of the ground σ = 1 mS/m, ε_r = 15

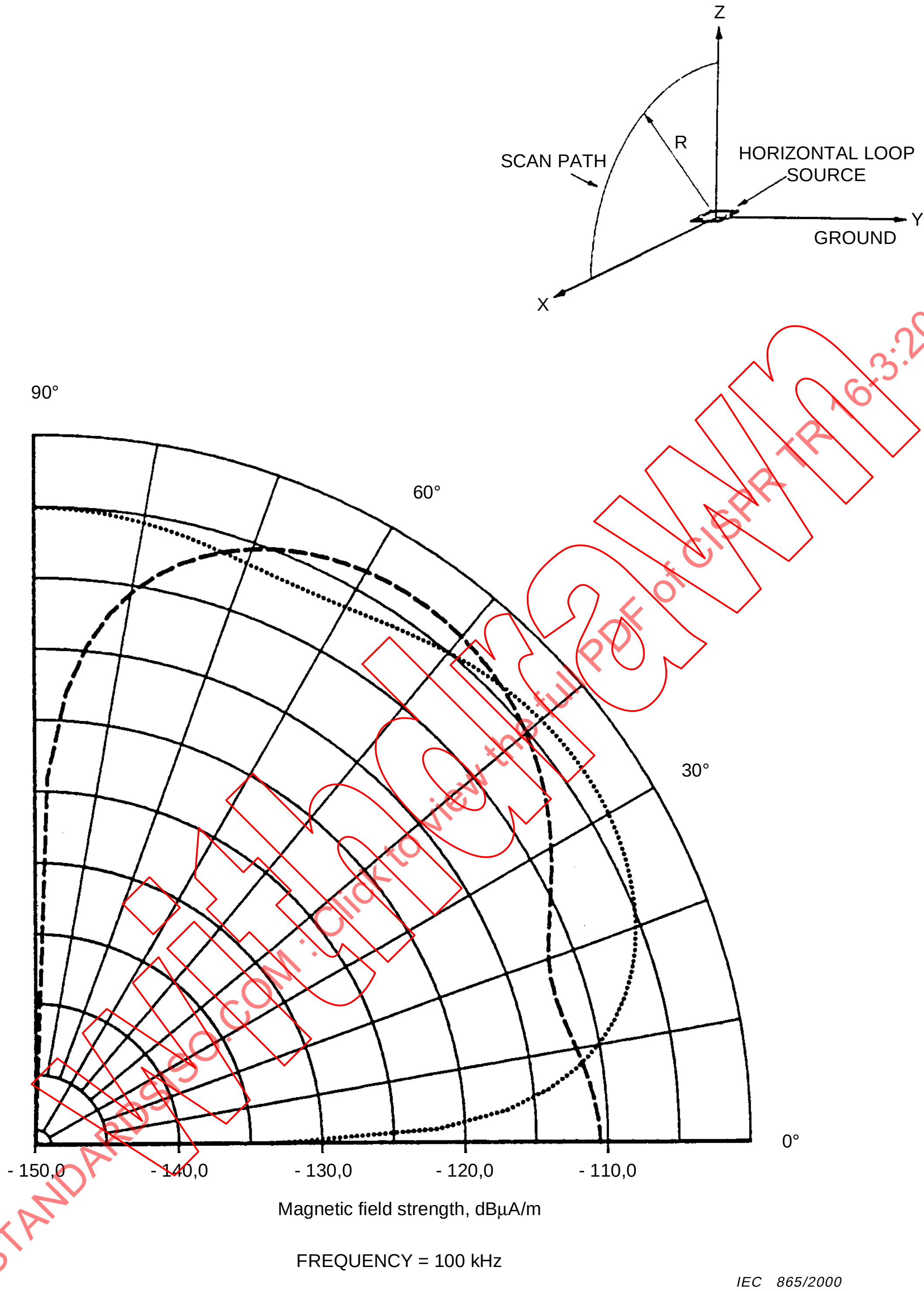

Figure 4.6-24 – Vertical radiation patterns of the *H*-fields emitted by a small vertical magnetic dipole (horizontal loop) located close to the ground

Square loop 3 m × 3 m. Loop height above ground 1 m. Dipole moment 1 A·m^2.

Dashed line curve – horizontally oriented *Hx* at a scan distance of 3 000 m
Dotted line curve – vertically oriented *Hz* at a scan distance of 3 000 m
Electrical constants of the ground σ = 1 mS/m, ε_r = 15

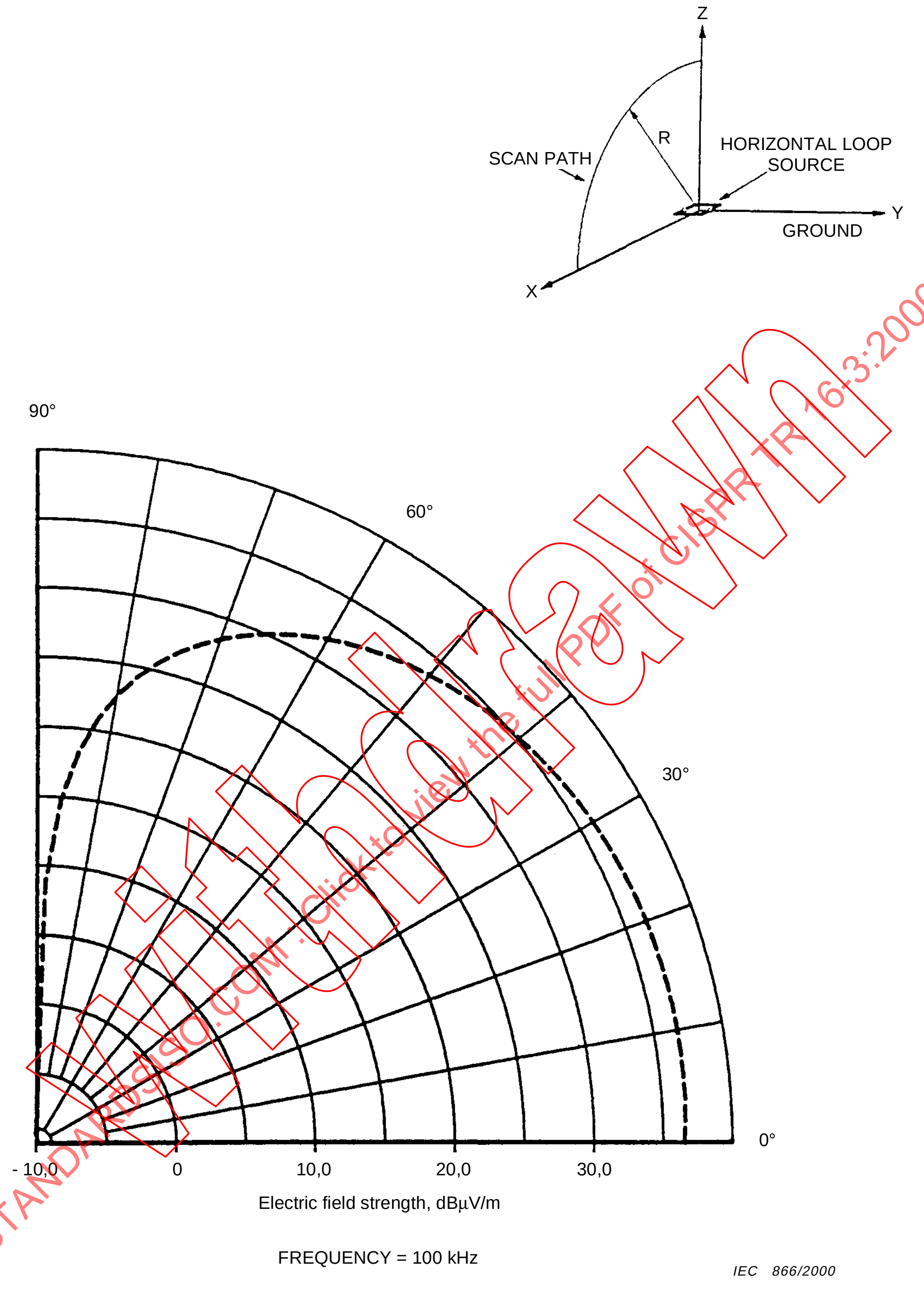

Figure 4.6-25 – Vertical radiation pattern of the *E*-field emitted by a small vertical magnetic dipole (horizontal loop) located close to the ground

Square loop 3 m × 3 m. Loop height above ground 1 m. Dipole moment 1 A·m^2.

Dashed line curve – horizontally oriented *Ey* at a scan distance of 30 m
Electrical constants of the ground σ = 1 mS/m, ε_r = 15

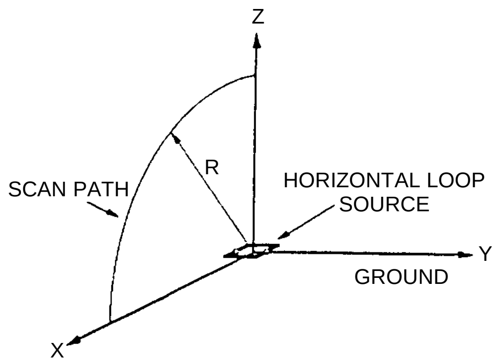

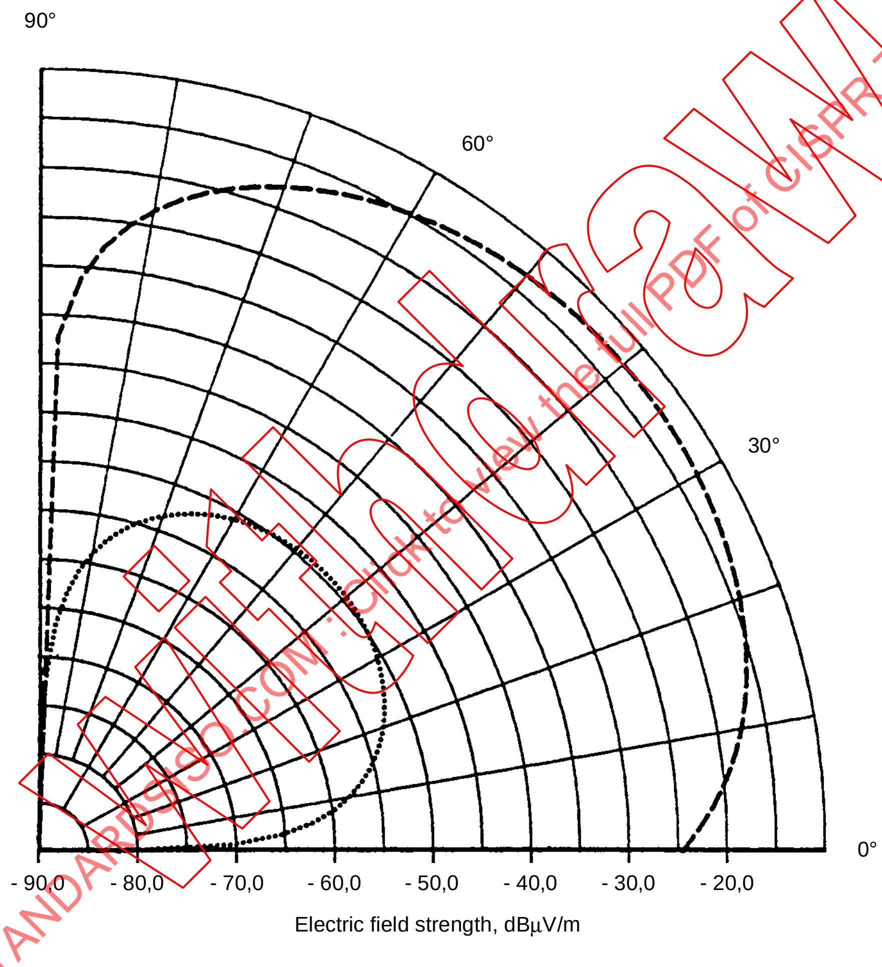

Figure 4.6-26 – Vertical radiation patterns of the *E*-fields emitted by a small vertical magnetic dipole (horizontal loop) located close to the ground

Square loop 3 m × 3 m. Loop height above ground 1 m. Dipole moment 1 A·m^2.

Dashed line curve – horizontally oriented *Ey* at a scan distance of 300 m
Dotted line curve – horizontally oriented *Ey* at a scan distance of 3 000 m
Electrical constants of the ground σ = 1 mS/m, ε_r = 15